PERFORMANCE ANALYSIS OF CONVENTIONAL AND WIRELESS POWERED DECODE-AND-FORWARD RELAY SYSTEMS

Pawan Kumar

PERFORMANCE ANALYSIS OF CONVENTIONAL AND WIRELESS POWERED DECODE-AND-FORWARD RELAY SYSTEMS

A

Thesis Submitted

in Partial Fulfilment of the Requirements

for the Degree of

DOCTOR OF PHILOSOPHY

By

PAWAN KUMAR

DEPARTMENT OF ELECTRONICS AND ELECTRICAL ENGINEERING

INDIAN INSTITUTE OF TECHNOLOGY GUWAHATI

GUWAHATI - 781039, ASSAM, INDIA

November 2018

Declaration

I hereby declare that the thesis entitled "**Performance Analysis of Conventional and Wireless Powered Decode-and-Forward Relay Systems**", submitted in the *Department of Electronics and Electrical Engineering, Indian Institute of Technology Guwahati, Assam, India*, for the award of the degree of **Doctor of Philosophy**, has been carried out by me under the supervision and guidance of Dr. Kalpana Dhaka. The results embodied in this thesis are original and have not been submitted to any other University or Institute for the award of any degree or diploma.

Dated:

Place: Guwahati

Pawan Kumar
Research Scholar
Dept. of Electronics and Electrical Engineering
Indian Institute of Technology Guwahati
Guwahati - 781039, Assam, India.

Certificate

This is to certify that the thesis entitled "**Performance Analysis of Conventional and Wireless Powered Decode-and-Forward Relay Systems**", submitted by **Pawan Kumar** (136102001), a research scholar in the *Department of Electronics and Electrical Engineering, Indian Institute of Technology Guwahati, Assam, India*, for the award of the degree of **Doctor of Philosophy**, is a record of an original research work carried out by him under my supervision and guidance. The thesis has fulfilled all requirements as per the regulations of the institute and in my opinion has reached the standard needed for submission. The results embodied in this thesis have not been submitted to any other University or Institute for the award of any degree or diploma.

Dated:

Place: Guwahati

Dr. Kalpana Dhaka
Assistant Professor
Dept. of Electronics and Electrical Engg.
Indian Institute of Technology Guwahati
Guwahati - 781039, Assam, India.

Acknowledgements

First and foremost, I feel it as a great privilege in expressing my deepest and most sincere gratitude to my supervisor Dr. Kalpana Dhaka for her excellent guidance throughout my Ph.D tenure. Her kindness, dedication, and attention to the details have been a source of great inspiration to me. My heartfelt thanks to my supervisor for her unlimited support and patience that she has shown towards me. I thank her from the bottom of my heart for always being there with me during my journey as a research scholar at IIT Guwahati. I would like to express my gratitude to my supervisor, Dr. A. Rajesh, and other committee members for selecting me in the interview and giving a chance to pursue doctoral research in this Institute.

I would like to thank my doctoral committee members: Prof. R. Bhattacharjee, Dr. S. Chouhan, and Dr. G. K. Das for sparing time out of their busy schedule to evaluate my progress and enrich this work with their valuable suggestions and feedbacks. I would further like to thank my M.Tech supervisor Dr. P. R. Sahu for motivating me with his magical words to pursue Ph.D. I extend my sincere thanks to all the staff members from EEE office and Academic office for helping me out in all sorts of ways during my stay at IIT Guwahati.

During my Ph.D, I found really wonderful lab-mates and fellow research scholars. I had a great time with my many friends at IIT Guwahati including but not limited to Dr. Saurabh Pandey, Arya Anuj Jee, Anoop P., Prateek Rathore, Arijit Roy, Niladri Das, Mohit Joshi, Ramanand Sagar, Vijith, Rahul, Kaushik. These guys made my stay at IIT Guwahati memorable. I will cherish the time spent with them. I thank them all for their friendship. I also express my sincere thanks to my seniors Dr. Brajesh Rawat, Mr. Pavan Kumar Manchi, Mr. Ripudaman Singh, Ms. Sonali Biswas and Mr. Shashank Dwivedi for their timely guidance. I would also like to thank my M.Tech friends Rahul Chhatwani, Kalpant Pathak, and Sandip Kumar Gupta for their consistent support and encouragement. Specifically, Kalpant Pathak has helped me in writing `MATLAB` codes for fading channel modeling. I also thank my B.Tech friend Surya Pratap Singh for his valuable role in my journey.

My deepest gratitude goes to my family for their continuous love and support throughout my studies. The opportunities that they have given me and their unlimited sacrifices are the reasons where I am and what I have accomplished so far. They have been and will remain my ultimate source

of inspiration to achieve every possible height in my journey.

Finally, I believe this research experience will greatly benefit my career in the future.

Pawan Kumar

Abstract

Relaying improves reliability and extends coverage range in wireless systems. Amplify-and-forward (AF) and decode-and-forward (DF) are two main relaying protocols. In conventional wireless systems, we assume that all communicating nodes are connected by continuous power sources or infinite storage batteries. In practice, most of the nodes are powered by batteries having finite storage which need to be recharged or replaced repeatedly in order to sustain the communication process. This may not be favorable in applications where energy-constrained nodes are not easily accessible or other convenient methods are available to provide power. Recently, radio frequency (RF)-based wireless power transfer to energy-constrained nodes has attracted the interest of a vast group of researchers. Performance analysis of both conventional and wireless powered (WP) relay systems is an important area of research which aims to investigate capability and reliability of the systems. In this thesis, we present the performance analysis of three-node DF relay systems when i) all nodes are conventionally powered by continuous power sources, ii) source node transfers wireless power to the energy-constrained relay node, and iii) RF signal radiated by the relay node powers the energy-constrained source node. In all three systems, the relay node operates in half-duplex mode and each node is equipped with a single antenna.

For the analysis, we consider average symbol error rate (SER) as the performance metric. We have derived the average SER expressions for all three systems and validated them by simulation results. Asymptotic average SER expressions are also obtained to simplify the analysis at high signal-to-noise ratio and analyze the diversity order of the systems. Data is modulated using M-ary phase-shift keying (M-PSK) or orthogonal M-ary frequency-shift keying (M-FSK) modulation schemes. M-PSK modulated data is coherently detected at the receiving ends, whereas noncoherent detection is considered for M-FSK modulated data. We have considered different fading environments for the

analysis.

The average SER of the conventional relay system is investigated under $\kappa-\mu$ and $\eta-\mu$ fading for M-PSK modulated data. The relay node employs selective DF protocol. Selective DF and fixed DF are two sub-categories of DF protocol. In selective DF, relay forwards only the correctly decoded data to the destination, whereas in fixed DF all the data received at the relay are forwarded. The direct link between the source and the destination node (SD link) exists and the two signals arriving at the destination node from source and the relay node are combined using maximum ratio combining (MRC) principle. The asymptotic average SERs are used to analyze optimal transmission power allocation at the source and the relay node.

Next, we propose a transmission technique for a WP three-node selective DF relay system where energy-constrained relay node is wirelessly powered by the source node. The end-to-end transmission occurs in three slots. The energy consumption in each slot is different. For the analysis, we consider two scenarios when a) SD link exists and b) SD link is deeply faded and hence ignored. In the first scenario, two signals arriving at the destination node via SD and relayed links are combined using equal-gain combining (EGC) principle. EGC performs close to MRC for reduced complexity. The average SERs of this system have been analyzed under Nakagami-m fading for M-PSK modulated data. The derived asymptotic average SER expressions are used to allocate optimal resources, namely, energy, power and time in different transmission slots.

Performance of the WP relay system, where the source node is energy-constrained and wirelessly powered by the relay node is also analyzed under Nakagami-m and $\kappa-\mu$ shadowed fading. The relay node employs fixed DF protocol. SD link is assumed to be in deep fade. We investigate the average SER of this system for M-PSK and M-FSK modulated data. The asymptotic average SERs are used to analyze the optimal relay location.

Contents

List of Figures

List of Tables

List of Acronyms

AF	Amplify-and-Forward
AWGN	Additive White Gaussian Noise
BDPSK	Binary Differential Phase-Shift Keying
BER	Bit Error Rate
BFSK	Binary Frequency-Shift Keying
BPSK	Binary Phase-Shift Keying
CDF	Cumulative Distribution Function
C-MRC	Cooperative Maximum Ratio Combining
CSI	Channel State Information
DC	Direct Current
DF	Decode-and-Forward
DO	Diversity Order
EGC	Equal-Gain Combining
EH	Energy Harvesting
FCC	Federal Communications Commission
HAP	Hybrid Access Point
ID	Information Decoding
IoT	Internet of Things
LOS	Line-of-Sight
M-ASK	M-ary Amplitude -Shift Keying
M-DPSK	M-ary Differential Phase-Shift Keying
M-FSK	M-ary Frequency-Shift Keying
MGF	Moment Generating Function
MIMO	Multiple Input Multiple Output

MISO	Multiple Input Single Output
ML	Maximum Likelihood
M-PSK	M-ary Phase-Shift Keying
M-QAM	M-ary Quadrature Amplitude Modulation
MRC	Maximum Ratio Combining
OFDM	Orthogonal Frequency Devision Multiplexing
PDF	Probability Density Function
PL	Piecewise-Linear
PS	Power Splitting
PSD	Power Spectral Density
RF	Radio Frequency
SC	Selection Combining
SER	Symbol Error Rate
SIMO	Single Input Multiple Output
SISO	Single Input Single Output
SNR	Signal-to-Noise Ratio
SWIPT	Simultaneous Wireless Information and Power Transfer
TS	Time Switching
WIT	Wireless Information Transfer
WP	Wireless Powered
WPCN	Wireless Powered Communication Network
WPT	Wireless Power Transfer

List of Publications

Journals Published

- P. Kumar and K. Dhaka, "Performance analysis of a decode-and-forward relay system in $\kappa-\mu$ and $\eta-\mu$ fading channels," *IEEE Transactions on Vehicular Technology*, vol. 65, no. 4, pp. 2768-2775, April 2016.
- P. Kumar and K. Dhaka, "Performance analysis of wireless powered DF relay system under Nakagami-m fading," *IEEE Transactions on Vehicular Technology*, vol. 67, no. 8, pp. 7073-7085, August 2018.
- P. Kumar and K. Dhaka, "Average BER and resource allocation in wireless powered decode-and-forward relay system," *IET Communications*, vol. 13, no. 4, pp. 379-386, March 2019.

Conferences Accepted for Publication

- P. Kumar and K. Dhaka, "Performance analysis of wireless powered decode-and-forward relay system", *25th National Conference on Communications, Bangalore, India.*

Manuscripts under Review

- P. Kumar and K. Dhaka, "Performance of wireless powered DF relay system under Nakagami-m fading: Relay assists energy-constrained source," *IEEE Systems Journal.*

1

Introduction

Contents

Relaying offers advantage in terms of increased coverage range and reliable communication. It finds application in communication networks including device-to-device communication, wireless body area networks, wireless sensor networks, Internet-of-things (IoT) entities, such as smart homes and medical implants, etc. In some applications nodes are physically unreachable and therefore, recharging and replacing batteries at the nodes when exhausted is not always feasible. In recent years, radio frequency (RF)-based wireless energy harvesting (EH) is considered as an effective solution for providing monitored energy to energy-constrained nodes. It has attracted the interest of a vast group of researchers. Wireless EH in relay systems is also a prominent area of research. In this thesis, we study the performance of relay systems when nodes transmit using i) continuous energy supply and ii) energy harvested from RF signal transmitted by the other nodes in the system. We analyze the performance of the relay systems under various fading environments. Before proceeding to the contributions of this thesis, we briefly take an overview of wireless communications and discuss fading channel modeling, relaying, and wireless EH.

1.1 An Overview of Wireless Communications

Signals transmitted over wireless propagation medium get affected by deteriorating effects of fading, which adversely affects the performance of wireless communication systems. Fading is basically categorized as large-scale fading and small-scale fading. Power dissipated and attenuation in the received signal due to propagation over a long distance is described by large-scale fading. Large-scale fading is sub-categorized as i) *path loss*, which delineates the reduction in power of the received signals, and ii) *shadowing*, which is caused by objects obstructing the propagation of signals. Further, due to scattering, reflection, and diffraction in the propagation medium, multiple replicas of the signal arrive at the destination/receiver. These replicas arrive via different paths with dissimilar delays and hence cause rapid fluctuations in the received signals amplitude and phase over a small distance or time duration. This fluctuation is described as small-scale fading. Due to the overlap of delayed multipath at the receiver side, there is spreading of signals energy over time. If the signals energy interferes with adjacent signals, then the fading is termed as *frequency-selective fading*, otherwise, it is called *frequency non-selective/flat fading*. These sub-categories of smallscale fading are characterized by the time-spreading phenomenon of fading channels. Based on the time-varying nature of the channel, small-scale fading can be further categorized as *time-selective/fast fading* and *slow fading*. Fast fading

implies the scenarios when the channel changes frequently over the symbol duration, while in slow fading the channel varies slowly over the symbol duration.

1.1.1 Transmission and Reception Over Fading Channels

In digital communication systems, transmitting nodes send data over wireless propagation media by altering the attributes of the carrier signal. This alteration scheme is widely known as modulation. If data changes amplitude, frequency, or phase of the carrier signal, it is called amplitude-shift keying (ASK), frequency-shift keying (FSK), or phase-shift keying (PSK) modulated data, respectively [1]. There exist modulation schemes which alter more than one attributes of the carrier signal to transmit the data. Such schemes are generally called hybrid modulation schemes. An example of such schemes is quadrature amplitude modulation (QAM) in which data modulates amplitude and phase of the carrier signal. Depending on whether the knowledge of carrier phase is required or not at the receiver for detection, modulation schemes are classified as coherent and noncoherent modulations, respectively. PSK and QAM are examples of coherent modulation schemes, while differential PSK (DPSK) modulation is an example of noncoherent modulation schemes. In DPSK modulation scheme, the phase of the data is shifted relative to the previous data. FSK modulated data can be detected coherently and noncoherently as well. Coherent modulation schemes are bandwidth efficient and provide better performance compared to noncoherent modulation schemes at an increased receiver design complexity. Noncoherent modulation schemes are power efficient and have simple receiver designs but suffer from poor performance as compared to the coherent modulation schemes. Data can be transmitted in the form of bits or by grouping bits as symbols. This leads to multi-level modulation. If $m \geq 1$ bits are grouped, there are $M = 2^m$ levels and the corresponding used modulation scheme is termed as M-ary ASK (M-ASK), -FSK (M-FSK), -PSK (M-PSK), -QAM (M-QAM), and -DPSK (M-DPSK). Let the constellation is defined by $\mathcal{S} = \{s_1, \ldots, s_M\}$, where s_ℓ is the ℓ^{th} symbol for $\ell = 1, 2, \ldots, M$. The grouping of bits is done for efficient utilization of the available resources, namely, power and bandwidth.

In a communication system comprising one source node and one destination node, consider $c(t) = A_c \exp(\jmath(2\pi f_c t + \theta_c))$ be the baseband representation of the carrier signal, where t represents time, $\jmath = \sqrt{-1}$, and A_c, f_c, and θ_c are the carrier signal's amplitude, frequency, and phase, respectively. The baseband equivalent of the modulating data signal is represented as $s(t) = a(t)\exp(\jmath(f(t)t + \theta(t)))$,

$0 \leq t < T_s$, where T_s is symbol duration, $a(t)$, $f(t)$ and $\theta(t)$ are data signal's amplitude, frequency and phase, respectively. A generalized form of the transmitted signal in passband domain is given by

$$\tilde{D}(t) = \mathrm{Re}\Big(s(t)\exp\left(\jmath(2\pi f_c t + \theta_c)\right)\Big), \tag{1.1}$$

where $\mathrm{Re}(\cdot)$ represents the real part. Due to disturbances present in the propagating medium, multiple copies of $\tilde{D}(t)$ arrives with different amplitude and delay at the receiving node. The received passband signal is represented as [2]

$$\tilde{R}(t) = \sum_n \alpha_n(t)\tilde{D}(t - \tau_n(t)) + \tilde{N}(t), \tag{1.2}$$

where n is the count of received copies, $\alpha_n(t)$ is amplitude of the nth copy, $\tau_n(t)$ is the delay, and $\tilde{N}(t)$ represents the induced noise. Using (1.1) and (1.2), the received signal can be represented as

$$\tilde{R}(t) = \mathrm{Re}\left(\sum_n \alpha_n(t)d(t - \tau_n(t))\exp(-\jmath 2\pi f_c\tau_n(t))\exp(\jmath(2\pi f_c t + \theta_c))\right) + \tilde{N}(t). \tag{1.3}$$

The baseband equivalent of the received signal can be represented as [3, Appendix A2.4]

$$r(t) = \sum_n \Big(\alpha_n(t)\exp(\jmath(\phi_n(t)))\Big)s(t - \tau_n(t))\exp(\jmath\theta_e) + n(t), \tag{1.4}$$

where θ_e is the phase error introduced due to the imperfect synchronization at the receiver, $\phi_n(t) = -2\pi f_c\tau_n(t)$ is the phase disturbance induced by fading, and $n(t) = \tilde{N}(t)\exp(-\jmath(2\pi f_c t + \theta_c))$ is complex noise component usually modeled using Gaussian distribution.

For delays $\tau_n(t) << T_s$, (1.4) can be given by

$$\begin{aligned} r(t) &= \sum_n \Big(\alpha_n(t)\exp(\jmath\phi_n(t))\Big)s(t)\exp(\jmath\theta_e) + n(t), &\text{(1.5a)}\\ &= g(t)s(t)\exp(\jmath\theta_e) + n(t), &\text{(1.5b)} \end{aligned}$$

where $g(t) = \sum_n \left(\alpha_n(t)\exp(\jmath(\phi_n(t)))\right)$ corresponds to fading. For coherent detection, $\theta_e = 0$ is desirable for the best attainable performance, whereas this phase error does not affect the performance of noncoherent modulation schemes. At the receiver, $r(t)$ is processed through matched filter(s) or correlator(s) to achieve the maximum energy, based on which the detection of the transmitted symbol is performed [3].

The fading gain $g(t) = h(t)\sqrt{\chi(t)d^{-\upsilon}}$ includes the effects of small-scale fading $h(t)$ and large-scale fading $\chi(t)d^{-\upsilon}$. $\chi(t)$ and $d^{-\upsilon}$ represent shadowing and path-loss, respectively where d (in meter) is the distance between transmitting and receiving nodes and υ is path-loss exponent. In this thesis, we consider that the effects of shadowing is relatively small and can be sufficiently described by the path-loss incurred. Hence, the fading gain can be represented as $g(t) = h(t)\sqrt{d^{-\upsilon}}$. In what follows, we refer to small-scale fading simply as *fading*. This consideration is general in the literature when the fluctuations in the received signal due to small-scale fading dominate over shadowing [4]. As such, we can write (1.5) on ignoring[1] θ_e as

$$r(t) = \sqrt{d^{-\upsilon}}h(t)s(t) + n(t)\,. \tag{1.6}$$

Note that, (1.5) is resulted considering that $\tau_n(t) << T_s$. The spread of multipaths over time is described by delay spread, $\sigma_d = f(\tau_n(t))$, where $f(\cdot)$ is a function of delays, and its frequency counterpart is called coherence bandwidth, $B_c \propto 1/\sigma_d$ [4]. Representing signal bandwidth as $B_s = 2/T_s$, the relation $\tau_n(t) << T_s$ is equivalent to $B_s < B_c$, that is, the signal bandwidth is smaller than the coherence bandwidth and the channel gain remains constant for all the frequency components of the signal. This implies that the channel is flat faded. The channel is frequency selective if signal bandwidth is greater than the coherence bandwidth, that is, $B_s > B_c$, and hence, channel gain is different for different frequency components of the signal. Furthermore, the time over which the channel condition changes is described by coherence time, T_c. If the channel remains constant during T_s, that is, $T_s < T_c$, then it is called slow fading channel. Otherwise, if $T_s > T_c$, the channel is fast fading. For slow fading channel, $h(t)$ in (1.6) can be simply represented by h assuming that the channel does not change over the symbol duration. Furthermore, the sampled output of the matched filter(s) (or the output of the correlator(s)) used for the decision can be given by

$$r = \sqrt{d^{-\upsilon}}hs + n. \tag{1.7}$$

1.1.2 Fading Channel Modeling

In the literature, there exist many models to characterize the fading environments. The *unbounded path-loss model* $d^{-\upsilon}$ in (1.6) is widely adopted in the literature. This model is not valid for small values

[1] θ_e can be ignored considering that there is no phase error in case of coherent detection and it does not affect the performance of noncoherent schemes.

of d due to the singularity at $d = 0$, thus *bounded path-loss model* is proposed [5]. For small d, bounded path-loss model is more effective when nodes are randomly deployed, which may cause some of the transmitting and receiving node pairs coincide and result in $d = 0$ [6]. However, in communication systems consisting of a few number of nodes with deterministic node location, unbounded path-loss model can be adopted ignoring the analysis for small d. In this thesis, we adopt the unbounded path-loss model. Methods such as two-ray model, two-slope two-ray model, etc., can be used to measure the path-loss incurred between a pair of transmitting and receiving nodes. Furthermore, attenuation occurred at reference distance plays an important role in measuring the path-loss [7]. However, in this thesis, we assume unity reference distance attenuation, which is a common practice in the literature.

Shadowing is basically modeled using lognormal and gamma distributions [4, 8, 9]. On the other hand, a variety of distributions can be used to model the small-scale fading. The channel gain $h = \sum_n \alpha_n \exp(\jmath\phi_n) = X + \jmath Y$, where X and Y respectively represent in-phase and quadrature components; the channel can be modeled using complex Gaussian distribution employing the central limit theorem for sufficiently large n. If there is no line-of-sight (LOS) component, the fading amplitude $|h|$ follows Rayleigh distribution. In presence of LOS component, the fading amplitude is modeled using Rician distribution. Figures 1.1(a) and (b) show the power delay profile of Rayleigh and Rician fading channels, respectively. Rayleigh and Rician models consider all mutipaths as a single cluster. There can be scenarios when multipaths arrive in clusters. Multipaths within a cluster possess similar delay but among different clusters, the delay is relatively large. Such scenarios can be modeled using Nakagami-m distribution [10]. The power delay profile for this model is shown in Figures 1.1 (c). The Nakagami-m fading parameter $m \geq 1/2$ characterizes the number of clusters. Non-integer values of m correspond to the correlation between in-phase and quadrature components. Nakagami-m fading is a generalized model which includes[2] Rayleigh fading when $m = 1$ and approximates Rician fading for $m > 1$. It provides a good fit to some experimental data of radio channels but may deviate adequately for the other data.

In [11], two more generalized fading models κ–μ and η–μ are proposed to characterize the environments with and without LOS components, respectively. These generalized models characterize the non-homogeneous scattering field and provide a better fit to the experimental data. Moreover, these models unify fading models including one-sided Gaussian, Hoyt, Rayleigh, Rician, Nakagami-m. The power delay profiles for κ–μ and η–μ fading channels are represented in Figures 1.1(d) and (e),

[2] Also, one-sided Gaussian fading and Hoyt fading for $m = 1/2$ and $1/2 < m < 1$, respectively.

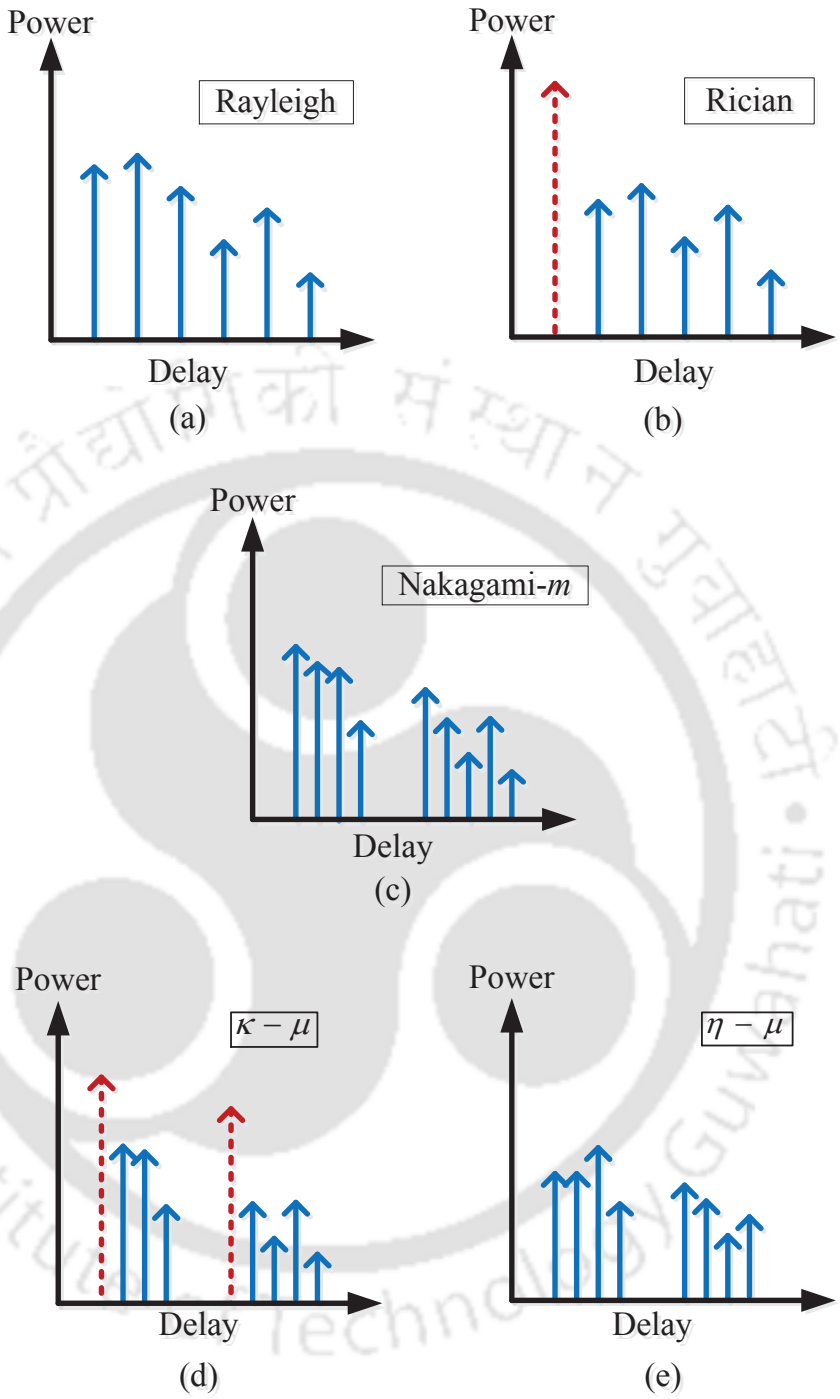

Figure 1.1: Power delay profile of different fading channels (red dashed lines: LOS components, blue solid lines: non LOS components).

respectively.

The parameters κ, η, and μ are real quantities. The parameter κ in $\kappa-\mu$ fading represents the ratio of power in the LOS components and power in the diffused (non-LOS) components. The parameter

Table 1.1: Special cases of $\kappa-\mu$ shadowed fading model.

	$\kappa-\mu$ fading	$\eta-\mu$ fading	$\kappa-\mu$ shadowed fading
Rayleigh	$\kappa \to 0$, $\mu = 1$	$\eta = 1$, $\mu = 0.5$	$\underline{\kappa} \to 0$, $\underline{\mu} = 1$ or $\underline{m} = 1$, $\underline{\mu} = 1$
Nakagami-m	$\kappa \to 0$, $\mu = m$	$\eta = 1$, $\mu = m/2$ or $\eta \to 0$, $\mu = m$	$\underline{\kappa} \to 0$, $\underline{\mu} = m$ or $\underline{m} = m$, $\underline{\mu} = m$
Nakagami-n (Rician)	$\mu = 1$		$\underline{\kappa} = K$, $\underline{\mu} = 1$, $\underline{m} = \infty$
Nakagami-q (Hoyt)		$\mu = 0.5$	$\underline{\kappa} \to (1-q^2)/2q^2$, $\underline{\mu} = 1$, $\underline{m} = 0.5$
One-sided Gaussian	$\kappa \to 0$, $\mu = 0.5$	$\eta \to 0$, $\mu = 0.5$ or $\eta \to \infty$, $\mu = 0.5$	$\underline{\kappa} \to 0$, $\underline{\mu} = 0.5$ or $\underline{m} = 0.5$, $\underline{\mu} = 0.5$
$\kappa-\mu$ fading	κ, μ		$\underline{\kappa} \to \kappa$, $\underline{\mu} = \mu$, $\underline{m} = \infty$
$\eta-\mu$ fading		η, μ	$\underline{\kappa} = (1-\eta)/2\eta$, $\underline{\mu} = 2\mu$, $\underline{m} = \mu$
Rician shadowed			$\underline{\kappa} = K$, $\underline{\mu} = 1$, $\underline{m} = m$

η in $\eta-\mu$ fading describes the correlation between in-phase and quadrature components or the power imbalance between these components. The parameter $\mu > 0$ in both fading models characterizes the number of clusters, and its non-integer values correspond to the correlation among clusters. In [12], $\kappa-\mu$ shadowed fading is proposed to characterize the environment having shadowed LOS components. Using experimental setup in [13] and [14], it is shown that $\kappa-\mu$ fading and $\kappa-\mu$ shadowed fading provide a good fit to empirical data in body-to-body communication networks and device-to-device communication networks, respectively. Table 1.1 lists the mapping of the generalized fading models to the other fading models [15]. In Table 1.1, the parameters $\underline{\kappa}$, $\underline{\mu}$, and $\underline{m}$ correspond to the fading parameters for $\kappa-\mu$ shadowed fading. Parameters $\underline{\kappa}$ and $\underline{\mu}$ are defined in the same manner as the parameters κ and μ in $\kappa-\mu$ fading. The parameter $\underline{m}$ captures the shadowing effect. Moreover, the parameters q and K are the fading parameters of Hoyt fading and Rician fading, respectively.

In the literature, many more fading models have been reported to describe specific wireless environments. In [16], two waves with diffuse power (TWDP) fading model is proposed to describe typical narrow-band receiver operations. In [17], $\alpha-\mu$ distribution is suggested which considers non-linearity of the propagation medium. Further, $\kappa-\mu$ extreme fading model is proposed in [18] to describe the environments such as airplanes, trains, buses, and shopping malls.

1.1.3 Combating the Effects of Fading

The deteriorating effects of fading can be minimized by means of various techniques explored in the literature [2, 19–21]. Equalization methods, orthogonal frequency division multiplexing (OFDM), vector encoding, etc., are useful in minimizing the degradation effects of frequency-selective fading channels [19]. Techniques such as robust modulation, signal redundancy, coding, and interleaving, etc., can be effective in mitigating the effects of time-selective fading channels [2, 20, 21]. If the channel is both frequency-selective and time-selective then conventional OFDM along with polyphase filtering and partial-response coding can be utilized to mitigate the distortion incurred [2]. Degradation in systems performance due to flat fading can be mitigated by employing various diversity techniques. Diversity techniques take advantage of randomness in the channel which enables to provide redundant copies of the source data at the destination(s). This can be accomplished in various ways, for example, by transmitting the source data in multiple time slots or frequency bands, using multiple antennas at transmitting and/or receiving nodes, etc.

Employing multiple antennas at communicating nodes can improve the systems performance considerably. Diversity gain is usually considered to measure the improvement in the performance with an increase in the number of antennas. Depending on the number of antennas at the transmitting and receiving nodes communication systems can be categorized as multiple-input single-output (MISO) systems, single-output multiple-input (SIMO) systems, and multiple-input multiple-output (MIMO) systems. In MISO, transmitting nodes are equipped with more than one antenna and receiving nodes uses a single antenna. On the other side, single antenna at transmitting nodes and multiple antennas at the receiving nodes are employed in SIMO systems. In MIMO systems, both transmitting and receiving nodes are equipped with multiple antennas. MISO and SIMO systems can provide improved diversity gain whereas, MIMO systems can additionally provide enhanced transmission data rate [19].

1.1.4 Performance Analysis

The performance analysis of wireless communication systems is broadly categorized under information theoretic approach and communication theoretic approach. In information theoretic approach mainly outage probability, outage capacity, ergodic capacity, and throughput are considered as the performance metrics. On the other hand, average bit error rate (BER) and average symbol error rate (SER) are the main performance metrics in communication theoretic approach. Information theoretic

approach takes transmission data rate into consideration, whereas communication theoretic approach considers modulation, demodulation, and detection of data. The performance analysis based on the latter approach provides better insights and is more reliable.

Average SER of communication systems are basically analyzed using i) cumulative distribution function (CDF), ii) probability density function (PDF), and iii) moment generating function (MGF) based approaches. Given the conditional SER, the average SER is obtained using the CDF, PDF, and MGF of the instantaneous received signal-to-noise ratio (SNR). These three approaches produce the same analytical results and can be chosen depending on the mathematical complexity involved in the analysis.

1.2 An Overview of Relay Systems

Employing multiple antennas at the transmitting and/or receiving nodes can assist in mitigating the effects of fading. In communication networks, such as wireless sensor networks, IoT entities, wireless body area network, etc., installation of multiple antennas at nodes may not be feasible due to hardware size constraints. In such scenarios, extra nodes can be deployed between the transmitting and receiving nodes to improve the end-to-end performance. These extra nodes are generally called *relays* and can form virtual antenna array in order to improve the diversity gain [22]. In communication systems like cellular networks, fixing multiple antennas at nodes (including relays) can further enhance the systems performance [23, 24]. In systems where relay nodes are introduced between the source and destination nodes to improve the diversity gain are known as *parallel relay systems*. Scenarios can also exist when the destination node is not in the coverage range of the source node or the channel between source and destination is blocked such that the source data cannot be conveyed to the destination. Under such circumstances, multiple relay nodes can be arranged in between source and destination nodes such that the source data is communicated to the destination in multiple hops and hence the coverage range is extended. The systems employing arrangement of relays in multiple hop fashion are commonly known as *multihop relay systems* [25, 26]. The hybrid arrangement of relay nodes is also appealing when there is a requirement of diversity enhancement in individual hop [26]. In networks such as device-to-device communications, usually user devices act as the relay and cooperate with each other to convey their data to the destination(s). Such user devices are generally called cooperative relays.

The advantage of relaying in terms of improved performance comes at the cost of increased overhead, which is caused by the requirement for additional channel state information (CSI), relay selection, and coordination. The increment in overhead in relay systems results in higher end-to-end delay as compared to point-to-point communications. In the literature, considerable efforts are made to investigate methods for minimization of the end-to-end delay [27–29], etc. Particularly, in parallel relay systems, the end-to-end delay can be minimized by appropriately modeling the transmission duration, applying suitable relay selection methods, etc. [27, 28]. The end-to-end delay in multihop relay systems is minimum when relays are placed at an equal distance [29]. Usually, half-duplex mode of operation is considered for the relays which imposes low system throughput. Schemes such as two-way relaying [30], full-duplex relaying [31], mimicking full-duplex relaying [32], etc., can be useful in improving the throughput, though this comes at the cost of increased system complexity. Network coding in relaying systems is also a potential candidate in improving the system throughput [33–35].

The relay nodes basically employ amplify-and-forward (AF) and decode-and-forward (DF) protocols to process the received signal. In AF, relays simply amplify the received signal with some gain and forward it further, whereas in DF, they first decode the received data, re-encode it and then forward. Depending on whether the gain by which relays forward the amplified signal is fixed or varying, AF protocol is called *fixed-gain AF* or *variable-gain AF*, respectively. Fixed AF requires no knowledge of instantaneous channel state information (CSI), whereas CSI of source-to-relay links are required at the relays in variable-gain AF. DF protocol is sub-categorized as *fixed DF* and *selective DF*. In fixed DF, relays forward all the decoded data, while in selective DF only the correctly decoded data is forwarded. Correct decoding at the relay nodes can be accomplished using cyclic redundancy check codes or threshold-based checking. AF protocol has lower complexity, whereas DF protocol outperforms AF protocol at high SNRs [26, 29].

1.2.1 Three-node Relay System

Three-node relay system has a relay node assisting the source and the destination nodes. In case the direct link connecting the source to destination node is deeply faded, then the relay node is useful for coverage extension. This arrangement of nodes is widely known as *two-hop* relay system. Further, if the direct link exists, the relay node assist in improving the diversity gain by means of diversity combining schemes such as selection combining (SC), equal-gain combining (EGC), and maximum

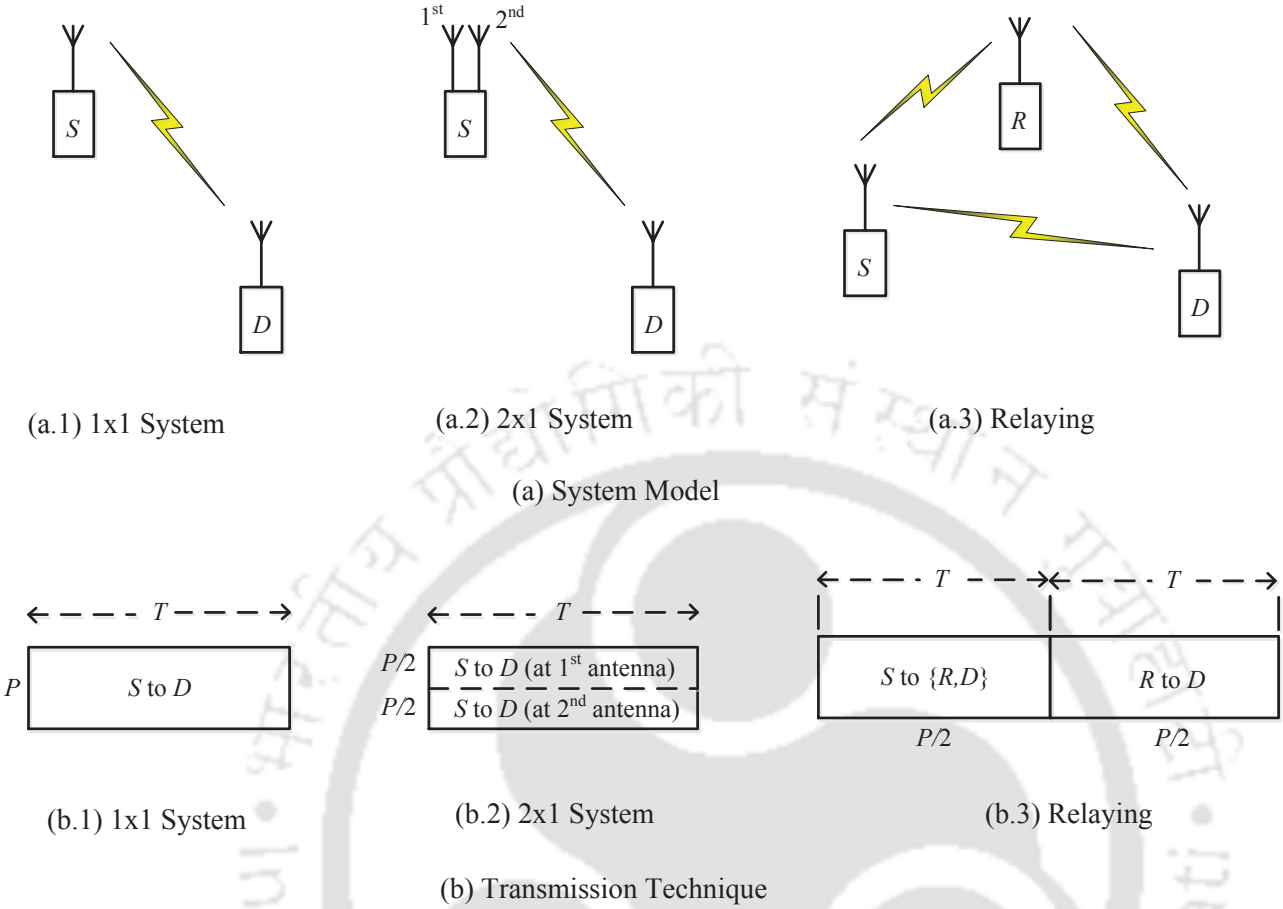

Figure 1.2: System model and transmission technique of 1×1 system, 2×1 system and relaying system.

ratio combining (MRC) [36]. In two-hop relay system, fixed-gain AF may outperform variable-gain AF at low to medium SNRs but exhibits relatively poor performance at high SNRs [37]. Fixed DF can outperform AF (both fixed-gain and variable-gain) at low to medium SNRs, although at high SNRs, these protocols perform identically [37]. In system with direct link, selective DF protocol possesses better performance than the other protocols [22].

Performance Comparison of Selective DF: Here we compare the performance of a three-node relay system with that of SISO (single-input and single-output) and MISO systems. Figure 1.2 presents the system model and transmission techniques for three systems: 1) SISO, where source node S and destination node D are mounted with single antenna, 2) MISO, where node S is equipped with two antenna and node D with single antenna, and 3) three-node relay system, where each node has a single antenna. SISO and MISO systems are represented by 1×1 system and 2×1 system, respectively. In the relay system, the relay node R employs selective DF protocol and operates in half-duplex mode.

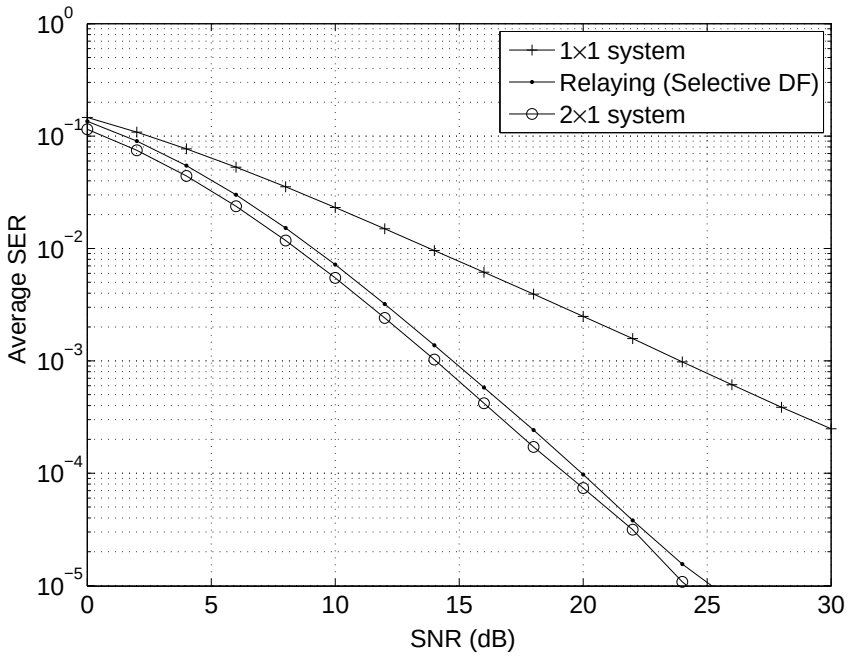

Figure 1.3: Average SER comparison of a three-node selective DF relay system with direct transmission and 2×1 MISO system for BPSK modulated data under Rayleigh fading.

The direct link between the source and destination nodes exists and the two signals arriving at the destination via the direct link and relayed link are combined using MRC principle. Each transmission requires T time. Hence, the relaying system requires a total $2T$ time of the end-to-end transmission. This causes a reduction in throughput by half as compared to the other two systems. The total transmission power in each system is taken as P. In 1×1 system, node S transmits with power P whereas in 2×1 system, each transmitting antenna at node S transmit with power $P/2$. In the relay system, source and relay nodes transmit with power $P/2$. The background noise is assumed to be additive white Gaussian noise (AWGN) with mean zero and variance N_0. The mean power of the fading gain is assumed to be unity. Hence, the received SNR is P/N_0. Data is considered to be binary PSK (BPSK) modulated and the fading environment is modeled by Rayleigh distribution. These three systems are emulated in `MATLAB` and the corresponding simulated average SER results are presented in Figure 1.3. We assume unit transmission time duration, that is, $T = 1$ for simulation. In Figure 1.3, we observe that the diversity gain of 2×1 system is better than that of the other two systems. The relay system exhibits diversity gain close to 2×1 system. 1×1 system possesses diversity order (DO) of one, whereas the other two systems have a DO of two. DO is diversity gain at high SNRs and can be

interpreted as the negative slope of average SER versus SNR curves on the log-log scale. We conclude that the performance of a communication system having a source and a destination, each equipped with a single antenna can be improved considerably by introducing a relay node in the system. The relay system and 2×1 MISO system perform close and both have DO of two.

Conventionally, it is assumed that nodes are powered by infinite energy capacity or rechargeable batteries. Although, in practice, energy storage is finite and in some applications communicating nodes are physically unreachable for recharging and replacing batteries when exhausted. In such circumstances, the end-to-end communication terminates if there is no sufficient amount of energy at any of the transmitting nodes. Renewable energy resources, such as wind, solar, mechanical vibration, etc., are looked upon as prominent solutions for scavenging energy at the energy-constrained nodes and extending the communication lifetime [38]. Though the quantity of energy arrival is dependent on geography, weather and many other factors, which make these resources unpredictable and unreliable [39]. This limits the applicability of these energy harvesting (EH) solutions when there is a requirement to transmit vital information but harnessed energy is insufficient to support the communication. Wireless EH in such scenarios is being considered as an effective solution for providing energy to energy-constrained nodes when required. It has attracted the interest of a vast group of researchers. Wireless EH in relay systems is also a prominent area of research [40, 41]. In the next section, we briefly discuss about wireless EH and its applicability in communication systems.

1.3 Wireless Energy Harvesting

Wireless EH or wireless power transfer (WPT) is attractive and promising as it can provide seamless, constant and controllable on-demand power to energy-constrained nodes. WPT can be accomplished in near-field and far-field of electromagnetic wave [39]. Near-field WPT relies on the coupling of magnetic fields of electromagnetic waves between two coils and EH is feasible over a tiny air-gap between the coils, typically few centimeters. The WPT distance can be increased for a reduced EH efficiency. Inductive coupling due to the magnetic field and magnetic resonance coupling are the two major techniques for near-field WPT. Far-field WPT enables EH over distances in the range of meters using electric field of the electromagnetic wave. Near-field WPT is non-radiative in nature. Whereas, far-field WPT is radiative which can have hazardous effects on the human body hence regularization of power transmission limit is required. Due to its capability to provide power to nodes located at

longer distances, far-field or radio-frequency (RF)/microwave-based EH looks more attractive in communication networks. Next, we discuss the past developments and major technical breakthroughs in WPT before focusing our attention to the applicability of far-field WPT in communication networks.

1.3.1 Background and Technical Breakthroughs

Wireless media are conventionally exploited to transmit information from transmitters to receivers. Several experimental demonstrations have been reported in the literature over years in an attempt to make WPT possible [39]. The first confirmed experimentation of WPT was accomplished by H. R. Hertz in 1888. He used induction coils to transfer power over a tiny air-gap. Later, at the end of the 19th century, N. Tesla performed experiments to transfer wireless power over longer distances. Specifically, he realized transmission of 10^8 Volts of electric power over 48 miles to light 200 bulbs and run an electric motor. Due to limited technology and therefore possibilities of hazardous effects of the high electric voltage on human beings and surroundings, further advancement and commercialization were shelved at that time. Long distance WPT again came into attention after the invention of magnetron in 1920s and 1930s. But still, the problem remained with the inability to harvest energy. Later, in 1964, W. C. Brown realized conversion of microwave energy in electric energy using rectenna and demonstrated WPT to a model helicopter. In 1968, the concept of WPT was introduced to satellite systems where solar energy is collected at satellites and then it is transmitted back to the earth through electromagnetic waves. In 1971, M. Cardullo patented first modern radio-frequency identification (RFID).

1.3.1.1 Near-Field Wireless EH

In the past decade, products launched for WPT has made it a reality from the theories. *Qi* standard developed by Wireless Power Consortium in 2008 is capable of WPT using inductive coupling at a distance up to 4 centimeters [42]. It targets to provide wireless power to mobile devices. Mobile device manufacturers, namely, Apple, Asus, HTC, Huawei, LG Electronics, Motorola Mobility, Nokia, Samsung, are working with the Qi standard. *Rezence* standard developed by Alliance for Wireless Power (A4WP) in 2012 is a competitor of Qi standard. Rezence is based on the principles of magnetic resonance and supports WPT of up to 50 Watt over a distance of 5 centimeters [43]. In 2015, Rezence merged with Power Matters Alliance (PMA) to form *AirFuel Alliance*, which standardizes WPT technology for a range of devices including smartphone, laptops, and wearables [44]. *Open Dots*

is another competitor of Qi standards and uses conductive charging method for WPT. *WiTtricity* technology is founded in 2007 following the demonstration of wirelessly lighting a 60 Watt bulb placed at a distance of 2.5 meters [45]. It uses magnetic resonance coupling for WPT and mainly targets to provide wireless power solutions to electric vehicles. The company has collaborated with car makers Audi, BMW, Chrysler, Jaguar, Nissan, and Toyota.

1.3.1.2 Far-Field Wireless EH

WPT via RF signal enables to wirelessly power energy-constrained nodes located at larger distances when compared to the WPT via coupling. Yet no standardization for RF-based WPT exists. But companies, namely, *Cota*, *Pawercast*, and *Energous*, have launched products capable of transferring power at long distances. Founded in 2008, Cota system works similar to Wi-Fi, except it transmits wireless power instead of data [46]. It is capable to transmit 1 Watt power which can be delivered at few meters distance. Powercast system is established in 2011 and uses Powercast transmitters to transmit wireless power and charge Prodcast receivers [47]. *Powercaster* and *PowerSpot* are the two Federal Communications Commission (FCC) approved transmitters launched by Powercast for consumer use. In 2015, Energous demonstrated powering an iPhone at 15 feet distance and has developed *WattUp* transmitter and receiver exchanging power within 30 feet envelope. WattUp products target to provide wireless power in far-field and near-field as well [48].

Recent standardizations and commercialization of products for WPT has made wireless EH at energy-constrained nodes a reality by opening promising directions for further development. RF-based EH is more attractive in communication networks because of its capability to provide wireless power to devices located at larger distances. Conventionally, it is considered that RF signals can only be used for wireless information transfer (WIT). In 2008, L. R. Varshney suggested that RF signals can be utilized to transport wireless information along with wireless power using information-energy tradeoff [49]. This has attracted the interest of a vast group of researchers who are working towards enabling the realization of EH using the ambient and/or dedicated RF signals at energy-constrained nodes.

The state-of-the-art technologies and products are capable of delivering wireless power in the range of milliwatt and microwatt [50]. This makes WPT feasible in communication networks supporting low power devices and sensors, such as wireless sensor networks, wireless body area networks, IoT entities, etc. In existing cellular networks, most of the devices are complied with 4G standards.

Such devices require power typically in the range of a few hundred milliwatt [50], which cannot be adhered by the present WPT technologies and products. Furthermore, devices complying 5G standards are set for deployment world-wide by 2020. Batteries, hard-wiring, and increased connectivity of heterogeneous devices in 5G networks would not be able to keep up with the requirements for wireless EH [46]. Although, it is expected that the further advancement in WPT will comply with the high power requirement in cellular network devices and other similar devices. Among various technologies, distributed laser charging (DLC) would play important role in enabling deliver high power wirelessly [51]. In this regard, wireless EH is considered as a key technology for Beyond 5G cellular networks [52].

1.3.2 Wireless Power Transfer in Communication Networks

Communication networks enabled with WIT and WPT are basically categorized by simultaneous wireless information and power transfer (SWIPT) networks and wireless powered communication networks (WPCNs). In SWIPT networks, the RF signals transmitted by nodes are processed for simultaneous WIT and WPT. Time-switching (TS) and power-splitting (PS) are two practical receiver designs used for simultaneous information decoding (ID) and EH at receiving nodes [53, 54]. In WPCNs, different RF signals are used for WIT and WPT, and energy-constrained nodes switch over time to choose between ID and EH modes. The works in [55–57] provides a study of WPNCs. The RF signal received at energy-constrained nodes is processed through a rectenna which can convert electromagnetic energy into electric energy. The electric energy can be used for further operations. Next, an overview on conversion of electromagnetic energy into electric energy is provided.

1.3.2.1 RF-based EH

Electromagnetic energy can be converted into electrical energy by employing rectenna at the energy-constrained nodes. Rectenna is basically formed by concatenating antenna and rectifier. Figure 1.4 illustrates a basic RF-based energy receiver. The received RF signal $y(t)$ at the antenna is processed through the rectifier, which comprises of a diode and a low pass filter. The output of the rectifier is direct current (DC) which is managed by a power management unit for further utilization of the electric energy.

The received signal $y(t)$ over a flat fading channel, can be given using (1.5) as

$$y(t) = \mathrm{Re}\Big(g(t)s(t)\exp(\jmath 2\pi f_c t)\Big) + n_a(t), \tag{1.8}$$

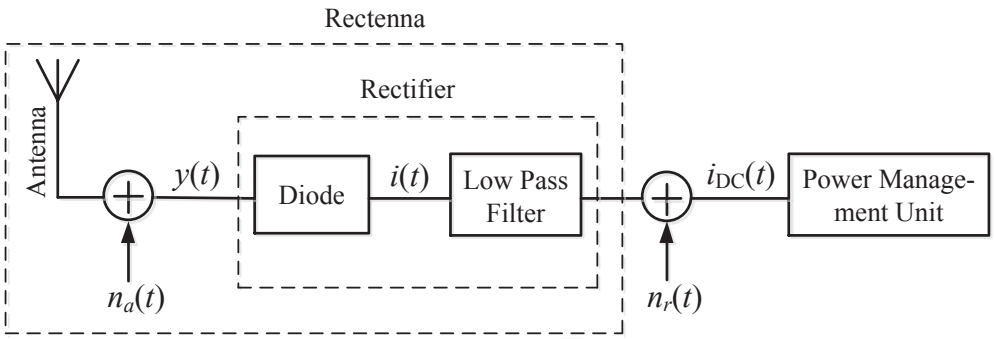

Figure 1.4: RF-based energy receiver.

where $n_a(t)$ is the noise introduced by the antenna [53]. $y(t)$ is the input voltage to the diode, and the corresponding output current can be represented as

$$i(t) = i_s \left(\exp(v_s y(t)) - 1\right), \tag{1.9}$$

where i_s is diode saturation current and v_s is reciprocal of the diode thermal voltage. Using Taylor series expansion, (1.9) can be given by [53, eq. (6)]

$$i(t) = \sum_{k=1}^{\infty} a_k (y(t))^k, \quad a_k = i_s v_s / k!. \tag{1.10}$$

When $i(t)$ passed through a low pass filter, all high-frequency components are filtered out and only DC component remains at the output. The DC output can be used for further processing or energy storage, which is handled by a power management unit. Assuming data is transmitted with power P, the energy harvested over the symbol duration can be given by [53, eq. (14)]

$$E_h = \zeta |g|^2 P T_s + N_0', \tag{1.11}$$

where $\zeta \in (0, 1)$ is *energy conversion efficiency* and N_0' is the total energy of antenna and rectifier noise components, $n_a(t)$ and $n_r(t)$, respectively. N_0' can be ignored for a small noise contribution.

The energy harvested at a node can be used in three different ways – *harvest-use*, *harvest-store-use*, and *harvest-use-store* [58]. In harvest-use approach, the incoming energy is directly used to power the communicating node. Harvest-store-use approach first stores the harvested energy in a buffer and then activates communicating node for data transmission if a minimum amount of required energy is

accumulated. In harvest-use-store approach, a fraction of the harvested energy is used to power the communicating node and remaining fraction is stored in a buffer for later use.

Furthermore, (1.11) corresponds to a linear energy harvester. Although, due to nonlinearity of diode(s), capacitors and inductors (in low pass filter block), linear energy harvester is not practical. Modeling of nonlinear energy harvester is explored in [59–61]. The nonlinear model proposed in [59] possesses analytical intractability and is simplified using a piecewise linear approximation suggested in [62]. [60, 61] focus on signal designing for WPT based on the nonlinearities of the energy harvester.

A detailed study of fundamental concepts and recent developments on WPT are provided in [39, 63, 64]. Extensive research on systems employing WPT has been carried out in the literature [65–67]. The main focus of the research comprises: improving EH circuitry and signal designing [60,65]; proposing novel EH methods and systems [39,41,66–68]; analyzing the performance of systems employing RF-based EH [41, 54, 69–71]. The performance analysis of systems involves examining their capability and reliability in terms of achievable throughput, outage performance, error-rate performance, etc.

1.4 Motivation of the Present Work

In three node systems, maximum DO can be exploited by employing AF and selective DF protocol at the relay node. Out of the two, selective DF protocol performs better than the AF protocol [22]. Therefore, we have considered selective DF protocol at the relay node. Further, fading can have severe effects on the performance of the wireless networks. The accuracy of analytical results depends upon the accuracy with which the fading model fits with the experimental data and characterizes the environment. Any deviation from the actual characteristics of the channel can accordingly cause uncertainty in the analysis. Generalized fading models provide a better fit to the experimental data under multiple scenarios. Following these motivations, in the first part of our work, we analyze the average SER for a three-node selective DF relay system under $\kappa-\mu$ and $\eta-\mu$ fading. Data is considered to be M-PSK modulated. In literature, average SER of a three-node selective DF relay systems is analyzed in [72] and [73] under Rayleigh fading and Nakagami-m fading, respectively.

In systems such as wireless sensor networks, body area network, etc., nodes may be physically unaccessible in order to recharge or replace batteries [41]. This can permanently terminate the communication between the nodes. Moreover, in applications such as device-to-device communication,

the user relay may not be willing to use its own power for transmitting other user's data [74]. In such circumstances, wireless EH at the energy-constrained relay node can enable participation of nodes in communication. In the literature, most of the works available on wireless powered (WP) relay systems considers information theoretic approach for the analysis. In [71, 75, 76], communication theoretic analysis for SWIPT networks is explored. However, for three-node WPCNs the analysis is not present in the literature. Communication theoretic analysis of such systems can be investigated to get better insights. Under these motivations, we analyze the average SER of a WPCN where energy-constrained relay node is wirelessly powered by the source node. Relay employs selective DF protocol and data is M-PSK modulated. The analysis of the system under generalized $\eta-\mu$, $\kappa-\mu$, and $\kappa-\mu$ shadowed fading has mathematical complexity. Hence, we consider that the system is affected under Nakagami-m fading for simplified analysis.

In applications like medical implants, sensor networks, etc., source nodes may be physically unreachable and hence eventually drained batteries can obstruct the transmission of vital data [77]. The communication lifetime can be extended if the energy-constrained source nodes are wirelessly powered by other nodes in the network or dedicated power transmitter(s). We consider a dual-hop relay system where energy-constrained source node harvests energy using the RF signal transmitted by the relay node. Relay node employs fixed DF protocol. Nakagami-m and $\kappa-\mu$ shadowed fading models are considered for performance analysis of the system. Data is considered to be M-PSK or orthogonal M-FSK modulated.

1.5 Thesis Contributions

This thesis aims at communication theoretic performance analysis of conventional and WP three-node DF relay system under different fading environments. All nodes are equipped with a single antenna and operate in half-duplex mode. The main contributions of the thesis are summarized as follows.

I. Conventional DF Relay System under $\kappa-\mu$ and $\eta-\mu$ Fading

We analyze the average SER of a conventional three-node selective DF relay system under generalized $\kappa-\mu$ and $\eta-\mu$ fading for M-PSK modulated data. We derive the high SNR approximation of the average SER which is used to find the systems DO and optimal power allocation at the source and relay nodes. Effects of modulation order, channel conditions, and node location on performance

of the system are examined.

II. WP DF Relay System under Nakagami-m Fading (EH at Relay Node)

Next, we present the average SER analysis of a WP three-node selective DF relay system under Nakagami-m fading for M-PSK modulated data. The relay node is energy-constrained and for transmission, it relies on WPT by the source node. EH model is linear and harvest-use approach is considered for processing harvested energy. We derive analytical average SER expressions and their approximations at high SNR. The high SNR approximations are used to optimize resource allocation in different slots and obtain DO of the system. For the analysis, two cases are considered i) the direct link between the source and destination nodes exists and ii) the direct link is blocked. The two cases are then compared with the conventional point-to-point communication. The effects of modulation order, channel conditions, relay location on performance of the system are investigated.

III. WP DF relay system under Nakagami-m and $\kappa-\mu$ Shadowed Fading (EH at Source Node)

Further, we consider that in a three-node relay system the source node is energy-constrained and harvests energy using the RF signal transmitted by the relay node. We assume linear EH model employing harvest-use approach to process the harvested energy. The source node utilizes the harvested energy for data transmission and relay node employs fixed DF protocol to process the received data. The direct link between the source and destination nodes is assumed to be in deep fade and other links are characterized by Nakagami-m or $\kappa-\mu$ shadowed fading. Data is considered to be M-PSK modulated with coherent or orthogonal M-FSK modulated with non-coherent detection. We derive average SER expressions for both the modulation schemes under two fading environments. High SNR approximation of the average SERs are also derived which are used to analyze the DO and optimal relay location. The effects of modulation schemes/order, channel conditions, and relay location on the performance are analyzed.

1.6 Thesis Organization

This thesis is organized into seven chapters. The summary of each chapter is briefly outlined as follows. A structural organization of the thesis is shown in Figure 1.5.

- **Chapter 1**: An overview of point-to-point wireless communication system, models of fading channels, relay-based communication systems, and wireless EH are presented in this chapter.

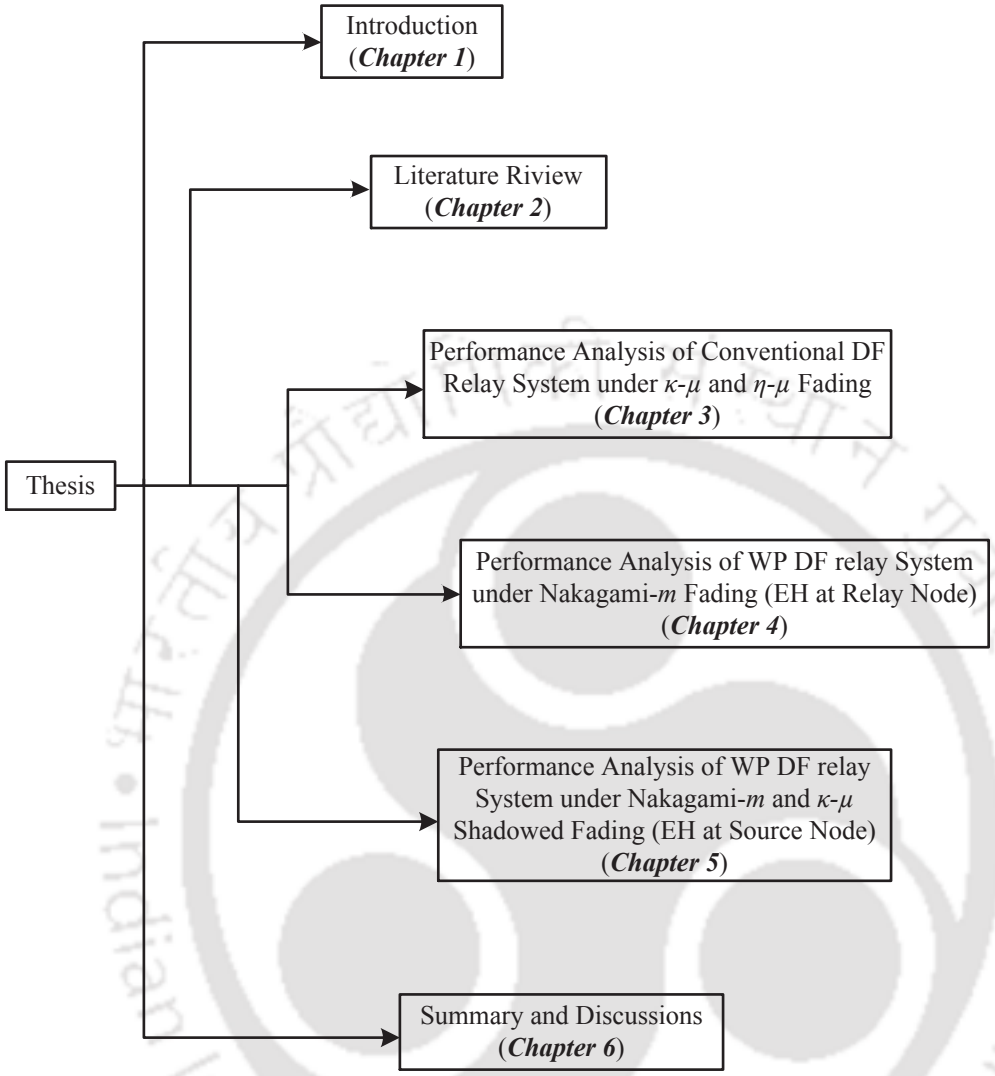

Figure 1.5: Thesis organization.

The fundamental concepts and terminologies defined in this chapter are used in later part of the thesis. This chapter also briefs some of the existing work in the literature which motivated our present work, summarizes the thesis contribution, and provides an outline of the thesis organization.

- **Chapter 2**: This chapter lists works available in the literature on performance analysis of conventional and WP relay systems.

- **Chapter 3**: In this chapter, we present average SER analysis of a conventional three-node DF relay system under $\kappa-\mu$, $\eta-\mu$, and mixed $\kappa-\mu$ and $\eta-\mu$ fading. Data is modulated using M-PSK

scheme. The signals received at destination node from source and relay nodes are combined using MRC principle. Analytical average SER expressions are derived in terms of fourth Lauricella function. Asymptotic approximation of average SERs at high SNRs are also derived to simplify the analysis and obtain the DO and optimal power allocation at source and relay nodes of the system. Effects of channel conditions, modulation order, node location, and power allocation on performance of the system are demonstrated using numerical examples.

- **Chapter 4**: In this chapter, we analyze average SER of a WP three-node DF relay system under Nakagami-m fading. Data is M-PSK modulated. Relay node is energy-constrained and wirelessly powered by the source node. We examined the performance for two cases i) source-to-destination link exists and ii) source-to-destination link is blocked. In the former case, the signals arriving from the source and relay nodes are combined using EGC principle. Analytical average SER expressions are derived in terms of univariate Meijer-G function and bivariate Fox-H function. For simplified analysis, an asymptotic approximation of the average SER is also obtained which is used to find DO and optimal resource allocation. Effects of modulation order, channel conditions, relay location on performance of the system with and without source-to-destination link are investigated. Throughput of the system is also analyzed.

- **Chapter 5**: In this chapter, we consider a two-hop DF relay system where source node is energy-constrained and relies on the energy harvested using the RF signal transmitted by the relay node for data transmission. Nakagami-m and $\kappa-\mu$ shadowed fading are considered. Data is modulated using either M-PSK or orthogonal M-FSK modulation scheme. M-PSK modulated data is coherently detected at the receiving node, while noncoherent detection is performed for orthogonal M-FSK modulated data. Average SER and its asymtotic approximation are derived for the two modulation schemes. Asymptotic results are used to analyze DO and optimal relay location of the system. Effects of modulation schemes/order, channel conditions, and relay location on performance of the system are also investigated.

- **Chapter 6**: This chapter concludes the work done in the thesis and provides some suggestions which may be considered for future research.

Abstract-TH-2151_136102001

2

Literature Review: Performance Analysis

Contents

In the previous chapter, we have discussed some of the works available in the literature on fading channel models, relaying, and wireless EH. In this chapter, we further discuss some of the related works on performance analysis of both conventional and WP relay systems.

2.1 Conventional Relay Systems

Over the past two decades, performance analysis of conventional relay systems has been an interesting area of research as relaying is looked upon as one of the prominent solutions for boosting the performance of various state-of-the-art technologies. The research aims to analyze the performance of multihop relaying [25, 78, 79], parallel relaying [80, 81], two-way relaying [82–84], full-duplex relaying [85–87], multiple access techniques in relaying [88, 89], relay systems equipped with multiple antennas [90, 91], physical layer secrecy in relay systems [92–94], etc. Research work on relay systems, such as i) full-duplex multihop relaying [95], ii) multihop MIMO [96], iii) multiple access techniques in multiple antenna assisted relaying [97], multihop relaying [98], two-way relaying [99] and full-duplex relaying [100, 101], etc is also reported in the literature. In this thesis, we mainly discuss the literature on performance analysis of one-way half-duplex relay systems where each node is equipped with a single antenna. First, we present the early stage developments in relay-assisted wireless powered communications systems. Then the literature on performance analysis of conventional AF and DF relay systems under different fading environments is presented.

2.1.1 Initial Developments

In [37,102,103], Hasna and Alouini analyzed the outage performance of a two-hop AF relay system. The results are also compared with the average BER of AF and fixed-DF protocols for binary DPSK (BDPSK) modulated data. MGF based approach is used for the average BER analysis. Fixed-gain and variable-gain AF relaying are considered in [102] and [37, 103], respectively. The authors provide analysis considering Rayleigh fading in [37, 102]. Nakagami-m fading environment is assumed in [103] and the analysis is presented in the presence of co-channel interferences. These works suggest that fixed DF protocol performs better than AF protocol at low to medium SNRs. The performance of fixed DF and AF protocols is comparable at high SNRs.

Laneman *et. al.* investigated outage performance of a cooperative relay system under Rayleigh fading in [22]. The performance of different relaying protocols is compared. It is found that except

fixed DF protocol, all other protocols, namely, selective DF, fixed-gain AF, and variable-gain AF, can achieve full diversity. Also, among these protocols, selective DF protocol possesses the best performance.

In a two-hop relay system with the direct link, full diversity cannot be exploited if fixed-gain DF relaying is employed. In order to achieve full diversity, optimal and suboptimal detectors are investigated in [104,105]. Chen and Laneman considered a parallel relay system and studied optimal maximum likelihood (ML) detector for coherent and noncoherent binary FSK (BFSK) modulation schemes in [104]. ML detector is nonlinear and incurs mathematical intractability in the average error rate analysis. A suboptimal detector with piecewise-linear (PL) combiner is used to approximate the ML detector to derive the closed-form expression for the average BER. PL detector utilizes the knowledge of average BER of source-to-relay link at the destination. In [105], Wang *et. al.* considered multihop-parallel relay system and utilized the knowledge of instantaneous BER of source-to-relay links to propose cooperative-MRC (C-MRC) detector. C-MRC provides low-complexity and high-performance compared to PL detector and it is applicable to modulation schemes of higher constellation size. The PDF-based approach is considered in [104, 105] to analyze the performance under Rayleigh fading.

2.1.2 Conventional AF Relay Systems

Communication theoretic analysis of AF relaying is presented in [106, 107]. In [106], Anghel and Kaveh considered a parallel relay system under Rayleigh fading. They analyzed average SER for M-PSK modulated data. Lower bound, upper bound, and asymptotic approximation of the average SER are also presented. In [107], Shin and Song analyzed average SER of three-node (cooperative) AF relay system for M-PSK modulated data. The destination node is equipped with multiple antennas and the system is considered to be affected under Nakagami-m fading. In [106,107], signals arriving at the destination node are combined using MRC principle and the performance is analyzed using MGF based approach.

Performance of dual-hop AF relay systems under $\kappa-\mu$ and/or $\eta-\mu$ fading is analyzed in [108–111]. In [108], Peppas *et. al.* investigated outage probability and average BER for binary modulation schemes using CDF based approach. Mixed $\kappa-\mu$ and $\eta-\mu$ fading are considered for the analysis. In [109], Zhang *et. al.* derived high SNR approximations of ergodic capacity and cutoff rate (a measure of effects of communication reliability on information rate) of the relay system under $\kappa-\mu$

and $\eta-\mu$ fading. Hussain *et. al.* provide information theoretic and communication theoretic analysis in [110]. CDF based approach is considered for the analysis of binary modulated data. In [111], Yang *et. al.* investigated outage probability of a cognitive relay system in the presence of a primary user under $\eta-\mu$ fading.

In [112], Kodide *et. al.* analyzed outage probability of a parallel relay system considering $\kappa-\mu$ shadowed fading environment for AF and DF protocols.

2.1.3 Conventional DF Relay Systems

Su *et. al.* analyzed the average SER of a three-node selective DF relay system for M-PSK and M-QAM modulated data in [72]. MGF based approach is considered for the analysis. High SNR approximations of the average SER are obtained to analyze optimal transmission power at source and relay nodes. In [113], Sadek *et. al.* consider parallel selective DF relay system and derived high SNR approximation of the average SER for M-PSK modulated data. Rayleigh fading environment is considered in [72, 113].

In [73, 114, 115], performance analysis of three-node DF relay systems under Nakagmi-m fading is investigated. In [114], Suraweera *et. al.* analyzed the outage probability of selective DF relaying. In [115], Ikki and Ahmed found the average BER of fixed and selective DF relaying when data is BPSK modulated. The communication theoretic analysis presented in [72] is extended by Lee and Tsai in [73].

Performance analysis of two-hop DF relay systems under $\kappa-\mu$ and $\eta-\mu$ fading is explored in [116–118]. Information theoretic analysis is presented by Li *et. al.* in [116] for the system affected under $\kappa-\mu$ and $\eta-\mu$ fading. In [117], Biswas and Chandra examined communication theoretic based energy efficient relay node placement under $\eta-\mu$ fading. In [118], Peppas provided information theoretic and communication theoretic analysis of the system in the presence of co-channel interference. All the links are affected by $\eta-\mu$ fading. Dixit and Sahu have explored the performance of selective DF relay systems under generalized fading in [119–121]. In [119], outage probability and average BER of multihop relay system are analyzed under $\eta-\mu$ fading. Average BER of multihop relay system under $\kappa-\mu$ fading is analyzed in [120]. PDF and CDF based approaches are used for the analysis in [119] and [120], respectively. Data is M-QAM modulated in both works. In [121], outage probability of parallel relay system is investigated under mixed $\eta-\mu$ and $\kappa-\mu$ fading.

In [122–124], the information theoretic performance of cognitive DF relay system under $\kappa-\mu$ shadowed fading is examined. In [122, 123], Kumar and Chouhan provided analysis for a single relay assisted system. Poreddy *et. al.* considered parallel relays in [124]. Selective DF protocol is considered in [122–124].

Table 2.1 presents a comparative study of related works on conventional DF relay systems. The table indicates that no work is reported in the literature that provides average SER analysis of conventional DF relay system under $\kappa-\mu$, $\eta-\mu$, and $\kappa-\mu$ shadowed fading for M-PSK and M-FSK modulation schemes. Note that, Fikadu *et. al.* has investigated the average SER of parallel DF relay system under $\eta-\mu$ fading for M-PSK and M-QAM modulation schemes in [81]. In this thesis, we present the average SER analysis under $\kappa-\mu$ and $\eta-\mu$ fading for M-PSK modulation scheme in Chapter 3.

Table 2.1: Performance analysis of conventional DF relay systems.

Reference	System	Protocol	Analysis	Modulation	Fading
Hasna and Alouini [37], 2003	Single relay	Fixed DF*	Communication Theoretic	BDPSK	Rayleigh
Hasna and Alouini [102], 2004	Single relay	Fixed DF*	Communication Theoretic	BDPSK	Rayleigh
Hasna and Alouini [103], 2004	Single relay	Fixed DF*	Communication Theoretic	BDPSK	Nakagami-m
Laneman *et. al.* [22], 2004	Single relay	Selective & Fixed DF	Information Theoretic	–	Rayleigh
Chen and Laneman [104], 2006	Parallel relays	Fixed DF	Communication Theoretic	BFSK	Rayleigh
Wang *et. al.* [105], 2007	Multihop and parallel relays	Fixed DF	Communication Theoretic	BFSK	Rayleigh
Su *et. al.* [72], 2005	Single relay	Selective DF	Communication Theoretic	M-PSK, M-QAM	Rayleigh
Sadek *et. al.* [113], 2005	Parallel relays	Selective DF	Communication Theoretic	M-PSK	Rayleigh

Continued on the next page

Table 2.1 – *Continued from the previous page*

Reference	System	Protocol	Analysis	Modulation	Fading
Suraweera *et. al.* [114], 2006	Parallel relays	Selective DF	Information Theoretic	–	Nakagami-m
Ikki and Ahmed [115], 2007	Single relay	Selective & Fixed DF	Communication Theoretic	BPSK	Nakagami-m
Lee and Tsai [73], 2009	Single relay	Selective DF	Communication Theoretic	M-PSK, M-QAM	Nakagami-m
Li *et. al.* [116], 2010	Single relay	Fixed DF	Information Theoretic	–	$\kappa-\mu$, $\eta-\mu$
Biswas and Chandra [117], 2013	Single relay	Selective DF	Communication Theoretic	M-QAM	$\eta-\mu$
Peppas [118], 2013	Single relay	Fixed DF	Communication Theoretic$^{\#}$	BPSK	$\eta-\mu$
Dixit and Sahu [119], 2014	Multihop relays	Selective DF	Communication Theoretic$^{\#}$	M-QAM	$\eta-\mu$
Dixit and Sahu [120], 2017	Multihop relays	Selective DF	Communication Theoretic	M-QAM	$\kappa-\mu$
Dixit and Sahu [121], 2017	Parallel relays	Selective DF	Information Theoretic	–	$\kappa-\mu$, $\eta-\mu$
Kodide *et. al.* [112], 2016	Parallel relays	Fixed DF*	Information Theoretic	–	$\kappa-\mu$ shadowed
Kumar and Chouhan [123], 2016	Single relay, cognitive	Selective DF	Information Theoretic	–	$\kappa-\mu$ shadowed
Poreddy *et. al.* [124], 2017	Parallel relays, cognitive	Selective DF	Information Theoretic	–	$\kappa-\mu$ shadowed

$*$ Analysis of AF protocol is also provided.

$^{\#}$ Information theoretic analysis is also presented.

2.2 WP Relay Systems

In the previous section, we discussed some of the prominent works available in the literature on performance analysis of conventional relay systems. Next, we list related works on performance analysis of WP relay systems. In the literature on WP relay systems, it is generally considered that relay node(s) is energy-constrained and wirelessly powered by the source node, interferers, or dedicated power transmitters [41, 62, 69, 70, 125]. The idea is to involve relay node enabled by RF-based EH in the communication process to extend the communication lifetime. Other scenario has also been considered in the literature where the destination node is energy-constrained and wirelessly powered by relay node, source node, and/or interferers to extend the communication lifetime [126,127]. In the literature, relatively less attention is given to systems where source node is energy-constrained. The analysis of such systems is vital when energy-constrained source node(s) cannot support the installation of batteries due to its size constraint. In [77, 128, 129], systems are considered where energy-constrained source nodes rely on RF signal transmitted by the relay and/or destination nodes for EH.

In the literature, scenarios is also considered when the communicating nodes provide wireless power to different EH node(s) of the system [130]. In most of the works linear EH model and harvest-use approach are considered to process the harvested energy. To incorporate more practical aspects in the analysis, nonlinear EH models are considered in [62] and harvest-store-use in [131, 132] and harvest-use-store in [133]. Performance analysis of various relaying systems, such as, supporting MIMO [134], multiple access techniques [135], full-duplex [136], multihop [137], two-way [138], random node deployment [139], etc., is also reported in literature. In this section, we mainly focus on the performance analysis of the WP one-way relay systems where nodes operate in half-duplex mode. In the works mentioned below, energy-constrained nodes employ harvest-use approach and linear energy harvester and all communicating nodes are considered to be equipped with a single antenna unless specified otherwise. The study is categorized as analysis of WP relay systems with energy-constrained i) relay node(s) and ii) source node(s).

2.2.1 EH at Relay Node(s)

The existing works provide performance analysis of WP relay systems with energy-constrained relay node(s) for both SWIPT networks and WPCNs.

2.2.1.1 SWIPT Networks

TS and PS EH techniques for point-to-point communications [53, 54] are explored by Nasir *et. al.* in [41] to investigate the performance of two-hop AF relay system. Information theoretic approach is considered for the analysis. Nasir *et. al.* further extended the analysis for two-hop DF protocol in [125]. In [69], Liu *et. al.* investigated the average SER of a parallel DF relay system where relays are energy-constrained. Data is assumed to be modulated using M-DPSK and M-FSK modulation schemes with noncoherent detection. Simulation based results using the proposed detectors are provided. Gu and Aïssa analyzed information theoretic performance of a WP DF relay system in the presence of interferences in [70].

The analysis in [41, 69, 70, 125] is carried out for Rayleigh fading environment. Several works are also available in the literature which consider Nakagami-m fading environment for the analysis [71, 75, 76, 140–142]. In [75], Tran *et. al.* analyzed outage probability and average SER of two-hop AF relay system for M-PSK modulated data. The relay node is equipped with multiple antennas when the source-to-relay link is Nakagami-m faded and the relay-to-destination link is Rayleigh faded. In [140], Wand *et. al.* analyzed outage probability of the system when DF relay is equipped with multiple antennas and the source-to-relay and relay-to-destination links are Nakagami-m faded. Chen *et. al.* analyzed the performance of two-hop AF and DF relaying in the presence of interfering signals using information theoretic approach in [141] and [142], respectively. In [76], Gao *et. al.* analyzed performance of two-hop DF relay system using information theoretic and communication theoretic approaches. Babaei *et. al.* investigated average BER of AF and DF relaying for M-PSK and M-QAM modulations in [71]. In [143], Ye *et. al.* analyzed performance of a two-hop DF relaying using information theoretic approach when relay nodes are randomly deployed around the source node and wirelessly powered by the destination node. Relay and destination nodes use multiple antennas for reception.

The works in [144–147] consider generalized fading models for the analysis of WP DF relay systems. Hussain *et. al.* provided information theoretic analysis under $\kappa-\mu$ fading and $\eta-\mu$ fading in [144] and [145], respectively. In [144], the system consists of source and destination nodes equipped with multiple antennas and multiple single antenna relays. Nonlinear energy harvester is considered in [145]. In [146], Badarneh *et. al.* presented information theoretic and communication theoretic analysis under mixed $\kappa-\mu$ and $\eta-\mu$ fading. Hussain *et. al.* analyzed information theoretic performance under $\kappa-\mu$

shadowed fading in [147].

2.2.1.2 WPCNs

The Works in [57, 148–151] provide information theoretic analysis of relay-assisted WPCNs under Rayleigh fading. Haghifam *et. al.* in [148] analyzed the performance of two-hop DF relay system considering the operational power consumption at the relay node. In [149], Ju and Zhang considered a WPCN comprising of one hybrid access point (HAP) and two users. HAP transmits wireless power to users in downlink and users cooperate with each other to transmit their data to the HAP in the uplink. Time and power is optimized to maximize the sum-rate. Aboelwafa *et. al.* in [57] generalized the analysis for multiple users and incorporated relay selection along with the optimal time and power allocation. DF and AF relaying is considered in [149] and [57], respectively. Di *et. al.* in [150] considered a WPCN consisting of one multiple antenna HAP and two single antenna users and jointly optimized the energy beamforming, time and power allocation to maximize the sum-rate. The user acting as relay employs DF protocol. In [151], Chen *et. al.* introduced a pricing mechanism to help relay user to sell their excess energy. Harvest-use approach is considered in [57, 149, 150] to process the incoming energy flow, while [151] considered the harvest-store-use approach.

Table 2.2 lists the works available in the literature that provide performance analysis of WP relay systems where relay node(s) is energy-constrained, operates in half-duplex mode, and employs harvest-use approach. Interfering signals are not considered in the listed work. We observe that no work is found in the literature analyzing the average SER of DF relay assisted WPCNs. The table can also be useful in finding other research gaps in this domain.

Table 2.2: Performance analysis of WP DF relay systems: EH at relay node(s).

Reference	Network	System	Protocol	Analysis	Fading
Nasir *et. al.* [41], 2013	SWIPT	Single relay	AF	Information theoretic	Rayleigh
Nasir *et. al.* [125], 2014	SWIPT	Single relay	DF	Information theoretic	Rayleigh
Ye *et. al.* [143], 2017	SWIPT	Parallel relays	DF	Information theoretic	Nakagami-m

Continued on the next page

Table 2.2 – *Continued from the previous page*

Reference	Network	System	Protocol	Analysis	Fading
Liu *et. al.* [69], 2016	SWIPT	Parallel relays	DF	Communication theoretic (noncoherent M-DPSK & M-FSK)	Rayleigh
Tran *et. al.* [75], 2015	SWIPT	Single relay	AF	Communication$^{\#}$ theoretic (M-PSK)	Rayleigh, Nakagami-m
Wang *et. al.* [140], 2016	SWIPT	Single relay	DF	Information theoretic	Nakagami-m
Gao *et al.* [76], 2017	SWIPT	Single relay	DF	Communication$^{\#}$ theoretic (BPSK, BFSK, M-PAM)	Nakagami-m
Babaei *et. al.* [71], 2018	SWIPT	Single relay	AF & DF	Communication theoretic (M-PSK, M-QAM)	Nakagami-m
Hussain *et. al.* [144], 2018	SWIPT	Parallel relays	DF	Information theoretic	$\kappa-\mu$
Hussain *et. al.* [145], 2018	SWIPT	Single relay	DF	Information theoretic	$\eta-\mu$
Badarneh *et. al.* [146], 2017	SWIPT	Single relay	DF	Communication$^{\#}$ theoretic (M-PSK, M-QAM)	$\kappa-\mu$, $\eta-\mu$
Hussain *et. al.* [147], 2018	SWIPT	Single relay	DF	Information theoretic	$\kappa-\mu$ shadowed
Haghifam *et. al.* [148], 2016	WPCN	Single relay	DF	Information theoretic	Rayleigh
Ju and Zhang [149], 2014	WPCN	Single relay	DF	Information theoretic	Rayleigh

Continued on the next page

Table 2.2 – *Continued from the previous page*

Reference	Network	System	Protocol	Analysis	Fading
Aboelwafa [57], 2017	WPCN	Parallel relays	AF	Information theoretic	Rayleigh
Di *et. al.* [150], 2017	WPCN	Single relay	DF	Information theoretic	Rayleigh

Information theoretic analysis is also presented.

2.2.2 EH at Source Node(s)

In [77,128,129,152,153], WPCNs are considered where energy-constrained source node(s) harvests energy using the RF signals transmitted by relay and/or destination nodes. Information theoretic approach is considered to investigate the performance of the system in terms of throughput. In [128], Chen *et. al.* considered a system with HAP, an energy-constrained source, and a relay. Relay employs AF protocol and source is wirelessly powered by the relay and HAP. In [129], Huang and Ansari considered a three-node DF relay system where energy-constrained source node relies on power transmitted at relay for EH. Zlatanov *et. al.* provided analysis for a full-duplex DF relay system in [152]. In [77], Yang *et. al.* considered a machine-to-machine communication enabled cellular network where machine type gateways act as DF relay. Energy-constrained source nodes are wirelessly powered by relays and adopt nonlinear EH model. In [77, 128, 129, 152], the effect of fading is either ignored or assumed constant. In a practical scenario, fading can have severe consequences on the performance of the system and hence its effects cannot be ignored. Moreover, analytical results obtained without considering fading can largely deviate from the actual outcome. Luo *et. al.* in [153] considered mixed fading environment when source-to-relay and relay-to-destination links are Rician and Rayleigh faded, respectively. The relay employs DF protocol to process the received source data, and the source node harvests energy using the RF signal radiated by the relay. Harvest-use and harvest-store-use EH approaches are considered in [77,153] and [128,129], respectively. Whereas, both harvest-use and harvest-store-use approaches are considered in [152].

Table 2.3 lists the works available in the literature that provide performance analysis of WP relay systems where source node(s) is energy-constrained. All the works listed here consider information

Table 2.3: Performance analysis of WP DF relay systems: EH at source node(s).

Reference	System model
Chen *et. al.* [128], 2014	- AF relaying - Fading gains are assumed constant - Information theoretic analysis
Huang and Ansari [129], 2016	- DF relaying - Fading gains are assumed constant - Information theoretic analysis
Zlatanov *et. al.* [152], 2017	- Full-duplex DF relaying - Nonfading, AWGN channels are considered - Information theoretic analysis
Yang *et. al.* [77], 2018	- Machine-to-machine enabled cellular network - Gateways acting as relay emply DF protocol - Effects of fading is ignored - Information theoretic analysis
Luo *et. al.* [153], 2016	- DF parallel relay system - Rayleigh/Rician fading - Information theoretic analysis

theoretic approach for analysis and fading is either ignored or assumed constant in most of them.

2.3 Summary

This chapter provides a thorough review of works on performance analysis of the conventional and WP relay systems. We found the research gaps which are not addressed in the literature which include average SER analysis of i) conventional relay systems under generalized fading and ii) WPCNs. This work is carried out in the thesis.

3

Conventional DF Relay System under $\kappa-\mu$ and $\eta-\mu$ Fading

Contents

In this chapter, we consider a conventional three-node DF relay system where the direct link between the source and destination nodes exists and the fading environment is modeled using $\kappa-\mu$ and $\eta-\mu$ fading. MRC principle is employed to combine the two signal arriving at the destination node via the direct and relayed paths. We provide communication theoretic analysis of the system.

3.1 Introduction

Performance analysis of conventional three-node DF system under Rayleigh fading is presented in [72, 154]. The analysis in [72] is further extended for Nakagami-m fading in [73]. Nakagami$-m$ distribution generalizes the fading model, however, it does not fit closely to the experimental data for non-homogeneous environments [11]. More generalized fading models, $\kappa-\mu$ and $\eta-\mu$ are proposed in [11] for the non-homogeneous fading environments with LOS components and non-LOS component, respectively. In [116–118], performance analysis of a two-hop conventional DF relay system is explored for $\kappa-\mu$ and $\eta-\mu$ fading models. The works in [116–118] ignore the presence of the direct link between the source and destination nodes. If the direct link is considered, then the performance of the system can be significantly improved by the means of diversity combining schemes.

The main contributions of this chapter are summarized as

- Average SER for M-PSK modulated data considering the fading environment is modeled using $\kappa-\mu$, $\eta-\mu$, and mixtures of the two fading models. The analysis can be generalized for a wide range of channel conditions considering mixed fading scenario.
- Asymptotic approximations of the average SER are also obtained to get a better insight about the dependence of performance on the fading parameters at high SNRs. Optimal transmission power allocation at source and relay nodes is done using the asymptotic results.

The rest of the chapter is organized as follows. Section 3.2 describes the system model. Expressions of the average SER and corresponding high SNR approximations are derived for $\kappa-\mu$ and $\eta-\mu$ fading channels in Section 3.3. In Section 3.4, the expressions are deduced for mixed $\kappa-\mu$ and $\eta-\mu$ faded environment. The asymptotic average SER expressions are utilized for optimal power allocation and DO analysis in Section 3.5. Numerical and simulation results are presented in Section 3.6. Section 3.7 gives some concluding remarks.

3.2 System Model

Consider a relay system comprises of a source node S, a relay node R, and a destination node D. All nodes are assumed to be powered by unobstructed supply or batteries having infinite storage. Each node is equipped with a single antenna. The end-to-end transmission takes place in two-time slots, T_1 and T_2. Both time slots are of equal duration, that implies $T_1 = T_2$. Without loss of generality, we assume $T_1 = T_2 = 1$. In the first time slot, node S broadcasts data with power P_S which can be received at nodes R and D. Node R operates in half-duplex mode and employs selective DF protocol to process the received data. The relay decodes the received data and if decoding is correct, the data is re-encoded and then forwarded to the destination with power P_R in the second time slot. Correct decoding at the relay node can be achieved by using cyclic-redundancy-check codes or threshold-based checking [72, 73]. The inter-node channels are independent, flat-slow faded, and modeled by either $\kappa-\mu$ or $\eta-\mu$ fading.

Source S transmits M-PSK modulated data with equal energy and equal *a priori* probability. In M-PSK, constellation $\mathcal{S}$ is given by $\mathcal{S} = \exp(\jmath 2\pi(m-1)/M)$, where $m = 1, 2, ..., M$ and $\jmath = \sqrt{-1}$. Nodes S and R transmit symbol s with energy $E[ss^*] = 1$, where $s \in \mathcal{S}$. $E[\cdot]$ denotes the expectation operator and $(\cdot)^*$ represents the complex conjugate. When symbol s is transmitted at the ith node, the baseband signal received at the jth node in the kth time slot is given by

$$y_{k,j} \;=\; \sqrt{\tilde{P}_i\,(d_{ij})^{-\alpha_{ij}}}\,h_{ij}\,s_k + n_{k,j}\,, \quad k = 1, 2, \tag{3.1}$$

where $i \in \{S, R\}$, $j \in \{R, D\}$, $ij \in \{SD, SR, RD\}$, $\tilde{P}_i$ is the power transmitted at the ith node, h_{ij} is the channel fading coefficient of the ij link, $(d_{ij})^{-\alpha_{ij}}$ represents path loss of the ij link over distance d_{ij} (in meter) with path loss exponent α_{ij} (ranging from 2 to 6 for wireless medium) and n_{ij} is AWGN with zero mean and N_0 variance at the jth node. At the source node, the symbol is transmitted with power $\tilde{P}_S = P_S$. If the relay node correctly decodes the received symbol, the power forwarded to the destination node is $\tilde{P}_R = P_R$ otherwise no transmission occurs and relay remains idle, that is $\tilde{P}_R = 0$. The total power P is given by

$$P \;=\; P_S + P_R, \quad \text{for} \quad 0 < P_S, P_R < P. \tag{3.2}$$

The two signals received at the destination node are combined using MRC principle [73, p. 1219]

$$y = w_1 y_{1,D} + w_2 y_{2,D}, \tag{3.3}$$

where $w_1 = \sqrt{P_S} h_{SD}^*/N_0$ and $w_2 = \sqrt{P_R} h_{RD}^*/N_0$. The data is detected at node R in the first slot using the decision rule

$$\hat{s} = \arg\left\{\max_{p\in\mathcal{S}} \mathrm{Re}\big(p^* h_{SR}^* y_{SR}\big)\right\}. \tag{3.4}$$

When node R detects incorrectly, then node D decides the data in the second slot using the decision rule

$$\hat{s} = \arg\left\{\max_{p\in\mathcal{S}} \mathrm{Re}\big(p^* h_{RD}^* y_{RD}\big)\right\}. \tag{3.5}$$

Otherwise, in case of correct detection at node R, node D applies the decision rule

$$\hat{s} = \arg\left\{\max_{p\in\mathcal{S}} \mathrm{Re}\Big(p^* y\Big)\right\}, \tag{3.6}$$

where y is given in (3.3).

Let the instantaneous SNRs of the SD, SR and RD links are

$$\gamma_{SD} = \frac{P_S|h_{SD}|^2}{N_0 (d_{SD})^{\alpha_{SD}}}, \tag{3.7a}$$

$$\gamma_{SR} = \frac{P_S|h_{SR}|^2}{N_0 (d_{SR})^{\alpha_{SR}}} \quad \text{and} \tag{3.7b}$$

$$\gamma_{RD} = \frac{\tilde{P}_R|h_{RD}|^2}{N_0 (d_{RD})^{\alpha_{RD}}}, \tag{3.7c}$$

respectively. The equivalent instantaneous SNR of the combined signal in (3.3) is given by

$$\begin{aligned}\gamma_{\mathrm{MRC}} &= \frac{P_S|h_{SD}|^2}{N_0 (d_{SD})^{\alpha_{SD}}} + \frac{P_R|h_{RD}|^2}{N_0 (d_{RD})^{\alpha_{RD}}} \\ &= \gamma_{SD} + \gamma_{RD}.\end{aligned} \tag{3.8}$$

The PDF of instantaneous SNR γ_{ij} under $\kappa-\mu$ and $\eta-\mu$ fading is given by [155]

$$f_{\gamma_{ij}}(\gamma_{ij}) = \frac{\mu_{ij}(1+\kappa_{ij})^{\frac{\mu_{ij}+1}{2}}(\gamma_{ij})^{\frac{\mu_{ij}-1}{2}}}{\exp(\kappa_{ij}\mu_{ij})(\kappa_{ij})^{\frac{\mu_{ij}-1}{2}}(\bar{\gamma}_{ij})^{\frac{\mu_{ij}+1}{2}}} \exp\left(-\frac{\mu_{ij}(1+\kappa_{ij})\gamma_{ij}}{\bar{\gamma}_{ij}}\right) I_{\mu_{ij}-1}\left(2\mu_{ij}\sqrt{\frac{\kappa_{ij}(1+\kappa_{ij})\gamma_{ij}}{\bar{\gamma}_{ij}}}\right) \quad (3.9)$$

and

$$f_{\gamma_{ij}}(\gamma_{ij}) = \frac{2\sqrt{\pi}(\mu_{ij})^{\mu_{ij}+1/2}(v_{ij})^{\mu_{ij}}(\gamma_{ij})^{\mu_{ij}-1/2}}{\Gamma(\mu_{ij})(V_{ij})^{\mu_{ij}-1/2}(\bar{\gamma}_{ij})^{\mu_{ij}+1/2}} \exp\left(-\frac{2\mu_{ij}v_{ij}\gamma_{ij}}{\bar{\gamma}_{ij}}\right) I_{\mu_{ij}-1/2}\left(\frac{2\mu_{ij}V_{ij}\gamma_{ij}}{\bar{\gamma}_{ij}}\right), \quad (3.10)$$

respectively where $\bar{\gamma}_{ij} = E[\gamma_{ij}]$ is the average SNR of ijth link, the parameters κ_{ij}, μ_{ij} and η_{ij} are defined for the respective fading models in Table 1.1. In (3.10), $v_{ij} = (2+\eta_{ij}+\eta_{ij}^{-1}))/4$, $V_{ij} = (\eta_{ij}^{-1}-\eta_{ij})/4$ for *Format-1* $(0 \leq \eta_{ij} \leq \infty)$ and $v_{ij} = 1/(1-\eta_{ij}^2)$, $V_{ij} = \eta_{ij}/(1-\eta_{ij}^2)$ for *Format-2* $(-1 \leq \eta_{ij} \leq 1)$ [11]. In Format-1, η_{ij} is power-ratio between in-phase and quadrature phase components, whereas in Format-2 it represents correlation between in-phase and quadrature phase components. In Table 1.1, the column for $\eta-\mu$ fading corresponds to Format-1. For link mean power $\lambda_{ij} = E[|h_{ij}|^2]$, the average SNR of ijth link is given by

$$\bar{\gamma}_{SD} = \frac{P_S\lambda_{SD}}{N_0(d_{SD})^{\alpha_{SD}}}, \quad (3.11a)$$

$$\bar{\gamma}_{SR} = \frac{P_S\lambda_{SR}}{N_0(d_{SR})^{\alpha_{SR}}} \quad \text{and} \quad (3.11b)$$

$$\bar{\gamma}_{RD} = \frac{\tilde{P}_R\lambda_{SR}}{N_0(d_{RD})^{\alpha_{RD}}}. \quad (3.11c)$$

3.3 Performance Analysis under $\kappa-\mu$ and $\eta-\mu$ Fading

In this section, exact average SER expressions are analyzed for $\kappa-\mu$ and $\eta-\mu$ faded channels. We consider the input symbol s to be M-PSK modulated with coherent detection. The end-to-end average SER can be analyzed by averaging the conditional SER at node D given by [73, eq. (6)]

$$P_e(\gamma_{\text{MRC}},\gamma_{SR}) = P_e(\gamma_{SR})P_e(\gamma_{SD}) + P_e(\gamma_{\text{MRC}})(1-P_e(\gamma_{SR})). \quad (3.12)$$

In (3.12), the first summand corresponds to the possibility that if node R detects incorrectly, that is, transmission over SR link is in error, then no transmission occurs at node R and detection at node D is erroneous when node D incorrectly detects the symbol received over SD link. The second summand

tells about the possibility that if node R decodes correctly, then it forwards the data to node D where error occurs when the combined signal does not result in correct detection.

The SER averaging is done using MGF based approach [156, eq. (9.15)], that is,

$$P_{e,\phi} = \frac{1}{\pi}\int_0^{\frac{(M-1)\pi}{M}} M_{\gamma_\phi}\left(\frac{g}{\sin^2\theta}\right)d\theta\,, \tag{3.13}$$

where $g=\sin^2(\pi/M)$, $\phi \in \{SR, SD, \text{MRC}\}$, and $M_y(\cdot)$ is the MGF of y. By splitting the integral limits (0 to $(M-1)\pi/M$) into two parts ranging from (0 to $\pi/2$) and ($\pi/2$ to $(M-1)\pi/M$), (3.13) can be rewritten as

$$P_{e,\phi} = \frac{1}{\pi}\int_0^{\frac{\pi}{2}} M_{\gamma_\phi}\left(\frac{g}{\sin^2\theta}\right)d\theta + \frac{1}{\pi}\int_{\frac{\pi}{2}}^{\frac{(M-1)\pi}{M}} M_{\gamma_\phi}\left(\frac{g}{\sin^2\theta}\right)d\theta\,. \tag{3.14}$$

Equation (3.14) is used in the later part of this chapter to simplify the derivation for average SER. Now, averaging (3.12) over the instantaneous SNRs γ_{SR}, γ_{SD}, and γ_{MRC}, we get

$$P_e = P_{e,SR}P_{e,SD} + P_{e,\text{MRC}}(1-P_{e,SR})\,, \tag{3.15}$$

where $P_{e,SR}=E[P_e(\gamma_{SR})]$, $P_{e,SD}=E[P_e(\gamma_{SD})]$, and $P_{e,\text{MRC}}=E[P_e(\gamma_{\text{MRC}})]$. Using (3.13), (3.15) is written as

$$\begin{aligned} P_e = {} & \left(\frac{1}{\pi}\int_0^{\frac{(M-1)\pi}{M}} M_{\gamma_{SR}}\left(\frac{g}{\sin^2\theta}\right)d\theta\right)\left(\frac{1}{\pi}\int_0^{\frac{(M-1)\pi}{M}} M_{\gamma_{SD}}\left(\frac{g}{\sin^2\theta}\right)d\theta\right) \\ & + \left(\frac{1}{\pi}\int_0^{\frac{(M-1)\pi}{M}} M_{\gamma_{\text{MRC}}}\left(\frac{g}{\sin^2\theta}\right)d\theta\right)\left(1-\frac{1}{\pi}\int_0^{\frac{(M-1)\pi}{M}} M_{\gamma_{SR}}\left(\frac{g}{\sin^2\theta}\right)d\theta\right). \end{aligned} \tag{3.16}$$

The MGFs of γ_{ij} for $\kappa-\mu$ and $\eta-\mu$ faded links are given as [155]

$$M_{\gamma_{ij}}(s) = \exp(-\kappa_{ij}\mu_{ij})\sum_{l=0}^{\infty}\frac{(\kappa_{ij}\mu_{ij})^l}{l!}\left(\frac{\mu_{ij}(1+\kappa_{ij})}{\mu_{ij}(1+\kappa_{ij})+s\bar{\gamma}_{ij}}\right)^{\mu_{ij}+l} \tag{3.17}$$

and

$$M_{\gamma_{ij}}(s) = \left(\frac{4\mu_{ij}^2 v_{ij}(2(v_{ij}-V_{ij})\mu_{ij}+s\bar{\gamma}_{ij})^{-1}}{(2(v_{ij}+V_{ij})\mu_{ij}+s\bar{\gamma}_{ij})}\right)^{\mu_{ij}}, \tag{3.18}$$

respectively.

Next, the average SER in (3.16) is obtained for $\kappa-\mu$ and $\eta-\mu$ fading environment using (3.17) and

(3.18), respectively.

3.3.1 Analytical Average SER

In this subsection, the average SER expressions are analyzed in the terms of fourth Lauricella function of p-variables $F_D^{(p)}$ which is given as [157, eq. (20)]

$$\begin{aligned} F_D^{(p)}(a, b_1, b_2, \cdots, b_p; c, x_1, x_2, \cdots, x_p) &= \frac{1}{B(a, c-a)} \int_0^1 \frac{t^{a-1}(1-t)^{c-a-1}}{(1-tx_1)^{b_1} \cdots (1-tx_p)^{b_p}} dt \\ &= \sum_{(m_1, \cdots, m_p)} \frac{(a)_{m_1+\cdots+m_p} (b_1)_{m_1} \cdots (b_p)_{m_p} x_1^{m_1} \cdots x_p^{m_p}}{(c)_{m_1+\cdots+m_p} m_1! \cdots m_P!}, \end{aligned} \quad (3.19)$$

where summation is p-fold, $(\lambda)_\upsilon = \Gamma(\lambda+\upsilon)/\Gamma(\lambda)$ is Pochhammer symbol,

$$B(x, y) = \int_0^1 t^{x-1}(1-t)^{y-1} dt \quad (3.20)$$

is beta function, and $\Gamma(\cdot)$ is gamma function.

3.3.1.1 $\kappa-\mu$ Fading

The average SER of link $\varphi_1 \in \{SD, SR\}$ under $\kappa-\mu$ fading is analyzed by substituting (3.17) in (3.14) as

$$P_{e,\varphi_1} = \frac{\exp(-\kappa_{\varphi_1}\mu_{\varphi_1})}{\pi} \sum_{l=0}^{\infty} \frac{(\kappa_{\varphi_1}\mu_{\varphi_1})^l}{l!} \left(\int_0^{\frac{\pi}{2}} Z_{\varphi_1}(\theta; l) d\theta + \int_{\frac{\pi}{2}}^{\frac{(M-1)\pi}{M}} Z_{\varphi_1}(\theta; l) d\theta \right), \quad (3.21)$$

where

$$Z_{\varphi_1}(\theta; l) = \left(\frac{\mu_{\varphi_1}(1+\kappa_{\varphi_1})}{\mu_{\varphi_1}(1+\kappa_{\varphi_1}) + g\bar{\gamma}_{\varphi_1}/\sin^2(\theta)} \right)^{\mu_{\varphi_1}+l}. \quad (3.22)$$

Integrals in (3.21) can be simplified by substituting $\cos^2(\theta) = t$ in the first integral and $\cos^2(\theta) = t\cos^2((M-1)\pi/M)$ in the second integral. Thus, we get

$$\begin{aligned} P_{e,\varphi_1} = \frac{\exp(-\kappa_{\varphi_1}\mu_{\varphi_1})}{2\pi} \sum_{l=0}^{\infty} \frac{(\kappa_{\varphi_1}\mu_{\varphi_1})^l}{l!} \Lambda_{\varphi_1}^{\mu_{\varphi_1}+l} \Bigg(& \int_0^1 t^{-1/2}(1-t)^{\mu_{\varphi_1}+l-1/2}(1-\Lambda_{\varphi_1}t)^{-\mu_{\varphi_1}-l} dt \\ & + \cos\left(\frac{\pi}{M}\right) \int_0^1 t^{-1/2} (1-\omega t)^{\mu_{\varphi_1}+l-1/2} (1-\omega\Lambda_{\varphi_1}t)^{-\mu_{\varphi_1}-l} dt \Bigg), \end{aligned} \quad (3.23)$$

where $\omega = \cos^2(\pi/M)$ and

$$\Lambda_{\varphi_1} = \frac{\mu_{\varphi_1}(1+\kappa_{\varphi_1})}{\mu_{\varphi_1}(1+\kappa_{\varphi_1}) + g\bar{\gamma}_{\varphi_1}}. \quad (3.24)$$

Using (3.19), (3.23) is further simplified as

$$P_{e,\varphi_1} = \frac{\exp(-\kappa_{\varphi_1}\mu_{\varphi_1})}{2\pi}\sum_{l=0}^{\infty}\frac{(\kappa_{\varphi_1}\mu_{\varphi_1})^l}{l!}\Lambda_{\varphi_1}^{\mu_{\varphi_1}+l}\left(B\left(\frac{1}{2},\mu_{\varphi_1}+l+\frac{1}{2}\right)F_D^{(1)}\left(\frac{1}{2},\mu_{\varphi_1}+l;\mu_{\varphi_1}+l+1,\Lambda_{\varphi_1}\right)\right.$$
$$\left.+\cos\left(\frac{\pi}{M}\right)B\left(\frac{1}{2},1\right)F_D^{(2)}\left(\frac{1}{2},\frac{1}{2}-\mu_{\varphi_1}-l,\mu_{\varphi_1}+l;\frac{3}{2},\omega,\omega\Lambda_{\varphi_1}\right)\right). \quad (3.25)$$

Next, when the signal is perfectly detected at the relay node, the signal received at the destination node is MRC of the direct and the relayed signals. As SD and RD links are independent, the MGF of γ_{MRC} is product of the MGFs of γ_{SD} and γ_{RD}, that is,

$$M_{\gamma_{\text{MRC}}}(s) = M_{\gamma_{SD}}(s)M_{\gamma_{RD}}(s). \quad (3.26)$$

Hence, the average SER $P_{e,\text{MRC}}$ can be analyzed using (3.17) and (3.26) in (3.14) for $\phi = \text{MRC}$ as

$$P_{e,\text{MRC}} = \frac{1}{\pi}\sum_{l_1=0}^{\infty}\sum_{l_2=0}^{\infty}\frac{(\kappa_{SD}\mu_{SD})^{l_1}(\kappa_{RD}\mu_{RD})^{l_2}}{l_1!l_2!\exp(\kappa_{SD}\mu_{SD}+\kappa_{RD}\mu_{RD})}$$
$$\times\left(\int_0^{\frac{\pi}{2}}Z_{SD}(\theta;l_1)Z_{RD}(\theta;l_2)d\theta+\int_{\frac{\pi}{2}}^{\frac{(M-1)\pi}{M}}Z_{SD}(\theta;l_1)Z_{RD}(\theta;l_2)d\theta\right), \quad (3.27)$$

where $Z_{\varphi_2}(\theta;l)$ is defined in (3.22) for $\varphi_2 \in \{SD, RD\}$. By substituting $\cos^2(\theta)=t$ in the first integral and $\cos^2(\theta) = t\cos^2((M-1)\pi/M)$ in the second integral and then using (3.19), (3.27) is simplified as

$$P_{e,\text{MRC}} = \frac{1}{2\pi}\sum_{l_1=0}^{\infty}\sum_{l_2=0}^{\infty}\frac{(\kappa_{SD}\mu_{SD})^{l_1}(\kappa_{RD}\mu_{RD})^{l_2}\Lambda_{SD}^{\mu_{SD}+l_1}\Lambda_{RD}^{\mu_{RD}+l_2}}{l_1!l_2!\exp(\kappa_{SD}\mu_{SD}+\kappa_{RD}\mu_{RD})}\left(\left(B\left(\frac{1}{2},\mu_{SD}+\mu_{RD}+l_1+l_2+\frac{1}{2}\right)\right.\right.$$
$$\left.\times F_D^{(2)}\left(\frac{1}{2},\mu_{SD}+l_1,\mu_{RD}+l_2;\mu_{SD}+\mu_{RD}+l_1+l_2+1,\Lambda_{SD},\Lambda_{RD}\right)\right)+\left(\cos\left(\frac{\pi}{M}\right)B\left(\frac{1}{2},1\right)\right.$$
$$\left.\left.\times F_D^{(3)}\left(\frac{1}{2},\frac{1}{2}-\mu_{SD}-\mu_{RD}-l_1-l_2,\mu_{SD}+l_1,\mu_{RD}+l_2;\frac{3}{2},\omega,\omega\Lambda_{SD},\omega\Lambda_{RD}\right)\right)\right), \quad (3.28)$$

where Λ_{φ_2} is defined in (3.24) for φ_1 replaced by $\varphi_2 \in \{SD, RD\}$.

The end-to-end average SER under $\kappa-\mu$ fading can be analyzed substituting (3.25) and (3.28) in (3.15).

3.3.1.2 $\eta-\mu$ Fading

When the system is under $\eta-\mu$ fading, the average SER factor P_{e,φ_1} is obtained by substituting (3.18) in (3.14), and is given by

$$P_{e,\varphi_1} = \frac{1}{\pi}\int_0^{\frac{\pi}{2}} \left(\frac{4\mu_{\varphi_1}^2 v_{\varphi_1}}{2(v_{\varphi_1}-V_{\varphi_1})\mu_{\varphi_1}+\frac{g\bar{\gamma}_{\varphi_1}}{\sin^2(\theta)}}\right)^{\mu_{\varphi_1}} \left(\frac{1}{2(v_{\varphi_1}+V_{\varphi_1})\mu_{\varphi_1}+\frac{g\bar{\gamma}_{\varphi_1}}{\sin^2(\theta)}}\right)^{\mu_{\varphi_1}} d\theta + \frac{1}{\pi}\int_{\frac{\pi}{2}}^{\frac{(M-1)\pi}{M}} \left(\frac{4\mu_{\varphi_1}^2 v_{\varphi_1}}{2(v_{\varphi_1}-V_{\varphi_1})\mu_{\varphi_1}+\frac{g\bar{\gamma}_{\varphi_1}}{\sin^2(\theta)}}\right)^{\mu_{\varphi_1}} \left(\frac{1}{2(v_{\varphi_1}+V_{\varphi_1})\mu_{\varphi_1}+\frac{g\bar{\gamma}_{\varphi_1}}{\sin^2(\theta)}}\right)^{\mu_{\varphi_1}} d\theta, \quad (3.29)$$

Substituting $\cos^2(\theta) = t$ and $\cos^2 = t\cos^2((M-1)\pi/M)$ respectively in the first and the second integral, (3.29) can be simplified using (3.19) as

$$P_{e,\varphi_1} = \frac{M_{\gamma_{\varphi_1},\eta-\mu}(g)}{2\pi}\left(B\left(\frac{1}{2},2\mu_{\varphi_1}+\frac{1}{2}\right)F_D^{(2)}\left(\frac{1}{2},\mu_{\varphi_1},\mu_{\varphi_1};2\mu_{\varphi_1}+1,C_{\varphi_1},D_{\varphi_1}\right) + \cos\left(\frac{\pi}{M}\right)B\left(\frac{1}{2},1\right)F_D^{(3)}\left(\frac{1}{2};\frac{1}{2}-2\mu_{\varphi_1},\mu_{\varphi_1},\mu_{\varphi_1};\frac{3}{2},\omega,\omega C_{\varphi_1},\omega D_{\varphi_1}\right)\right), \quad (3.30)$$

where $\omega = \cos^2((M-1)\pi/M)$,

$$M_{\gamma_{\varphi_1},\eta-\mu}(g) = \left(\frac{4\mu_{\varphi_1}^2 v_{\varphi_1}}{(2(v_{\varphi_1}-V_{\varphi_1})+g\gamma_{\varphi_1})(2(v_{\varphi_1}+V_{\varphi_1})+g\gamma_{\varphi_1})}\right)^{\mu_{\varphi_1}}, \quad (3.31a)$$

$$C_{\varphi_1} = \frac{2(v_{\varphi_1}-V_{\varphi_1})\mu_{\varphi_1}}{2(v_{\varphi_1}-V_{\varphi_1})\mu_{\varphi_1}+g\bar{\gamma}_{\varphi_1}} \quad \text{and} \quad (3.31b)$$

$$D_{\varphi_1} = \frac{2(v_{\varphi_1}+V_{\varphi_1})\mu_{\varphi_1}}{2(v_{\varphi_1}+V_{\varphi_1})\mu_{\varphi_1}+g\bar{\gamma}_{\varphi_1}}. \quad (3.31c)$$

For independent SD and RD links, the average SER factor $P_{e,\text{MRC}}$ is obtained using (3.18) and (3.26) in (3.14) for $\phi = \text{MRC}$, followed by simplification of integrals having limits (0 to $\pi/2$) and ($\pi/2$ to $(M-1)\pi/M$) with substitutions $\cos^2(\theta) = t$ and $\cos^2(\theta) = t\cos^2((M-1)\pi/M)$, respectively and then applying (3.19) as

$$P_{e,\text{MRC}} = \frac{M_{\gamma_{SD},\eta-\mu}(g)M_{\gamma_{RD},\eta-\mu}(g)}{2\pi}\left(\left(B\left(\frac{1}{2},2\mu_{SD}+2\mu_{RD}+\frac{1}{2}\right)F_D^{(4)}\left(\frac{1}{2},\mu_{SD},\mu_{SD},\mu_{RD},\mu_{RD};2\mu_{SD}+2\mu_{RD}+1,C_{SD},D_{SD},C_{RD},D_{RD}\right)\right) + \left(\cos\left(\frac{\pi}{M}\right)B\left(\frac{1}{2},1\right)F_D^{(5)}\left(\frac{1}{2},\frac{1}{2}-2\mu_{SD}-2\mu_{RD},\mu_{SD},\mu_{SD},\mu_{RD},\mu_{RD};\frac{3}{2},\omega,\omega C_{SD},\omega D_{SD},\omega C_{RD},\omega D_{RD}\right)\right)\right), \quad (3.32)$$

where $M_{\gamma_{\varphi_2},\eta-\mu}(g)$, C_{φ_2}, and D_{φ_2} are defined in (3.31a), (3.31b), and (3.31c), respectively for φ_1 replaced by $\varphi_2 \in \{SD, RD\}$.

The end-to-end average SER for η-μ faded channels can be analyzed on substituting (3.30) and (3.32) in (3.15).

3.3.2 Asymptotic Average SER

We obtain high SNR approximation for the average SER expressions to simplify the system analysis. At high SNRs, (3.15) can be approximated as

$$P_e^{\infty} = P_{e,SR}^{\infty} P_{e,SD}^{\infty} + P_{e,\mathrm{MRC}}^{\infty}, \tag{3.33}$$

where $P_{e,SR}^{\infty}$, $P_{e,SD}^{\infty}$, and $P_{e,\mathrm{MRC}}^{\infty}$ are the high SNR approximations of $P_{e,SR}$, $P_{e,SD}$, and $P_{e,\mathrm{MRC}}$, respectively, and derived below for the two fading types. The derivation requires high SNR approximation of the MGFs (3.17) and (3.18).

3.3.2.1 $\kappa-\mu$ Fading

In case of $\kappa-\mu$ fading, the MGF in (3.17) is approximated for $\bar{\gamma}_{\varphi_1} >> 1$ as

$$M_{\gamma_{ij}}^{\infty}(s) \approx \left(\frac{\mu_{ij}(1+\kappa_{ij})}{s\bar{\gamma}_{ij}}\right)^{\mu_{ij}} \exp\left(-\mu_{ij}\kappa_{ij}\right), \quad ij \in \{SR, SD, RD\}. \tag{3.34}$$

The corresponding asymptotic average SER for $\varphi_1 \in \{SR, SD\}$ link can be analyzed by substituting (3.34) in (3.14) as

$$P_{e,\varphi_1}^{\infty} \approx \frac{\exp(-\mu_{\varphi_1}\kappa_{\varphi_1})}{\pi}\left(\frac{\mu_{\varphi_1}(1+\kappa_{\varphi_1})}{g\bar{\gamma}_{\varphi_1}}\right)^{\mu_{\varphi_1}}\left(\int_0^{\frac{\pi}{2}}\left(\sin^2(\theta)\right)^{\mu_{\varphi_1}}d\theta + \int_{\pi/2}^{\frac{(M-1)\pi}{M}}\left(\sin^2(\theta)\right)^{\mu_{\varphi_1}}d\theta\right). \tag{3.35}$$

In (3.35), the first integral can be simplified using substitution $\cos^2(\theta)=t$ and the relation (3.20) as

$$\int_0^{\frac{\pi}{2}}\left(\sin^2(\theta)\right)^{\mu_{\varphi_1}}d\theta = \frac{1}{2}B\left(\frac{1}{2}, \mu_{\varphi_1}+\frac{1}{2}\right). \tag{3.36}$$

Similarly, the second integral can be simplified using substitution $\cos^2(\theta)=t\cos^2((M-1)\pi/M)$ and the relation (3.19) as

$$\int_{\frac{\pi}{2}}^{\frac{(M-1)\pi}{M}}\left(\sin^2(\theta)\right)^{\mu_{\varphi_1}}d\theta = \frac{1}{2}\cos\left(\frac{\pi}{M}\right)B\left(\frac{1}{2},1\right)F_D^{(1)}\left(\frac{1}{2},\frac{1}{2}-\mu_{\varphi_1};\frac{3}{2},\omega\right). \tag{3.37}$$

Using (3.36) and (3.37) in (3.35), we get

$$P_{e,\varphi_1}^{\infty} \approx \frac{\exp(-\mu_{\varphi_1}\kappa_{\varphi_1})}{2\pi}\left(\frac{\mu_{\varphi_1}(1+\kappa_{\varphi_1})}{g\bar{\gamma}_{\varphi_1}}\right)^{\mu_{\varphi_1}}\left(B\left(\frac{1}{2},\mu_{\varphi_1}+\frac{1}{2}\right) + \cos\left(\frac{\pi}{M}\right)B\left(\frac{1}{2},1\right)F_D^{(1)}\left(\frac{1}{2},\frac{1}{2}-\mu_{\varphi_1};\frac{3}{2},\omega\right)\right). \tag{3.38}$$

The high SNR approximation of $P_{e,\text{MRC}}$ is obtained using (3.34), (3.26) and (3.14) for $\phi = \text{MRC}$, ij replaced by $\varphi_2 \in \{SD, RD\}$, and then applying (3.36) and (3.37) as

$$P_{e,\text{MRC}}^{\infty} \approx \frac{\exp(-\mu_{RD}\kappa_{RD} - \mu_{SD}\kappa_{SD})}{2\pi} \left(\frac{\mu_{RD}(1+\kappa_{RD})}{g\bar{\gamma}_{RD}}\right)^{\mu_{RD}} \left(\frac{\mu_{SD}(1+\kappa_{SD})}{g\bar{\gamma}_{SD}}\right)^{\mu_{SD}} \times\left(B\left(\frac{1}{2}, \mu_{RD}+\mu_{SD}+\frac{1}{2}\right) + \cos\left(\frac{\pi}{M}\right) B\left(\frac{1}{2},1\right) F_D^{(1)}\left(\frac{1}{2}, \frac{1}{2} - \mu_{RD} - \mu_{SD}; \frac{3}{2}, \omega\right)\right). \quad (3.39)$$

The end-to-end asymptotic average SER under $\kappa-\mu$ fading can be analyzed using (3.38) and (3.39) in (3.33) as

$$P_e^{\infty} \approx \frac{\mathcal{A}_{SR}\mathcal{A}_{SD}}{(\bar{\gamma}_{SR})^{\mu_{SR}}(\bar{\gamma}_{SD})^{\mu_{SD}}} + \frac{\mathcal{A}_{\text{MRC}}}{(\bar{\gamma}_{RD})^{\mu_{RD}}(\bar{\gamma}_{SD})^{\mu_{SD}}}, \quad (3.40)$$

where

$$\mathcal{A}_{SR} = \frac{\exp(-\mu_{SR}\kappa_{SR})}{2\pi} \left(\frac{\mu_{SR}(1+\kappa_{SR})}{g}\right)^{\mu_{SR}} \times\left(B\left(\frac{1}{2}, \mu_{SR}+\frac{1}{2}\right) + \cos\left(\frac{\pi}{M}\right) B\left(\frac{1}{2},1\right) F_D^{(1)}\left(\frac{1}{2}, \frac{1}{2} - \mu_{SR}; \frac{3}{2}, \omega\right)\right), \quad (3.41)$$

$$\mathcal{A}_{SD} = \frac{\exp(-\mu_{SD}\kappa_{SD})}{2\pi} \left(\frac{\mu_{SD}(1+\kappa_{SD})}{g}\right)^{\mu_{SD}} \times\left(B\left(\frac{1}{2}, \mu_{SD}+\frac{1}{2}\right) + \cos\left(\frac{\pi}{M}\right) B\left(\frac{1}{2},1\right) F_D^{(1)}\left(\frac{1}{2}, \frac{1}{2} - \mu_{SD}; \frac{3}{2}, \omega\right)\right), \quad (3.42)$$

and

$$\mathcal{A}_{\text{MRC}} = \frac{\exp(-\mu_{RD}\kappa_{RD} - \mu_{SD}\kappa_{SD})}{2\pi} \left(\frac{\mu_{RD}(1+\kappa_{RD})}{g}\right)^{\mu_{RD}} \left(\frac{\mu_{SD}(1+\kappa_{SD})}{g}\right)^{\mu_{SD}} \times\left(B\left(\frac{1}{2}, \mu_{RD}+\mu_{SD}+\frac{1}{2}\right) + \cos\left(\frac{\pi}{M}\right) B\left(\frac{1}{2},1\right) F_D^{(1)}\left(\frac{1}{2}, \frac{1}{2} - \mu_{RD} - \mu_{SD}; \frac{3}{2}, \omega\right)\right). \quad (3.43)$$

3.3.2.2 $\eta-\mu$ Fading

In case of $\eta-\mu$ fading, the high SNR approximation of MGF in (3.18) is

$$M_{\gamma_{ij}}^{\infty}(s) \approx \left(\frac{4v_{ij}\mu_{ij}^2}{s^2\bar{\gamma}_{ij}^2}\right)^{\mu_{ij}}, \quad ij \in \{SR, SD, RD\}. \quad (3.44)$$

Substituting (3.44) in (3.14), the average SER for $\varphi_1 \in \{SR, SD\}$ link is given by

$$P_{e,\varphi_1}^{\infty} \approx \frac{1}{\pi}\left(\frac{4v_{\varphi_1}\mu_{\varphi_1}^2}{g^2\bar{\gamma}_{\varphi_1}^2}\right)^{\mu_{\varphi_1}}\left(\int_0^{\frac{\pi}{2}}(\sin\theta)^{4\mu_{\varphi_1}}\,d\theta + \int_{\frac{\pi}{2}}^{\frac{(M-1)\pi}{M}}(\sin\theta)^{4\mu_{\varphi_1}}\,d\theta\right), \tag{3.45}$$

which can be simplified using (3.36) and (3.37) as

$$P_{e,\varphi_1}^{\infty} \approx \frac{1}{2\pi}\left(\frac{4v_{\varphi_1}\mu_{\varphi_1}^2}{g^2\bar{\gamma}_{\varphi_1}^2}\right)^{\mu_{\varphi_1}}\left(B\left(\frac{1}{2}, 2\mu_{\varphi_1}+\frac{1}{2}\right)+\cos\left(\frac{\pi}{M}\right)B\left(\frac{1}{2},1\right)F_D^{(1)}\left(\frac{1}{2},\frac{1}{2}-2\mu_{\varphi_1};\frac{3}{2},\omega\right)\right). \tag{3.46}$$

The asymptotic expression of $P_{e,\mathrm{MRC}}^{\infty}$ is derived using (3.44), (3.26), and (3.14) for $\phi = \mathrm{MRC}$, $ij = \varphi_2$, $\varphi_2 \in \{SD, RD\}$, and then applying (3.36) and (3.37) as

$$\begin{aligned} P_{e,\mathrm{MRC}}^{\infty} \approx{}& \frac{1}{2\pi}\left(\frac{4v_{RD}\mu_{RD}^2}{g^2\bar{\gamma}_{RD}^2}\right)^{\mu_{RD}}\left(\frac{4v_{SD}\mu_{SD}^2}{g^2\bar{\gamma}_{SD}^2}\right)^{\mu_{SD}} \\ &\times\left(B\left(\frac{1}{2}, 2(\mu_{RD}+\mu_{SD})+\frac{1}{2}\right)+\cos\left(\frac{\pi}{M}\right)B\left(\frac{1}{2},1\right)F_D^{(1)}\left(\frac{1}{2},\frac{1}{2}-2(\mu_{RD}+\mu_{SD});\frac{3}{2},\omega\right)\right). \end{aligned} \tag{3.47}$$

The end-to-end asymptotic average SER for $\eta-\mu$ fading can be obtained on substituting (3.46) and (3.47) in (3.33) as

$$P_e^{\infty} \approx \frac{\mathcal{B}_{SR}\mathcal{B}_{SD}}{(\bar{\gamma}_{SR})^{2\mu_{SR}}(\bar{\gamma}_{SD})^{2\mu_{SD}}} + \frac{\mathcal{B}_{\mathrm{MRC}}}{(\bar{\gamma}_{RD})^{2\mu_{RD}}(\bar{\gamma}_{SD})^{2\mu_{SD}}}, \tag{3.48}$$

where

$$\mathcal{B}_{SR} = \frac{1}{2\pi}\left(\frac{4v_{SR}\mu_{SR}^2}{g^2}\right)^{\mu_{SR}}\left(B\left(\frac{1}{2}, 2\mu_{SR}+\frac{1}{2}\right)+\cos\left(\frac{\pi}{M}\right)B\left(\frac{1}{2},1\right)F_D^{(1)}\left(\frac{1}{2},\frac{1}{2}-2\mu_{SR};\frac{3}{2},\omega\right)\right), \tag{3.49}$$

$$\mathcal{B}_{SD} = \frac{1}{2\pi}\left(\frac{4v_{SD}\mu_{SD}^2}{g^2}\right)^{\mu_{SD}}\left(B\left(\frac{1}{2}, 2\mu_{SD}+\frac{1}{2}\right)+\cos\left(\frac{\pi}{M}\right)B\left(\frac{1}{2},1\right)F_D^{(1)}\left(\frac{1}{2},\frac{1}{2}-2\mu_{SD};\frac{3}{2},\omega\right)\right), \tag{3.50}$$

and

$$\begin{aligned} \mathcal{B}_{\mathrm{MRC}} ={}& \frac{1}{2\pi}\left(\frac{4v_{RD}\mu_{RD}^2}{g^2}\right)^{\mu_{RD}}\left(\frac{4v_{SD}\mu_{SD}^2}{g^2}\right)^{\mu_{SD}} \\ &\times\left(B\left(\frac{1}{2}, 2\mu_{SD}+\frac{1}{2}\right)+\cos\left(\frac{\pi}{M}\right)B\left(\frac{1}{2},1\right)F_D^{(1)}\left(\frac{1}{2},\frac{1}{2}-2\mu_{SD};\frac{3}{2},\omega\right)\right). \end{aligned} \tag{3.51}$$

3.4 Performance Analysis under Mixed $\kappa-\mu$ and $\eta-\mu$ Fading

In this section, the average SER of the relay system is analyzed when the three links connecting source to destination are differently faded. For two kind of fading models, in mixed sense the three links together can be affected in six ways, that is, three combinations of one link as $\kappa-\mu$ faded and other two links as $\eta-\mu$ faded and similarly three combinations of one link as $\eta-\mu$ faded and other two links as $\kappa-\mu$ faded. We analyze the case where the SD link is $\eta-\mu$ faded and the SR and RD links are $\kappa-\mu$ faded. This combination suggests that there is no LOS component in the SD link, while LOS components exist in the other two links. In the same manner, the other five combinations of the fading models can also be analyzed.

The average SER P_e in mixed fading is obtained by substituting $P_{e,SR}$, $P_{e,SD}$, and $P_{e,\mathrm{MRC}}$ for respective fading in (3.15). For the considered mixed fading case, $P_{e,SR}$ and $P_{e,SD}$ can be evaluated using (3.25) and (3.30), respectively. The analytical expression of $P_{e,\mathrm{MRC}}$ is derived as fallows. Substituting the MGFs (3.17) (for $ij = RD$) and (3.18) (for $ij = SD$) in (3.26), we get the MGF

$$\begin{aligned} M_{\gamma_{\mathrm{MRC}}}(s) &= \left(\frac{4\mu_{SD}^2 v_{SD}(2(v_{SD}-V_{SD})\mu_{SD}+s\bar{\gamma}_{SD})^{-1}}{(2(v_{SD}+V_{SD})\mu_{SD}+s\bar{\gamma}_{SD})}\right)^{\mu_{SD}} \\ &\quad \times \exp(-\kappa_{RD}\mu_{RD})\sum_{l=0}^{\infty}\frac{(\kappa_{RD}\mu_{RD})^l}{l!}\left(\frac{\mu_{RD}(1+\kappa_{RD})}{\mu_{RD}(1+\kappa_{RD})+s\bar{\gamma}_{RD}}\right)^{\mu_{RD}+l}. \end{aligned} \tag{3.52}$$

Substituting (3.52) in (3.14) and solving the integrals using (3.19) with the help of substitutions $\cos^2(\theta) = t$ and $\cos^2(\theta) = t\cos^2((M-1)\pi/M)$ respectively in the integral with limit (0 to $\pi/2$) and ($\pi/2$ to $(M-1)\pi/M$), we get

$$\begin{aligned} P_{e,\mathrm{MRC}} &= \frac{\exp(-\kappa_{RD}\mu_{RD})M_{\gamma_{SD,\,\eta-\mu}}(g)}{2\pi}\sum_{l=0}^{\infty}\frac{(\kappa_{RD}\mu_{RD})^l}{l!}\Lambda_{RD}^{\mu_{RD}+l}\Bigg(\Bigg(B\left(\frac{1}{2},\mu_{RD}+2\mu_{SD}+k+\frac{1}{2}\right) \\ &\quad \times F_D^{(3)}\left(\frac{1}{2},\mu_{RD}+l,\mu_{SD},\mu_{SD};\mu_{RD}+2\mu_{SD}+l+1,\Lambda_{RD},C_{SD},D_{SD}\right)\Bigg)+\Bigg(\cos\left(\frac{\pi}{M}\right)B\left(\frac{1}{2},1\right) \\ &\quad \times F_D^{(4)}\left(\frac{1}{2},\frac{1}{2}-\mu_{RD}-2\mu_{SD}-l,\mu_{RD}+l,\mu_{SD},\mu_{SD};\frac{3}{2},\omega,\omega\Lambda_{RD},\omega C_{SD},\omega D_{SD}\right)\Bigg)\Bigg), \end{aligned} \tag{3.53}$$

where Λ_{RD} and $M_{\gamma_{SD,\,\eta-\mu}}(g)$ are defined in (3.24) (for $\varphi_1 = RD$) and (3.31a) (for $\varphi_1 = SD$), respectively.

Similarly, the end-to-end asymptotic average SER can be analyzed on substituting $P_{e,SR}^{\infty}$, $P_{e,SD}^{\infty}$, and $P_{e,\mathrm{MRC}}^{\infty}$ for the given fading combination in (3.33). $P_{e,SR}^{\infty}$ and $P_{e,SD}^{\infty}$ are derived as in (3.38) and

(3.46), respectively. $P_{e,\mathrm{MRC}}^{\infty}$ is obtained on substituting approximate MGFs (3.34) and (3.44) in (3.26) and putting the resulting MGF in (3.14), followed by applying (3.36) and (3.37). We get

$$P_{e,\mathrm{MRC}}^{\infty} = \frac{\exp(-\mu_{RD}\kappa_{RD})}{2\pi}\left(\frac{\mu_{RD}(1+\kappa_{RD})}{g\bar{\gamma}_{SD}}\right)^{\mu_{RD}}\left(\frac{4v_{SD}\mu_{SD}^2}{g^2\bar{\gamma}_{SD}^2}\right)^{\mu_{SD}} \times\left(B\left(\frac{1}{2},\mu_{RD}+2\mu_{SD}+\frac{1}{2}\right)+\cos\left(\frac{\pi}{M}\right)B\left(\frac{1}{2},1\right)F_D^{(1)}\left(\frac{1}{2},\frac{1}{2}-\mu_{RD}-2\mu_{SD};\frac{3}{2},\omega\right)\right). \quad (3.54)$$

Hence, the end-to-end asymptotic average SER is given by

$$P_e^{\infty} \approx \frac{\mathcal{A}_{SR}\mathcal{B}_{SD}}{(\bar{\gamma}_{SR})^{\mu_{SR}}(\bar{\gamma}_{SD})^{2\mu_{SD}}} + \frac{\mathcal{C}_{\mathrm{MRC}}}{(\bar{\gamma}_{RD})^{\mu_{RD}}(\bar{\gamma}_{SD})^{2\mu_{SD}}}, \quad (3.55)$$

where $\mathcal{A}_{SR}$, $\mathcal{B}_{SD}$ are defined as in (3.41), (3.50), respectively and

$$\mathcal{C}_{\mathrm{MRC}} = \frac{\exp(-\mu_{RD}\kappa_{RD})}{2\pi}\left(\frac{\mu_{RD}(1+\kappa_{RD})}{g}\right)^{\mu_{RD}}\left(\frac{4v_{SD}\mu_{SD}^2}{g^2}\right)^{\mu_{SD}} \times\left(B\left(\frac{1}{2},\mu_{RD}+2\mu_{SD}+\frac{1}{2}\right)+\cos\left(\frac{\pi}{M}\right)B\left(\frac{1}{2},1\right)F_D^{(1)}\left(\frac{1}{2},\frac{1}{2}-\mu_{RD}-2\mu_{SD};\frac{3}{2},\omega\right)\right). \quad (3.56)$$

3.5 Optimal Power Allocation and Diversity Order

The derived end-to-end asymptotic average SER expressions can be used to allocate optimal power at nodes S and R and obtain DO of the system.

3.5.1 Optimal Power Allocation

In relay systems, equal power allocation at transmitting nodes is generally considered, but this is not energy efficient. Optimal power allocation is an efficient assignment and can improve performance on the system significantly. Transmitting power at nodes can be optimally allocated if nodes have partial knowledge of the CSI [72, 73]. In this section, we have analyzed expressions for the optimal power allocation at the source and the relay node for the given mixed faded relay system. The asymptotic average SER expression in (3.55) is represented using (3.11) in terms of P_S and P_R as

$$P_e^{\infty}(P_S,P_R) = \frac{\Xi_1}{(P_S)^{2\mu_{SD}+\mu_{SR}}} + \frac{\Xi_2}{(P_S)^{2\mu_{SD}}(P_R)^{\mu_{RD}}}, \quad (3.57)$$

where

$$\Xi_1 = \mathcal{A}_{SR}\mathcal{B}_{SD}\left(\frac{N_0(d_{SR})^{\alpha_{SR}}}{\lambda_{SR}}\right)^{\mu_{SR}}\left(\frac{N_0(d_{SD})^{\alpha_{SD}}}{\lambda_{SD}}\right)^{2\mu_{SD}} \quad (3.58)$$

and

$$\Xi_2 \;=\; \mathcal{C}_{\text{MRC}} \left(\frac{N_0 (d_{RD})^{\alpha_{RD}}}{\lambda_{RD}}\right)^{\mu_{RD}} \left(\frac{N_0 (d_{SD})^{\alpha_{SD}}}{\lambda_{SD}}\right)^{2\mu_{SD}}. \tag{3.59}$$

Applying the second order conditions [158] it is easy to show that (3.57) is a convex function of $(P_S, P_R) \in [0, P]$, where $P = P_S + P_R$ is the total power used for the transmission. Using (3.57), the power optimization problem can be formulated as

$$\min_{P_S, P_R} \frac{\Xi_1}{(P_S)^{2\mu_{SD}+\mu_{SR}}} + \frac{\Xi_2}{(P_S)^{2\mu_{SD}} (P_R)^{\mu_{RD}}} \tag{3.60}$$

subject to

$$P \;=\; P_S + P_R\,.$$

Now, using Lagrange's method, the objective function is written as

$$f(P_S, P_R, \lambda) \;=\; \frac{\Xi_1}{(P_S)^{2\mu_{SD}+\mu_{SR}}} + \frac{\Xi_2}{(P_S)^{2\mu_{SD}} (P_R)^{\mu_{RD}}} + \lambda(P_S + P_R - P)\,. \tag{3.61}$$

On differentiating (3.61) with respect to P_S, P_R and λ, and equating to zero, we get the relation in terms of P_S as

$$\Xi_2 P_S^{\mu_{SR}} \big(2\mu_{SD} P - (2\mu_{SD} + \mu_{RD}) P_S\big) \;=\; -\Xi_1 (2\mu_{SD} + \mu_{SR})(P - P_S)^{\mu_{RD}+1}\,. \tag{3.62}$$

Equation (3.62) is valid for $2\mu_{SD} P - (2\mu_{SD} + \mu_{RD}) P_S < 0$, this gives ranges for P_S and P_R as $2\mu_{SD}/(2\mu_{SD} + \mu_{RD}) P < P_S \leq P$ and $0 \leq P_R \leq \mu_{RD}/(2\mu_{SD} + \mu_{RD}) P$, respectively. For $2\mu_{SD} \geq \mu_{RD}$, the optimal power allotted to the source node will always be greater than $P/2$, whereas for $2\mu_{SD} < \mu_{RD}$, the optimal power allotted to the source node can be less than $P/2$. On solving (3.62), we can obtain the optimal power allotted at the source and the relay node.

For $\mu_{SR} = \mu_{RD} = 2\mu_{SD} = \delta$ and $\xi = P_S/P_R$, (3.62) can be written as

$$\Xi_2 \xi^{\delta} (\xi - 1) - 2\Xi_1 \;=\; 0. \tag{3.63}$$

For $\delta = 1$, the solutions of ξ in (3.63) are

$$\xi \;=\; \frac{1 + \sqrt{1 + 8\Xi_1/\Xi_2}}{2},\; \frac{1 - \sqrt{1 + 8\Xi_1/\Xi_2}}{2}. \tag{3.64}$$

Using (3.58) and (3.59), it can be shown that $\sqrt{1+8\Xi_1/\Xi_2} > 1$. Hence, the second solution which is negative can be discarded. Using the relation $P = P_S + P_R$ and (3.64), we get

$$P_S = \frac{1+\sqrt{1+8\,\Xi_1/\Xi_2}}{3+\sqrt{1+8\,\Xi_1/\Xi_2}}\,P \tag{3.65}$$

and

$$P_R = \frac{2}{3+\sqrt{1+8\,\Xi_1/\Xi_2}}\,P\,, \tag{3.66}$$

respectively.

Relation with the result existing in the literature: When all links are $\kappa-\mu$ faded, then instead of $2\mu_{SD}$ in (3.57) we have μ_{SD}. On assuming $\mu_{ij} = \delta$, we can write the optimization equation for $\kappa-\mu$ faded channels as (3.63). For $\mu_{ij} = 1$, all the channels are Rician faded and the optimal power at the source and the relay node is given by (3.65), in which

$$\frac{\Xi_1}{\Xi_2} = \frac{\exp(-\kappa_{SR}+\kappa_{RD})}{2\pi}\frac{(1+\kappa_{SR})\lambda_{RD}(d_{SR})^{\alpha_{SR}}}{(1+\kappa_{RD})\lambda_{SR}(d_{RD})^{\alpha_{RD}}}\frac{(C_1)^2}{C_2}, \tag{3.67}$$

where $\mathrm{C}_1 = B(0.5,1.5) + B(0.5,1)\cos(\pi/M)F_D^{(1)}(0.5,-0.5;1.5,\omega)$ and $\mathrm{C}_2 = B(0.5,2.5) + B(0.5,1)\cos(\pi/M)F_D^{(1)}(0.5,-1.5;1.5,\omega)$. Furthermore, as κ_{ij} tends to 0, the optimal power allocation expression reduces to [72, eqs. (21) (22)] for Rayleigh faded channels. Also, C_1 and C_2 are same as A and B defined in [72, eqs. (16) and (17)].

The expressions of the optimal power for any value of fading parameters in $\kappa-\mu$, $\eta-\mu$, and mixed $\kappa-\mu$ and $\eta-\mu$ faded channel can be obtained after appropriate changes in (3.62) and solving it in mathematical softwares like `MATHEMATICA`, `MAPLE`, and `MATLAB`.

3.5.2 Diversity Order

If expression of the asymptotic average SER is known, then DO of the system can be analyzed using [159, eq. (15)]

$$\mathrm{DO} = -\lim_{\bar{\gamma}\to\infty}\frac{\log(P_e^{\infty}(\bar{\gamma}))}{\log(\bar{\gamma})}. \tag{3.68}$$

Now, the end-to-end asymptotic average SER in (3.57) can be rewritten as

$$P_e^{\infty}(\bar{\gamma}) = \frac{\Xi_1'(P_S/P)^{-2\mu_{SD}-\mu_{SR}}}{\bar{\gamma}^{2\mu_{SD}+\mu_{SR}}} + \frac{\Xi_2'(P_S/P)^{-2\mu_{SD}}(P_R/P)^{-\mu_{RD}}}{\bar{\gamma}^{2\mu_{SD}+\mu_{RD}}}, \tag{3.69}$$

where $\bar{\gamma} = P/N_0$, $\Xi_1' = \Xi_1 (N_0)^{-2\mu_{SD}-\mu_{SR}}$, and $\Xi_2' = \Xi_2 (N_0)^{-2\mu_{SD}-\mu_{RD}}$. Using (3.68) and (3.69), we have

$$\begin{aligned} \text{DO} &= \min \left\{ - \lim_{\bar{\gamma}\to\infty} \frac{\log\left(\Xi_1' (P_S/P)^{-2\mu_{SD}-\mu_{SR}} / \bar{\gamma}^{2\mu_{SD}+\mu_{SR}}\right)}{\log(\bar{\gamma})}, \right. \\ &\quad \left. - \lim_{\bar{\gamma}\to\infty} \frac{\log\left(\Xi_2' (P_S/P)^{-2\mu_{SD}} (P_R/P)^{-\mu_{RD}} / \bar{\gamma}^{2\mu_{SD}+\mu_{RD}}\right)}{\log(\bar{\gamma})} \right\}. \end{aligned} \tag{3.70}$$

Solving (3.70), we get

$$\text{DO} = 2\mu_{SD} + \min\{\mu_{SR}, \mu_{RD}\}. \tag{3.71}$$

Similarly, we can obtain the DO when all links are $\kappa-\mu$ faded as

$$\text{DO} = \mu_{SD} + \min\{\mu_{SR}, \mu_{RD}\} \tag{3.72}$$

and for $\eta-\mu$ faded channels as

$$\text{DO} = 2\mu_{SD} + \min\{2\mu_{SR}, 2\mu_{RD}\}. \tag{3.73}$$

3.6 Numerical Results

In this section, we present numerical results for average SER of the relay system under $\kappa-\mu$ and $\eta-\mu$ fading channels. The system model described in Section 3.2 is emulated in `MATLAB` to get the simulation results. The analytical results are obtained using the end-to-end average SER expressions derived in Sections 3.3 and 3.4. The analytical expressions obtained for $\kappa-\mu$ fading are in infinite series form, however these series converge rapidly with increase in number of summation terms (N), for example, $N = 10$ is sufficient to achieve accuracy up to 5th term of decimal. The corresponding analysis is done for $N = 15$ for a better and assured accuracy. The channel gains are considered to be normalized to unity, that is, $\lambda_{ij}(d_{ij})^{-\alpha_{ij}} = 1$, unless otherwise stated.

The average SER versus SNR plots are shown in Figures 3.1 (a) and (b) for different modulation orders under $\kappa-\mu$ and $\eta-\mu$ fading, respectively. Analytical results under $\kappa-\mu$ fading are plotted using (3.15), (3.25), (3.28), and under $\eta-\mu$ fading using (3.15), (3.30), (3.32). Simulation results are found to be in perfect agreement with analytical results, hence validating our analysis. Asymptotic results are plotted using (3.40), (3.48), and (3.55) for $\kappa-\mu$, $\eta-\mu$, and mixed $\kappa-\mu$ and $\eta-\mu$ faded channels,

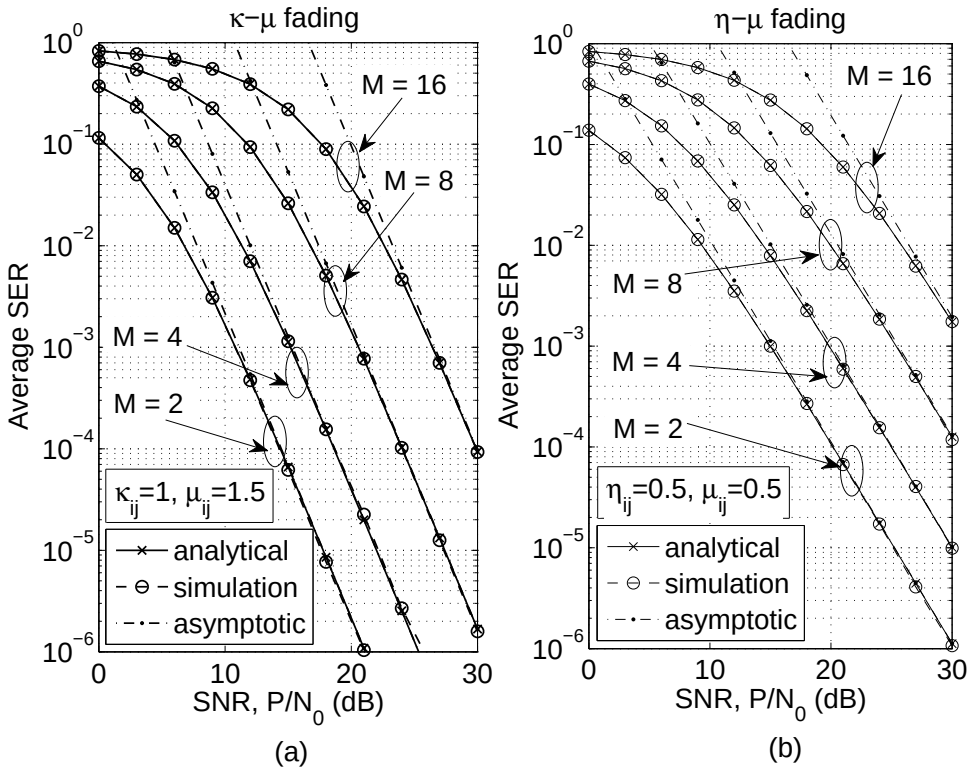

Figure 3.1: Average SER performance of the relay system under $\kappa-\mu$ and $\eta-\mu$ fading for different modulation orders.

respectively. We observe that asymptotic results provide good approximation at high SNRs.

Figure 3.2 presents performance comparison based on channel quality under $\kappa-\mu$ fading. Data is considered to be 8-PSK modulated. In Figure 3.2 (a), the average SER is plotted for fixed μ_{SD} and κ_{ij}, and varying μ_{SR} and μ_{RD}. In Figure 3.2 (a), we observe that the increment in performance is more for increase in μ_{RD} as compared to increase in μ_{SR}. In Figure 3.2 (b), μ_{ij} and κ_{ij} are kept constant for SR and SD links, and varied for RD link. We observe that increase in μ_{RD} has better impact on performance than increase in κ_{RD}. The SR and RD links with greater values of fading parameters κ and μ show better performance and among them the parameters of RD link dominate. Moreover, increase in μ_{RD} has better impact compared to increase in κ_{RD}.

In Figure 3.3, average SER is plotted for different channel conditions under $\eta-\mu$ fading. 4-PSK modulation is considered. In Figure 3.3 (a), the average SER is plotted for fixed μ_{ij} and η_{SD}, and varying η_{SR} and η_{RD}. We find from the plots that the performance improvement is higher with increase in η_{RD} as compared to increase in η_{SR}. In Figure 3.3 (b), parameters of SR and SD links are kept constant and the effect of change in parameters of RD link is observed. As seen from plots, increase

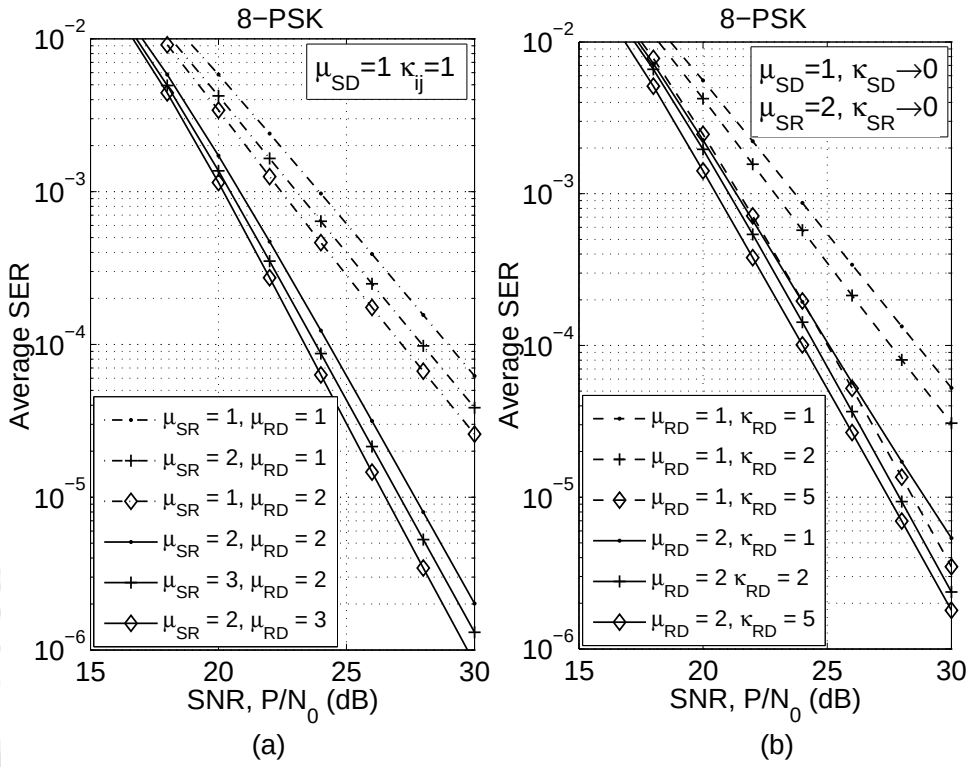

Figure 3.2: Average SER performance of 8-PSK under $\kappa-\mu$ fading channels with different values of κ_{ij} and μ_{ij}.

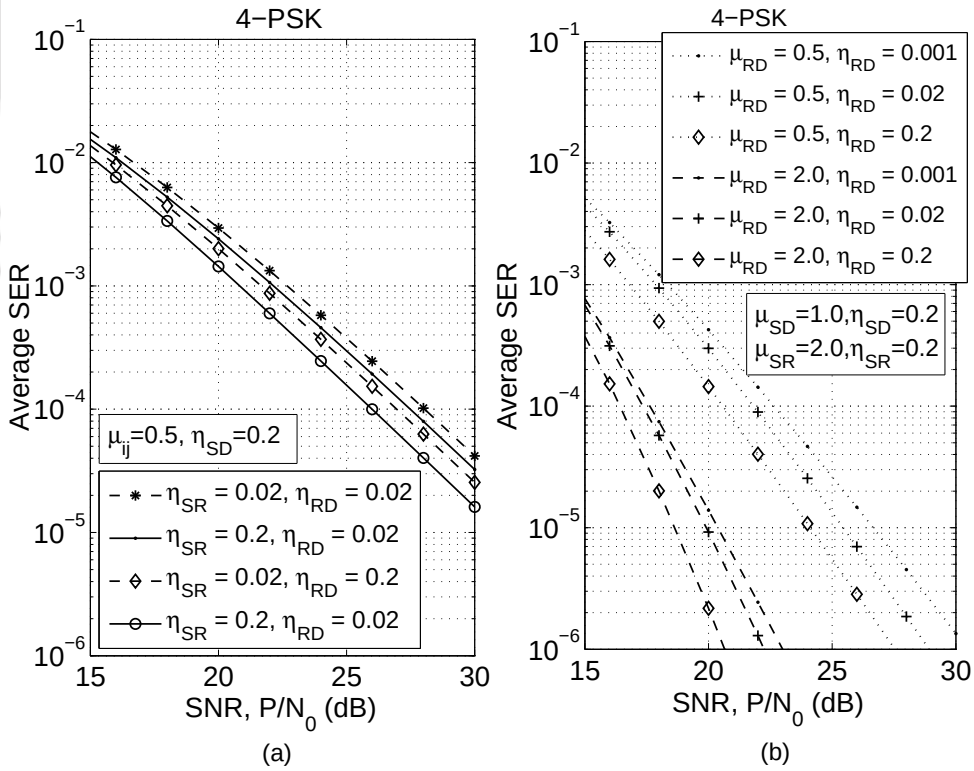

Figure 3.3: Average SER performance of 4-PSK under $\eta-\mu$ fading channels with different values of η_{ij} and μ_{ij}.

in μ_{RD} gives better performance as compared to increase in η_{RD}. The performance improvement is more for increase in parameters of the RD link compared to increase in parameters of SR link, and increase in μ_{RD} has better impact compared to increase in η_{RD}.

In Figure 3.4, the average SER results for the relay system with equal and optimal power allocation are presented. Mixed fading environment is considered, where SD link is $\eta-\mu$ faded and SR and RD links are $\kappa-\mu$ faded. 4-PSK and 8-PSK modulated data is considered in Figure 3.4 (a) and (b), respectively. Optimal power allocated to nodes S and R are evaluated by implementing and solving (3.61) in `MATLAB`. The results are also compared with that of direct transmission. Total transmission power in relay system and direct transmission is considered same, that is, P. In both system, each transmission requires equal duration, that implies relay system requires twice the time required in the direct transmission. We observe in Figure 3.4 that for better SD link quality, direct transmission can outperform the relay system with equal power allocation scheme. Although, optimal power allocation in the relay system performs better than direct transmission under all channel conditions. It also outperforms the equal power allocation in the relay system.

Assume $N_0 = 1$, the variation in average SER in Figure 3.4 is with total transmission power P. Furthermore, in (3.62), we can see that the optimal power allocated to node S, P_S depends on power P and the channel conditions. Although, through numerical computation we observed that there is not much variation in the optimal power-ratio P_S/P obtained for different values of P. Moreover, for a wide range of channel conditions, the corresponding average SER is close to the average SER obtained for $P = 24$ dB. In Figure 3.4, the curves with *circle* marker correspond to the average SER with optimal power allocation that depends on P. The average SERs obtained for $P = 24$ dB are found to overlap with the optimal curves, but not shown in the figure for the sake of clarity. In Figure 3.4, the value $x^* = P_S/P$ corresponds to the optimal power allocated to node S for $P = 24$ dB. We observe that for higher modulation order, the optimal power allotted to the source node increases (and hence the optimal power allotted to the relay node decreases).

In order to compare the derived analytical results with those presented in [72] and [73], the average SER of system with Nakagami-m faded channel and 4-PSK modulated data is shown in Figure 3.5. $\eta-\mu$ fading and $\kappa-\mu$ fading reduce to Nakagami-m fading for $\eta_{ij} = 1$ (Format-1) and $\kappa_{ij} \to 0$, respectively. The results are shown for the mixed fading scenario[1] when $\mu_{SD} = \{0.25, 0.5, 0.75, 1\}$ and

[1] SD link is under $\eta-\mu$ fading and SR and RD links are under $\kappa-\mu$ fading. SD link reduces to Nakagami-m fading for $\eta_{SD} = 1$ and SR and RD links correspond to Nakagami-m fading for κ_{SR}, $\kappa_{RD} \to 0$.

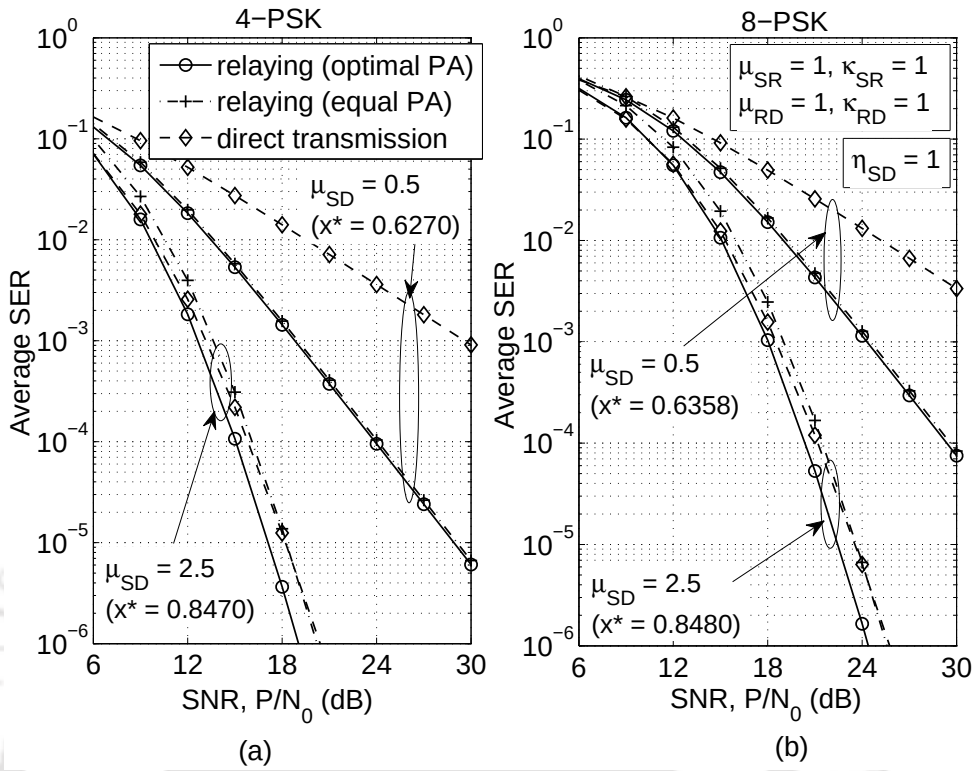

Figure 3.4: Average SER versus average SNR plots showing comparison of the relay system with optimal and equal power allocation (PA) and direct transmission under mixed $\kappa-\mu$ and $\eta-\mu$ faded (SD link as $\eta-\mu$, SR and RD links as $\kappa-\mu$ faded).

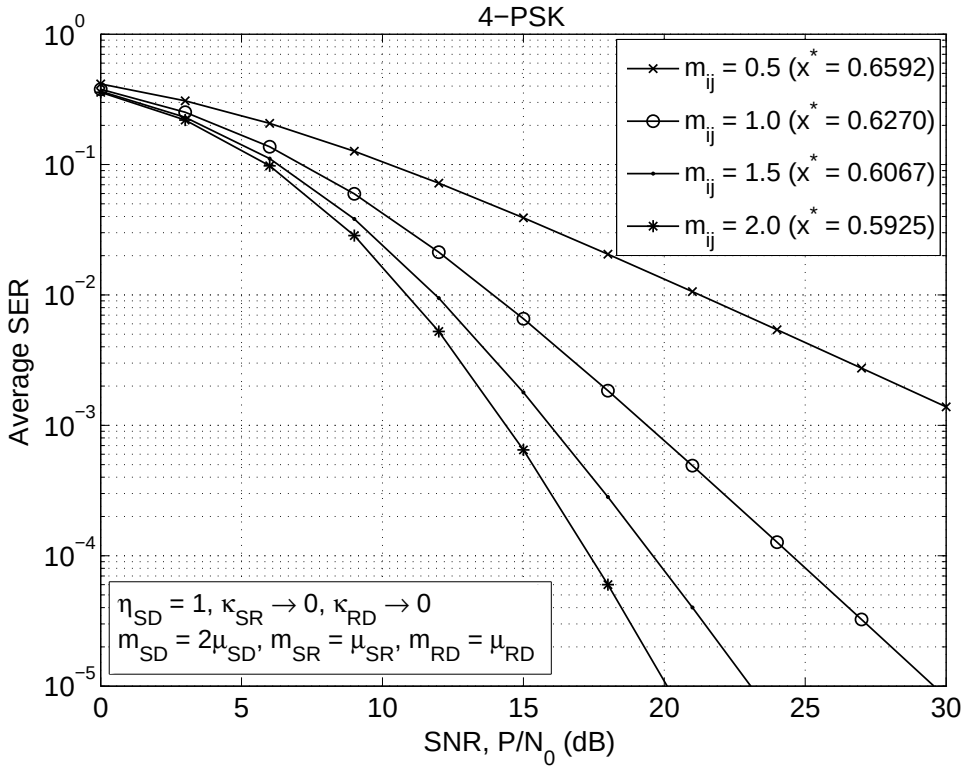

Figure 3.5: Average SER versus SNR plot for 4-PSK under Nakagami-m fading as a special case of the fixed fading scenario.

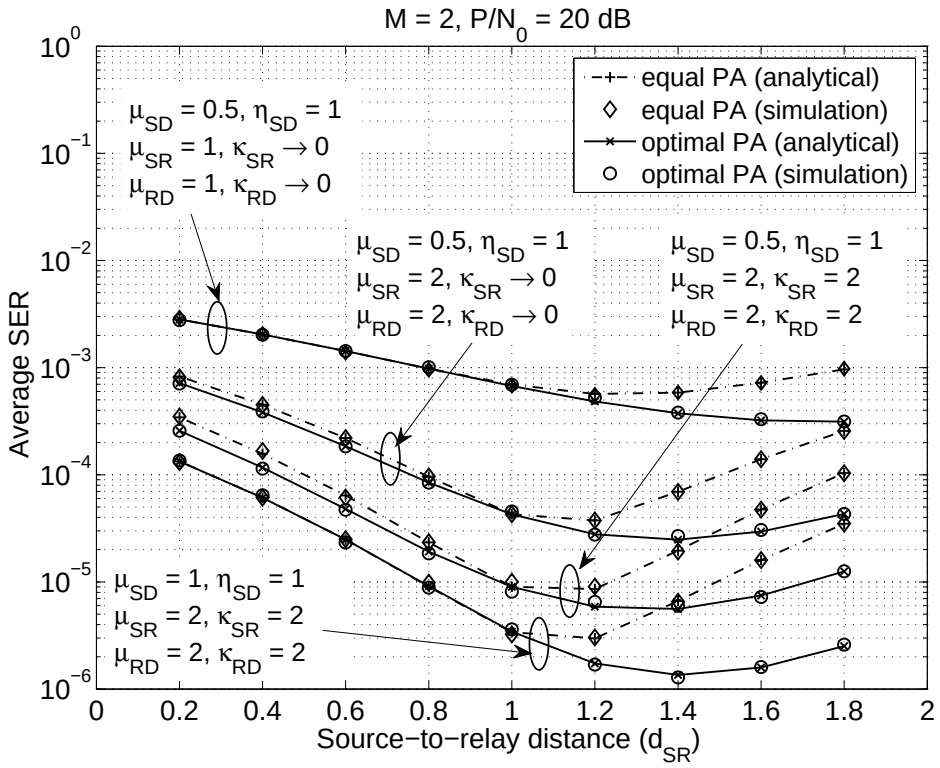

Figure 3.6: Average SER versus source-to-relay distance for the relay system with equal and optimal PA under mixed fading for different fading parameters, $d_{SR}+d_{RD}=d_{SD}$, $d_{SD}=2$ unit, $\alpha_{ij}=3$, $\lambda_{ij}=1$.

$\mu_{SR},\mu_{RD}\in\{0.5,1.0,1.5,2\}$. Let the Nakagami-$m$ fading parameters of the links be $m_{SD}=2\mu_{SD}$, $m_{SR}=\mu_{SR}$, and $m_{RD}=\mu_{RD}$. Thus we have $m_{ij}\in\{0.5,1,1.5,2\}$. It can be noted that the plot for different values of m_{ij} resembles that for the corresponding value of the fading parameter m in [73, Figure 3] for Nakagami-m fading. Furthermore, for $m_{ij}=1$ the plot resembles that in [72, Figure 4] for Rayleigh fading environment. Moreover, the optimal fractions of total power allotted to the source node is obtained as $x^*=P_S/P=0.6270$, which is identical to that obtained in [72, Figure 4]. This suggests that the average SER expressions for Rayleigh fading and Nakagami-m fading can be traced using expressions for the generalized fading models.

In Figure 3.6, the average SER is plotted with variation in source-to-relay distance for the relay system with equal and optimal power allocation under different channel conditions. The nodes are considered to be collinear and follow the relation $d_{SR}+d_{RD}=d_{SD}$. The results are shown for $d_{SD}=2$ unit, $\alpha_{ij}=3$, and $\lambda_{ij}=1$. We observe that when power at nodes S and R are equally allocated then the optimal relay location lies near midway with approximate distance ratio $d_{SR}/d_{SD}\approx 0.6$. This is in accordance with the result in [160]. Furthermore, when power is optimally allocated and channel

Table 3.1: Fraction of the total power allocated at the source node (P_S/P) in case of optimal power allocation for 4-PSK modulated data under the considered mixed fading scenario, $P = 24$ dB, $N_0 = 1$.

$\mu_{SR} = 1, \kappa_{SR} = 0;$ $\mu_{RD} = 0.5, \kappa_{RD} = 0$			$\mu_{SD} = 0.5, \eta_{SD} = 1;$ $\mu_{RD} = 0.5, \kappa_{RD} = 0$			$\mu_{SD} = 0.5, \eta_{SD} = 1;$ $\mu_{SR} = 0.5, \kappa_{SR} = 0$		
μ_{SD}	η_{SD}	P_S/P	μ_{SR}	κ_{SR}	P_S/P	μ_{RD}	κ_{RD}	P_S/P
	0.01	0.55511		0	0.80784		0	0.68339
0.25	0.1	0.55511	0.5	1	0.74548	0.5	1	0.68586
	1	0.55511		4	0.70280		4	0.71252
	0.01	0.68866		0	0.68866		0	0.60712
0.5	0.1	0.68866	1	1	0.68339	1	1	0.62704
	1	0.68866		4	0.66894		4	0.78139
	0.01	0.80784		0	0.67204		0	0.64977
1	0.1	0.80784	1.5	1	0.67010	1.5	1	0.68582
	1	0.80784		4	0.66682		4	0.87797

condition improves, the optimal relay location moves toward the destination node. Similar observations can be made for different values of d_{SD}, α_{ij}, and λ_{ij}.

In Table 3.1, the fraction of the total power allocated to the source node (P_S/P) in case of optimal power allocation is tabulated corresponding to the parameters of the SD, SR, and RD link for 4-PSK modulated data under the considered mixed fading case. Following observations can be made from the table: i) P_S/P increases with increase in μ_{SD} but is not affected by change in η_{SD}, ii) P_S/P decreases with improvement in SR link quality, and iii) P_S/P increases with improvement in RD link quality.

3.7 Conclusion

We have deduced exact expressions of the average SER for a conventional DF system under $\kappa-\mu$, $\eta-\mu$, and mixed $\kappa-\mu$ and $\eta-\mu$ fading when input data is M-PSK modulated. At high SNRs, asymptotic approximations of average SERs are also analyzed. Optimal power allocation expressions for the power allotted to the source and the relay node are obtained. DO for the different fading types is analyzed and the effect of distance on performance is traced. We observe that the performance improvement is more for increase in fading parameters of RD link when compared to increase in fading

parameters of SR link. Also, among κ and μ parameters in $\kappa-\mu$ fading and η and μ parameters in $\eta-\mu$ fading, the improvement in performance with increase in μ parameter dominates. The performance for shorter SD links is better when compared to longer links. Also, the relative increment in performance is more when the fading parameters of the SD link increases. In case of high SD link quality, direct transmission may outperform communication using relay with equal power allocation at source and relay node. However, the relaying system outperforms the direct transmission in case of optimal power allocation at nodes, under all channel conditions. Furthermore, the power allotted to the source node raises with the increase in the modulation order, decline in SR link quality, and improvement in RD link quality.

4

WP DF Relay System under Nakagami-m Fading: EH at Relay Node

Contents

The previous chapter provides the performance analysis of a conventional three-node DF relay system. In conventional systems, nodes are considered to be powered by batteries which can be replaced or recharged if drained. In systems, such as wireless sensor networks, wireless body networks, etc., the nodes are generally inaccessible and therefore providing power with the aid of such batteries may not be always feasible. In such a scenario, end-to-end communication is hampered if batteries of the participating relay node(s) exhaust in-between the communication. Also, there could be a possibility when the relay node(s) does not want to use its own power for relaying. Under such circumstances, if the node can be supported by wireless EH methods, it may encourage participation of the node in communication. In this chapter, we present communication theoretic analysis of a relay-assisted WPCN under Nakagami-m fading for M-PSK modulated data. The energy-constrained relay node is wirelessly powered by the source node.

4.1 Introduction

In the literature, performance analysis of WP networks is widely explored. In [41, 70, 125], the performance of SWIPT networks is analyzed using the information theoretic approach. Energy-constrained relay node harvests energy using the received RF signals radiated by the source node and/or interferences. AF and DF protocols are considered in [41] and [70, 125], respectively. In [69], the average symbol-error-rate (SER) of parallel DF relaying SWIPT network with energy-constrained relay nodes is given for the noncoherent M-DPSK and M-FSK modulation schemes. Information theoretic analysis of WPCNs with AF and DF relaying is presented in [57] and [149], respectively. The works done in [41,57,69,70,125,149] consider Rayleigh fading environment for the analysis. In a practical scenario, wireless medium is lossy in nature and therefore the applicability of WP systems is limited to short-range communications. Thus, the possibility that LOS components exist cannot be ignored. Rician, $\kappa-\mu$, and $\kappa-\mu$ shadowed fading models are more applicable for short-range communications. However, analysis for these fading models is difficult and mathematically intractable under some circumstances. Nakagami-m fading is a generalized model which is Rayleigh model for $m = 1$ and approximates to Rician fading for $m > 1$. In [62,71,76,141–143], the performance of WP relay systems under Nakagami-m fading is analyzed. Information theoretic analysis is carried out in [62, 141–143] whereas communication theoretic analysis is presented in [71]. [76] exhibit both information theoretic and communication theoretic analyses. DF protocol is considered in [76,142,143], whereas AF protocol

in [62, 141]. Both AF and DF protocols are considered in [71]. These references provide performance analysis of SWIPT networks. Moreover, the effect of direct link between the source and destination is ignored. If the direct link exists and is considered for the analysis, performance of the system can be significantly improved by employing diversity combining schemes at the destination node.

In this chapter, performance analysis of a three-node relay-assisted WPCN is presented. The end-to-end transmission is executed in three slots. In the first slot, the relay node is powered by the source. In the next two slots, selective DF relaying is employed to transfer the information from the source to the destination using the energy harvested in the first slot. The received SNRs are expressed as the ratio of signal energy and noise power spectral density (PSD) [69], unlike in Chapter 4, where these are defined as the ratio of signal power and noise power. By defining the SNRs in terms of the energy ratio, the energy assigned for each slot can be optimized for the minimum average SER, which in turn can be used to judiciously optimize the corresponding power transmitted or the slot duration [161]. We consider two scenarios for the analysis i) direct link is present between the source and the destination and ii) direct link is ignored. In the latter case, the direct link is considered to be in deep fade. When a direct link exists, the two signals arriving at the destination via direct and relayed links are combined using EGC scheme as it performs close to MRC for reduced system complexity [36].

The main contributions of this chapter are summarized as

- Motivated by the WPT and WIT technique [55] for point-to-point communication in WPCN, we propose a transmission technique for a relay assisted WPCN. Analytical expressions of the average SER are derived for M-PSK modulated data under Nakagami-m fading environment.
- We also derive the asymptotic expression of the average SERs to simplify the analysis at high SNRs. The high SNR approximations are utilized to find the optimal energy assigned for transmission in each slot. Since energy is related to the power transmitted at a node and the slot duration, the optimal energy expression can be judiciously used to optimize power and time for the corresponding slot.
- We further analyze the DO and the throughput of the system.
- The effects of modulation order and fading parameters on system performance is also investigated.

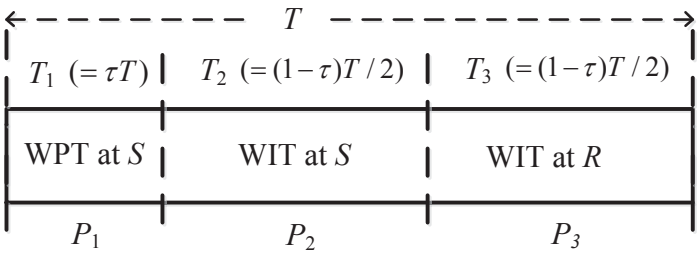

Figure 4.1: Illustration of the transmission technique.

Rest of the chapter is organized as follows. The system model is described in Section 4.2. Expressions for average SER and corresponding asymptotic approximations are obtained in Section 4.3. In Section 4.4, asymptotic expressions are used to find the optimal energy assigned in different slots for minimum SER, which then determines the corresponding optimal power and the slot duration. In Section 4.5, DO and throughput are analyzed. Numerical results are presented in Section 4.6 and the concluding remarks are written in Section 4.7.

4.2 System Model

We consider a three-node WPCN with EH at the relay node R. M-PSK modulated symbols are communicated from the source node S to the destination node D. Each node is having a single antenna. We assume half-duplex mode of communication. Each information symbol at the source is communicated to the destination in a slot of duration T which is further divided in three time slots as shown in Figure 4.1. In the first slot T_1, wireless power P_1 transmitted by node S is used to harvest energy at the energy-constrained node R. The second time slot T_2 and the third time slot T_3 are equally divided ($T_2 = T_3$) and are engaged in WIT. Let τ be the fraction of T used for harvesting energy. Then, the three time slots are $T_1 = \tau T$ and $T_2 = T_3 = (1-\tau)T/2$. Node S broadcasts the data in slot T_2 with power P_2. Selective DF is employed at node R, thus the received source data is checked for its correctness. In case of correct reception, the relay R uses the harvested energy to forward the re-encoded data to node D in slot T_3 with power P_3. Correct decoding at node R can be accomplished by using threshold-based checking or cyclic-redundancy-check codes [72, 73]. We consider harvest-use approach to process the incoming energy flow [58, 68].

We assume that the power consumption in operational circuits (like modulator, demodulator, encoder, decoder, etc.) is comparatively smaller and therefore can be neglected [70, 125]. The energy

harvested at node R in T_1 is completely used to forward the encoded data to node D. Data transmitted is M-PSK modulated with equal *a priori* probabilities. The M-PSK constellation $\mathcal{S}$ is given by $\mathcal{S} = \exp(\jmath 2\pi(n-1)/M)$, where $n = 1, 2, \ldots, M$ and $\jmath = \sqrt{-1}$. In the kth time slot, $x_k = \sqrt{P_k T_k} s_k$ is transmitted with energy $E[x_k x_k^*] = P_k T_k$, where $s_k \in \mathcal{S}$ and $k = 1, 2, 3$. $E[\cdot]$ denotes the expectation operator and $(\cdot)^*$ represents the complex conjugate. We assume links between nodes S, R, and D are independent, slow-flat Nakagami-m faded, and link gains are assumed to be constant for time T.

In the kth time slot, the baseband equivalent of the received RF signal at node j is given by

$$y_{kj} = \sqrt{P_k T_k \, {d_{ij}}^{-\alpha_{ij}}} \, h_{ij} \, s_k + n_{kj}, \quad k = 1, 2, 3, \tag{4.1}$$

where $i \in \{S, R\}$, $j \in \{R, D\}$, h_{ij} is the fading coefficient of the link connecting node i and node j having mean power $E[|h_{ij}|^2] = \lambda_{ij}$, ${d_{ij}}^{-\alpha_{ij}}$ represents path loss of the link between node i and j, d_{ij} is in meters with path loss exponent α_{ij} ranging from 2 to 6, and n_{kj} is additive white Gaussian noise at node j having PSD N_0. For a comparatively small noise component, the harvested energy in T_1 can be approximated as

$$E_R \approx \frac{\zeta |h_{SR}|^2 P_1 T_1}{(d_{SR})^{\alpha_{SR}}}, \tag{4.2}$$

where ζ is energy conversion efficiency, $\zeta \in (0, 1)$. In T_2, s_2 is transmitted at node S and selective DF relaying is employed at node R in T_3. This implies, if node R correctly decodes the symbol s_2, the symbol is forwarded to the destination D with power P_3 $(= E_R/T_3)$ in the time slot T_3. Otherwise node R remains idle ($P_3 = 0$). The signals received at node D via direct and relay links on correct decoding at the relay are combined in slot T_3 using EGC [36] as

$$\begin{aligned} y &= \exp(-\jmath \angle h_{SD}) y_{2D} + \exp(-\jmath \angle h_{RD}) y_{3D} \\ &= \left(\sqrt{P_2 T_2 (d_{SD})^{-\alpha_{SD}}} \, |h_{SD}| + \sqrt{P_3 T_3 (d_{RD})^{-\alpha_{RD}}} \, |h_{RD}| \right) s_2 \\ &\quad + \Big(\exp(-\jmath \angle h_{SD}) n_{2D} + \exp(-\jmath \angle h_{RD}) n_{3D} \Big), \end{aligned} \tag{4.3}$$

where $\angle(\cdot)$ represents the argument's angle.

The data is detected at node R in slot T_2 using the decision rule

$$\hat{s} = \arg \left\{ \max_{p \in \mathcal{S}} \mathrm{Re}\Big(p^* \exp(-\jmath \angle h_{SR}) y_{2R} \Big) \right\}. \tag{4.4}$$

If the detection is incorrect at node R, then node D decides the data in slot T_3 using the decision rule

$$\hat{s} = \arg\left\{\max_{p\in\mathcal{S}} \mathrm{Re}\Big(p^* \exp(-\jmath\angle h_{RD}) y_{3D}\Big)\right\}. \tag{4.5}$$

Otherwise, in case of correct detection at node R, node D uses the decision rule

$$\hat{s} = \arg\left\{\max_{p\in\mathcal{S}} \mathrm{Re}\Big(p^* y\Big)\right\}, \tag{4.6}$$

where y is given in (4.3).

The ratio of the power exponent of the equivalent signal and noise components in (4.3) gives the equivalent instantaneous SNR at node D. That is

$$\begin{aligned}\gamma_{\mathrm{EGC}} &= \frac{\left(\sqrt{P_2T_2(d_{SD})^{-\alpha_{SD}}}|h_{SD}| + \sqrt{P_3T_3(d_{RD})^{-\alpha_{RD}}}|h_{RD}|\right)^2}{\Big(\exp(-\jmath\angle h_{SD})n_{2D} + \exp(-\jmath\angle h_{RD})n_{3D}\Big)^2} \\ &= \left(\nu_1|h_{SD}| + \nu_2|h_{SR}||h_{RD}|\right)^2, \end{aligned} \tag{4.7}$$

where $\nu_1 = \sqrt{P_2T_2\,(d_{SD})^{-\alpha_{SD}}/(2N_0)}$ and $\nu_2 = \sqrt{\zeta P_1T_1\,(d_{SR})^{-\alpha_{SR}}(d_{RD})^{-\alpha_{RD}}/(2N_0)}$. The instantaneous SNRs of SR, RD, and SD links are given by

$$\gamma_{SR} = \frac{P_2T_2|h_{SR}|^2}{(d_{SR})^{\alpha_{SR}}N_0}, \tag{4.8a}$$

$$\gamma_{RD} = \frac{\zeta P_1T_1|h_{SR}|^2|h_{RD}|^2}{(d_{SR})^{\alpha_{SR}}(d_{RD})^{\alpha_{RD}}N_0}, \quad \text{and} \tag{4.8b}$$

$$\gamma_{SD} = \frac{P_2T_2|h_{SD}|^2}{(d_{SD})^{\alpha_{SD}}N_0}, \tag{4.8c}$$

respectively. Owing to Nakagami-m fading, the PDF of the fading amplitude $|h_{ij}|$ is given by

$$f_{|h_{ij}|}(|h_{ij}|) = \frac{2m_{ij}^{m_{ij}}|h_{ij}|^{2m_{ij}-1}}{\Gamma(m_{ij})\lambda_{ij}^{m_{ij}}} \exp\left(-\frac{m_{ij}|h_{ij}|^2}{\lambda_{ij}}\right), \tag{4.9}$$

where m_{ij} is Nakagami-m fading parameter of $ij \in \{SR, SD, RD\}$ link and $\Gamma(\cdot)$ is gamma function. The average link SNRs for the SR, RD, and SD links are obtained by taking expectation of the

instantaneous link SNRs in (4.8) as

$$\bar{\gamma}_{SR} = \frac{P_2 T_2 \lambda_{SR}}{(d_{SR})^{\alpha_{SR}} N_0}, \tag{4.10a}$$

$$\bar{\gamma}_{RD} = \frac{\zeta P_1 T_1 \lambda_{SR} \lambda_{RD}}{(d_{SR})^{\alpha_{SR}} (d_{RD})^{\alpha_{RD}} N_0}, \quad \text{and} \tag{4.10b}$$

$$\bar{\gamma}_{SD} = \frac{P_2 T_2 \lambda_{SD}}{(d_{SD})^{\alpha_{SD}} N_0}, \tag{4.10c}$$

respectively.

Let P be the average transmission power required to communicate data from the source S to the destination D. Then, the total energy consumed in the time slots T_1, T_2, and T_3 is PT, where $T = T_1 + T_2 + T_3$. The energy in the three slots are P_1T_1, P_2T_2, and P_3T_3, respectively. Since the relay node is WP; energy harvested in the time slot T_1 is used to forward the data at node R in T_3. That is, the relay does not consume any additional energy and therefore, we have $PT = P_1T_1 + P_2T_2$. This can be rewritten as

$$\tau P_1 + \Big(\frac{1-\tau}{2}\Big) P_2 = P \quad \text{or} \quad \beta_1 + \beta_2 = 1, \tag{4.11}$$

where fractions of total energy consumed in T_1 and T_2 are given by

$$\beta_1 = \tau \frac{P_1}{P} \qquad \text{and} \qquad \beta_2 = \frac{1-\tau}{2} \frac{P_2}{P}, \tag{4.12}$$

respectively.

We note that for $P_1 = P_2 = P$ (or $\beta_1 = \tau$) the analysis presented in this work for WPCN is reduced to the analysis for TS based SWIPT network [71]. $\beta_1 = \tau$ corresponds to the time fraction of the received signal allocated for EH and $\beta_2 = (1-\tau)/2$ corresponds to the remaining time fraction used for ID at the relay R in the SWIPT network. Hence, the optimization for energy fraction is reduced to the optimization for time fraction. In [71], the analysis is presented for TS and PS based two-hop DF relaying. Though, the corresponding optimization of time and power fractions is not provided there.

4.3 Performance Analysis

In this section, expressions of average SER are analyzed for the system when i) SD link assists in data transmission and ii) SD link does not assist in data transmission because it is deeply faded. The

expressions are derived in the terms of univariate Meijer-G and bivariate Fox-H functions. Univariate Meijer-G function is represented in single Mellin-Barnes integral form as [162, eq. (8.2.1.1)]

$$G_{p_1,q_1}^{m_1,n_1}\left[x\middle|\begin{matrix}a_1,\ldots,a_{p_1}\\ b_1,\ldots,b_{q_1}\end{matrix}\right] = \frac{1}{2\pi\jmath}\int_{\mathcal{C}}\theta(p)x^{-p}dp, \tag{4.13}$$

where $\mathcal{C}$ is the contour of the integration and

$$\theta(p) = \frac{\prod_{j=1}^{m_1}\Gamma(b_j+p)\prod_{j=1}^{n_1}\Gamma(1-a_j-p)}{\prod_{j=m_1+1}^{q_1}\Gamma(1-b_j-p)\prod_{j=n_1+1}^{p_1}\Gamma(a_j+p)}.$$

The double Mellin-Barnes integral representation of bivariate Fox-H function is given as [163, eq. (1.1)]

$$H\left[\begin{matrix}x\\ y\end{matrix}\middle|\begin{matrix}\begin{pmatrix}0,n_1\\ p_1,q_1\end{pmatrix}\\ \begin{pmatrix}m_2,n_2\\ p_2,\ q_2\end{pmatrix}\\ \begin{pmatrix}m_3,n_3\\ p_3,\ q_3\end{pmatrix}\end{matrix}\middle|\begin{matrix}(a_j;\alpha_j,A_j)_1,p_1\\ (b_j;\varpi_j,B_j)_1,q_1\\ (c_j,\zeta_j)_1,p_2\\ (d_j,\delta_j)_1,q_2\\ (e_j,E_j)_1,p_3\\ (f_j,F_j)_1,q_3\end{matrix}\right] = \frac{1}{(2\pi\jmath)^2}\int_{\mathcal{C}_1}\int_{\mathcal{C}_2}\phi(p,q)\theta_1(p)\theta_2(q)x^{-p}y^{-q}dpdq, \tag{4.14}$$

where $\mathcal{C}_1$ and $\mathcal{C}_2$ represent integral contours, and the definition of $\phi(p,q)$, $\theta_1(p)$, and $\theta_2(q)$ is followed from [163, eqs. (1.2), (1.3), and (1.3a)], respectively for $p=-s$ and $q=-t$. In this chapter, contours of the integrals in (4.13) and (4.14) are lines[1] parallel to the imaginary axis. Therefore, it is possible to numerically evaluate Meijer-G and bivariate Fox-H functions in mathematical softwares, such as `MATLAB` and `MATHEMATICA` by performing line integration along the strip of analyticity (SoA) [164], [165]. In the literature, different representations for the Meijer-G and the Fox-H functions are used. In [163, eq. (1.1)], [166, eq. (9.301)], and [167], the SoA of the corresponding integrals is considered to be in the left-half of the complex plane whereas in [162, eqs. (8.2.1.1) and (8.3.1.1)] and [165], the right-half of the complex plane is considered. In this chapter, we use (4.13) and (4.14), where SoA of the integrals lies in the right-half of the complex plane.

[1]Contours are loops ensuring poles of complex gamma functions in numerator of the integrand are separated to guarantee the convergence of integrals [163, 164].

4.3.1 Analytical Average SER

The average SER for the two cases is analyzed using MGF based approach. The PDF and MGF of γ_{SR}, γ_{SD}, γ_{RD}, and γ_{EGC} are used in the intermediate steps of the analysis.

4.3.1.1 With SD Link

We analyze the end-to-end average SER for the case when SD link assists in data transmission and the signals received from SD and RD links are combined using EGC principle (4.7) at the destination. Therefore, using (4.7) the equivalent instantaneous SNR at the destination is

$$\gamma_{\text{EGC}} \;=\; (t_1{+}t_2)^2;\;\; t_1{=}\nu_1|h_{SD}| \text{ and } t_2{=}\nu_2|h_{SR}|\,|h_{RD}|, \tag{4.15}$$

where t_1 follows Nakagami-m distribution with fading parameter m_{SD} and mean power $\bar{\gamma}_1 = E[(t_1)^2] = \lambda_{SD}(\nu_1)^2$. The PDF of t_2 is analyzed in Appendix A.1 as

$$f_{t_2}(t_2) \;=\; \frac{2m_{SR}m_{RD}t_2}{\Gamma(m_{SR})\Gamma(m_{RD})\bar{\gamma}_2} G_{0,2}^{2,0}\left[\frac{m_{SR}m_{RD}(t_2)^2}{\bar{\gamma}_2}\middle|\begin{matrix}-\\ m_{SR}-1, m_{RD}-1\end{matrix}\right], \tag{4.16}$$

where $\bar{\gamma}_2 = \lambda_{SR}\lambda_{RD}(\nu_2)^2$. The PDFs of t_1 and t_2 are used in Appendix A.2 to analyze the PDF for γ_{EGC} in (4.15), thus, the PDF is

$$f_{\gamma_{\text{EGC}}}(\gamma_{\text{EGC}}) \;=\; \frac{m_{SD}m_{SR}m_{RD}\,\gamma_{\text{EGC}}}{\Gamma(m_{SD})\Gamma(m_{SR})\Gamma(m_{RD})\bar{\gamma}_1\bar{\gamma}_2} H\left[\begin{matrix}\dfrac{m_{SR}m_{RD}\gamma_{\text{EGC}}}{\bar{\gamma}_2}\\[2ex] \dfrac{m_{SD}\gamma_{\text{EGC}}}{\bar{\gamma}_1}\end{matrix}\middle|\begin{matrix}\begin{pmatrix}0,0\\0,1\end{pmatrix}\\ \begin{pmatrix}2,1\\1,2\end{pmatrix}\\ \begin{pmatrix}1,2\\2,2\end{pmatrix}\end{matrix}\middle|\begin{matrix}-\\ (-3;2,2))\\ (-1,2)\\ (m_{SR}{-}1{,}1),(m_{RD}{-}1{,}1)\\ (0,1),(-2,2)\\ (m_{SD}{-}1,1),(-1,1)\end{matrix}\right]. \tag{4.17}$$

Next, the end-to-end conditional SER at node D on selective DF relaying is given by (3.12)

$$P_e(\gamma_{SR},\gamma_{SD},\gamma_{\text{EGC}}) \;=\; P_e(\gamma_{SR})P_e(\gamma_{SD}) + (1-P_e(\gamma_{SR}))P_e(\gamma_{\text{EGC}}), \tag{4.18}$$

where $P_e(\gamma_\varphi)$ is the conditional SER and γ_φ is the instantaneous SNR of link $\varphi \in \{SR, SD, \text{EGC}\}$. The instantaneous SNRs γ_{SR}, γ_{SD}, and γ_{EGC} are defined in (4.8a), (4.8c) and (4.7), respectively. The

end-to-end average SER is obtained by taking expectation of (4.18), given by

$$\begin{aligned} P_e &= E[P_e(\gamma_{SD}, \gamma_{SR}, \gamma_{\text{EGC}})] \\ &= P_{e,SR}P_{e,SD} + (1 - P_{e,SR})P_{e,\text{EGC}}\,, \end{aligned} \tag{4.19}$$

where $P_{e,SR} = E[P_e(\gamma_{SR})]$, $P_{e,SD} = E[P_e(\gamma_{SD})]$, and $P_{e,\text{EGC}} = E[P_e(\gamma_{\text{EGC}})]$. The expectation of $P_e(\gamma_\varphi)$ is obtained using the MGF based approach [156, eq. (9.15)], that is expressed as

$$P_{e,\,\varphi} = \frac{1}{\pi}\int_0^{\frac{(M-1)\pi}{M}} M_{\gamma_\varphi}\left(\frac{g}{\sin^2\theta}\right) d\theta\,, \tag{4.20}$$

where $g = \sin^2(\pi/M)$ and $M_{\gamma_\varphi}(s)$ is MGF of γ_φ given by

$$M_{\gamma_\varphi}(s) = \int_0^\infty \exp(-s\gamma_\varphi) f_{\gamma_\varphi}(\gamma_\varphi) d\gamma_\varphi\,. \tag{4.21}$$

The MGF of the SR (or SD) link under Nakagami-m fading is given using [156, Table 2.2] as

$$M_{\gamma_{\varphi_1}} = \left(1 + s\frac{\bar{\gamma}_{\varphi_1}}{m_{\varphi_1}}\right)^{-m_{\varphi_1}}, \tag{4.22}$$

where $\varphi_1 \in \{SR, SD\}$ and $\bar{\gamma}_{\varphi_1} = P_2 T_2 \lambda_{\varphi_1} (d_{\varphi_1})^{-\alpha_{\varphi_1}}/N_0$ is the average SNR at the receiving node. Substituting (4.22) in (4.20), the average SER of link φ_1 can be expressed as

$$P_{e,\,\varphi_1} = \frac{1}{\pi}\int_0^{\frac{(M-1)\pi}{M}} \left(1 + \frac{g\bar{\gamma}_{\varphi_1}}{m_{\varphi_1}\sin^2(\theta)}\right)^{-m_{\varphi_1}} d\theta\,. \tag{4.23}$$

The closed-form expression for $P_{e,\,\varphi_1}$ in (4.23) is given in [168, eq. (19)]. Similarly, the MGF of γ_{EGC} at node D is given by

$$M_{\gamma_{\text{EGC}}}(s) = \int_0^\infty \exp(-s\gamma_{\text{EGC}}) f_{\gamma_{\text{EGC}}}(\gamma_{\text{EGC}}) d\gamma_{\text{EGC}}\,, \tag{4.24}$$

where $M_{\gamma_{\text{EGC}}}(s)$ is simplified using (4.14), (4.17), and (B.7) as

$$M_{\gamma_{\text{EGC}}}(s) = \frac{m_{SD}m_{SR}m_{RD}}{\Gamma(m_{SD})\Gamma(m_{SR})\Gamma(m_{RD})\bar{\gamma}_1\bar{\gamma}_2 s^2} H\left[\begin{array}{c|c} \dfrac{m_{SR}m_{RD}}{s\bar{\gamma}_2} & \begin{matrix}0,1\\1,1\\2,1\\1,2\end{matrix} \\ \dfrac{m_{SD}}{s\bar{\gamma}_1} & \begin{matrix}1,2\\2,2\end{matrix} \end{array} \left| \begin{matrix} (-1;1,1) \\ (-3;2,2)) \\ (-1,2) \\ (m_{SR}-1,1),(m_{RD}-1,1) \\ (0,1),(-2,2) \\ (m_{SD}-1,1),(-1,1) \end{matrix} \right.\right]. \tag{4.25}$$

Using (4.20) and (4.25), an exact expression of the $P_{e,\mathrm{EGC}}$ can be obtained on splitting the limits of integral in (4.20) into two parts ranging from (0 to $\pi/2$) and ($\pi/2$ to $(M-1)\pi/M$). The expression can be written in terms of bivariate Fox-H function and trivariate Fox-H function [169, eq. (1.1)]. Trivariate Fox-H function is a triple contour integral, which has computational challenges in mathematical softwares like `MATLAB`. The issues are (i) identifying the SoA, which may not be straight forward and (ii) long computation time. Therefore, we use an approximation of (4.20) to simplify the numerical evaluation. The approximation can be obtained using the conditional SER expression $P_e(\gamma_\varphi) \approx a_M Q(\sqrt{2g\gamma_\varphi})$ mentioned in [19, Table 6.1], (4.24), and [156, eq. (4.2)]. That is

$$P_{e,\varphi} \approx \frac{a_M}{\pi}\int_0^{\frac{\pi}{2}} M_{\gamma_\varphi}\left(\frac{g}{\sin^2\theta}\right)d\theta\,, \tag{4.26}$$

where $a_M = 1$ for $M = 2$ (BPSK modulation scheme) and $a_M = 2$ for $M \geq 4$. The approximation in (4.26) is exact for BPSK and close for higher modulation orders. A simplified expression of $P_{e,\mathrm{EGC}}$ is analyzed in Appendix A.3 on substituting (4.25) in (4.26) for $\varphi = \mathrm{EGC}$ as

$$P_{e,\mathrm{EGC}} \approx \frac{a_M m_{SD} m_{SR} m_{RD}}{2\sqrt{\pi}\,\Gamma(m_{SD})\Gamma(m_{SR})\Gamma(m_{RD})\bar{\gamma}_1\bar{\gamma}_2 g^2} H\left[\begin{array}{c|c} \dfrac{m_{SR}m_{RD}}{g\bar{\gamma}_2} & \begin{matrix}(0,2)\\(2,2)\end{matrix} \\ & \begin{matrix}(2,1)\\(1,2)\end{matrix} \\ \dfrac{m_{SD}}{g\bar{\gamma}_1} & \begin{matrix}(1,2)\\(2,2)\end{matrix} \end{array}\middle| \begin{matrix}(-1;1,1),(-3/2;1,1)\\(-3;2,2),(-2;1,1)\\(-1,2)\\(m_{SR}-1,1),(m_{RD}-1,1)\\(0,1),(-2,2)\\(m_{SD}-1,1),(-1,1)\end{matrix}\right]. \tag{4.27}$$

An approximate expression of the end-to-end average SER can be obtained on substituting (4.23) and (4.27) in (4.19).

4.3.1.2 Without SD Link

We analyze the end-to-end average SER for the system when SD link is deeply faded. Therefore, data at the source S is transmitted using SR and RD links (SRD link) only. The data is correctly decoded at the destination D only if it is correctly received over both SR and RD links. Thus, the end-to-end conditional SER is given by

$$P_e(\gamma_{SR},\gamma_{RD}) = 1-(1-P_e(\gamma_{SR}))(1-P_e(\gamma_{RD})), \tag{4.28}$$

where $P_e(\gamma_{\varphi_2})$ is the conditional SER of $\varphi_2 \in \{SR, RD\}$ link and γ_{φ_2} is the corresponding instantaneous SNR defined as in (4.8a) and (4.8b). The end-to-end average SER is obtained by taking expectation of (4.28) as

$$\begin{aligned} P_e &= E[P_e(\gamma_{SR}, \gamma_{RD})] \\ &= 1 - (1 - P_{e,SR})(1 - P_{e,RD}), \end{aligned} \tag{4.29}$$

where $P_{e,SR} = E[P_e(\gamma_{SR})]$ and $P_{e,RD} = E[P_e(\gamma_{RD})]$. $P_{e,SR}$ is given in (4.23) for $\varphi_1 = SR$ and $P_{e,RD}$ is obtained using the MGF based approach. The PDF of the instantaneous link SNR $\gamma_{RD} = 2(t_2)^2$, where $t_2 = \nu_2|h_{SR}||h_{RD}|$ is obtained using (4.16) as

$$f_{\gamma_{RD}}(\gamma_{RD}) = \frac{m_{SR} m_{RD}}{\Gamma(m_{SR})\Gamma(m_{RD})\bar{\gamma}_{RD}} G_{0,2}^{2,0}\left[\frac{m_{SR} m_{RD}\gamma_{RD}}{\bar{\gamma}_{RD}}\middle| \begin{matrix} - \\ m_{SR}-1, m_{RD}-1 \end{matrix}\right], \tag{4.30}$$

where $\bar{\gamma}_{RD} = 2\bar{\gamma}_2$. The corresponding MGF is obtained on substituting (4.30) in (4.21) and following the steps adopted in Appendix A.1 as

$$M_{\gamma_{RD}}(s) = \frac{m_{SR} m_{RD}}{\Gamma(m_{SR})\Gamma(m_{RD}) s\bar{\gamma}_{RD}} G_{0,2}^{2,0}\left[\frac{m_{SR} m_{RD}}{s\bar{\gamma}_{RD}}\middle| \begin{matrix} 0 \\ m_{SR}-1, m_{RD}-1 \end{matrix}\right]. \tag{4.31}$$

An approximate and computationally efficient expression for the average SER of RD link can be analyzed on substituting (4.31) in (4.26) for $\varphi = RD$. Therefore, $P_{e,RD}$ is

$$P_{e,RD} \approx \frac{a_M\, m_{SR} m_{RD}}{\pi\Gamma(m_{SR})\Gamma(m_{RD})} \int_0^{\pi/2} \frac{\sin^2(\theta)}{g\bar{\gamma}_{RD}} G_{0,2}^{2,0}\left[\frac{m_{SR} m_{RD}\sin^2(\theta)}{g\bar{\gamma}_{RD}}\middle| \begin{matrix} 0 \\ m_{SR}-1, m_{RD}-1 \end{matrix}\right]. \tag{4.32}$$

A closed-form solution of (4.32) can be obtained using (4.13) and (A.11). Thus, we have

$$P_{e,RD} \approx \frac{a_M\, m_{SR} m_{RD}}{2\sqrt{\pi}\Gamma(m_{SR})\Gamma(m_{RD}) g\bar{\gamma}_{RD}} G_{2,3}^{2,2}\left[\frac{m_{SR} m_{RD}}{g\bar{\gamma}_{RD}}\middle| \begin{matrix} 0, -1/2 \\ m_{SR}-1, m_{RD}-1, -1 \end{matrix}\right]. \tag{4.33}$$

An approximate expression of the end-to-end average SER is obtained on substituting (4.23) and (4.33) in (4.29).

4.3.2 Asymptotic Average SER

In this subsection, high SNR approximations of the end-to-end average SER are analyzed for the system with and without SD link.

4.3.2.1 With SD Link

The end-to-end average SER in (4.19) for $\bar{\gamma}_\varphi \to \infty$ is given by

$$P_e^\infty \simeq P_{e,SR}^\infty P_{e,SD}^\infty + P_{e,\mathrm{EGC}}^\infty, \tag{4.34}$$

where $P_{e,SR}^\infty$, $P_{e,SD}^\infty$, and $P_{e,\mathrm{EGC}}^\infty$ are the high SNR approximations of $P_{e,SR}$, $P_{e,SD}$, and $P_{e,\mathrm{EGC}}$, respectively. Now, $P_{e,SD}^\infty$ and $P_{e,SR}^\infty$ can be obtained using the high SNR approximation of MGF in (4.22), that is, $M_{\varphi_1}(s) \approx (s\bar{\gamma}_{\varphi_1}/m_{\varphi_1})^{-m_{\varphi_1}}$ and (4.26) as

$$P_{e,\varphi_1}^\infty \approx \frac{a_M \Gamma(1/2+m_{\varphi_1})}{2\sqrt{\pi}\Gamma(1+m_{\varphi_1})} \left(\frac{m_{\varphi_1}}{g\bar{\gamma}_{\varphi_1}}\right)^{m_{\varphi_1}}. \tag{4.35}$$

In order to determine $P_{e,\mathrm{EGC}}^\infty$, we approximate PDF and MGF of γ_{EGC} at high SNR. Since EGC combines signal received via independent SD and RD links, PDF and MGF of γ_{EGC} are approximated at high SNR for each link individually.

The PDF in (4.16) is rewritten using (B.4) as

$$f_{t_2}(t_2) = \frac{4\,(t_2)^{(m_{SR}+m_{RD}-1)}}{\Gamma(m_{SR})\Gamma(m_{RD})} \left(\frac{m_{SR}m_{RD}}{\bar{\gamma}_2}\right)^{\left(\frac{m_{SR}+m_{RD}}{2}\right)} K_{m_{SR}-m_{RD}}\left(\sqrt{\frac{4m_{SR}m_{RD}(t_2)^2}{\bar{\gamma}_2}}\right), \tag{4.36}$$

where $K_r(y)$ is the r-th order modified Bessel's function of the second kind. Now, using the relation (B.6), (4.36) can be approximated for $\bar{\gamma}_2 \to \infty$. We find two cases while doing the approximation: *a)* $(m_{SR}-m_{RD})=0$ and *b)* $|m_{SR}-m_{RD}|>0$.

a) For $(m_{SR}-m_{RD})=0$: Let $m_{SR}=m_{RD}=m_a$, the approximation of (4.36) realized using (B.6) is

$$f_{t_2}^\infty(t_2) \approx \frac{-4\,(t_2)^{(2m_a-1)}}{(\Gamma(m_a))^2} \left(\frac{(m_a)^2}{\bar{\gamma}_2}\right)^{m_a} \ln\left(\sqrt{\frac{4{m_a}^2(t_2)^2}{\bar{\gamma}_2}}\right). \tag{4.37}$$

Using (4.37) and A.6, an approximation of $f_{\gamma_{\mathrm{EGC}}}(\gamma_{\mathrm{EGC}})$ is analyzed in Appendix A.4 as

$$\begin{aligned} f_{\gamma_{\mathrm{EGC}}}^\infty(\gamma_{\mathrm{EGC}}) \approx{}& \frac{2\Gamma(1+2m_{SD})\Gamma(2m_a)(m_{SD}+m_a)}{\Gamma(1+m_{SD})\Gamma(1+2m_{SD}+2m_a)(\Gamma(m_a))^2} \left(\frac{m_{SD}}{\bar{\gamma}_1}\right)^{m_{SD}} \left(\frac{(m_a)^2}{\bar{\gamma}_2}\right)^{m_a} \\ &\times\left(2\mathcal{D}_n - \frac{1}{(m_{SD}+m_a)} - \ln\left(\frac{4G^2(m_a)^2\gamma_{\mathrm{EGC}}}{\bar{\gamma}_2}\right)\right)(\gamma_{\mathrm{EGC}})^{(m_{SD}+m_a-1)}, \end{aligned} \tag{4.38}$$

where $\ln(G^2) = \sum_{n=1}^{\infty}(2(2m_a-1))/(n(n+2m_a-1))$ and $\mathcal{D}_n = (2m_{SD}+2m_a)\sum_{n=1}^{\infty}(\Gamma(n+2m_{SD}+2m_a))$

$/(n\Gamma(1+n+2m_{SD}+2m_a))$. The corresponding MGF is determined using (4.24), (4.38), (B.7) and (B.9) as

$$M^{\infty}_{\gamma_{\rm EGC}}(s) \approx \frac{2\Gamma(1+2m_{SD})\Gamma(2m_a)\Gamma(1+m_{SD}+m_a)}{\Gamma(1+m_{SD})\Gamma(1+2m_{SD}+2m_a)(\Gamma(m_a))^2}\left(\frac{m_{SD}}{s\bar{\gamma}_1}\right)^{m_{SD}}\left(\frac{(m_a)^2}{s\bar{\gamma}_2}\right)^{m_a} \times\left(2\mathcal{D}_n-\psi(m_{SD}+m_a)-\frac{1}{(m_{SD}+m_a)}-\ln\left(\frac{4G^2(m_a)^2}{s\bar{\gamma}_2}\right)\right), \quad (4.39)$$

where $\psi(\cdot)$ is digamma function [170, eq. (6.3.1)]. The high SNR approximation of $P_{e,\rm EGC}$ is obtained using (4.26) and (4.39) followed by some algebraic manipulations. The resultant expression is

$$P^{\infty}_{e,\rm EGC} \approx \frac{a_M\Gamma(1+2m_{SD})\Gamma(2m_a)\Gamma(1/2+m_{SD}+m_a)}{\sqrt{\pi}\Gamma(1+m_{SD})\Gamma(1+2m_{SD}+2m_a)(\Gamma(m_a))^2} \times\left(\frac{m_{SD}}{g\bar{\gamma}_1}\right)^{m_{SD}}\left(\frac{(m_a)^2}{g\bar{\gamma}_2}\right)^{m_a}\Bigg(-\psi(m_{SD}+m_a+1/2)+\psi(m_{SD}+m_a+1) -\psi(m_{SD}+m_a)-\frac{1}{(m_{SD}+m_a)}-\ln\left(\frac{4G^2(m_a)^2}{g\bar{\gamma}_2}\right)+2\mathcal{D}_n\Bigg). \quad (4.40)$$

We have used the relations $\int_0^{\pi/2}(\sin^2(\theta))^{m_{SD}+m_a}d\theta=(\sqrt{\pi}\Gamma(m_{SD}+m_a+1/2))/(2\Gamma(m_{SD}+m_a+1))$ and (B.10) to obtain the outcome presented in (4.40).

b) For $|m_{SR}-m_{RD}|>0$: In this case, an approximation of (4.36) is obtained using (B.6) as

$$f^{\infty}_{t_2}(t_2) \approx \frac{2\Gamma(|m_{SR}-m_{RD}|)}{\Gamma(m_{SR})\Gamma(m_{RD})}\left(\frac{m_{SR}m_{RD}}{\bar{\gamma}_2}\right)^{m_b}(t_2)^{2m_b-1}, \quad (4.41)$$

where $m_b=(m_{SR}+m_{RD}-|m_{SR}-m_{RD}|)/2$. Next, we obtain $f_{\gamma_{\rm EGC}}(\gamma_{\rm EGC})$ using (4.41) and adopting steps followed for analyzing (4.38) as

$$f^{\infty}_{\gamma_{\rm EGC}}(\gamma_{\rm EGC}) \approx \frac{\Gamma(1+2m_{SD})\Gamma(|m_{SR}-m_{RD}|)\Gamma(2m_b)}{\Gamma(1+m_{SD})\Gamma(m_{SR})\Gamma(m_{RD})\Gamma(2m_{SD}+2m_b)} \times\left(\frac{m_{SD}}{\bar{\gamma}_1}\right)^{m_{SD}}\left(\frac{m_{SR}m_{RD}}{\bar{\gamma}_2}\right)^{m_b}(\gamma_{\rm EGC})^{m_{SD}+m_b-1}. \quad (4.42)$$

Using (4.24) and (4.42), the approximate expression of MGF is written as

$$M^{\infty}_{\gamma_{\rm EGC}}(s) \approx \frac{\Gamma(1+2m_{SD})\Gamma(|m_{SR}-m_{RD}|)\Gamma(2m_b)}{\Gamma(1+m_{SD})\Gamma(m_{SR})\Gamma(m_{RD})\Gamma(2m_{SD}+2m_b)} \times\Gamma(m_{SD}+m_b)\left(\frac{m_{SD}}{s\bar{\gamma}_1}\right)^{m_{SD}}\left(\frac{m_{SR}m_{RD}}{s\bar{\gamma}_2}\right)^{m_{RD}}. \quad (4.43)$$

$P^{\infty}_{e,\mathrm{EGC}}$ can be analyzed using (4.26) and (4.43) as

$$P^{\infty}_{e,\mathrm{EGC}} \approx \frac{a_M \Gamma(1+2\,m_{SD})\Gamma(|m_{SR}-m_{RD}|)\Gamma(2m_b)\Gamma(m_{SD}+m_b)}{2\pi\Gamma(1+m_{SD})\Gamma(m_{SR})\Gamma(m_{RD})\Gamma(2m_{SD}+2m_b)} \times B\left(\frac{1}{2}, m_{SD}+m_b+\frac{1}{2}\right)\left(\frac{m_{SD}}{g\bar{\gamma}_1}\right)^{m_{SD}}\left(\frac{m_{SR}m_{RD}}{g\bar{\gamma}_2}\right)^{m_b}, \tag{4.44}$$

where $B(x,y)=\Gamma(x)\Gamma(y)/\Gamma(x+y)$ is beta function.

The high SNR approximations of $P^{\infty}_{e,\mathrm{EGC}}$ for $(m_{SR}-m_{RD})=0$ and $|m_{SR}-m_{RD}|>0$ in (4.40) and (4.44), respectively are unified as

$$P^{\infty}_{e,\mathrm{EGC}} \approx \frac{\mathcal{A}_1(\mathcal{B}_1+\rho_1\ln(\bar{\gamma}_2))}{(\bar{\gamma}_1)^{m_{SD}}(\bar{\gamma}_2)^{\mu_1}}. \tag{4.45}$$

$\mathcal{A}_1$, $\mathcal{B}_1$, μ_1, and ρ_1 are defined for each case as follows

a) For $(m_{SR}-m_{RD})=0$: $\mu_1=m_a$, $\rho_1=1$,

$$\mathcal{A}_1 = \frac{a_M\Gamma(1+2m_{SD})\Gamma(2m_a)\Gamma(1/2+m_{SD}+m_a)(m_{SD})^{m_{SD}}(m_a)^{2m_a}}{\sqrt{\pi}\Gamma(1+m_{SD})\Gamma(1+2m_{SD}+2m_a)(\Gamma(m_a))^2 g^{m_{SD}+m_a}}$$

and

$$\mathcal{B}_1 = \Bigg(-\psi(m_{SD}+m_a+1/2)+\psi(m_{SD}+m_a+1)-\psi(m_{SD}+m_a) - \frac{1}{(m_{SD}+m_a)}-\ln\left(\frac{4G^2(m_a)^2}{g}\right)+2\mathcal{D}_n\Bigg).$$

b) For $|m_{SR}-m_{RD}|>0$: $\mu_1=m_b$, $\rho_1=0$, $\mathcal{B}_1=1$ and

$$\mathcal{A}_1 = B\left(1/2, m_{SD}+m_b+1/2\right)(m_{SD})^{m_{SD}}(m_{SR}m_{RD})^{m_{SR}} \times\frac{a_M\Gamma(1+2m_{SD})\Gamma(|m_{SR}-m_{RD}|)\Gamma(2m_b)\Gamma(m_{SD}+m_b)}{2\pi\Gamma(1+m_{SD})\Gamma(m_{SR})\Gamma(m_{RD})\Gamma(2m_{SD}+2m_b)g^{m_{SD}+m_b}}.$$

Using (4.34), (4.35) and (4.45), asymptotic expression of the end-to-end average SER is given by

$$P^{\infty}_{e} \approx \frac{\mathcal{Z}_1}{(\bar{\gamma}_{SD})^{m_{SD}}(\bar{\gamma}_{SR})^{m_{SR}}}+\frac{\mathcal{A}_1(\mathcal{B}_1+\rho_1\ln(\bar{\gamma}_2))}{(\bar{\gamma}_1)^{m_{SD}}(\bar{\gamma}_2)^{\mu_1}}, \tag{4.46}$$

where

$$\mathcal{Z}_1 = \frac{(a_M)^2\Gamma(1/2+m_{SD})\Gamma(1/2+m_{SR})(m_{SD})^{m_{SD}}(m_{SR})^{m_{SR}}}{4\pi\Gamma(1+m_{SD})\Gamma(1+m_{SR})g^{m_{SD}+m_{SR}}}.$$

4.3.2.2 Without SD Link

The high SNR approximation of the end-to-end SER in (4.29) is given by

$$P_e^{\infty} \simeq P_{e,SR}^{\infty} + P_{e,RD}^{\infty}, \tag{4.47}$$

where $P_{e,SR}^{\infty}$ and $P_{e,RD}^{\infty}$ are the high SNR approximation of $P_{e,SR}$ and $P_{e,RD}$, respectively. $P_{e,SR}^{\infty}$ is same as (4.35) for $\varphi_1 = SR$ and $P_{e,RD}^{\infty}$ is determined using the high SNR approximation of the PDF expression in (4.30). Now, to determine $P_{e,RD}^{\infty}$, $f_{\gamma_{RD}}^{\infty}(\gamma_{RD})$ is obtained using (4.30), (B.4) and (B.6) for the cases: *a*) $(m_{SR} - m_{RD}) = 0$ and *b*) $|m_{SR} - m_{RD}| > 0$ as

$$f_{\gamma_{RD}}^{\infty}(\gamma_{RD}) \approx -\frac{(\gamma_{RD})^{m_a-1}}{(\Gamma(m_a))^2}\left(\frac{(m_a)^2}{\bar{\gamma}_{RD}}\right)^{m_a} \ln\left(\frac{4(m_a)^2\gamma_{RD}}{\bar{\gamma}_{RD}}\right) \tag{4.48}$$

and

$$f_{\gamma_{RD}}^{\infty}(\gamma_{RD}) \approx \frac{\Gamma(|m_{SR} - m_{RD}|)(\gamma_{RD})^{m_b-1}}{\Gamma(m_{SR})\Gamma(m_{RD})}\left(\frac{m_{SR}m_{RD}}{\bar{\gamma}_{RD}}\right)^{m_b}, \tag{4.49}$$

respectively. The corresponding average SER expressions for cases *a*) and *b*) can be analyzed on adopting the steps followed to analyze (4.40) and (4.44), respectively. Thus, the unified expression of $P_{e,RD}^{\infty}$ for the two cases can be written as

$$P_{e,RD}^{\infty} \approx \frac{\mathcal{A}_2(\mathcal{B}_2 + \rho_2 \ln(\bar{\gamma}_{RD}))}{(\bar{\gamma}_{RD})^{\mu_2}}. \tag{4.50}$$

$\mathcal{A}_2$, $\mathcal{B}_2$, ρ_2, and μ_2 are defined for each case as follows

a) For $(m_{SR} - m_{RD}) = 0$: $\mu_2 = m_a$, $\rho_2 = 1$, $\mathcal{A}_2 = (a_M\Gamma(1/2 + m_a)(m_a)^{2m_a})/(2\sqrt{\pi}\Gamma(m_a)\Gamma(1 + m_a)g^{m_a})$, and $\mathcal{B}_2 = -\psi(m_a) - \psi(m_a + 1/2) + \psi(m_a + 1) - \ln(4(m_a)^2/g)$.

b) For $|m_{SR} - m_{RD}| > 0$: $\mu_2 = m_b$, $\rho_2 = 0$, $\mathcal{B}_2 = 1$, and

$$\mathcal{A}_2 = \frac{a_M\Gamma(|m_{SR} - m_{RD}|)\Gamma(1/2 + m_b)\Gamma(m_b)(m_{SR}m_{RD})^{m_b}}{2\sqrt{\pi}\Gamma(m_{SR})\Gamma(m_{RD})\Gamma(1 + m_b)g^{m_b}}.$$

The asymptotic expression for the end-to-end average SER is obtained using (4.35), (4.47) and (4.50) as

$$P_e^{\infty} \approx \frac{\mathcal{Z}_2}{(\bar{\gamma}_{SR})^{m_{SR}}} + \frac{\mathcal{A}_2(\mathcal{B}_2 + \rho_2 \ln(\bar{\gamma}_{RD}))}{(\bar{\gamma}_{RD})^{\mu_2}}, \tag{4.51}$$

where

$$\mathcal{Z}_2 = \frac{a_M\Gamma(1/2 + m_{SR})(m_{SR})^{m_{SR}}}{2\sqrt{\pi}\Gamma(1 + m_{SR})g^{m_{SR}}}.$$

4.4 Resources Optimization

In this section, we optimize the fractions of the total energy assigned for slots T_1 and T_2, such that the asymptotic average SER obtained in (4.46) and (4.51) are minimum. The optimal value of energy is then used to determine the power transmitted in slots T_1 and T_2 and the corresponding slot duration.

The asymptotic average SER of the system with and without SD link in (4.46) and (4.51), respectively can be rewritten in terms of average link SNRs on considering[2] $\bar{\gamma}_1 = \bar{\gamma}_{SD}/2$ and $\bar{\gamma}_2 = \bar{\gamma}_{RD}/2$. Therefore, P_e^{∞} for the system with and without SD link are rewritten as

$$P_e^{\infty} = \frac{\mathcal{Z}_1}{(\mathrm{A}\bar{\gamma})^{m_{SD}}(\mathrm{B}\bar{\gamma})^{m_{SR}}(1-\beta_1)^{m_{SD}+m_{SR}}} + \frac{\mathcal{A}_1(\mathcal{B}_1 + \rho_1 \ln(\eta \mathrm{C}\bar{\gamma}\beta_1/2))}{(\mathrm{A}\bar{\gamma}/2)^{m_{SD}}(\eta \mathrm{C}\bar{\gamma}/2)^{\mu_1}(1-\beta_1)^{m_{SD}}(\beta_1)^{\mu_1}} \tag{4.52}$$

and

$$P_e^{\infty} = \frac{\mathcal{Z}_2}{(\mathrm{B}\bar{\gamma})^{m_{SR}}(1-\beta_1)^{m_{SR}}} + \frac{\mathcal{A}_2\big(\mathcal{B}_2 + \rho_2 \ln(\eta \mathrm{C}\bar{\gamma}\beta_1)\big)}{(\eta \mathrm{C}\bar{\gamma})^{\mu_2}(\beta_1)^{\mu_2}}, \tag{4.53}$$

respectively, where $\bar{\gamma} = PT/N_0$ and A, B, and C are channel gains of SD, SR, and SRD links, respectively. The channel gains are defined as $\mathrm{A} = \lambda_{SD}/(d_{SD})^{\alpha_{SD}}$, $\mathrm{B} = \lambda_{SR}/(d_{SR})^{\alpha_{SR}}$, and $\mathrm{C} = \lambda_{SR}\lambda_{RD}/\big((d_{SR})^{\alpha_{SR}}(d_{RD})^{\alpha_{RD}}\big)$. On applying the second-order conditions [158], it is easy to show that (4.52) and (4.53) are convex functions of $\beta_1 \in (0,1)$. This guarantees that an optimal value of β_1 exists in the range. We employ Golden-section search method [73] to identify optimal value of β_1 for the system with and without SD link. The optimal value of β_1 for the system with and without SD link are denoted by β_w^* and β_{wo}^*, respectively.

Using (4.11), the optimal solution of the energy consumed in T_2 is $(1-\beta_\iota^*)$, $\iota \in \{w, wo\}$. The optimal power transmitted by node S in the first two slots and the corresponding slot duration can be obtained using (4.12) and the optimal solution of energy for slots T_1 and T_2. Considering the optimal solution of τ is same for all the slots, that is, $\tau^* = 1/3$, (or $T_1 = T_2 = T_3 = T/3$); using (4.11) we get $P_1 + P_2 = 3P$, which implies the power-ratios P_1/P, $P_2/P \in (0,3)$. Hence, using (4.12) the optimal power allotted to slots T_1 and T_2 are given by $P_1^* = 3\beta_1^* P$ and $P_2^* = 3\beta_2^* P$, respectively. Similarly, considering the optimal solution of power transmitted in slots T_1 and T_2 is same, that is, $P_1^* = P_2^*$

[2]Substituting ν_1 and ν_2 from (4.7) into the definition of $\bar{\gamma}_1$ and $\bar{\gamma}_2$ in Section 4.3 and comparing the result with (4.10) yield the relation between $\bar{\gamma}_1$, $\bar{\gamma}_{SD}$, $\bar{\gamma}_2$, and $\bar{\gamma}_{RD}$.

$(= 2P/(1+\tau^*))$, then the optimal time-ratio is obtained using (4.11) and (4.12) as $\tau^* = \beta_1^*/(2-\beta_1^*)$.

4.4.1 Special Case: $m_{ij} = 1$ (Rayleigh Fading)

If the system is Rayleigh faded, the corresponding asymptotic expression of average SER can be realized by setting $m_{ij} = 1$ in (4.52) and (4.53) for the system with and without SD link, respectively. For fading parameter $m_{ij} = 1$, we have $\rho_1 = 1$, $\mu_1 = 1$, $\rho_2 = 2$, and $\mu_2 = 1$ in (4.52) and (4.53). Also, we get $\mathcal{Z}_1 = (a_M)^2/(16g^2)$, $\mathcal{A}_1 = a_M/(16g^2)$, $\mathcal{B}_1 = 0.0769 + \ln(g)$ for (4.52) and $\mathcal{Z}_2 = a_M/(4g)$, $\mathcal{A}_2 = a_M/(4g)$, $\mathcal{B}_2 = -0.4228 + \ln(g)$ for (4.53). `MATLAB` is used to solve the digamma function $\psi(\cdot)$ and simplify these constants. The values $\ln(G^2) = \sum_{n=1}^{\infty} 2(n(n+1))^{-1} \simeq 2$ and $\mathcal{D}_n = 4\sum_{n=1}^{\infty}(n(n+4))^{-1} \simeq 4 \times 0.5208$ are used to get the simplified form of $\mathcal{B}_1$. Thence, (4.52) and (4.53) can be written as

$$P_e^{\infty} = \frac{(a_M)^2}{16g^2 \mathrm{AB}\bar{\gamma}^2(1-\beta_1)^2} + \frac{a_M(\mathrm{D}_1 + \ln(\beta_1))}{4g^2\zeta \mathrm{AC}\bar{\gamma}^2(1-\beta_1)\beta_1} \tag{4.54}$$

and

$$P_e^{\infty} = \frac{a_M}{4g\mathrm{B}\bar{\gamma}(1-\beta_1)} + \frac{a_M(\mathrm{D}_2 + \ln(\beta_1))}{4g\zeta \mathrm{C}\bar{\gamma}\beta_1}, \tag{4.55}$$

respectively where $\mathrm{D}_1 = (0.0769 + \ln(g\zeta \mathrm{C}\bar{\gamma}/2))$ and $\mathrm{D}_2 = (-0.4228 + \ln(g\zeta \mathrm{C}\bar{\gamma}))$. The optimal value of β_1 can be obtained by differentiating (4.54) and (4.55) with respect to β_1 and equating it to zero, that is,

$$\frac{(a_M)^2}{8g^2\mathrm{AB}\bar{\gamma}^2(1-\beta_1)^3} - \frac{a_M\big((\mathrm{D}_1+\ln(\beta_1))(1-2\beta_1) - (1-\beta_1)\big)}{4g^2\zeta \mathrm{AC}\bar{\gamma}^2(\beta_1)^2(1-\beta_1)^2} = 0 \tag{4.56}$$

and

$$\frac{a_M}{4g\mathrm{B}\bar{\gamma}(1-\beta_1)^2} - \frac{a_M\big(-1 + (\mathrm{D}_2+\ln(\beta_1))\big)}{4g\zeta \mathrm{C}\bar{\gamma}(\beta_1)^2} = 0, \tag{4.57}$$

respectively. Equations (4.56) and (4.57) have a logarithmic term, which makes it difficult to simplify these equations to obtain the exact expression for optimal β_1. Therefore, we use the least square (LS) based approximation of $\ln(\beta_1)$ to obtain a suboptimal solution for β_1. In (4.56) and (4.57), $\ln(\beta_1)$ can be approximated as $\ln(\beta_1) \approx b_1\beta_1 + b_2$, where the coefficients $b_1 = 2.0209$ and $b_2 = -1.7963$ are evaluated in `MATLAB` using the relations of b_1 and b_2 given in [171]. Thus, (4.56) and (4.57) are

rewritten as

$$\frac{a_M}{2\mathrm{B}(1-\beta_1)} - \frac{\big(-1+b_2+\mathrm{D}_1+(1+b_1-2(b_2+\mathrm{D}_1))\beta_1-2b_1(\beta_1)^2\big)}{\zeta\mathrm{C}(\beta_1)^2} \;=\; 0 \tag{4.58}$$

and

$$\frac{1}{\mathrm{B}(1-\beta_1)^2} - \frac{-1+\mathrm{D}_2+b_2+b_1\beta_1}{\zeta\mathrm{C}(\beta_1)^2} \;=\; 0, \tag{4.59}$$

respectively. Equations (4.58) and (4.59) are cubic polynomials of the form

$$(\beta_1)^3 + a(\beta_1)^2 + b\beta_1 + c \;=\; 0\,, \tag{4.60}$$

where the coefficients are defined as

$$\begin{aligned} a &= \big(-1-3b_1+2(b_2+\mathrm{D}_1)-\zeta a_M\mathrm{C}/(2\mathrm{B})\big)/(2b_1), \\ b &= \big(2+b_1-3(b_2+\mathrm{D}_1)\big)/(2b_1), \quad \text{and} \\ c &= \big(-1+b_2+\mathrm{D}_1\big)/(2b_1) \end{aligned}$$

for the system with SD link and

$$\begin{aligned} a &= \big((-1+b_2+D_2)-2b_1-\zeta\mathrm{C}/\mathrm{B}\big)/b_1, \\ b &= \big(-2(-1+b_2+\mathrm{D}_2)+b_1\big)/b_1, \quad \text{and} \\ c &= \big(-1+b_2+\mathrm{D}_2\big)/b_1 \end{aligned}$$

for the system without SD link. We can see that the coefficients for the system with SD link are independent of the channel quality of SD link. Hence, the suboptimal resource allocation is independent of SD link quality under Rayleigh fading environment. Furthermore, the suboptimal resource allocation for the system without SD link is independent of a_M, that is, modulation oder.

Coefficients a, b, and c are real. Let $U = (a^2 - 3b)/9$ and $V = (2a^3 - 9ab + 27c)/54$, then at high SNRs $V^2 < U^3$ holds. The three real roots of (4.60) are obtained using [172, p. 179] as $\beta_{1,1} = -2\sqrt{U}\cos(\theta/3) - a/3$, $\beta_{1,2} = -2\sqrt{U}\cos((\theta+2\pi)/3) - a/3$, and $\beta_{1,3} = -2\sqrt{U}\cos((\theta-2\pi)/3) - a/3$, where $\theta = \arccos\big(V/\sqrt{U^3}\big)$. Hence, the suboptimal solution of β_1 for the system with and without

SD link denoted by β_w^+ and β_{wo}^+, respectively can be obtained as

$$\beta_\iota^+ = \beta_{1,\ell}\,, \quad \text{if} \quad \beta_{1,\ell} \in (0,1)\,, \quad \text{for} \quad \ell = \{1,2,3\}, \quad \iota \in \{w, wo\}\,. \tag{4.61}$$

Using (4.11) and (4.61), the suboptimal solution for the energy consumed in T_2 is $(1-\beta_\iota^+)$. Since, the suboptimal value for the fraction of total energy consumed in T_1 and T_2 is known, the suboptimal power and time for the respective slot can be found using (4.12). Similar to the optimal resource allocation in case of Nakagami-m fading, we consider two cases when i) the three time slots are equally divided, that is, $T_1 = T_2 = T_3 = T/3$ or $\tau = 1/3$ and ii) power transmitted in slots T_1 and T_2 is same, that is, $P_1 = P_2$. In case i), the suboptimal power allocated in slots T_1 and T_2 can be obtained using (4.12) as $P_1^+ = 3\beta_1^+ P$ and $P_2^+ = 3\beta_2^+ P$, respectively. In case ii), the suboptimal value of τ found using (4.11) and (4.12) is $\tau^+ = \beta_1^+/(2-\beta_1^+)$.

4.5 Diversity Order and Throughput

The analytical and asymptotic average SER expressions obtained in the earlier sections can be used to investigate the DO and the throughput of the system.

4.5.1 Diversity Order

The asymptotic average SER expressions in (4.46) and (4.51) can be used to analyze the achievable DO of the system with and without SD link, obtained using (3.68) as

$$\mathrm{DO}_1 \;=\; \min\left\{m_{SD} + m_{SR}, \left(m_{SD} + \mu_1 - \rho\frac{\ln(\ln(\bar{\gamma}))}{\ln(\bar{\gamma})}\right)\right\} \tag{4.62}$$

and

$$\mathrm{DO}_2 \;=\; \min\left\{m_{SR}, \left(\mu_2 - \rho\frac{\ln(\ln(\bar{\gamma}))}{\ln(\bar{\gamma})}\right)\right\}, \tag{4.63}$$

respectively, where $\rho = 1$ for $m_{SR} = m_{RD}$ and $\rho = 0$ otherwise. At high SNRs, $\bar{\gamma} = PT/N_0$ is the limiting variable in (4.62) and (4.63). Consider $m_{SR} = m_{RD}$, then at high SNRs DO_1 and DO_2 vary logarithmically with SNR and the maximum value is achieved when $\ln(\ln(\bar{\gamma}))/\ln(\bar{\gamma})$ tends to 0. This suggests that when the fading parameters of SR and RD links are identical, maximum DO is achieved at a rate slower than that of the conventional relay systems [72, 73].

4.5.2 Throughput

We define throughput for the system as

$$\xi \;=\; \left(\frac{1-\tau}{2}\right)\left(\frac{\log_2(M)}{2}\right)(1-P_b), \tag{4.64}$$

where $(1-\tau)/2$ is the fraction of total time used for non-repeated data transmission, that is, T_2/T, $(\log_2(M))/2$ is the count of bits communicated per second per Hertz (bps/Hz) for the given modulation order M [3, eq. (6.52)], and P_b is the average BER at the destination. The average BER can be defined in terms of average SER by $P_b \approx P_e/\log_2(M)$, where P_e is the average end-to-end SER for the system. In case of system without direct link, P_e is obtained on substituting (4.23) and (4.33) in (4.29), whereas for the system with direct link P_e is found by putting (4.23) and (4.27) in (4.19). At high SNR, $P_b \to 0$, thus

$$\xi \;\approx\; \left(\frac{1-\tau}{2}\right)\left(\frac{\log_2(M)}{2}\right). \tag{4.65}$$

Note that, throughput of the system employing the transmission technique given in Figure 4.1 is less than that of the conventional relay system by a factor of $(1-\tau)$. Throughput of the conventional relay system can be approximated as $\log_2(M)/4$. As τ tends to 0, throughput of the system is close to that of the conventional relay system. Furthermore, the throughput defined in (4.64) is a communication theoretic performance metric and differs from that used in [41, 125] and other references, which measure the throughput as a function of information theoretic performance matrices, outage probability, capacity, etc.

4.6 Numerical Results

In this section, numerical results for the performance metrics analyzed in Sections 4.3, 4.4, and 4.5 are plotted to examine the performance of the WP DF relay system. The expressions for the average SER are derived in terms of univariate Meijer-G and bivariate Fox-H functions which are evaluated in `MATLAB 13a` using the *Mupad* package and [165, Appendix], respectively. The system model described in Section 4.2 is emulated in `MATLAB` to obtain the simulation results. Energy conversion efficiency ζ, time T, and channel gains are considered to be unity unless otherwise stated, thus $\zeta = 1$, $T = 1$, and $\lambda_{ij}(d_{ij})^{-\alpha_{ij}} = 1$. $\zeta = 1$ corresponds to maximum energy conversion efficiency. The noise PSD is considered as $N_0 = 10^{-4}$ watts per hertz (W/Hz) and the average transmission power P is represented in dBm.

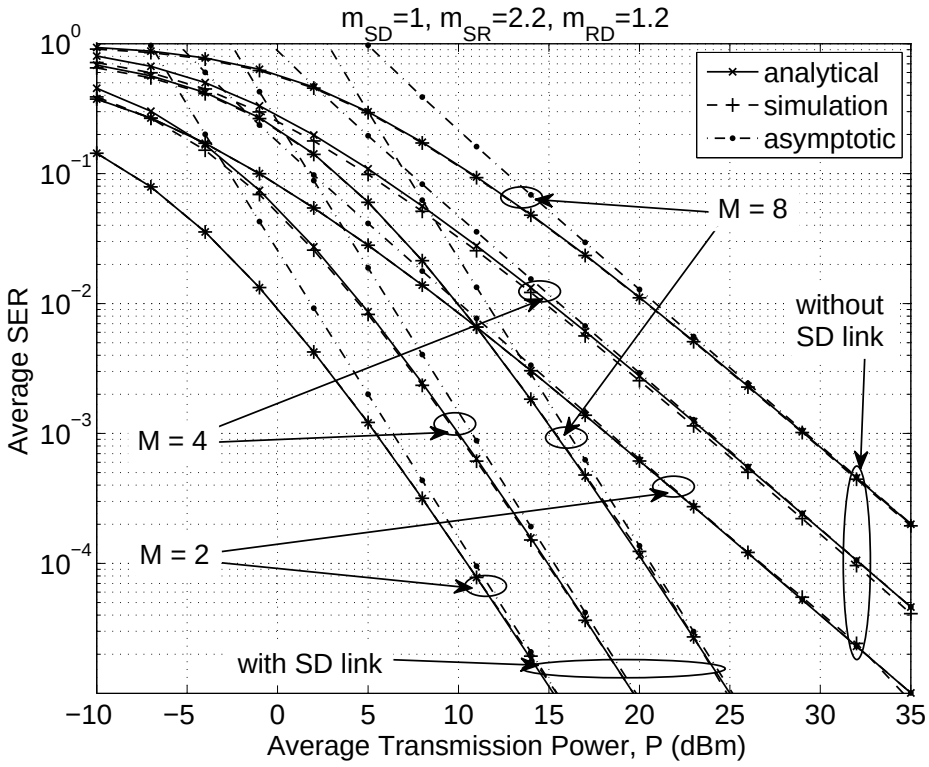

Figure 4.2: Comparison of average SER for WP three-node DF relay system with and without direct (SD) link with respect to average transmission power P.

Figure 4.2 compares the average SER performance of the WP DF relay system with and without direct (SD) link with respect to the average transmission power P. The results are plotted for modulation orders $M = 2, 4, 8$ and fading parameters $m_{SD} = 1$, $m_{SR} = 2.2$, $m_{RD} = 1.2$. We consider that the total transmission time is equally divided among all the three slots, that is, $\tau = 1/3$. The power assigned to the source in T_1 is assumed as $P_1/P = x = 1$, therefore using (4.11) $P_2/P = 3 - x = 2$. In case of the system with SD link, analytical results are computed by substituting (4.23) and (4.27) in (4.19), whereas for the system without SD link average SER is plotted using (4.23), (4.29), and (4.33). Simulation results are also shown and they are found to be in perfect agreement with the analytical results, thus validating our analysis. The corresponding asymptotic results are plotted using (4.46) and (4.51), and they are found to be close approximation of the average SER at high SNRs. Note that, for $|m_{SR} - m_{RD}| = 0$ asymptotic average SER may result in a relatively loose bound.

In Figure 4.3, plots for average SER versus average transmission power are shown for different fading parameters m_{ij} and 4-PSK ($M = 4$) when direct link is considered. Slot durations and trans-

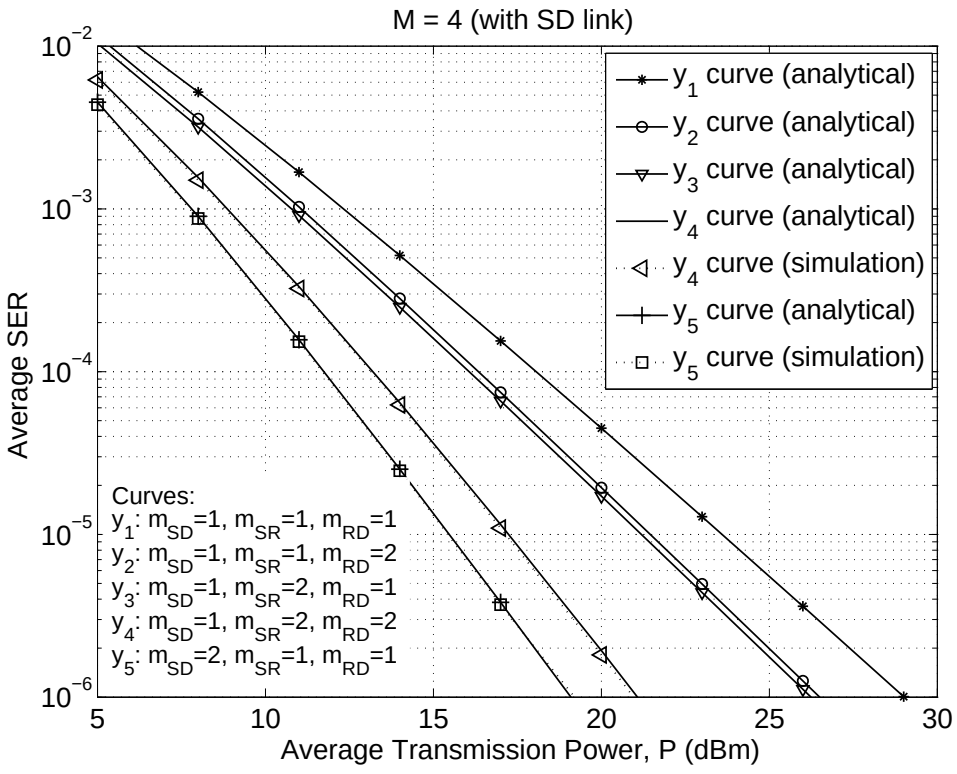

Figure 4.3: Average SER versus average transmission power P with variation in fading parameters m_{ij}.

mission power are assumed to be same as considered for Figure 4.2. In Figure 4.3, it is observed that the average SER decreases with increase in m_{ij}, implying improvement in performance of the system. Also, the effect of increment in m_{SR} is more on the system performance when compared to m_{RD}. This is because the increment in m_{SR} corresponds to better connectivity between the source and the relay. Thus, enhancing EH and the detection capability at node R. Increment in m_{RD} corresponds to better RD link quality, which adds to the system performance if data is correctly decoded at node R. It can also be observed from the figure that there is a significant improvement in performance when fading parameter of both SR and RD links increases.

In Figures 4.4 and 4.5, variation of average SER versus average transmission power is plotted for the WP relay system with and without SD link for different value of β_1. 4-PSK modulation scheme ($M = 4$) is considered and fading parameters are taken as $m_{SD} = 1$, $m_{SR} = 2$, and $m_{RD} = 2$. In Figure 4.4, τ is considered to be 1/3, that is, $T_1 = T_2 = T_3$, and plots corresponding to different fractions of total transmitted power in the first time slot $x = P_1/P$ are shown. Plot for optimal $x^*(= 3\beta_1^*)$ is also shown in Figure 4.4. In Figure 4.5, power transmitted in slots T_1 and T_2 are considered to be equal $P_1 = P_2$ and plots for different value of τ are shown. Plot for optimal $\tau^*(= \beta_1^*/(2 - \beta_1^*)$ is

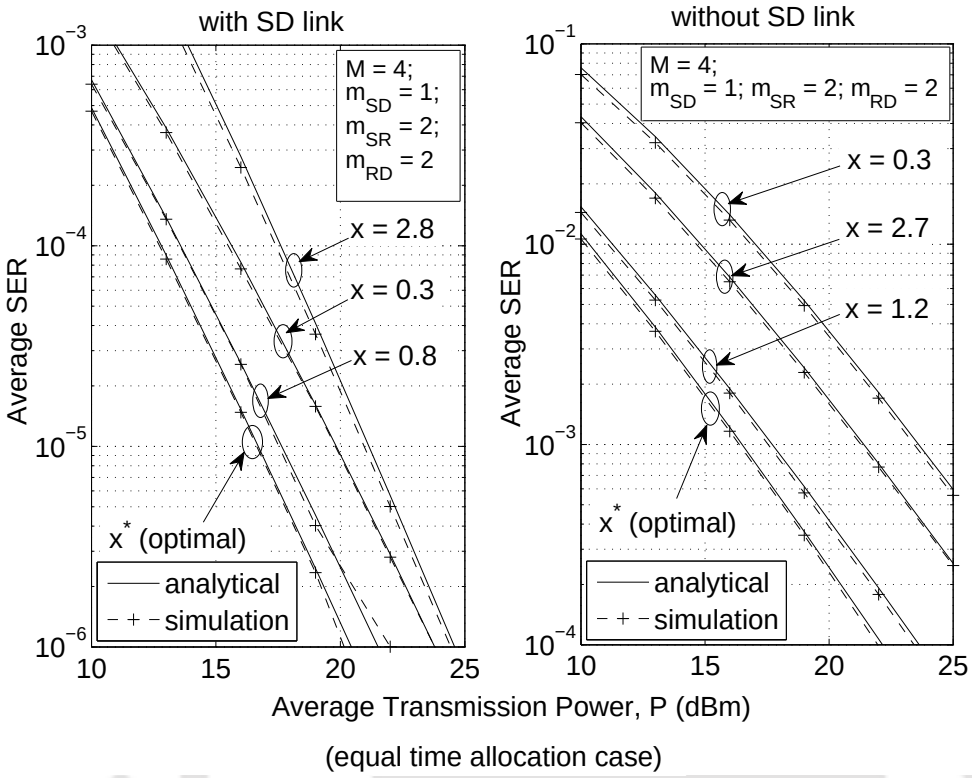

Figure 4.4: Variation of average SER with the average transmission power P for $\tau = 1/3$.

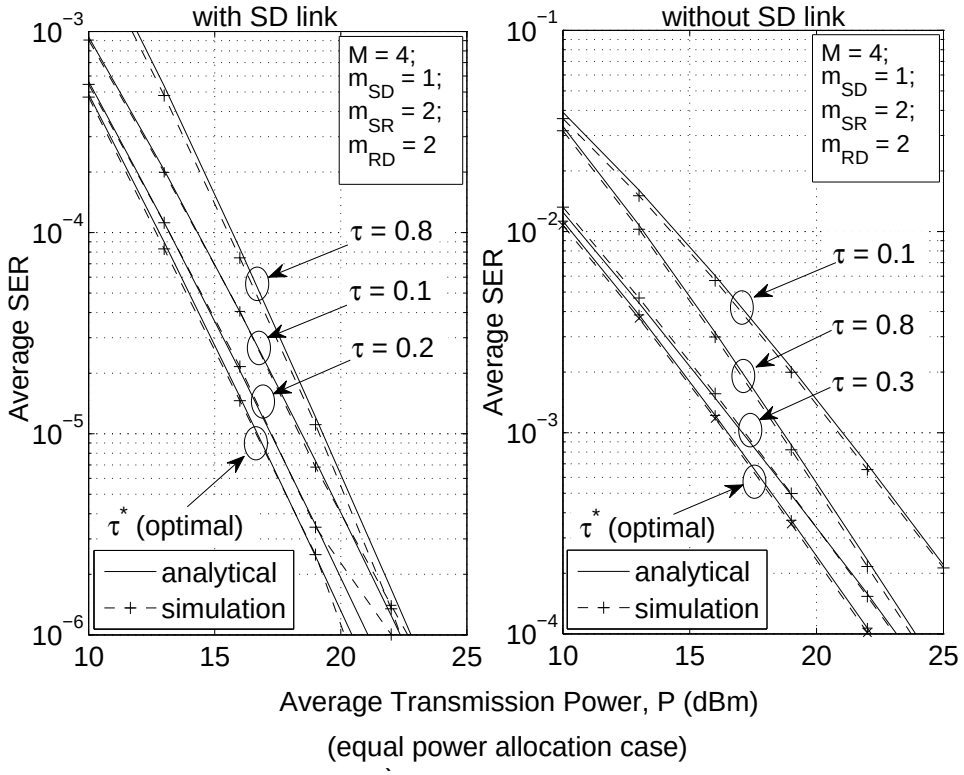

Figure 4.5: Variation of average SER with the average transmission power P for $P_1 = P_2$.

Abstract-TH-2151_136102001

also shown. We observe that the average SER for optimal resource allocation is minimum as seen in Figures 4.4 and 4.5. It is also observed that the average SER for plots corresponding to optimal power and optimal time allocation are same. This is because of the same optimal energy consumption in the respective phases. Furthermore, values of x^* and τ^* are smaller for the system with SD link than that of the system without SD link. The reason is, presence of direct link offers diversity advance and improves the performance of the system. Thus, reducing the optimal value of x^* and τ^* for the slot T_1. In this scenario, more energy can be assigned to the source for transmission in T_2.

Variation of average SER for different d_{SR} is shown in Figure 4.6 for average transmission power $P = 20$ dBm, $x = 0.5$, and $\tau = 1/3$. 4-PSK modulation scheme ($M = 4$) is considered and fading parameters are taken as $m_{SD} = 0.6$, $m_{SR} = 2.1$, and $m_{RD} = 1.5$. The three nodes are considered to be coplanar, therefore $d_{SR} + d_{RD} \geq d_{SD}$. A pictorial representation of a two-dimensional nodes placement and relay location is shown in Figure 4.7.[3] In Figure 4.6, Nodes S and D are 2 unit apart and the path loss exponent of all the links is considered to be $\alpha_{ij} = 3$. We further assume that each link possesses unit mean power, that is, $\lambda_{ij} = 1$. The analysis we present below follows for different values of d_{SD}, α_{ij}, and λ_{ij} as well. It is observed from Figure 4.6 that the performance is better if node R is located close to node S. The performance degrades when node R moves away from node S and then improves when node R is close to node D. This is due to the fact that when node R is close to node S, more energy can be harvested at R in slot T_1, hence higher P_3 is available at node R for transmission in slot T_3, covering a relatively farther destination. Similarly, when node R is close to node D, relatively small energy can be stored at node R in slot T_1, but the energy is sufficient for communication to the destination. Since the distance d_{RD} is relatively smaller. Hence, the system performs better when node R is close to either the source or the destination. We observe from Figure 4.6, the optimal location of node R is closer to node S [41,75]. Also, the improvement in performance on the optimum resource allocation for different d_{SR} is more in the system without SD link. The crossover of curves suggests that on optimal resource allocation the system without SD link may perform better than the system with SD link. The possibilities are more when node R is located close

[3] In Figure 4.7, the inter-node distance follows the relation $d_{SR} + d_{RD} = \beta d_{SD}$, $\beta \geq 1$. The three nodes are collinear for $\beta = 1$, which is represented by path β_0. The non-collinear paths are represented by β_1, β_2 for $\beta_2 > \beta_1 > \beta$, $\beta > 1$. For any value of β other than unity there exist two paths, one in the upper half of the SD line and another in the lower half. The analysis for the two paths corresponding to β_1, β_2 or any $\beta > 1$ remain same. A more compact two-dimensional node placement has been considered in [126], where relay location follows an elliptical path. The consideration of nodes placement as in Figure 4.7 provides relatively simplified analysis, as relay paths are controlled by a single factor β. Note that, the notations β_1, β_2 refer to relay paths only when we refer to Figure 4.7, otherwise they are meant for energy fractions (4.12).

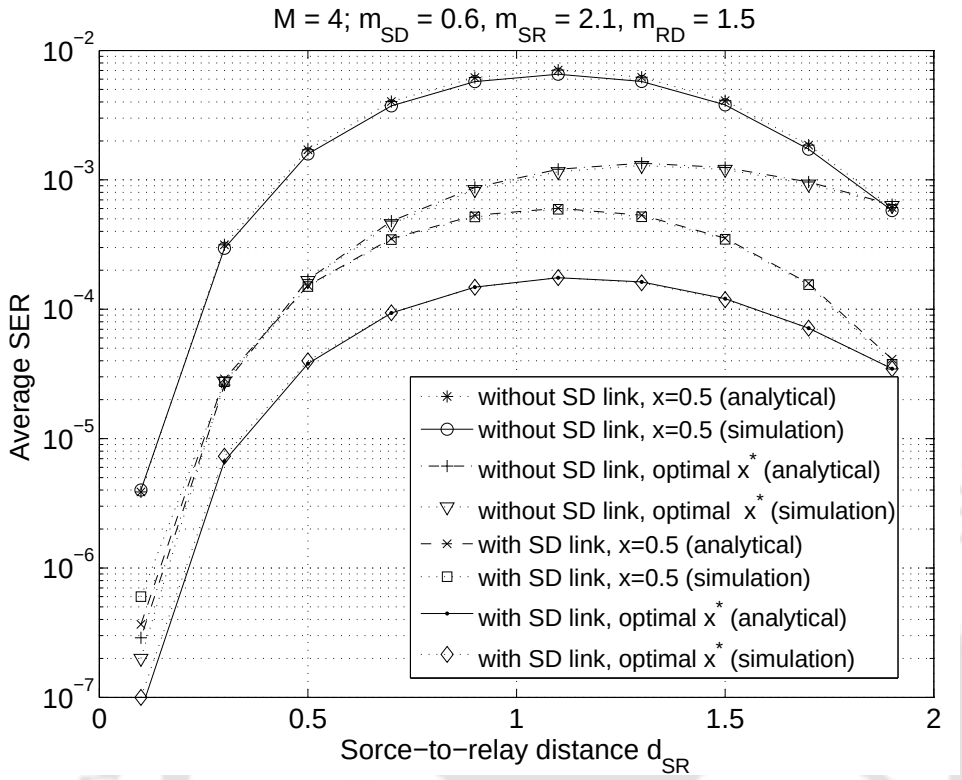

Figure 4.6: Variation of average SER with d_{SR} for $d_{SR} + d_{RD} = \beta d_{SD}$, $\beta = 1.1$, $d_{SR} \in (0, d_{SD})$, $d_{SD} = 2$ unit.

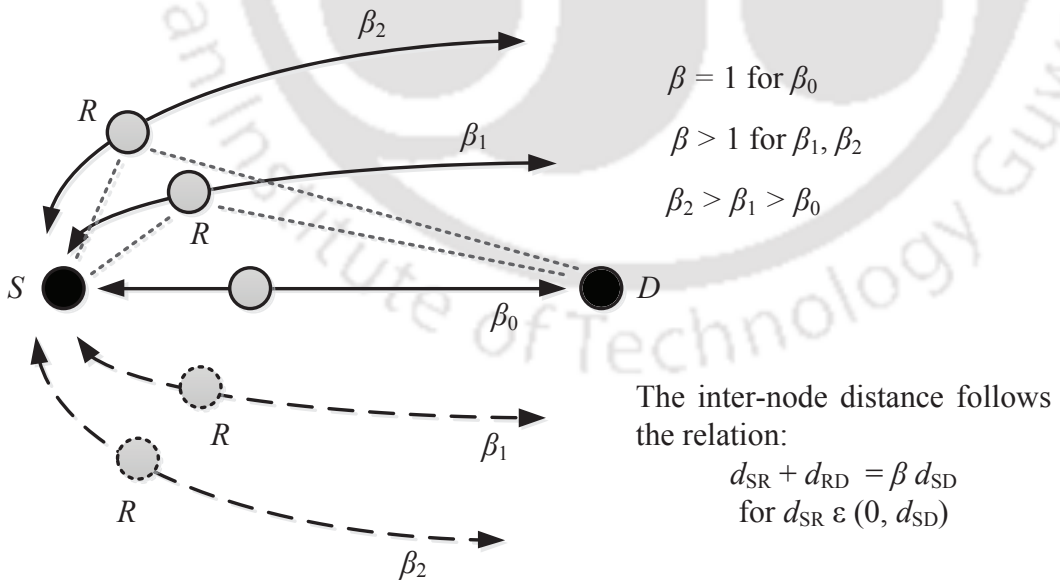

Figure 4.7: An illustration of a two-dimensional nodes placement and relay location.

to node S. On optimal resource allocation the system with SD link outperforms the system without SD link.

In Figure 4.8, average SER versus d_{SR} plots are shown to check the variation in the optimal relay location with change in the values of energy conversion efficiency, $\zeta \in \{0.4, 0.6, 0.8, 1.0\}$. The system with SD link is considered and results are shown for 4-PSK modulated data. The nodes placement, fading parameters, and values of P, x, τ are considered as in Figure 4.6. We observe from Figure 4.8 that the optimal relay location lies near the source node for all values of ζ. With increase in ζ, the system's performance improves and the relative improvement in the performance decreases. Similar analysis follows for the system without SD link and the systems enabled with optimal resource allocation.

Further, variation of average SER with d_{SR} for different values of $\beta \in \{1.0, 1.1, 1.3, 1.5, 1.7, 1.9\}$ is shown in Figure 4.9. The system with SD link is considered. The modulation scheme, resource allocation, and fading parameters are chosen as in Figures 4.6 and 4.8. Maximum energy conversion efficiency is assumed, that is, $\zeta = 1$. We observe from Figure 4.9 that the system's performance degrades with increase in β, as expected. Moreover, the optimal relay location lies near the source node for all values of β. Similar analysis follows for the system without SD link and the systems enabled with optimal resource allocation.

In Figure 4.10, average SER of WP relaying system with and without SD link is plotted with P_1/P for $\lambda_{SR} \in \{1, 10\}$, $\lambda_{RD} \in \{1, 10\}$, $\lambda_{SD} = 1$, and $\tau = 1/3$. BPSK modulation scheme is considered and fading parameters are taken as $m_{ij} = 1$. The performance is compared with that of direct transmission for mean power $\lambda_{SD} = 1$. Nodes are considered to be coplanar and node R is placed at $d_{SR} = 0.3 d_{SD}$ for the node arrangement as in Figure 4.6. The path loss exponent of all the links is considered to be equal, $\alpha_{ij} = 3$. The average transmission power for the WP relay system is taken as 20 dBm, which is same as the transmission power in case of direct transmission. We consider equal total transmission time for WP relaying and direct transmission.

In WP system, the power-ratio varies in the range $P_1/P \in (0, 3)$, whereas it is constant for direct transmission. Therefore, direct transmission exhibits constant average SER for different P_1/P. For the assumptions considered, it can be observed from the figure that the WP relaying system with SD link outperforms the other two systems. Also, the WP relaying system without SD link performs better than direct transmission for improved channel conditions. On optimal resource allocation (power in

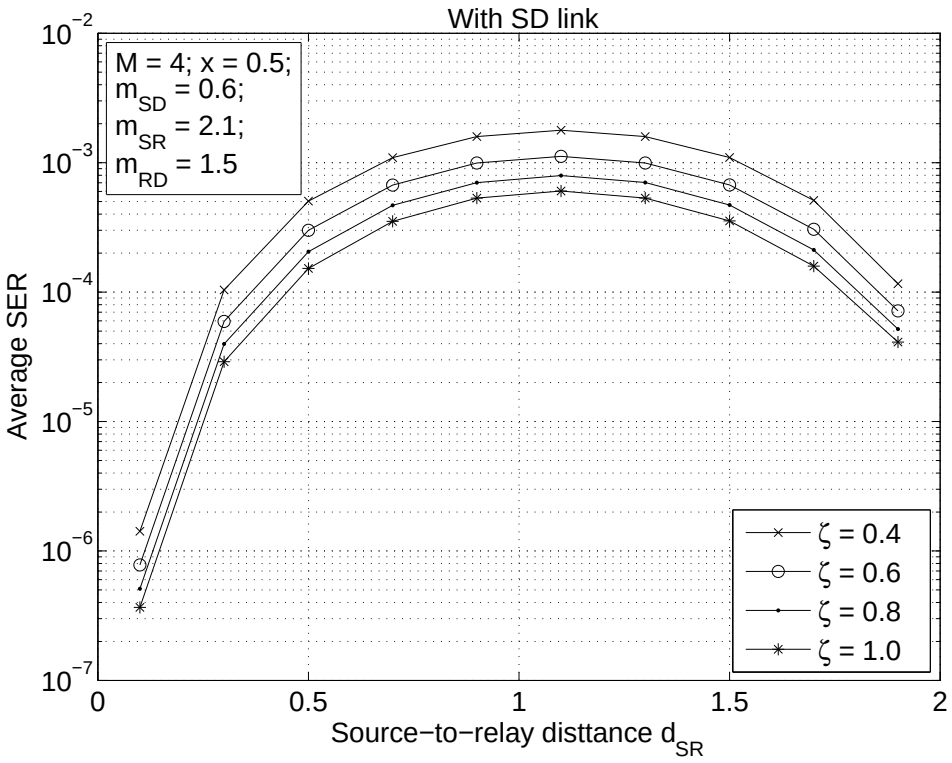

Figure 4.8: Variation of average SER with d_{SR} for different values of ζ, $d_{SR} + d_{RD} = \beta d_{SD}$, $\beta = 1.1$, $d_{SR} \in (0, d_{SD})$, $d_{SD} = 2$ unit.

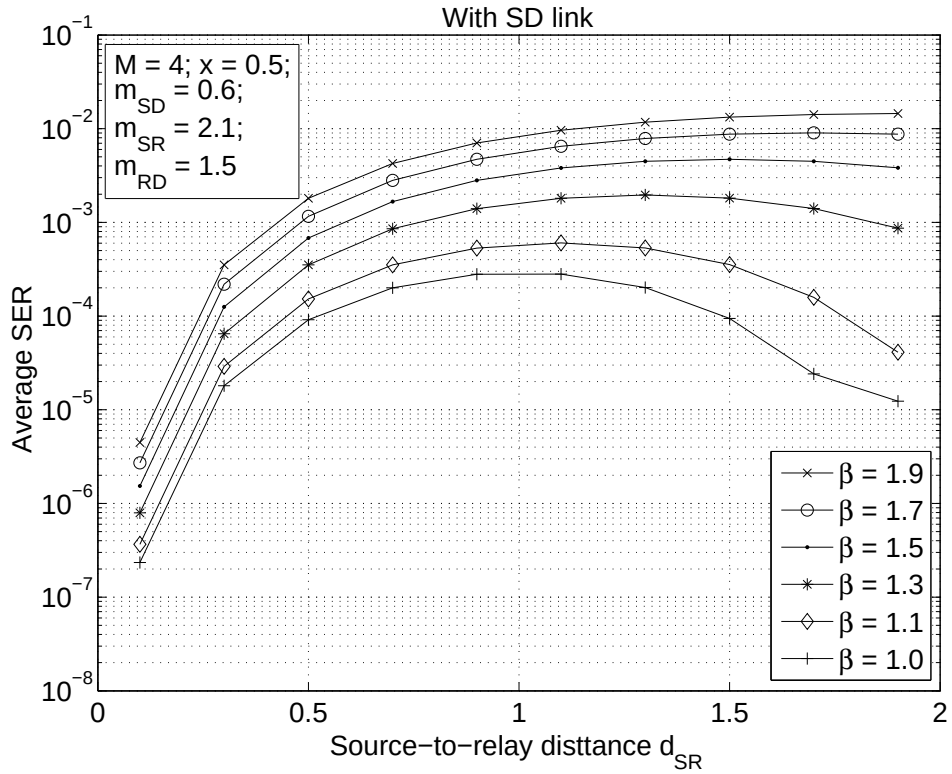

Figure 4.9: Variation of average SER with d_{SR} for different values of β, $d_{SR} + d_{RD} = \beta d_{SD}$, $d_{SR} \in (0, d_{SD})$, $d_{SD} = 2$ unit, $\zeta = 1$.

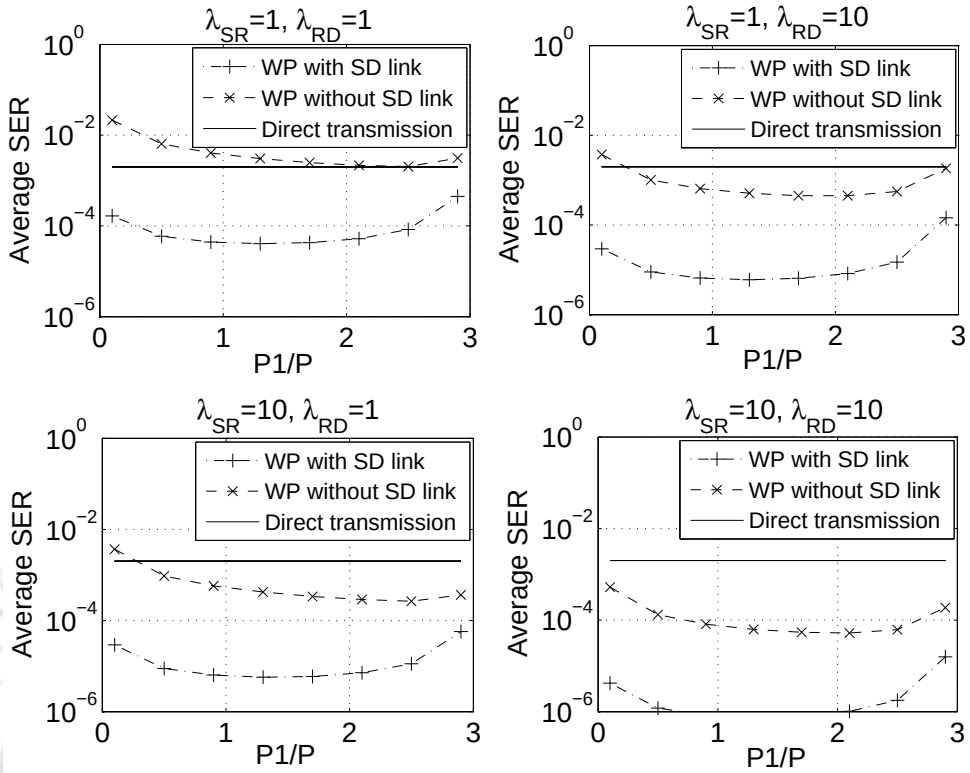

Figure 4.10: Average SER comparison of the WP relay system and direct transmission for $M = 2$, $m_{ij} = 1$, and different mean power for each link $\lambda_{SR} \in \{1, 10\}$, $\lambda_{RD} \in \{1, 10\}$, and $\lambda_{SD} = 1$.

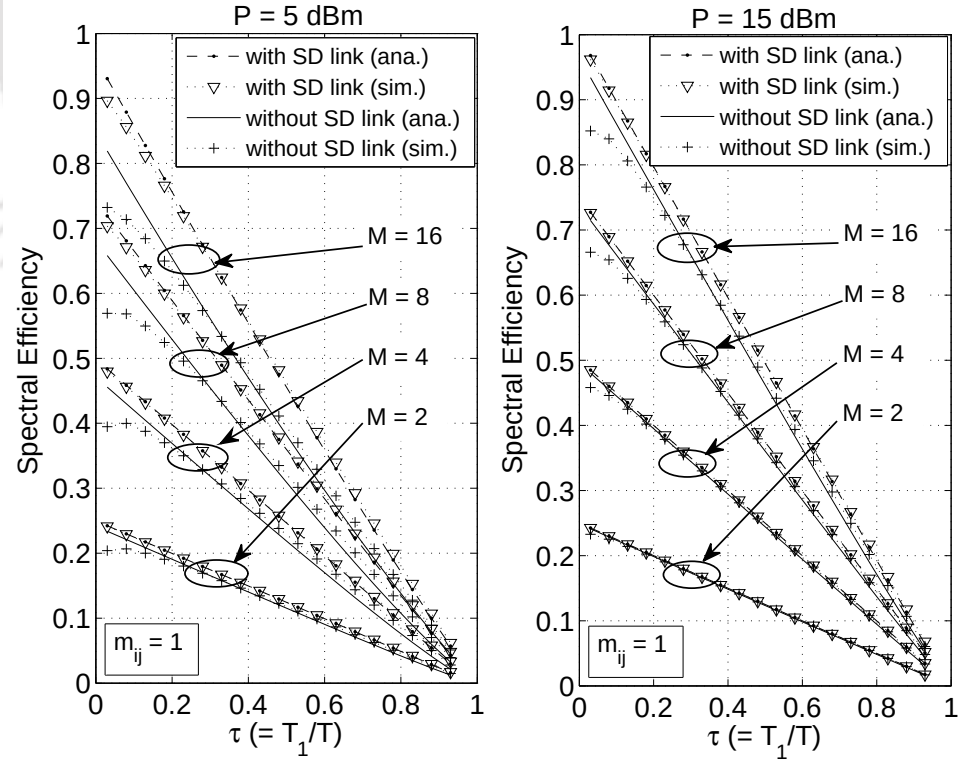

Figure 4.11: Plot for throughput versus τ in WP DF relay system with and without SD link. Abbreviations: ana. – analytical, sim. – simulation.

this case), the performance can be significantly improved when compared to direct transmission. This analysis can be useful for power allocation in different time slots assimilating Federal Communications Commission limits. A similar analysis can be followed for $P_1 = P_2$, which can be useful in setting different data transmission rate for varying channel conditions. Moreover, depending on the channel conditions, the analysis can be used in deciding whether to transmit data directly from source to destination or through the relay in presence or absence of SD link.

In Figure 4.11, we consider equal power allocation case ($P_1 = P_2 = 2P/(1+\tau)$) to plot throughput in (4.64) versus τ for WP system with and without SD link. Modulation orders $M = 2, 4, 8, 16$ are considered and fading parameter of each link is taken as $m_{ij} = 1$. The deviation between the analytical and the simulation results is because of the approximate relationship between the BER and the SER. We observe from the plot that the throughput improves with increase in modulation order M and the average transmission power (P). The system with SD link posses better throughput than the system without SD link.

Table 4.1 compares the suboptimal solution (β_1^+) obtained using (4.61) and the optimal solution (β_1^*) numerically evaluated solving (4.54) and (4.55) with the help of Golden-section search method for the system with and without SD link under Rayleigh fading. Comparison is shown for BPSK and 4-PSK modulation schemes with variation in P. The corresponding asymptotic average SERs evaluated for β_1^+ and β_1^* are also shown. It is observed that the solutions β_1^+ and β_1^* obtained using these two methods are in close proximity and the difference reduces further with the increase in P. Moreover, line search methods involve multiple iterations to find out the optimal solution and hence can take long computational time. Therefore, (4.60) and (4.61) can be used to efficiently compute suboptimal solutions of the energy assigned to each slot for minimum average SER under Rayleigh fading. We further observe that the average SERs computed for β_1^+ and β_1^* are same. Also, the energy allocations and corresponding average SERs in the system without SD link are independent of modulation order.

4.7 Conclusion

This chapter presents performance analysis of a three-node DF relay system with WP relay node. Data is considered to be M-PSK modulated and channels are Nakagami-m faded. The data at source is communicated to destination in three time slots; the first slot is employed for WPT and the other two slots are used for WIT. The source node is assumed to have a dedicated power supply. The analysis is

Table 4.1: Comparison of suboptimal (β_1^+) and optimal (β_1^*) energy allotted to slot T_1 and corresponding average SER under Rayleigh fading for $\lambda_{ij}(d_{ij})^{-\alpha_{ij}} = 1$.

System	M	Energy and average SER	P (dBm)			
			10	15	20	25
with SD link	2	β_1^+	0.3750	0.4123	0.4318	0.4440
		P_e^∞	3.4×10^{-4}	4.6×10^{-5}	5.8×10^{-6}	6.9×10^{-7}
		β_1^*	0.3778	0.4140	0.4329	0.4447
		P_e^∞	3.4×10^{-4}	4.6×10^{-5}	5.8×10^{-6}	6.9×10^{-7}
	4	β_1^+	0.3040	0.3753	0.4057	0.4236
		P_e^∞	2.2×10^{-3}	3.2×10^{-4}	4.2×10^{-5}	5.1×10^{-6}
		β_1^*	0.3579	0.3975	0.4186	0.4321
		P_e^∞	2.2×10^{-3}	3.2×10^{-4}	4.2×10^{-5}	5.1×10^{-6}
without SD link	2	β_1^+	0.6189	0.6632	0.6929	0.7148
		P_e^∞	2.1×10^{-2}	8.2×10^{-3}	3.0×10^{-3}	1.1×10^{-3}
		β_1^*	0.6220	0.6646	0.6935	0.7151
		P_e^∞	2.1×10^{-2}	8.2×10^{-3}	3.0×10^{-3}	1.1×10^{-3}
	4	β_1^+	0.6189	0.6632	0.6929	0.7148
		β_1^*	0.6220	0.6646	0.6935	0.7151

presented for the system with and without the SD link. We consider MGF based approach to analyze the expressions of the average SER. High SNR approximations of the average SER are also obtained to optimize the resources assigned for each slot and determine DO and throughput of the system. The following observations are made: i) the system performs best on optimal resource allocation, ii) the average SER and the throughput of the system enhance with increase in M, iii) increment in m_{SR} results in better performance when compared to increase in m_{RD}, and iv) the performance improves if the relay node is placed close to either source or destination; optimal results are achieved when relay is placed close to source. The average SER and the throughput of the system with direct link is always better when compared to the system without direct link for given energy assigned to each slot or on optimal resource allocation. We also analyze suboptimal resource allocation for the special case when $m_{ij} = 1$, which corresponds to Rayleigh fading. The suboptimal and optimal resource allocation are in close proximity at high SNRs.

Abstract-TH-2151_136102001

5

WP DF Relay System under Nakagami-m and $\kappa-\mu$ Shadowed Fading: EH at Source Node

Contents

In this chapter, we examine the average SER of a WP relay system where the source node is energy-constrained and harvests energy using RF signal radiated by the relay node. The energy-constrained source node needs to harvest energy before it starts transmitting data. The analysis for such systems can be vital in applications like wireless sensor networks, wireless body area networks, machine-to-machine communication, and internet of things (IoT) entities, such as, smart home, medical implant, etc., [66, 67].

5.1 Introduction

In the literature on wireless EH, relay node(s) are mostly considered to be energy-constrained and wirelessly powered by source node(s), interferes, or dedicated power transmitter(s) [41, 70, 71, 74]. However, in certain scenarios relay nodes can also be considered as energy suppliers when they are in the range of source and destination node(s). In the literature, relatively less attention is given to systems where source node is energy-constrained. In [77, 128, 129, 152, 153], energy-constrained source node(s) rely on RF signals transmitted at relay and/or destination node(s) for EH. The performance of these systems is analyzed in terms of throughput. In [77,128,129,152], the performance is investigated either ignoring fading or assuming it constant. In a practical scenario, fading cannot be ignored due to its adverse effects on the performance. The analytical results obtained without considering fading can largely deviate from the actual results. In [153], the analysis is provided considering mixed Rayleigh and Rician fading environment. In this chapter, the average SER of the system is derived on considering that the fading environment is modeled by Nakagami-m distribution, which is then extended for $\kappa-\mu$ shadowed fading. We consider the direct link connecting the source and destination is blocked. Data is either M-PSK or orthogonal M-FSK modulated and transmitted in two time slots. Coherent detection is performed for M-PSK modulated data, while noncoherent detection for orthogonal M-FSK modulated data. The relay node employs fixed DF protocol to decode the received source data and forward the re-encoded data to the destination. Source and destination nodes are considered to be located in the coverage range of the relay. Hence, both source and destination simultaneously receive RF signal broadcasted by the relay. Source node utilizes the received RF signal for EH, while destination node performs detection. The energy harvested at source is used for data transmission in the following slot. The process is pursued in an iterative manner to transmit data from source to destination. The main contributions of this chapter include:

- Average SER analysis of a WP DF relay system under Nakagami-m and $\kappa-\mu$ shadowed fading for M-PSK and orthogonal M-FSK modulated data.
- High SNR approximations of the average SERs to find the optimal relay location and DO of the system.
- Examining the effects of modulation scheme/order, relay location, and fading parameters on performance of the system.

Nakagami-m fading is a special case of $\kappa-\mu$ shadowed fading as shown in Table 1.1. Hence, the analysis for the former can be traced from that for the latter with appropriate fading parameter setting. However, we present analysis for the two fading models separately because the average SER for $\kappa-\mu$ shadowed fading involves infinite series of integrals which can take long computational time in mathematical softwares, such as, `MATLAB`. The average SER expressions for Nakagami-m fading involves a single integral only, which is a relatively simpler form for computation in mathematical softwares and obtaining asymptotic approximation and optimal relay location.

The organization of this chapter is as follows. In Section 5.2, the system model is described. The system's performance is investigated in terms of average SER in Section 5.3 and Section 5.4 for Nakagami-m and $\kappa-\mu$ shadowed fading, respectively. Optimal relay location and DO are also analyzed in Section 5.3 and Section 5.4. Section 5.5 presents numerical results. Finally, conclusions are written in Section 5.6.

5.2 System model

We consider a WPCN comprising an energy-constrained source node S, a relay node R, and a destination node D. We assume half-duplex mode of communication and all nodes are equipped with single antenna. The direct link between nodes S and D is considered to be deeply faded and hence it is ignored. Relay R employs fixed DF protocol to process the received source data. Nodes S and D lie in the coverage range of node R and hence the signal transmitted at node R is received at both S and D. The system model is illustrated in Figure 5.1. We consider a traditional two-hop DF relay system in this chapter, that is, node S transmits data to the node R in odd time slot and node R relays data to node D in even time slot. In addition, node S harvests energy using RF signal received in even time slot. Node S communicates data in the following odd slot using the harvested energy

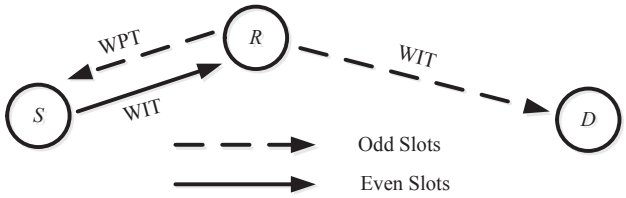

(a) System model

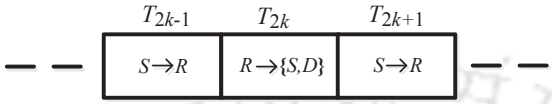

(b) Transmission protocol

Figure 5.1: The system model and the transmission technique.

only. That is, in the odd time slot $(2k-1)$ (k is a positive integer), node S transmits data to node R using energy harvested in the previous time slot. Further, in the even time slot $2k$, node R broadcasts RF signal which on reception at node S and node D is used for EH and detection, respectively. The process is repeated in the following odd and even slots. We consider the slots are of equal duration. For notational convenience, we refer odd and even time slots as $T_O = [2(k-1)T_s, (2k-1)T_s)$ and $T_E = [(2k-1)T_s, 2kT_s)$, respectively where T_s is symbol duration and $k = 1, 2, \ldots$.

We consider harvest-use approach to process the incoming energy flow [38,68]. Power consumptions in operational circuits such as encoder, modulator, etc., is comparatively small and therefore can be neglected [70, 125]. Hence, the energy harvested at node S in even slots is entirely used to send data sequentially to node R in odd slots. We consider two M-ary signaling schemes M-PSK and orthogonal M-FSK for data transmission. At receiving nodes, coherent detection is performed for orthogonal M-PSK and noncoherent detection for M-FSK. The symbols are transmitted with equal *a priori* probability. The constellation $\mathcal{S}$ is given by $\mathcal{S} = \{S_1, \ldots, S_M\}$, where $S_1, \ldots, S_M$ are the constellation points corresponding to M symbols $1, \ldots, M$, respectively. In case of M-PSK, the constellation is given by

$$S_m = \exp\left(\jmath 2\pi(m-1)/M\right), \quad m = 1, \ldots, M\,, \tag{5.1}$$

where $\jmath = \sqrt{-1}$. The orthogonal M-FSK constellation can be represented as

$$S_m = \exp\left(\jmath\, 2\pi\, (\Delta f_m)\, t\right)\,, \quad m = 1, \ldots, M, \tag{5.2}$$

where Δf_m denotes the shift of the mth frequency from the carrier such that

$$\frac{1}{T_s}\int_0^{T_s} S_m S_u^* dt = \begin{cases} 1, & m = u \\ 0, & m \neq u \end{cases} . \tag{5.3}$$

We assume links between nodes are independent and slow-flat Nakagami-m or $\kappa-\mu$ Shadowed faded.

The baseband equivalent of received RF signal at node R in slot T_O is given by

$$y_{SR}^O = \sqrt{P_S T_s \, (d_{SR})^{-\alpha_{SR}}}\, h_{SR}\, x + n_R^O , \tag{5.4}$$

where $x \in \mathcal{S}$ is the symbol transmitted by node S with power P_S, h_{SR} is the fading coefficient of SR link, $(d_{SR})^{\alpha_{SR}}$ represents path loss of SR link, d_{SR} is distance in meters with path loss exponent α_{SR}, and n_R^O is AWGN at node R. Here, P_S depends on the energy harvested at node S in the previous even time slot. As node S relies for data transmission on the energy harvested in the previous slot, an arbitrary RF signal can be transmitted by the relay (say, in time slot T_0) to start the communication. Further, in the subsequent slot T_E, the baseband equivalent of signal communicated by node R to node j is

$$y_{Rj}^E = \sqrt{P_R T_s \, (d_{Rj})^{-\alpha_{Rj}}}\, h_{Rj}\, \hat{x} + n_j^E , \quad j = S, D \tag{5.5}$$

where $\hat{x}$ is the estimate of symbol x transmitted in slot T_O, P_R is power transmitted by node R, h_{Rj} is the fading coefficient of Rj link, $(d_{Rj})^{\alpha_{Rj}}$ represents path loss of Rj link, d_{Rj} is distance in meters with path loss exponent α_{Rj}, and n_j^O is AWGN at node j. Path loss exponent ranges from 2 to 6 based on environmental conditions. The noise components n_R^O and n_j^E are independent of each other and the channel fading coefficients. They are zero-mean complex Gaussian with PSD N_0.

For a comparatively small noise component, the energy harvested at node S in slot T_E can be approximated as

$$E_S \approx \frac{\zeta P_R T_s \, |h_{RS}|^2}{(d_{RS})^{\alpha_{RS}}} , \tag{5.6}$$

where ζ is energy conversion efficiency. Since, $E_S = P_S T_s$, (5.6) can be re-written as

$$P_S \approx \frac{\zeta P_R \, |h_{RS}|^2}{(d_{RS})^{\alpha_{RS}}} . \tag{5.7}$$

In case of M-PSK, the detected data $\hat{x}$ resulting from coherent detection at node R in slot T_O is

obtained from the decision rule

$$\hat{x} = \arg\left\{\max_{s\in\mathcal{S}} \ \mathrm{Re}\left(s^* h_{SR}^* y_{SR}^O\right)\right\}, \tag{5.8}$$

where $\mathrm{Re}(\cdot)$ represents the real component of the argument. At the destination, we get the detected symbol $\hat{\hat{x}}$ in slot T_E, given by

$$\hat{\hat{x}} = \arg\left\{\max_{s\in\mathcal{S}} \ \mathrm{Re}\left(s^* h_{RD}^* y_{RD}^E\right)\right\}. \tag{5.9}$$

In case of orthogonal M-FSK, the detected data $\hat{x}$ resulting from noncoherent detection at node R in slot T_O is obtained from the decision rule

$$\hat{x} = \arg\left\{\max_{s\in\mathcal{S}} \ \left|s^* y_{SR}^O\right|^2\right\}, \tag{5.10}$$

and, finally, at the destination, we get the detected symbol $\hat{\hat{x}}$ in slot T_E, given by

$$\hat{\hat{x}} = \arg\left\{\max_{s\in\mathcal{S}} \ \left|s^* y_{RD}^E\right|^2\right\}. \tag{5.11}$$

5.2.1 PDF and MGF of Instantaneous SNRs

The instantaneous received SNRs at nodes R and D can be expressed using (5.4), (5.5), and (5.7) as

$$\gamma_{SR} = \frac{\zeta P_R T_s |h_{RS}|^2 |h_{SR}|^2}{(d_{RS})^{\alpha_{RS}} (d_{SR})^{\alpha_{SR}} N_0} \quad \text{and} \tag{5.12a}$$

$$\gamma_{RD} = \frac{P_R T_s |h_{RD}|^2}{(d_{RD})^{\alpha_{RD}} N_0}, \tag{5.12b}$$

respectively. On taking expectation of the instantaneous SNRs in (5.12), we can obtain the corresponding average received SNRs as

$$\bar{\gamma}_{SR} = \frac{\zeta \lambda_{RS} \lambda_{SR} P_R T_s}{(d_{SR})^{\alpha_{SR}+\alpha_{RS}} N_0} \quad \text{and} \tag{5.13a}$$

$$\bar{\gamma}_{RD} = \frac{\lambda_{RD} P_R T_s}{(d_{RD})^{\alpha_{RD}} N_0}. \tag{5.13b}$$

In (5.13), the $E[|h_{ij}|^2] = \lambda_{ij}$ is mean power of ij link is, where $E[\cdot]$ represents expectation operator. The PDF and the MGF of γ_{SR} and γ_{RD} for Nakagami-m and $\kappa-\mu$ shadowed fading are given below.

They are used to analyze the average SERs in the later part this chapter.

5.2.1.1 Nakagami-m Fading

For Nakagami-m fading, the power variates of the channel coefficients $|h_{ij}|^2$ are gamma distributed with PDF

$$f_{|h_{ij}|^2}(|h_{ij}|) = \frac{(m_{ij})^{m_{ij}}|h_{ij}|^{m_{ij}-1}}{\Gamma(m_{ij})(\lambda_{ij})^{m_{ij}}}\exp\left(-\frac{m_{ij}|h_{ij}|}{\lambda_{ij}}\right), \tag{5.14}$$

where m_{ij} is Nakagami-m fading parameter of link $ij \in \{SR, RS, RD\}$ and $\Gamma(\cdot)$ is gamma function.

The instantaneous received SNRs given in (5.12a) and (5.12b) can be expressed as $\gamma_{SR} = b_{SR}|h_{RS}|^2 |h_{SR}|^2$ and $\gamma_{RD} = b_{RD}|h_{RD}|^2$, respectively where $b_{SR} = \zeta P_R T_s/ (N_0 {d_{RS}}^{\alpha_{RS}+\alpha_{SR}})$ and $b_{RD} = P_R T_s/ (N_0 {d_{RD}}^{\alpha_{RD}})$. Using the relation for the PDF of the product of two random variables,

$$f_{\gamma_{SR}}(\gamma_{SR}) = \int_0^\infty \frac{1}{b_{SR}\,t} f_{|h_{RS}|^2}\left(\frac{\gamma_{SR}}{b_{SR}\,t}\right) f_{|h_{SR}|^2}(t)dt, \tag{5.15}$$

the PDF of γ_{SR} is obtained on substituting (5.14) and (B.14) in (5.15) as

$$f_{\gamma_{SR}}(\gamma_{SR}) = \frac{2}{\Gamma(m_{SR})\Gamma(m_{RS})\gamma_{SR}}\left(\frac{m_{RS}m_{SR}\gamma_{SR}}{\bar{\gamma}_{SR}}\right)^{\frac{m_{RS}+m_{SR}}{2}} K_{m_{SR}-m_{RS}}\left(2\sqrt{\frac{m_{RS}m_{SR}\gamma_{SR}}{\bar{\gamma}_{SR}}}\right), \tag{5.16}$$

where $\bar{\gamma}_{SR} = b_{SR}\lambda_{RS}\lambda_{SR}$ and $K_r(\cdot)$ is the r-th order modified Bessel's function of the second kind. The PDF of γ_{RD} is obtained using the relation $f_{\gamma_{RD}}(\gamma_{RD}) = 1/b_{RD} f_{|h_{RD}|^2}(\gamma_{RD}/b_{RD})$ as

$$f_{\gamma_{RD}}(\gamma_{RD}) = \frac{{m_{RD}}^{m_{RD}}{\gamma_{RD}}^{m_{RD}-1}}{\Gamma(m_{RD})(\bar{\gamma}_{RD})^{m_{RD}}}\exp\left(-\frac{m_{RD}\gamma_{RD}}{\bar{\gamma}_{RD}}\right), \tag{5.17}$$

where $\bar{\gamma}_{RD} = b_{RD}\lambda_{RD}$. The MGF of γ_φ for $\varphi \in \{SR, RD\}$ is

$$M_{\gamma_\varphi}(s) = \int_0^\infty \exp(-s\gamma_\varphi) f_{\gamma_\varphi}(\gamma_\varphi)d\gamma_\varphi\,. \tag{5.18}$$

Substituting (5.16) in (5.18) and using (B.15), we get the MGF of γ_{SR} as

$$M_{\gamma_{SR}}(s) = \left(\frac{m_{RS}m_{SR}}{s\bar{\gamma}_{SR}}\right)^{\frac{m_{RS}+m_{SR}-1}{2}} \exp\left(\frac{m_{RS}m_{SR}}{2s\bar{\gamma}_{SR}}\right) W_{\frac{1-m_{RS}-m_{RS}}{2},\frac{m_{RS}-m_{SR}}{2}}\left(\frac{m_{RS}m_{SR}}{s\bar{\gamma}_{SR}}\right), \tag{5.19}$$

where $W_{s,t}(\cdot)$ is Whittaker's function. Next, substituting (5.17) in (5.18) and using (B.7), the MGF

of γ_{SR} is given by

$$M_{\gamma_{RD}}(s) = \left(1 + s\frac{\bar{\gamma}_{RD}}{m_{RD}}\right)^{-m_{RD}}. \tag{5.20}$$

The expression for MGF in (5.20) is a well known result.

5.2.1.2 $\kappa-\mu$ Shadowed Fading

The PDF of the power variate for $\kappa-\mu$ shadowed fading link gains is given by [12, eq. (4)]

$$\begin{aligned} f_{|h_{ij}|^2}(|h_{ij}|) &= \frac{{\mu_{ij}}^{\mu_{ij}} {m_{ij}}^{m_{ij}} (1+\kappa_{ij})^{\mu_{ij}}}{\Gamma(\mu_{ij})\lambda_{ij}(\mu_{ij}\kappa_{ij}+m_{ij})^{m_{ij}}} \left(\frac{|h_{ij}|}{\lambda_{ij}}\right)^{\mu_{ij}-1} \\ &\quad \times \exp\left(-\frac{\mu_{ij}(1+\kappa_{ij})|h_{ij}|}{\lambda_{ij}}\right) {}_1F_1\left(m_{ij}, \mu_{ij}; \frac{{\mu_{ij}}^2\kappa_{ij}(1+\kappa_{ij})|h_{ij}|}{(\mu_{ij}\kappa_{ij}+m_{ij})\lambda_{ij}}\right), \end{aligned} \tag{5.21}$$

where κ_{ij} is the ratio of total power of the LOS components and the total power of non-LOS components, μ_{ij} corresponds to the number of clusters, m_{ij} captures the shadowing effect of the fading environment, ${}_1F_1(\cdot)$ represents confluent hypergeometric function [166, eq. (9.210.1)], and $\lambda_{ij} = E[|h_{ij}|^2]$ is the mean power of $|h_{ij}|$. Deriving the average SER using the PDF (5.21) requires dealing with the integration of integrands involving confluent hypergeometric function. This makes it difficult to derive the closed-form expression of the average SER for SR link. To simplify the derivation, we use the series form representation of the PDF[1] given in [173]. In [173], the series form representation of confluent hypergeometric function [166, eq. (9.210.1)] is used to get the PDF

$$f_{|h_{ij}|^2}(|h_{ij}|) = \sum_{l_n=0}^{\infty} p_{ij}(c_{ij})^{l_n+\mu_{ij}} |h_{ij}|^{l_n+\mu_{ij}-1} \exp(-c_{ij}|h_{ij}|), \tag{5.22}$$

where p_{ij} and c_{ij} are defined as

$$p_{ij,l_n} = \frac{(m_{ij})_{l_n}}{\Gamma(m_{ij})l_n!(\mu_{ij})_{l_n}} \left(\frac{\mu_{ij}\kappa_{ij}}{\mu_{ij}\kappa_{ij}+m_{ij}}\right)^{l_n} \left(\frac{m_{ij}}{\mu_{ij}\kappa_{ij}+m_{ij}}\right)^{m_{ij}} \quad \text{and} \quad c_{ij} = \frac{\mu_{ij}(1+\kappa_{ij})}{\lambda_{ij}}, \tag{5.23}$$

[1]Another series form representation of the PDF is provided in [15, eq. (12)] which requires computation of N moments of h [15, eq. (11)], where N is number of terms in the series. Although, for small value of $\kappa_{ij}mu_{ij}/m_{ij}$ the series in [15, eq. (12)] converges to the exact PDF faster than (5.22) but as $\kappa_{ij}mu_{ij}/m_{ij}$ increases it requires large N. For large N and $\kappa_{ij}mu_{ij}/m_{ij}$, the higher order moments cannot be evaluated in `MATLAB` due to computational limitation and, hence, for some cases [15, eq. (12)] can diverge from the exact PDF. This can be observed through numerical results, which are included to avoid the deviation. We further observed that (5.22) does not converge to the exact PDF for higher $\kappa_{ij}mu_{ij}/m_{ij}$, especially at tails. However, (5.22) is considered in this work due to the simplicity it offers in the analysis.

with $n = 1$ for $ij = RS$, $n = 2$ for $ij = SR$, and $n = 3$ for $ij = RD$.

The PDF of γ_{SR} obtained by substituting (5.22) and (B.14) in (5.15) is

$$f_{\gamma_{SR}}(\gamma_{SR}) = \frac{2a_{SR}}{\bar{\gamma}_{SR}} \sum_{l_1=0}^{\infty} \sum_{l_2=0}^{\infty} p_{RS,l_1}\, p_{SR,l_2} \left(\frac{a_{SR}\gamma_{SR}}{\bar{\gamma}_{SR}}\right)^{\frac{l_1+l_2+\mu_{RS}+\mu_{RS}}{2}-1} K_{l_2+\mu_{SR}-l_1-\mu_{RS}}\left(2\sqrt{\frac{a_{SR}\gamma_{SR}}{\bar{\gamma}_{SR}}}\right), \quad (5.24)$$

where $\bar{\gamma}_{SR} = b_{SR}\lambda_{RS}\lambda_{SR}$ and $a_{SR} = \mu_{RS}\mu_{SR}(1+\kappa_{RS})(1+\kappa_{SR})$. The PDF of γ_{RD} is obtained using the relation $f_{\gamma_{RD}}(\gamma_{RD}) = 1/b_{RD} f_{|h_{RD}|^2}(\gamma_{RD}/b_{RD})$ and (5.22) as

$$f_{\gamma_{RD}}(\gamma_{RD}) = \frac{a_{RD}}{\bar{\gamma}_{RD}} \sum_{l_3=0}^{\infty} p_{RD,l_3} \left(\frac{a_{RD}\gamma_{RD}}{\bar{\gamma}_{RD}}\right)^{l_3+\mu_{RD}-1} \exp\left(-\frac{a_{RD}\gamma_{RD}}{\bar{\gamma}_{RD}}\right), \quad (5.25)$$

where $\bar{\gamma}_{RD} = b_{RD}\lambda_{RD}$ and $a_{RD} = \mu_{RD}(1+\kappa_{RD})$.

Substituting (5.24) in (5.18) and applying (B.15), the MGF of γ_{SR} is given by

$$M_{\gamma_{SR}}(s) = \sum_{l_1=0}^{\infty} \sum_{l_2=0}^{\infty} p_{RS,l_1}\, p_{SR,l_3} \Gamma(l_1+\mu_{RS})\Gamma(l_2+\mu_{SR}) \left(\frac{a_{SR}}{s\bar{\gamma}_{SR}}\right)^{\frac{l_1+l_2+\mu_{RS}+\mu_{RS}}{2}-1} \times \exp\left(\frac{a_{SR}}{2s\bar{\gamma}_{SR}}\right) W_{\frac{1-l_2-\mu_{SR}-l_1-\mu_{RS}}{2}, \frac{l_2+\mu_{SR}-l_1-\mu_{RS}}{2}}\left(\frac{a_{SR}}{s\bar{\gamma}_{SR}}\right), \quad (5.26)$$

where $W_{s,t}(\cdot)$ is Whittaker's function. Similarly, on replacing (5.25) in (5.18) and using (B.7), the MGF of γ_{RD} is written as

$$M_{\gamma_{RD}}(s) = \sum_{l_3=0}^{\infty} p_{RD,l_3} \Gamma(l_2+\mu_{RD}) \left(1+\frac{s\bar{\gamma}_{RD}}{a_{RD}}\right)^{-l_3-\mu_{RD}}. \quad (5.27)$$

5.3 Performance Analysis under Nakagami-m Fading

In this section, we analyze the average SER of the system in Figure 4.1 for M-PSK modulation scheme with coherent detection and orthogonal M-FSK modulation scheme with noncoherent detection. Both the signaling schemes have symmetric constellations. Consider symbol S_p is transmitted at node S in slot T_O and detected as S_q at node R. Further, in slot T_E symbol S_q is transmitted at node R and detected as S_r at node D. Note that $S_p, S_q, S_r \in \mathcal{S}$. Now, the symbol transmitted at node S can be correctly detected at node D, only if, $S_p = S_r$. Thus, the end-to-end probability of correct reception is a function of the possibilities when symbol S_p transmitted at node S is detected as S_q at node R, which when forwarded by R is detected as S_p at node D.

Let $P_{p,q}(\gamma_\varphi)$ represents conditional probability to transmit symbol S_p and receive S_q over link φ, where $S_p, S_q \in \mathcal{S}$ and $\varphi \in \{SR, RD\}$. $P_{p,q}(\gamma_\varphi)$ for $p \neq q$ corresponds to conditional paired error probabilities, conditioned on the instantaneous SNR γ_φ [25, 174]. The conditional end-to-end probability of correct detection at node D can be expressed as [174]

$$P_c(\gamma_{SR}, \gamma_{RD}) = \frac{1}{M}\sum_{\ell=1}^{M}\sum_{m=1}^{M} P_{\ell,m}(\gamma_{SR}) P_{m,\ell}(\gamma_{RD}) \,. \tag{5.28}$$

The end-to-end average probability of correct detection can be obtained by taking expectation of the conditional probability in (5.28), given by

$$P_c = \frac{1}{M}\sum_{\ell=1}^{M}\sum_{m=1}^{M} P_{\ell,m}^{SR} P_{m,\ell}^{RD} , \tag{5.29}$$

where $P_{\ell,m}^{SR} = E[P_{\ell,m}(\gamma_{SR})]$ and $P_{m,\ell}^{RD} = E[P_{m,M}(\gamma_{RD})]$ are the average error probabilities. Let Ψ be a set of SR and RD links, that is, $\Psi = \{SR, RD\}$. In signaling schemes with symmetric constellations, the paired error probability is dependent on the Euclidean distance between the two constellation points, therefore $P_{\ell,m}^{\varphi} = P_{m,\ell}^{\varphi}$, $\varphi \in \Psi$. We represent $P_{\ell,m}^{\varphi} = P_{m,\ell}^{\varphi} = P_{|\ell-m|}^{\varphi}$, for $\ell, m \in \{1, \ldots, M\}$. Thus, (5.29) can be re-written as

$$\begin{aligned} P_c &= \frac{1}{M}\sum_{\ell=1}^{M}\sum_{m=1}^{M} P_{|\ell-m|}^{SR} P_{|\ell-m|}^{RD} \\ &= \sum_{\nu=0}^{M-1} P_\nu^{SR} P_\nu^{RD} \,. \end{aligned} \tag{5.30}$$

The average probabilities of correct decision corresponding to $\nu = 0$ in (5.30) are represented as $P_0^{SR} = (1 - P_{e,SR})$ and $P_0^{RD} = (1 - P_{e,RD})$. $P_{e,SR}$ and $P_{e,RD}$ are the average error probabilities for SR and RD links, respectively. Thus, end-to-end probability of correct decision can be represented in terms of the average link error probabilities and the pairwise error probabilities as

$$P_c = (1 - P_{e,SR})(1 - P_{e,RD}) + \sum_{\nu=1}^{M-1} P_\nu^{SR} P_\nu^{RD} \,. \tag{5.31}$$

Using (5.31), the end-to-end average SER is given by

$$P_e = P_{e,SR} + P_{e,RD} - P_{e,SR}P_{e,RD} - \sum_{\nu=1}^{M-1} P_\nu^{SR} P_\nu^{RD} \,. \tag{5.32}$$

5.3.1 Analytical Average SER

Next, we obtain the factors $P_{e,SR}$, $P_{e,RD}$, P_{ν}^{SR}, and P_{ν}^{RD} used for the average SER analysis for the two modulation schemes.

5.3.1.1 M-PSK

The average error terms in (5.32) are represented in integral form using [174, eqs. (7) and (8)] as

$$P_{e,\varphi} = \frac{1}{\pi}\int_0^{\phi_0} M_{\gamma_\varphi}\left(\frac{g_0}{\sin^2\theta}\right)d\theta \quad \text{and} \tag{5.33}$$

$$P_{\ell}^{\varphi} = \frac{1}{2\pi}\int_0^{\phi_1} M_{\gamma_\varphi}\left(\frac{g_1}{\sin^2\theta}\right)d\theta - \frac{1}{2\pi}\int_0^{\phi_2} M_{\gamma_\varphi}\left(\frac{g_2}{\sin^2\theta}\right)d\theta, \quad \varphi \in \Psi, \tag{5.34}$$

where $\phi_0 = (M-1)\pi/M$, $g_0 = \sin^2(\pi-\phi_0)$, $\phi_1 = (\pi - 2\pi\ell/M + \pi/M)$, $g_1 = \sin^2(\pi-\phi_1)$, $\phi_2 = (\pi - 2\pi\ell/M - \pi/M)$, $g_2 = \sin^2(\pi-\phi_2)$, and $M_{\gamma_\varphi}(s)$ is the MGF of γ_φ.

The end-to-end average SER for M-PSK modulation scheme under Nakagami-m fading can be obtained by substituting (5.33) and (5.34) in (5.32) and using (5.19) and (5.20).

5.3.1.2 Orthogonal M-FSK

In case of orthogonal M-FSK, the Euclidean distance between different constellations points is same, therefore the paired error probabilities are related as $P_1^{\varphi} = \ldots = P_{M-1}^{\varphi}$, $\varphi \in \Psi$ [25]. Thus, the end-to-end average probability of error in (5.32) is modified as

$$P_e = P_{e,SR} + P_{e,RD} - P_{e,SR}P_{e,RD} - (M-1)P_1^{SR}P_1^{RD}, \tag{5.35}$$

where $P_1^{SR} = P_{e,SR}/(M-1)$ and $P_1^{RD} = P_{e,RD}/(M-1)$. Hence, (5.35) can be re-written as

$$P_e = P_{e,SR} + P_{e,RD} - \frac{M}{M-1}P_{e,SR}P_{e,RD}\,. \tag{5.36}$$

The conditional error probability expression for link φ in orthogonal M-FSK with noncoherent detection is given by [1, eq. (13.59c)]

$$P_{e,\varphi}(\gamma_\varphi) = \sum_{l=1}^{M-1}\frac{(-1)^{l+1}}{(l+1)}\binom{M-1}{l}\exp\left(-\frac{l\gamma_\varphi}{(l+1)}\right). \tag{5.37}$$

The average error probability $P_{e,SR}$ can be obtained by taking expectation of (5.37) using the PDF in (5.16). The simplified expression obtained on applying (B.15) is written as

$$P_{e,SR} = \sum_{l=1}^{M-1} \frac{(-1)^{l+1}}{(l+1)} \binom{M-1}{l} \exp\left(\frac{(l+1)m_{RS}m_{SR}}{2l\bar{\gamma}_{SR}}\right) \times W_{\frac{1-m_{RS}-m_{RS}}{2},\frac{m_{RS}-m_{SR}}{2}}\left(\frac{(l+1)m_{RS}m_{SR}}{l\bar{\gamma}_{SR}}\right)\left(\frac{(l+1)m_{RS}m_{SR}}{l\bar{\gamma}_{SR}}\right)^{\left(\frac{m_{RS}+m_{SR}-1}{2}\right)}. \quad (5.38)$$

Averaging (5.37) with the PDF of γ_{RD} (5.17) and using (B.7), $P_{e,RD}$ in (5.36) is analyzed as

$$P_{e,RD} = \sum_{l=1}^{M-1} \frac{(-1)^{l+1}}{(l+1)} \binom{M-1}{l} \left(1+\frac{l\bar{\gamma}_{RD}}{(l+1)m_{RD}}\right)^{-m_{RD}}. \quad (5.39)$$

The end-to-end average SER for orthogonal M-FSK modulation scheme under Nakagami-m fading can be obtained on substituting (5.38) and (5.39) in (5.36).

5.3.2 Asymptotic Average SER

At high SNRs, the end-to-end average SER expression in (5.32) can be approximated as

$$P_e^{\infty} \approx P_{e,SR}^{\infty} + P_{e,RD}^{\infty}, \quad (5.40)$$

where P_e^{∞}, $P_{e,SR}^{\infty}$, and $P_{e,RD}^{\infty}$ are asymptotic approximation of P_e, $P_{e,SR}$, and $P_{e,RD}$, respectively.

5.3.2.1 M-PSK

The high SNR approximation of P_e in (5.40) can be obtained by determining the asymptotic approximation of $P_{e,SR}$ and $P_{e,RD}$. $P_{e,SR}^{\infty}$ can be obtained by approximating $f_{\gamma_{SR}}(\gamma_{SR})$ for the cases when $a)\,(m_{RS}-m_{SR})=0$ and $b)\,|m_{RS}-m_{SR}|>0$ using (B.6). The PDF expressions thus obtained for the two cases are then used to analyze the corresponding MGF $M_{\gamma_{SR}}^{\infty}(s)$ and the error term $P_{e,SR}^{\infty}$ as follows:

$a)\,(m_{RS}-m_{SR})=0$: For this case, the PDF in (5.16) is approximated as

$$f_{\gamma_{SR}}^{\infty}(\gamma_{SR}) \approx \frac{-2(\gamma_{SR})^{m_a-1}}{(\Gamma(m_a))^2}\left(\frac{(m_a)^2}{\bar{\gamma}_{SR}}\right)^{m_a} \ln\left(\sqrt{\frac{4(m_a)^2\gamma_{SR}}{\bar{\gamma}_{SR}}}\right), \quad (5.41)$$

where $m_a = m_{RS} = m_{SR}$. The corresponding MGF is obtained by substituting (5.41) in (5.18) and

using (B.9) as

$$M^{\infty}_{\gamma_{SR}}(s) \approx \frac{1}{\Gamma(m_a)}\left(\ln\left(\frac{s\bar{\gamma}_{SR}}{4(m_a)^2}\right)-\psi(m_a)\right)\left(\frac{(m_a)^2}{s\bar{\gamma}_{SR}}\right)^{m_a}, \tag{5.42}$$

where $\psi(\cdot)$ is digamma function. Substituting (5.42) in (5.33) followed by solving the integral using (B.10) gives the approximation of $P^{\infty}_{e,SR}$ as

$$P^{\infty}_{e,SR} \approx \frac{1}{\pi\Gamma(m_a)}\left(\frac{(m_a)^2}{g_0\bar{\gamma}_{SR}}\right)^{m_a}\left(\mathcal{J}(m_a,\phi_0;\theta)+\left(\ln\left(\frac{g_0\bar{\gamma}_{SR}}{4(m_a)^2}\right)-\psi(m_a)\right)\mathcal{I}(m_a,\phi_0;\theta)\right), \tag{5.43}$$

where

$$\mathcal{I}(p,\phi_0;\theta) = \int_0^{\phi_0}(\sin^2\theta)^p d\theta, \quad \text{and} \tag{5.44}$$

$$\mathcal{J}(p,\phi_0;\theta) = \int_0^{\phi_0}(\sin^2\theta)^p \ln\left(\sin^2\theta\right) d\theta. \tag{5.45}$$

b) $|m_{RS}-m_{SR}|>0$: For this case, the PDF in (5.16) is approximated as

$$f^{\infty}_{\gamma_{SR}}(\gamma_{SR}) \approx \frac{\Gamma(|m_{RS}-m_{SR}|)}{\Gamma(m_{RS})\Gamma(m_{SR})}\left(\frac{m_{RS}m_{SR}}{\bar{\gamma}_{SR}}\right)^{m_b}(\gamma_{SR})^{m_b-1}, \tag{5.46}$$

where $m_b=(m_{RS}+m_{SR}-|m_{RS}-m_{SR}|)/2$. The corresponding MGF is obtained by substituting (5.46) in (5.18), thus

$$M^{\infty}_{\gamma_{SR}}(s) \approx \frac{\Gamma(|m_{RS}-m_{SR}|)\Gamma(m_b)}{\Gamma(m_{RS})\Gamma(m_{SR})}\left(\frac{m_{RS}m_{SR}}{s\bar{\gamma}_{SR}}\right)^{m_b}. \tag{5.47}$$

Further, $P^{\infty}_{e,SR}$ is obtained by using (5.33) and (5.47) as

$$P^{\infty}_{e,SR} \approx \frac{\Gamma(|m_{RS}-m_{SR}|)\Gamma(m_b)}{\pi\Gamma(m_{RS})\Gamma(m_{SR})}\left(\frac{m_{RS}m_{SR}}{g_0\bar{\gamma}_{SR}}\right)^{m_b}\mathcal{I}(m_b,\phi_0;\theta), \tag{5.48}$$

where $\mathcal{I}(m_b,\phi_0;\theta)$ is defined in (5.44). $P^{\infty}_{e,SR}$ in (5.43) and (5.48) can be unified as

$$P^{\infty}_{e,SR} \approx \frac{\mathcal{A}}{(\bar{\gamma}_{SR})^{m_r}}\big((\mathcal{B}+\rho_1\ln(\bar{\gamma}_{SR}))\mathcal{I}(m_r,\phi_0;\theta)+\rho_2\mathcal{J}(m_r,\phi_0;\theta)\big), \tag{5.49}$$

where $\mathcal{A}$, $\mathcal{B}$, m_r, ρ_1, and ρ_2 are defined for the two cases as follows:

a) For $(m_{RS}-m_{SR})=0$, we have $m_r=m_a$, $\rho_1=1$, $\rho_2=1$,

$$\mathcal{A} = \frac{1}{\pi\Gamma(m_a)}\left(\frac{(m_a)^2}{g_0}\right)^{m_a},$$

$$\mathcal{B} = \ln\left(\frac{g_0}{4(m_a)^2}\right)-\psi(m_a).$$

b) For $|m_{RS} - m_{SR}| > 0$, we have $\mathcal{B} = 1$, $m_r = m_b$, $\rho_1 = 0$, $\rho_2 = 0$,

$$\mathcal{A} = \frac{\Gamma(|m_{RS} - m_{SR}|)\Gamma(m_b)}{\pi\Gamma(m_{RS})\Gamma(m_{SR})} \left(\frac{m_{RS}m_{SR}}{g_0}\right)^{m_b}.$$

Next, $P_{e,RD}^{\infty}$ in (5.40) can be obtained using the asymptotic approximation of MGF $M_{\gamma_{RD}}(s)$. For $(s\bar{\gamma}_{RD}/m_{RD}) >> 1$, the MGF in (5.20) is approximated as

$$M_{\gamma_{RD}}^{\infty}(s) \approx \left(\frac{m_{RD}}{s\bar{\gamma}_{RD}}\right)^{m_{RD}}. \tag{5.50}$$

Substituting (5.50) in (5.33), $P_{e,RD}$ is obtained as

$$P_{e,RD}^{\infty} \approx \frac{1}{\pi}\left(\frac{m_{RD}}{g_0\bar{\gamma}_{RD}}\right)^{m_{RD}} \mathcal{I}(m_{RD}, \phi_0; \theta). \tag{5.51}$$

The asymptotic end-to-end average SER for M-PSK can be expressed substituting (5.49) and (5.51) in (5.40) as

$$P_e^{\infty} \approx \frac{\mathcal{A}}{(\bar{\gamma}_{SR})^{m_r}}\Big((\mathcal{B}+\rho_1 \ln(\bar{\gamma}_{SR}))\,\mathcal{I}(m_r, \phi_0; \theta) + \rho_2\mathcal{J}(m_r, \phi_0; \theta)\Big) + \frac{\mathcal{C}}{(\bar{\gamma}_{RD})^{m_{RD}}}\mathcal{I}(m_{RD}, \phi_0; \theta), \tag{5.52}$$

where $\mathcal{C} = (m_{RD}/g_0)^{m_{RD}}/\pi$.

Following (4.26), integrals (5.44) and (5.45) can be approximated as $\mathcal{I}(p, \phi_0; \theta) \approx a_M \int_0^{\pi/2} (\sin^2\theta)^p d\theta$ and $\mathcal{J}(p, \phi_0; \theta) \approx b_M \int_0^{\pi/2} (\sin^2\theta)^p \ln\left(\sin^2\theta\right) d\theta$, respectively, where a_M, $b_M = 1$ for $M = 2$ and a_M, $b_M = 2$ for $M \geq 4$. The approximation is exact for $M = 2$ and close for $M \geq 4$. Using [166, eq. (3.621.1)] and (B.10), the closed-form representation of the approximations for $\mathcal{I}(p, \phi_0; \theta)$ and $\mathcal{J}(p, \phi_0; \theta)$ are

$$\mathcal{I}(p, \phi_0; \theta) \approx a_M 2^{2p-1} B\big(p + 1/2, p + 1/2\big) \tag{5.53}$$

and

$$\mathcal{J}(p, \phi_0; \theta) \approx b_M \frac{\sqrt{\pi}\Gamma(p + 1/2)}{2\Gamma(p + 1)}\big(\psi(p + 1/2) - \psi(p + 1)\big), \tag{5.54}$$

respectively, where $B(s, t) = \Gamma(s)\Gamma(t)/\Gamma(s + t)$ is beta function.

5.3.2.2 Orthogonal M-FSK

To obtain $P_{e,SR}^{\infty}$ for orthogonal M-FSK modulation, the conditional SER in (5.37) is averaged using the approximate expression of $f_{\gamma_{SR}}(\gamma_{SR})$. Two cases are observed for approximation, that is, *a*)

$(m_{RS} - m_{SR}) = 0$ and $b)$ $|m_{RS} - m_{SR}| > 0$. The approximations of $f_{\gamma_{SR}}(\gamma_{SR})$ for the cases $a)$ and $b)$ are given by (5.41) and (5.46), respectively. Thus, $P_{e,SR}^{\infty}$ for the two cases is given as follows:

$a)$ $(m_{RS} - m_{SR}) = 0$: The resulting expression for $P_{e,SR}^{\infty}$ is obtained on taking expectation of (5.37) using (5.41) and (B.9) as

$$P_{e,SR}^{\infty} \approx \frac{1}{\Gamma(m_a)} \left(\frac{(m_a)^2}{\bar{\gamma}_{SR}} \right)^{m_a} \sum_{v=1}^{M-1} \mathcal{D}(v) \left(\ln \left(\frac{l\bar{\gamma}_{SR}}{4(v+1)(m_a)^2} \right) - \psi(m_a) \right), \tag{5.55}$$

where

$$\mathcal{D}(v) = \frac{(-1)^{v+1}}{(v+1)} \binom{M-1}{v} \left(\frac{(v+1)}{v} \right)^{m_r}, \tag{5.56}$$

with $m_r = m_a$.

$b)$ $|m_{RS} - m_{SR}| > 0$: Averaging (5.37) using (5.46) gives

$$P_{e,SR}^{\infty} \approx \frac{\Gamma(|m_{RS} - m_{SR}|)\Gamma(m_b)}{\Gamma(m_{RS})\Gamma(m_{SR})} \left(\frac{m_{RS} m_{SR}}{\bar{\gamma}_{SR}} \right)^{m_b} \sum_{v=1}^{M-1} \mathcal{D}(v), \tag{5.57}$$

for $m_r = m_b$. $P_{e,SR}^{\infty}$ in (5.55) and (5.57) are unified as

$$P_{e,SR}^{\infty} \approx \frac{\mathcal{A}(v;M) + \rho_1 \mathcal{B}(v;M) \ln(\bar{\gamma}_{SR})}{(\bar{\gamma}_{SR})^{m_r}}, \tag{5.58}$$

where m_r, ρ_1, $\mathcal{A}(v;M)$, and $\mathcal{B}(v;M)$ are defined as

$a)$ For $(m_{RS} - m_{SR}) = 0$, $m_r = m_a$, $\rho_1 = 1$,

$$\mathcal{A}(v;M) = \frac{(m_a)^{2m_a}}{\Gamma(m_a)} \sum_{v=1}^{M-1} \mathcal{D}(v) \left(\ln \left(\frac{v(m_a)^{-2}}{4(v+1)} \right) - \psi(m_a) \right)$$

and

$$\mathcal{B}(v;M) = \frac{(m_a)^{2m_a}}{\Gamma(m_a)} \sum_{v=1}^{M-1} \mathcal{D}(v). \tag{5.59}$$

$b)$ For $|m_{RS} - m_{SR}| > 0$, $m_r = m_b$, $\rho_1 = 0$, $\mathcal{B}(v;M) = 1$, and

$$\mathcal{A}(v;M) = \frac{\Gamma(|m_{RS} - m_{SR}|)\Gamma(m_b)(m_{RS} m_{SR})^{m_b}}{\Gamma(m_{RS})\Gamma(m_{SR})} \sum_{v=1}^{M-1} \mathcal{D}(v).$$

Further, in (5.39) $v\bar{\gamma}_{RD}/((v+1)m_{RD}) >> 1$ at high SNRs, thus the asymptotic approximation of

$P_{e,RD}$ is

$$P_{e,RD}^{\infty} \approx \sum_{v=1}^{M-1} \frac{(-1)^{v+1}}{(v+1)} \binom{M-1}{v} \left(\frac{(v+1)m_{RD}}{v\bar{\gamma}_{RD}} \right)^{m_{RD}}. \tag{5.60}$$

The asymptotic end-to-end average SER for orthogonal M-FSK obtained on substituting (5.58) and (5.60) in (5.40) is given by

$$P_e^{\infty} \approx \frac{\mathcal{A}(v;M) + \rho_1 \mathcal{B}(v;M) \ln(\bar{\gamma}_{SR})}{(\bar{\gamma}_{SR})^{m_r}} + \frac{\mathcal{C}(v;M)}{(\bar{\gamma}_{RD})^{m_{RD}}}, \tag{5.61}$$

where

$$\mathcal{C}(v;M) = \sum_{v=1}^{M-1} \frac{(-1)^{v+1}}{(v+1)} \binom{M-1}{v} \left(\frac{(v+1)m_{RD}}{v} \right)^{m_{RD}}.$$

5.3.3 Optimal Relay Location

In this subsection, (5.52) and (5.61) are used to analyze the optimal relay location for M-PSK and orthogonal M-FSK modulation schemes. Using (5.13a) and (5.13b), (5.52) can be rewritten as

$$\begin{aligned} P_e^{\infty} \approx\ & \mathcal{A}' \Big((\mathcal{B}' - \rho_1(\alpha_{RS}+\alpha_{SR}) \ln(d_{SR})) \mathcal{I}(m_r, \phi_0; \theta) + \rho_2 \mathcal{J}(m_r, \phi_0; \theta) \Big) (d_{SR})^{m_r(\alpha_{RS}+\alpha_{SR})} \\ & + \mathcal{C}' (\beta d_{SD} - d_{SR})^{m_{RD}\alpha_{RD}} \mathcal{I}(m_{RD}, \phi_0; \theta), \end{aligned} \tag{5.62}$$

where $\mathcal{A}' = \mathcal{A}\,(\mathcal{Z}_1)^{m_r}$, $\mathcal{B}' = \mathcal{B} - \rho_1(\ln(\mathcal{Z}_1))$, and $\mathcal{C}' = \mathcal{C}(\mathcal{Z}_2)^{m_{RD}}$, with $\mathcal{Z}_1 = 1/(\zeta \lambda_{RS} \lambda_{SR}\, \bar{\gamma})$, $\mathcal{Z}_2 = 1/(\lambda_{RD}\bar{\gamma})$, and $\bar{\gamma} = P_R T_s / N_0$. The nodes are considered to be planner (Figure 4.7) and inter link distances follow the relation $d_{SR} + d_{RD} = \beta d_{SD}$, $\beta \geq 1$. When $\beta = 1$, the nodes are collinear. Next, for orthogonal M-FSK (5.61) is written as

$$\begin{aligned} P_e^{\infty} \approx\ & \Big(\mathcal{A}(l;M) - \rho_1 \mathcal{B}(l;M) \big(\ln(\mathcal{Z}_1) + (\alpha_{RS}+\alpha_{SR}) \ln(d_{SR}) \big) \Big) (\mathcal{Z}_1)^{m_r} (d_{SR})^{m_r(\alpha_{RS}+\alpha_{SR})} \\ & + \mathcal{C}(l;M) (\mathcal{Z}_2)^{m_{RD}} (\beta d_{SD} - d_{SR})^{m_{RD}\alpha_{RD}}. \end{aligned} \tag{5.63}$$

Now, applying the second-order conditions [158], it is easy to show that (5.62) and (5.63) are convex functions of d_{SR}. Hence, at high SNRs an optimal relay location achieving minimum average SER for M-PSK and orthogonal M-FSK can be obtained using (5.62) and (5.63), respectively. Golden-section search method [73] is used to obtain the optimal values.

5.3.4 Diversity Order

The asymptotic average SER in (5.52) and (5.61) can be represented in the form

$$P_e^{\infty} = \frac{\mathcal{Y}_1(\mathcal{Y}_2 + \rho_1 \ln(\bar{\gamma}))}{(\bar{\gamma})^{m_r}} + \frac{\mathcal{Y}_3}{(\bar{\gamma})^{m_{RD}}}, \tag{5.64}$$

where $\mathcal{Y}_1$, $\mathcal{Y}_2$, and $\mathcal{Y}_3$ encapsulate the terms independent of $\bar{\gamma}$ $(= P_R T_s/N_0)$ and are different for M-PSK and orthogonal M-FSK modulation schemes. The DO of the system can be evaluated using the relation $\text{DO} = -\lim_{\bar{\gamma}\to\infty} \ln(P_e^{\infty})/\ln(\bar{\gamma})$ where P_e^{∞} is given in (5.64). We get

$$\text{DO} = \min\left\{\left(m_r - \rho\frac{\ln\ln(\bar{\gamma})}{\ln(\bar{\gamma})}\right), m_{RD}\right\}, \tag{5.65}$$

where $\rho = 1$ for case a) and $\rho = 0$ for case b). Essentially, at significantly high SNRs DO for case a) tends to the DO for case b), that is, $\text{DO} = \min\{m_r, m_{RD}\}$.

5.4 Performance Analysis under $\kappa-\mu$ Shadowed Fading

In this section, we derive the average SER for the two modulation schemes when the system is under $\kappa-\mu$ shadowed fading. We also obtain the high SNR approximations of the average SERs.

5.4.1 Analytical average SER

The derivation of average SERs for M-PSK and orthogonal M-FSK modulated data is given as follows.

5.4.1.1 M-PSK

The end-to-end average SER for M-PSK modulated data under $\kappa-\mu$ shadowed fading can be evaluated on putting (5.33) and (5.34) in (5.32) and using equations (5.26) and (5.27).

5.4.1.2 Orthogonal M-FSK

The average SER for $\kappa-\mu$ shadowed fading can be obtained by averaging the conditional SER in (5.37) using the PDF (5.24) and applying (B.15). We get

$$P_{e,SR} = \sum_{l_1=0}^{\infty}\sum_{l_2=0}^{\infty} p_{RS,l_1}\, p_{SR,l_2}\Gamma(l_1+\mu_{RS})\Gamma(l_2+\mu_{SR}) \sum_{v=1}^{M-1} \frac{(-1)^{v+1}}{v+1}\binom{M-1}{v} \exp\left(\frac{(v+1)a_{SR}}{2v\bar{\gamma}_{SR}}\right) \times\left(\frac{(v+1)a_{SR}}{v\bar{\gamma}_{SR}}\right)^{\frac{l_1+l_2+\mu_{RS}+\mu_{RS}-1}{2}} W_{\frac{1-l_2-\mu_{SR}-l_1-\mu_{RS}}{2}, \frac{l_2+\mu_{SR}-l_1-\mu_{RS}}{2}}\left(\frac{(v+1)a_{SR}}{v\bar{\gamma}_{SR}}\right), \tag{5.66}$$

Similarly, using (5.37) and the PDF (5.25), $P_{e,RD}$ is derived as

$$P_{e,RD} = \sum_{l_3=0}^{\infty} p_{RD,l_3}\Gamma(l_3+\mu_{RD})\sum_{v=1}^{M-1}\frac{(-1)^{v+1}}{v+1}\binom{M-1}{v}\left(1+\frac{v\bar{\gamma}_{RD}}{(v+1)a_{RD}}\right)^{l_3-\mu_{RD}}. \quad (5.67)$$

The end-to-end average SER for orthogonal M-FSK modulated data can be analyzed by replacing (5.66) and (5.67) in (5.36).

5.4.2 Asymptotic Average SER

At high SNRs, the end-to-end average SER in (5.32) can be simplified as

$$P_e^{\infty} = P_{e,SR}^{\infty} + P_{e,RD}^{\infty}, \quad (5.68)$$

where P_e^{∞}, $P_{e,SR}^{\infty}$, and $P_{e,RD}^{\infty}$ are approximations of P_e, $P_{e,SR}$, and $P_{e,RD}$, respectively. P_e^{∞} for the two modulation schemes are analyzed below.

5.4.2.1 M-PSK

In order to obtain P_e^{∞} in (5.68), an approximate expression of PDF $f_{\gamma_{SR}}(\gamma_{SR})$ is used to derive $P_{e,SR}^{\infty}$. The PDF in (5.24) is a series containing $K_r(\cdot)$. When $\gamma_{SR} >> 1$, $K_r(\cdot)$ can be approximated using (B.6) for the two cases $r=0$ and $|r|>0$, where $r=(l_2+\mu_{SR}-l_1-\mu_{RS})$. The approximation is done considering only the first term of (5.24), that is, the term for $l_1=0$ and $l_2=0$. The considered approximation of the average SER is good for $\kappa_{ij}\to 0$ and deviates with increase in the values of κ_{ij}. In order to get a better approximation for higher values of κ_{ij}, it is required to include more number of terms in the series which raises with increase in κ_{ij}. The method used for approximation of $\kappa_{ij}\to 0$ can be followed when κ_{ij} is large by choosing appropriate number of terms in the series dependent on κ_{ij}.

For $l_1=0$ and $l_2=0$, (5.24) can be written as

$$f_{\gamma_{SR}}(\gamma_{SR}) \approx 2p_{SR}\left(\frac{a_{SR}}{\bar{\gamma}_{SR}}\right)^{\frac{\mu_{RS}+\mu_{RS}}{2}}\gamma_{SR}^{\frac{\mu_{RS}+\mu_{RS}}{2}-1}K_{\mu_{SR}-\mu_{RS}}\left(2\sqrt{\frac{a_{SR}\gamma_{SR}}{\bar{\gamma}_{SR}}}\right), \quad (5.69)$$

where $p_{SR}=p_{RD,0}\,p_{SR,0}$, $p_{ij,0}=(\mu_{ij}\kappa_{ij}/(\mu_{ij}\kappa_{ij}+m_{ij}))^{m_{ij}}/\Gamma(\mu_{ij})$. Now, applying (B.6), (5.69) can be approximated for the two cases: *a*) $(\mu_{RS}-\mu_{SR})=0$ and *b*) $|\mu_{RS}-\mu_{SR}|>0$. The approximated

PDF for cases a) and b) are

$$f^{\infty}_{\gamma_{SR}}(\gamma_{SR}) \approx p_{SR}\left(\frac{a_{SR}}{\bar{\gamma}_{SR}}\right)^{\mu_a}{\gamma_{SR}}^{\mu_a-1}\ln\left(\frac{\bar{\gamma}_{SR}}{4a_{SR}\gamma_{SR}}\right) \tag{5.70}$$

and

$$f^{\infty}_{\gamma_{SR}}(\gamma_{SR}) \approx p_{SR}\Gamma(|\mu_{SR}-\mu_{RS}|)\left(\frac{a_{SR}}{\bar{\gamma}_{SR}}\right)^{\mu_b}{\gamma_{SR}}^{\mu_b-1}, \tag{5.71}$$

respectively where $\mu_a = \mu_{RS} = \mu_{SR}$ and $\mu_b = (\mu_{RS}+\mu_{SR}-|\mu_{RS}-\mu_{SR}|)/2$. The PDFs in (5.70) and (5.71) can be unified as

$$f^{\infty}_{\gamma_{SR}}(\gamma_{SR}) \approx p_{SR}(\Gamma(|\mu_{SR}-\mu_{RS}|))^{\rho_1}\left(\frac{a_{SR}}{\bar{\gamma}_{SR}}\right)^{\mu_r}{\gamma_{SR}}^{\mu_r-1}\left(1+\rho_2\ln\left(\frac{\bar{\gamma}_{SR}}{4ea_{SR}\gamma_{SR}}\right)\right), \tag{5.72}$$

where e is Euler's number, $\mu_r = \mu_a$, $\rho_1 = 0$, and $\rho_2 = 1$ for case a), and $\mu_r = \mu_b$, $\rho_1 = 1$, and $\rho_2 = 0$ for case b).

Putting (5.72) in (5.18) and applying (B.9), the approximated MGF is given by

$$M_{\gamma_{SR}}(s) \approx p_{SR}(\Gamma(|\mu_{SR}-\mu_{RS}|))^{\rho_1}\Gamma(\mu_r)\left(\frac{a_{SR}}{s\bar{\gamma}_{SR}}\right)^{\mu_r}\left(1+\rho_2\ln\left(\frac{s\bar{\gamma}_{SR}}{4ea_{SR}}\right)-\rho_2\psi(\mu_r)\right), \tag{5.73}$$

where $\psi(\cdot)$ is digamma function. Substituting (5.73) in (5.33) and using (B.10), the approximate average SER $P^{\infty}_{e,SR}$ is

$$\begin{aligned} P^{\infty}_{e,SR} \approx{}& \frac{p_{SR}(\Gamma(|\mu_{SR}-\mu_{RS}|))^{\rho_1}\Gamma(\mu_r)}{\pi}\left(\frac{a_{SR}}{g_0\bar{\gamma}_{SR}}\right)^{\mu_r} \\ &\times\left(\left(1+\rho_2\ln\left(\frac{g_0\bar{\gamma}_{SR}}{4ea_{SR}}\right)-\rho_2\psi(\mu_r)\right)\mathcal{I}(\mu_r,\phi_0;\theta)+\rho_2\mathcal{J}(\mu_r,\phi_0;\theta)\right), \end{aligned} \tag{5.74}$$

where $\mathcal{I}(\mu_r,\phi_0;\theta)$ and $\mathcal{J}(\mu_r,\phi_0;\theta)$ are defined in (5.44) and (5.44), respectively.

For $\bar{\gamma}_{RD} >> 1$ and $l_3 = 0$, (5.27) can be approximated as

$$M^{\infty}_{\gamma_{RD}}(s) \approx p_{RD}\Gamma(\mu_{RD})\left(\frac{a_{RD}}{s\bar{\gamma}_{RD}}\right)^{\mu_{RD}}, \tag{5.75}$$

where $p_{RD} = p_{RD,0} = (\mu_{RD}\kappa_{RD}/(\mu_{RD}\kappa_{RD}+m_{RD}))^{m_{RD}}/\Gamma(\mu_{RD})$. Substituting (5.75) in (5.33), we get

$$P^{\infty}_{e,RD} \approx \frac{p_{RD}\Gamma(\mu_{RD})}{\pi}\left(\frac{a_{RD}}{g_0\bar{\gamma}_{RD}}\right)^{\mu_{RD}}\mathcal{I}(\mu_{RD},\phi_0;\theta), \tag{5.76}$$

where $\mathcal{I}(\mu_r, \phi_0; \theta)$ is defined in (5.44).

The asymptotic end-to-end average SER for M-PSK modulated data can be expressed on replacing (5.74) and (5.76) in (5.68). Thus

$$P_e^{\infty} \approx \frac{\mathcal{A}}{(\bar{\gamma}_{SR})^{\mu_r}}\Big((\mathcal{B}+\rho_2 \ln(\bar{\gamma}_{SR}))\,\mathcal{I}(\mu_r, \phi_0; \theta) + \rho_2 \mathcal{J}(\mu_r, \phi_0; \theta)\Big) + \frac{\mathcal{C}}{(\bar{\gamma}_{RD})^{\mu_{RD}}}\mathcal{I}(\mu_{RD}, \phi_0; \theta), \quad (5.77)$$

where

$$\begin{aligned}
\mathcal{A} &= \frac{p_{SR}(\Gamma(|\mu_{SR}-\mu_{RS}|))^{\rho_1}\Gamma(\mu_r)}{\pi}\left(\frac{a_{SR}}{g_0}\right)^{\mu_r}, \\
\mathcal{B} &= 1+\rho_2 \ln\left(\frac{g_0}{4e a_{SR}}\right) - \rho_2 \psi(\mu_r) \quad \text{and} \\
\mathcal{C} &= \frac{p_{RD}\Gamma(\mu_{RD})}{\pi}\left(\frac{a_{RD}}{g_0}\right)^{\mu_{RD}}.
\end{aligned}$$

5.4.2.2 Orthogonal M-FSK

For orthogonal M-FSK modulated data, $P_{e,SR}^{\infty}$ is derived by averaging the conditional SER (5.37) using the PDF in (5.72) and using (B.9) as

$$\begin{aligned}
P_{e,SR}^{\infty} \approx\; & p_{SR}(\Gamma(|\mu_{RS}-\mu_{SR}|))^{\rho_1}\Gamma(\mu_r)\sum_{v=1}^{M-1}\frac{(-1)^{v+1}}{v+1}\binom{M-1}{v} \\
& \times\left(\frac{(v+1)a_{SR}}{v\bar{\gamma}_{SR}}\right)^{\mu_r}\left(1+\rho_2 \ln\left(\frac{v\bar{\gamma}_{SR}}{4e(v+1)a_{SR}}\right)-\rho_2\psi(\mu_r)\right). \quad (5.78)
\end{aligned}$$

For $v\bar{\gamma}_{RD}/((v+1)\mu_{RD}) >> 1$ and considering $l_3 = 0$, (5.67) is reduced to

$$P_{e,RD}^{\infty} \approx p_{RD}\Gamma(\mu_{RD})\sum_{v=1}^{M-1}\frac{(-1)^{v+1}}{v+1}\binom{M-1}{v}\left(\frac{(v+1)a_{RD}}{v\bar{\gamma}_{RD}}\right)^{\mu_{RD}}. \quad (5.79)$$

On substituting (5.78) and (5.79) in (5.68), the asymptotic end-to-end average SER for orthogonal M-FSK modulated data is given by

$$P_e^{\infty} \approx \frac{\mathcal{A}(v;M)+\rho_2\mathcal{B}(v;M)\ln(\bar{\gamma}_{SR})}{(\bar{\gamma}_{SR})^{\mu_r}} + \frac{\mathcal{C}(l;M)}{(\bar{\gamma}_{RD})^{\mu_{RD}}}, \quad (5.80)$$

where

$$\mathcal{A}(v;M) = \mathcal{B}(v;M)\left(1+\rho_2 \ln\left(\frac{v}{4e(v+1)a_{SR}}\right)-\rho_2\psi(\mu_r)\right), \quad (5.81)$$

$$\begin{aligned}
\mathcal{B}(v;M) &= p_{SR}(\Gamma(|\mu_{RS}-\mu_{SR}|))^{\rho_1}\Gamma(\mu_r)\left(\frac{a_{SR}}{\bar{\gamma}_{SR}}\right)^{\mu_r}\sum_{v=1}^{M-1}\mathcal{D}(v:M)\,,\\
\mathcal{C}(v;M) &= p_{RD}\Gamma(\mu_{RD})\sum_{v=1}^{M-1}\frac{(-1)^{v+1}}{(v+1)}\binom{M-1}{v}\left(\frac{(v+1)a_{RD}}{v}\right)^{\mu_{RD}}, \quad \text{and}\\
\mathcal{D}(v;M) &= \frac{(-1)^{v+1}}{(v+1)}\binom{M-1}{v}\left(\frac{(v+1)}{v}\right)^{\mu_r}. \qquad (5.82)
\end{aligned}$$

5.4.3 Optimal Relay Location

The end-to-end asymptotic average SERs (5.77) and (5.80) can be utilized to obtain the optimal relay location as in Section 5.3.3. However, the analysis is applicable only for $\kappa_{ij} \to 0$. Therefore a more reliable analysis for higher values of κ_{ij} can be investigated on considering appropriate number of terms in the infinite series (5.24).

5.4.4 Diversity order

The asymptotic average SER in (5.77) and (5.80) can be rearranged to get the form (5.64). Thence, the DO of the system can be obtained as

$$\text{DO} = \min\left\{\left(\mu_r - \rho\frac{\ln\ln(\bar{\gamma})}{\ln(\bar{\gamma})}\right), \mu_{RD}\right\}, \qquad (5.83)$$

where $\rho = 1$ for case *a*) and $\rho = 0$ for case *b*). At significantly high SNRs, the system possesses $\text{DO} = \min\{\mu_r, \mu_{RD}\}$.

5.5 Numerical Results

The different results derived in this chapter are plotted in this section. Simulated results are also obtained by emulating the system described in Section 5.2 in `MATLAB`. The end-to-end average SER expressions deduced in Sections 5.3 and 5.4 for Nakagami-m and $\kappa-\mu$ shadowed fading environment, respectively are plotted. The numerical results for these two fading models are also presented. Without loss of generality, we assume unit symbol duration, that is, $T_s = 1$ second. The transmission power at the relay is considered in dBm and the noise PSD is taken as $N_0 = 10^{-4}$ watts per hertz (W/Hz). Channel gains and energy conversion efficiency are assumed to be unity, that is, $\lambda_{ij}(d_{ij})^{-\alpha_{ij}} = 1$ and $\zeta = 1$, respectively, unless otherwise stated.

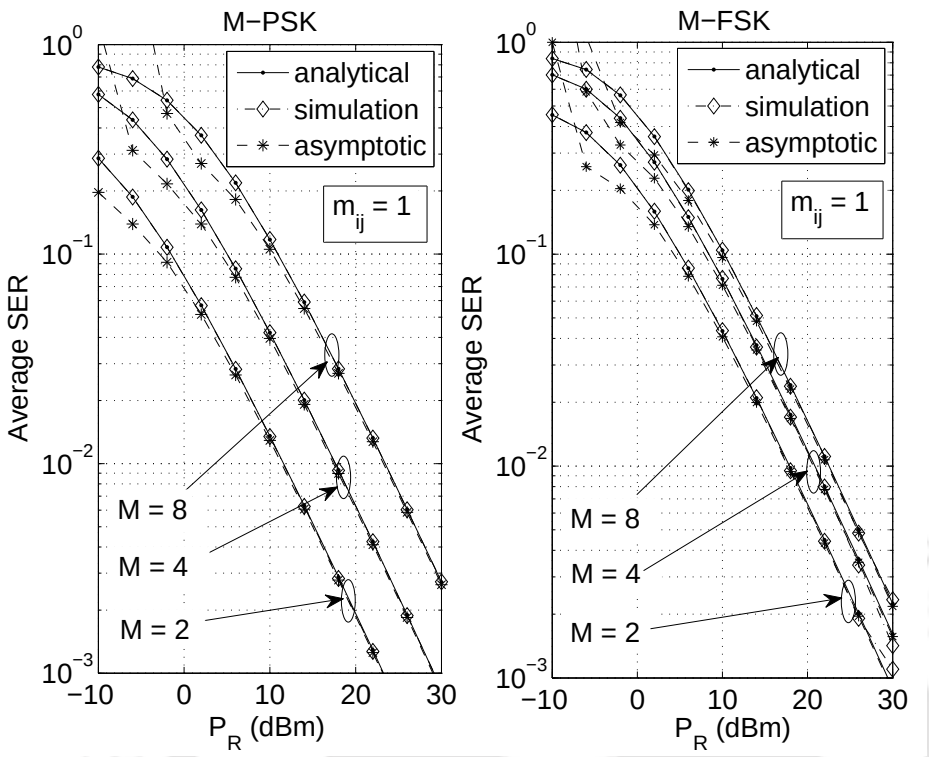

Figure 5.2: Average SER versus transmission power P_R for M-PSK and orthogonal M-FSK when $m_{ij} = 1$.

5.5.1 Nakagami-m Fading

In this subsection, we present numerical results for the end-to-end average SER of the system affected under Nakagami-m fading.

Figure 5.2 compares average SER of M-PSK and orthogonal M-FSK for different modulation orders when $m_{ij} = 1$. Analytical average SER (P_e) for M-PSK is obtained on substituting (5.33), (5.34), (5.19), and (5.20) in (5.32), whereas for orthogonal M-FSK the terms in (5.36) are evaluated using (5.38), (5.39). The plots in Figure 5.2 depict that the analytical result matches perfectly with the simulation results, hence validating our analysis. Asymptotic average SERs for M-PSK and orthogonal M-FSK are also presented using (5.52) and (5.61), respectively. The asymptotic results are found to be close approximation of the average SER at high SNRs. The plots in Figure 5.2 can be useful for selecting modulation scheme and order based on reliability, feasible system complexity, and available resources such as power and bandwidth, etc.

In Figures 5.3 and 5.4, plots showing variation in the average SER with source-to-relay distance d_{SR} are presented for 4-PSK and orthogonal 2-FSK schemes, respectively. Nodes are considered to be planner and inter link distances follow the relation $d_{SR} + d_{RD} = \beta d_{SD}$. Let $m_{RS} = m_{SR} = m_a$

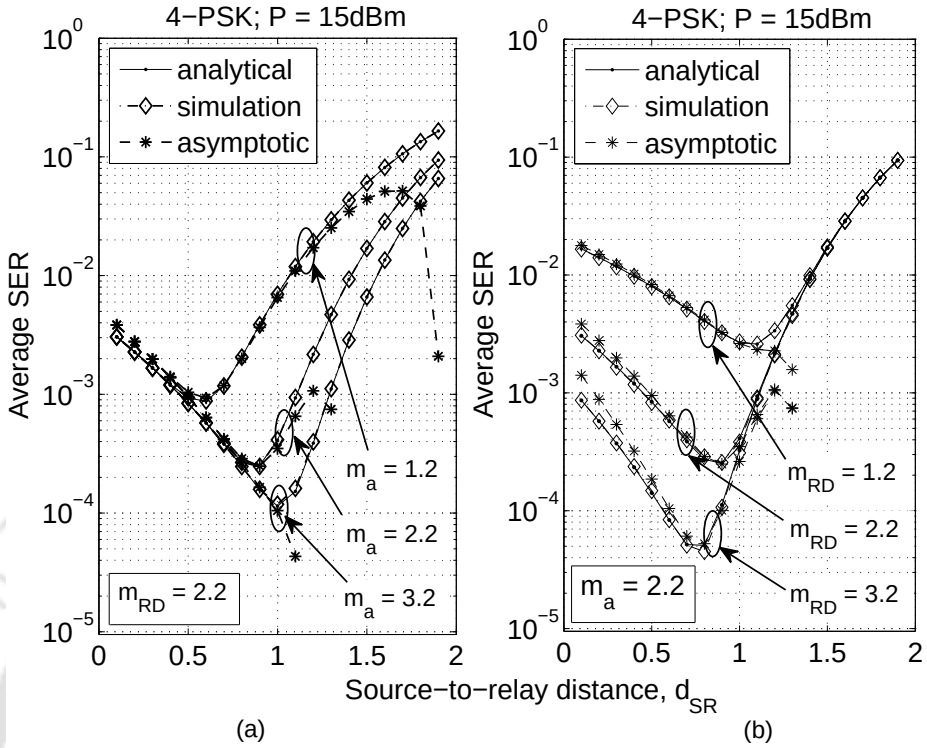

Figure 5.3: Variation in average SER for 4-PSK with fading parameters m_{ij} and distance d_{SR} for $d_{SR}+d_{RD} = \beta d_{SD}, \beta = 1.1, d_{SD} = 2$ unit, $\lambda_{ij} = 1$, $\alpha_{ij} = 3$.

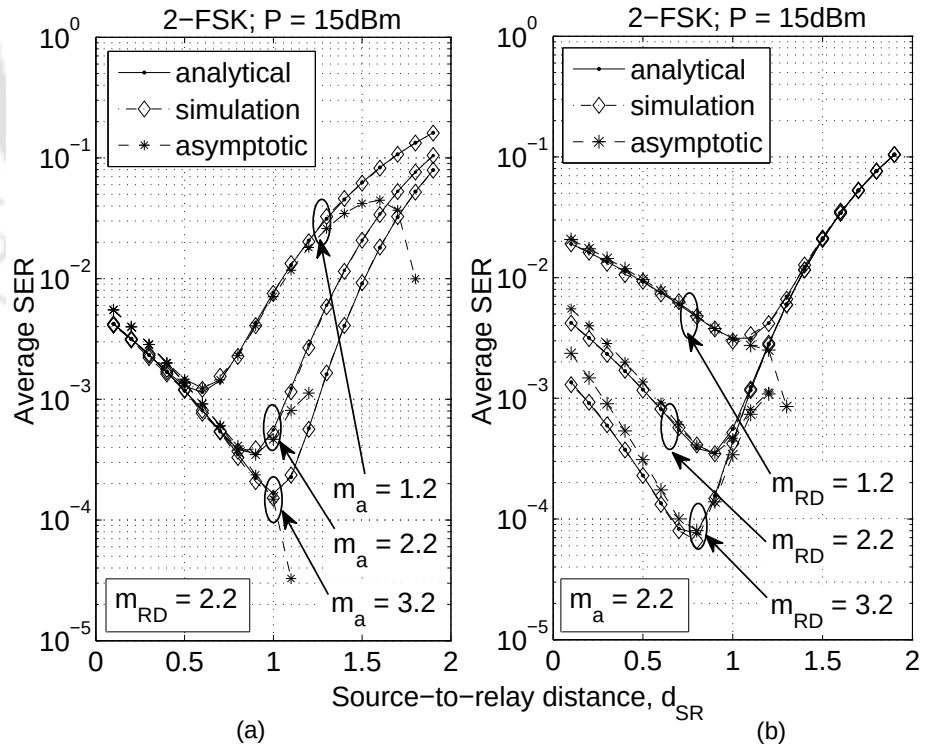

Figure 5.4: Variation in average SER for orthogonal 2-FSK with fading parameters m_{ij} and distance d_{SR} for $d_{SR} + d_{RD} = \beta d_{SD}, \beta = 1.1, d_{SD} = 2$ unit, $\lambda_{ij} = 1$, $\alpha_{ij} = 3$.

(Case a)), $d_{SD} = 2$ unit, λ_{ij}, and $\alpha_{ij} = 3$. In Figures 5.3(a) and 5.4(a), plots are shown for varying m_a when m_{RD} is fixed. Further, plots for different m_{RD} when m_a is constant are presented in Figures 5.3(b) and 5.4(b). We observe that the optimal relay location depends on links quality; it lies between the source and destination nodes and moves toward the node with poor link quality. In Figures 5.3(a) and 5.4(a), the optimal relay location inclines toward node S for small m_a and when m_a is increased the optimal solution shifts toward node D. Similarly, in Figure 5.3(b) and 5.4(b), the optimal relay location is close to node D for small m_{RD} and when m_{RD} is increased, it moves toward node S. For small m_a, if node S is located close to node R then the energy harvested at the node S is relatively high to support reliable end-to-end transmission. Otherwise, if node R is located close to node D then even for small m_{RD} the chances of reliable reception increases.

The optimal relay location in case of 4-PSK and orthogonal 2-FSK modulation schemes can be obtained by applying Golden-section search method on (5.62) and (5.63), respectively. In Figure 5.3(a), the optimal distance for $m_a = 1.2$ and $m_a = 2.2$ are obtained as $d_{SR} = 0.5871$ and $d_{SR} = 0.8847$, respectively. Similarly, in Figure 5.3(b), the optimal distances are $d_{SR} = 0.8847$ and $d_{SR} = 0.0.7719$ for $m_{RD} = 2.2$ and $m_{RD} = 3.2$, respectively. The optimal relay location in Figure 5.4(a) are obtained as 0.6080 and 0.8911 for $m_a = 1.2$ and $m_a = 2.2$, respectively. In Figure 5.4(b), the optimal relay location for $m_{RD} = 2.2$ and $m_{RD} = 3.2$ are obtained as 0.8911 and 0.7833, respectively. However, in Figures 5.3(a) and 5.4(a), we observe that the plot of P_e^{∞} for $m_a = 3.2$ is not convex. Therefore optimal relay location cannot be obtained for this case using the asymptotic approximation. Similarly, optimal relay locations cannot be obtained for $m_{RD} = 1.2$ in Figures 5.3(b) and 5.4(b). The conditions for which P_e^{∞} is not convex can be derived using (5.62) and (5.63).

In Figure 5.5, variation in average SER with energy conversion efficiency ζ and distance d_{SR} is shown for 4-PSK scheme, $d_{SR} + d_{RD} = \beta d_{SD}$, $d_{SD} = 2$ unit, $\beta = 1.1$, and $P_R = 15$ dBm. Fading parameters are taken as $m_a = 2.2$, $m_{RD} = 2.2$. We observe that with increase in ζ: i) the system's performance improves and ii) the relative improvement in the performance degrades. Further, the optimal relay location inclines toward the source node for smaller value of ζ.

In Figure 5.6, variation in average SER with β is shown for 4-PSK scheme, $d_{SR} + d_{RD} = \beta d_{SD}$, $d_{SD} = 2$ unit, $\zeta = 1$, and $P_R = 15$ dBm. Fading parameters are taken as $m_a = 2.2$, $m_{RD} = 2.2$. We observe that the optimal relay location shifts toward the destination node with increase in β.

The asymptotic average SER P_e^{∞} in (5.40) is sum of high SNR approximations $P_{e,SR}^{\infty}$ and $P_{e,RD}^{\infty}$.

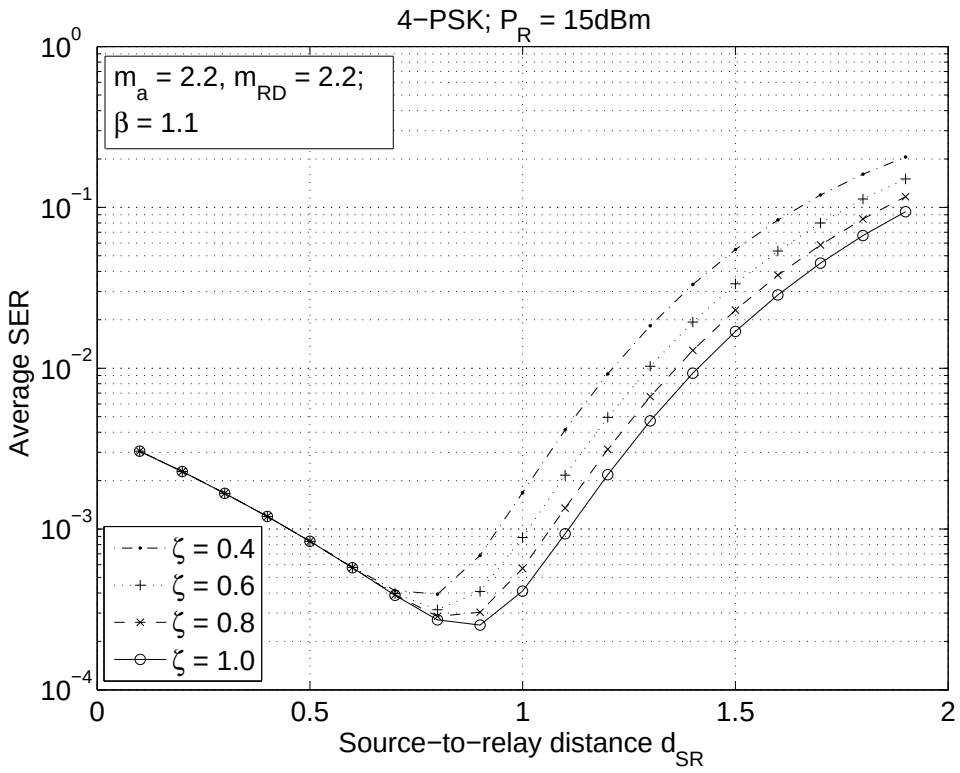

Figure 5.5: Variation in average SER for 4-PSK with energy conversion efficiency ζ and distance d_{SR} for $d_{SR} + d_{RD} = \beta d_{SD}, \beta = 1.1, d_{SD} = 2$ unit, $d_{SR} \in (0, d_{SD})$, $\lambda_{ij} = 1$, $\alpha_{ij} = 3$.

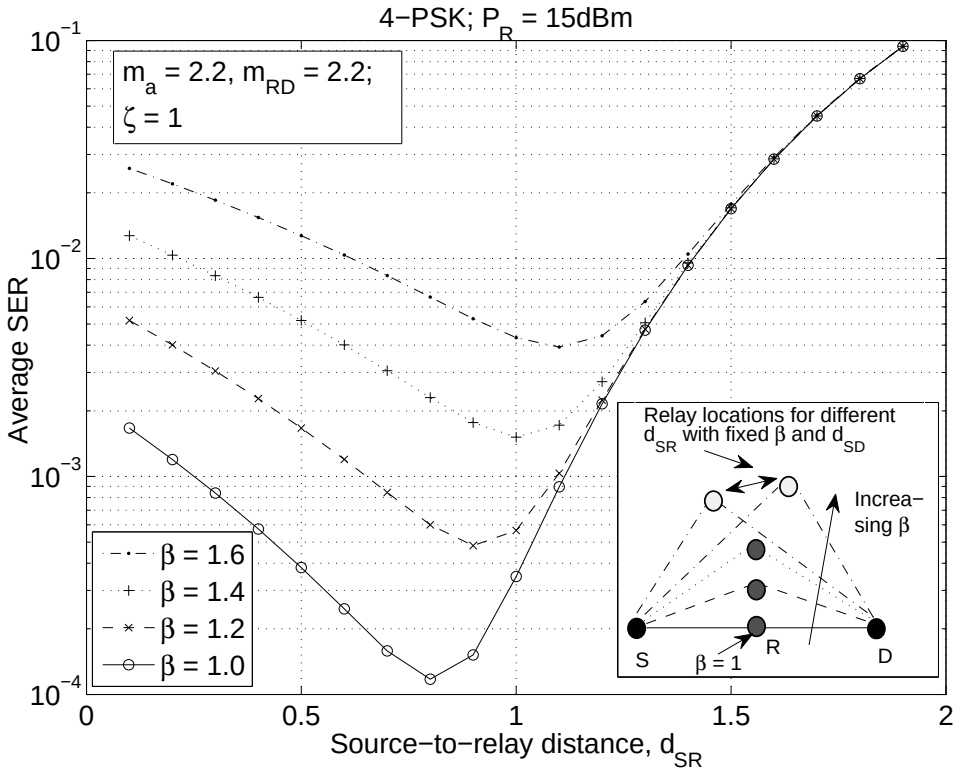

Figure 5.6: Variation in average SER for orthogonal 4-PSK with distance d_{SR} and β for $d_{SR} + d_{RD} = \beta d_{SD}, d_{SD} = 2$ unit, $d_{SR} \in (0, d_{SD})$, $\lambda_{ij} = 1$, $\alpha_{ij} = 3$, $\zeta = 1$.

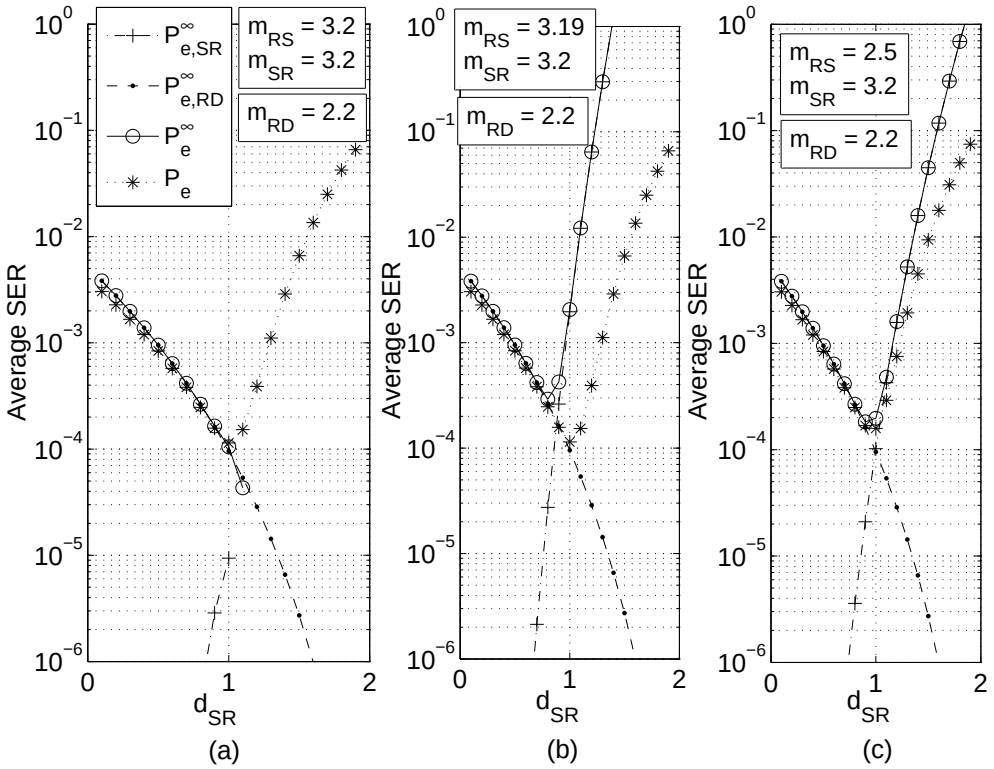

Figure 5.7: Variation in average SER for 4-PSK with source-to-destination distance d_{SR} and fading parameter m_{RS} for $d_{SR}+d_{RD}=\beta d_{SD}, \beta=1.1, d_{SD}=2$ unit, $\lambda_{ij}=1$, $\alpha_{ij}=3$, $P_R=15$ dBm.

Since $P^{\infty}_{e,SR}$, $P^{\infty}_{e,RD}$, and P^{∞}_{e} are error probabilities, therefore they must be individually positive. $P^{\infty}_{e,RD}$ in (5.51) and (5.60) for M-PSK and orthogonal M-FSK modulation schemes, respectively is always positive. Also, $P^{\infty}_{e,SR}$ for $|m_{RS}-m_{SR}|>0$ in (5.48) and (5.57) is positive in the two modulation schemes. When $(m_{RS}-m_{SR})=0$, $P^{\infty}_{e,SR}$ in (5.43) for M-PSK and (5.55) for orthogonal M-FSK can be negative because of the terms $\left(\ln\left(g_0\bar{\gamma}_{SR}/(4m_a^2)\right)-\psi(m_a)\right)$ and $\left(\ln\left(l\bar{\gamma}_{SR}/(4(l+1)m_a^2)\right)-\psi(m_a)\right)$, respectively. In case of M-PSK modulation scheme with $(m_{RS}-m_{SR})=0$, $P^{\infty}_{e,SR}$ in (5.43) is negative for

$$\bar{\gamma}_{SR}<\frac{4m_a^2}{g_0}\exp\left(\psi(m_a)-\frac{\mathcal{J}(m_a,\phi_0;\theta)}{\mathcal{I}(m_a,\phi_0;\theta)}\right),$$

where $\mathcal{I}(m_a,\phi_0;\theta)$ and $\mathcal{J}(m_a,\phi_0;\theta)$ are defined in (5.44) and (5.45), respectively. Similarly, in case of orthogonal M-FSK modulation schemes with $(m_{RS}-m_{SR})=0$, $P^{\infty}_{e,SR}$ in (5.55) is negative for

$$\bar{\gamma}_{SR}<\left(\frac{\exp(c_1\psi(m_a))}{c_2}\right)^{1/c_1},$$

where $c_1=\sum_{l=1}^{M-1}\mathcal{D}(l)$ and $c_2=\prod_{l=1}^{M-1}(l/(4(l+1)m_a^2))^{\mathcal{D}(l)}$ for $m_r=m_a$.

In Figure 5.7, $P_{e,SR}^{\infty}$, $P_{e,RD}^{\infty}$, P_e^{∞}, and P_e are plotted with d_{SR} considering $P_R = 15$ dBm and data is 4-PSK modulated. The markers used in Figure 5.7(a) also applies to Figures 5.7(b) and (c). We observe from plots that P_e^{∞} is mainly determined by $P_{e,RD}^{\infty}$ for small d_{SR} and a transition is observed for d_{SR} greater than optimal d_{SR} when dependency shifts to $P_{e,SR}^{\infty}$. For optimal d_{SR} sum of $P_{e,SR}^{\infty}$ and $P_{e,RD}^{\infty}$ is minimum. In Figure 5.7(a) for $(m_{RS} - m_{SR}) = 0$, $P_{e,SR}^{\infty}$ is negative and thus the plot of asymptotic average SER is non-convex. Next, we consider $|m_{RS} - m_{SR}| = 0.1$ in Figure 5.7(b) and observe that the asymptotic average SER is a loose bound for small value of $|m_{RS} - m_{SR}|$. This is because the approximation of $K_r(\cdot)$ in (5.16) used to obtain (5.41) and (5.46) is loose when $|m_{RS} - m_{SR}| \to 0$. Further, in Figure 5.7(c) with $|m_{RS} - m_{SR}| = 0.7$, the plot corresponding to asymptotic average SER is relatively close to the analytical results. This difference reduces further with increase in $|m_{RS} - m_{SR}|$. Thus we conclude that for negative $P_{e,SR}^{\infty}$, optimal d_{SR} cannot be determined using Golden-section search method if P_e^{∞} is non-convex. This can be true if i) the relay is close to the destination node, that is, d_{SR} is large or $(\beta d_{SD} - d_{SR})$ is small and ii) either m_a increases for fixed m_{RD} or m_{RD} decreases for fixed m_a. The optimal d_{SR} for $|m_{RS} - m_{SR}| > 0$ can be obtained using (5.62) and (5.63) for M-PSK and orthogonal M-FSK modulation schemes, respectively. The accuracy improves with increase in $|m_{RS} - m_{SR}|$.

5.5.2 $\kappa-\mu$ Shadowed Fading

For system affected under $\kappa-\mu$ shadowed fading, analytical results for M-PSK modulation scheme are obtained using (5.33), (5.34), (5.26), and (5.27) in (5.32), and for orthogonal M-FSK modulation scheme using (5.66) and (5.67) in (5.36). Analytical average SER evaluation requires computation of average SER factors $P_{e,SR}^{\infty}$ and $P_{e,SR}^{\infty}$ which are in infinite series form. These series converge faster with increase in the number of terms. Let N_1 and N_2 terms are required for the computation of $P_{e,SR}^{\infty}$ and $P_{e,SR}^{\infty}$, respectively. The required number of terms in the series varies with change in the value of fading parameters κ_{ij}, μ_{ij}, and m_{ij}. Analytical results in this section are obtained for $N_1 = 20$ and $N_2 = 20$. For M-PSK and orthogonal M-FSK, (5.26) and (5.66), respectively are two-fold summations. The number of terms N_1 is equally divided for the two summations, that is, the upper limit of each summation is $N_1/2 - 1$. Asymptotic average SER are also evaluated using (5.70) and (5.71) and plotted to check the accuracy of the approximation.

Figure 5.8 presents average SER versus relay transmission power P_R plots for the two modulation

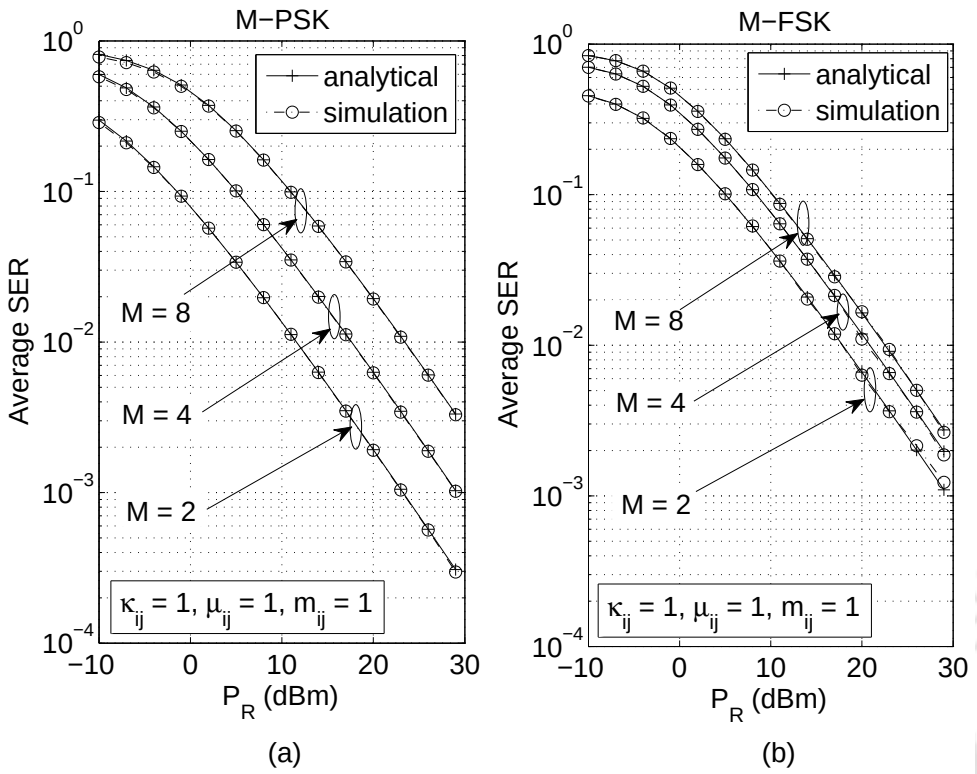

Figure 5.8: Average SER comparison of coherent M-PSK and noncoherent orthogonal M-FSK modulation scheme when the system is affected under $\kappa-\mu$ shadowed fading.

schemes. We choose $\kappa_{ij} = 1$, $\mu_{ij} = 1$, $m_{ij} = 1$. The analytical results match with the simulation results for all modulation schemes and orders. Hence, our analysis for the system is validated.

Figure 5.9 compares the closeness of asymptotic average SER with analytical average SER for different values of $\kappa_{RS} = \kappa_{SR} = \kappa_a \in \{0, 1, 2\}$. 4-PSK modulation scheme is considered. We observe that for $\kappa_a = 0$ the asymptotic average SER is a good approximation of the analytical average SER at high SNRs. However, it deviates for the higher values of κ_a. The asymptotic average SER is derived considering the first term of the series (5.24). A better approximation for higher values of κ_a can be attained using the asymptotic average SER expression derived by considering more than one term in the series. This comparison follows for case b) and other orders of both modulations schemes.

In Figure 5.10, we plot average SER versus source-to-relay distance for 4-PSK with variation in μ_{ij}. We consider nodes are located on a plane satisfying the distance relation $d_{SR} + d_{RD} = \beta d_{SD}$, for $\beta \geq 1$. We assume $\beta = 1.1$, $\alpha_{ij} = 3$, $\lambda_{ij} = 1$. Let $\mu_{RS} = \mu_{SR} = \mu_a$, $\kappa_{RS} = \kappa_{SR} = \kappa_a$ and $m_{RS} = m_{SR} = m_a$ for case a). In Figure 5.10(a), we fix the fading parameters $\mu_{RD} = 2$, $\kappa_{ij} = 2$ and $m_{ij} = 2$, except μ_a and plot average SER for $\mu_a \in \{1, 2, 3\}$. In Figure 5.10(b), plots are shown for

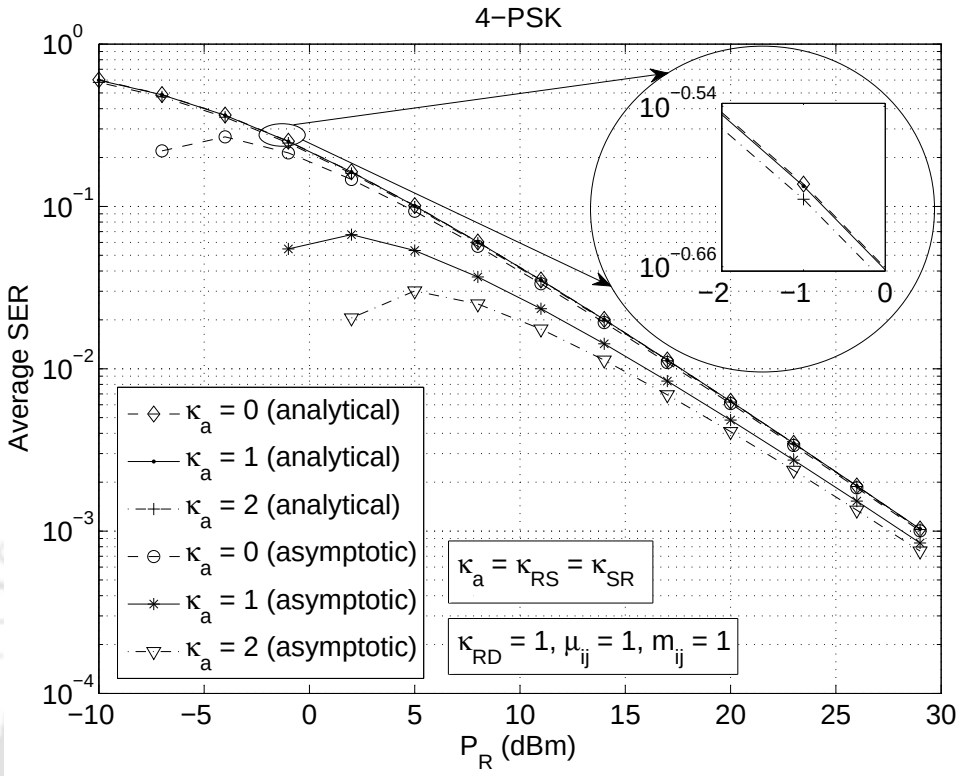

Figure 5.9: Analytical and asymptotic average SER comparison for different values of $\kappa_{RS} = \kappa_{SR}$.

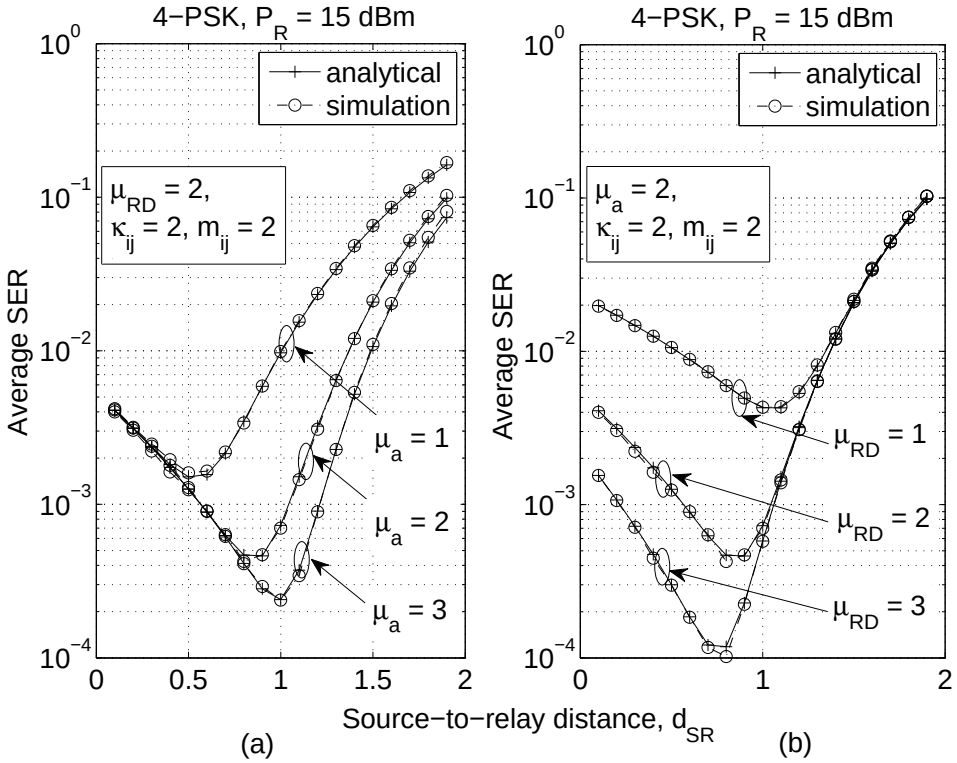

Figure 5.10: Average SER versus source-to-relay distance for coherent 4-PSK with variation in μ_a and μ_{RD}.

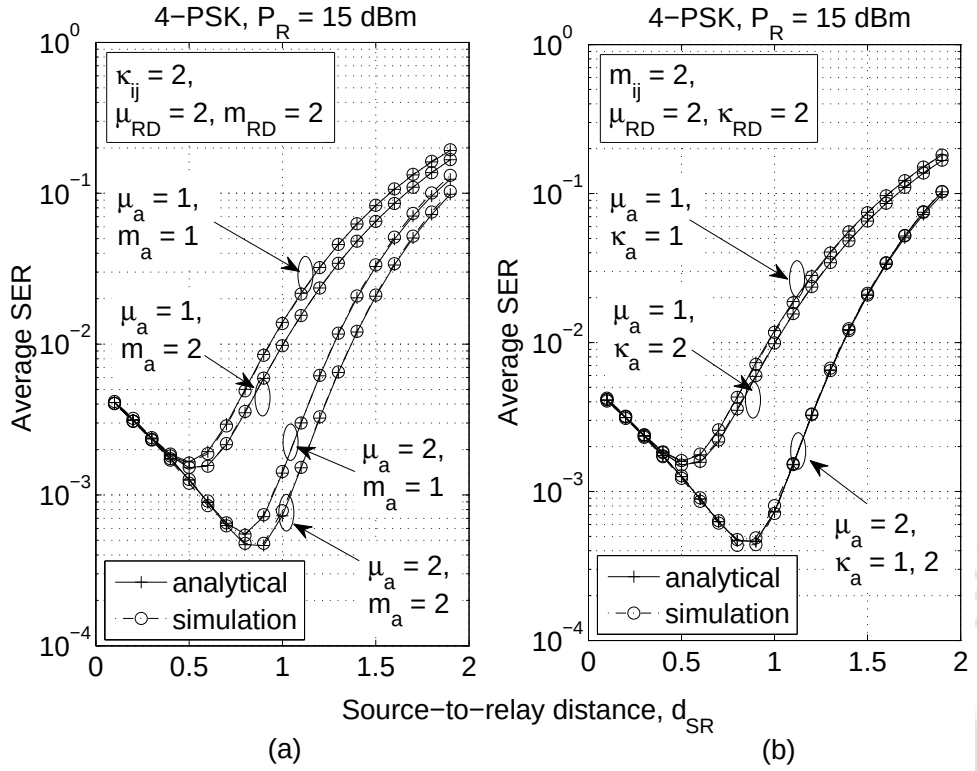

Figure 5.11: Average SER versus source-to-relay distance for coherent 4-PSK with variation in μ_a, κ_a and m_a.

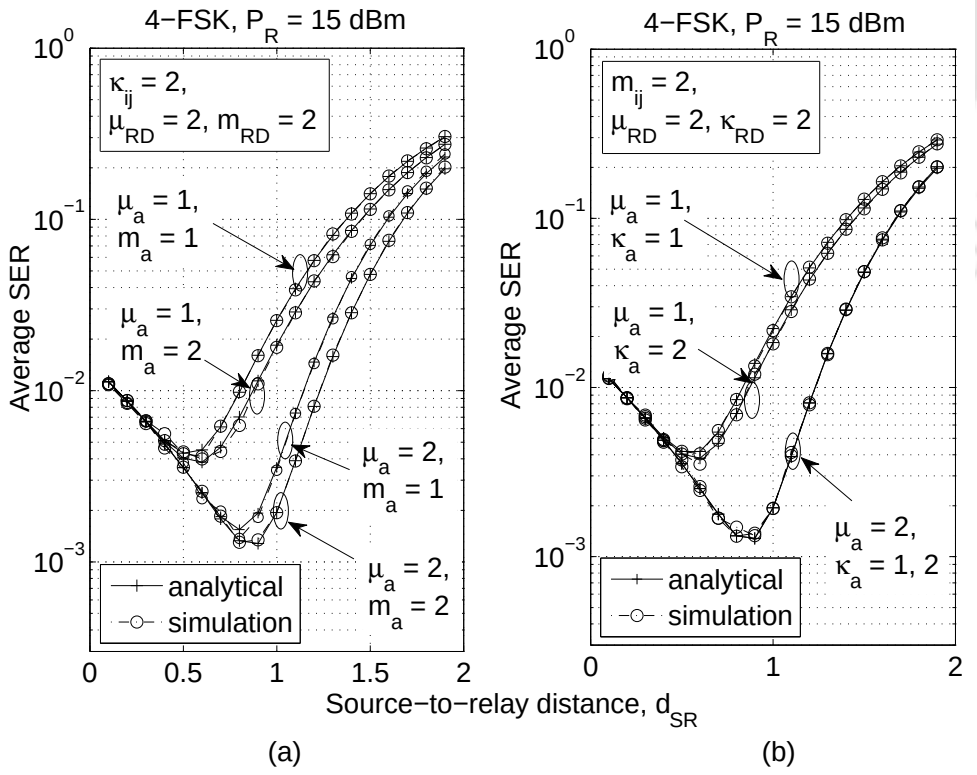

Figure 5.12: Average SER comparison of noncoherent 4-FSK for varying μ_a, κ_a and m_a.

Abstract-TH-2151_136102001

$\mu_{RD} \in \{1, 2, 3\}$ when other fading parameters are constant, that is, $\mu_a = 2$, $\kappa_{ij} = 2$, $m_{ij} = 2$. We observe that the optimal relay location is close to the node with poor link quality. We further observe that improvement in the performance is more for increase in μ_a as compared to μ_{RD} when relay is near to the destination node. To visualize this effect compare the change in average SER with μ_a and μ_{RD} in Figure 5.10(a) and Figure 5.10(b), respectively for $d_{SR} > 1$. When relay is located near the source node, that is, $d_{SR} < 1$, then improvement in the performance is more for increase in μ_{RD} as compared to μ_a. This analysis applies to case b) and other modulation orders/scheme as well.

In Figure 5.10, we compared the change in performance with μ_a and μ_{RD}. Now, we compare the change in performance with fading quality of SR link in Figure 5.11 and Figure 5.12 for 4-PSK and 4-FSK, respectively. The node location and other assumptions are made as in Figure 5.10. In Figure 5.11(a) and Figure 5.12(a), for fixed κ_{ij}, μ_{RD} and m_{RD}, plots are presented to compare the variation in the performance with μ_a and m_a. We observe that increase in the values of μ_a has better impact on the performance improvement as compared to that of m_a. Similarly, in Figure 5.11(b) and Figure 5.11(b), for constant m_{ij}, μ_{RD} and m_{RD} we compare the variation in the performance with μ_a and κ_a. The increase in μ_a dominates over the increase in κ_a. Moreover, comparing Figure 5.11(a) and Figure 5.11(b) for 4-PSK and Figure 5.12(a) and Figure 5.12(b) for 4-FSK, it can be observed that increase in m_a dominates over increase in κ_a. A similar analysis can be followed with variation in fading quality of RD link.

5.6 Conclusion

In this chapter, we deduce expressions for the average SER of a three-node WP DF relay system under Nakagami-m and κ−μ shadowed fading. Energy-constrained source node harvests energy using the RF signal radiated by the relay node. The analysis is presented for M-PSK and orthogonal M-FSK modulated data. We also obtained high SNRs approximation of the average SER for the two modulation schemes when links are Nakagami-m faded. In case of κ−μ shadowed fading, the approximations are satisfactory when κ parameter of SR link tend to zero ($\kappa_{RS}, \kappa_{SR} \to 0$). Through numerical results we observe that the optimal relay location lies almost halfway between source node and destination node with slight inclination towards the node having poor link quality. We also observe that if relay node is located near the source node then the performance improvement is more for increase in fading parameters of the RD link when compared with that of the SR link. Instead, if

relay is close to the destination then increase in fading parameter of the SR link dominates over that for the RD link. Furthermore, in $\kappa-\mu$ shadowed fading environment, among the fading parameters κ, μ and m, increment in μ has the best impact on the performance improvement, while increment in κ has the least impact.

6

Summary and Discussions

Contents

In this thesis, we analyze the average SER of conventional and WP three-node DF relay systems under different fading environments. High SNR approximations of the average SER are also obtained for each system to simplify the analysis. This chapter presents a summary of the thesis and suggests possible future directions.

6.1 Summary of the Present Work

This section briefly summarizes the thesis and discusses the main contributions and findings from the work.

- ✓ **Exhaustive literature review on performance analysis of conventional and WP relay systems:**

  We have done an in-depth review of the literature available on performance analysis of relay systems. The main focus of the work is analyzing the performance of one-way half-duplex relay systems where nodes are equipped with a single antenna. Some of the related works which consider more complex systems, including two-way relaying, full-duplex relaying, multiple antenna assisted relaying, multiple access in relaying, etc., are also discussed. The literature review is carried out for both conventional and WP relay systems. Different fading models and basics of RF-based EH have also been briefed.

- ✓ **Average SER analysis of conventional three-node DF relay system under $\kappa-\mu$, $\eta-\mu$, and mixed $\kappa-\mu$ and $\eta-\mu$ fading:**

  We considered a conventional three-node DF relay system where all nodes are powered by batteries, which have infinite storage or can be recharged or replaced when exhausted. Average SER analysis is presented for M-PSK modulated data when links are $\kappa-\mu$, $\eta-\mu$, and mixed $\kappa-\mu$ and $\eta-\mu$ faded. High SNR approximation of the average SER is also obtained to analyze DO of the system and allocate optimal power to source and relay node. Through numerical results, we observed that: i) when the total power is optimally assigned to the source and the relay node, the system performs better. ii) the optimal relay location lies almost halfway between the source and the destination node, and shifts toward the destination node when channel quality improves, iii) improvement in RD link quality results in better performance when compared to increase in that of SR link, and iv) among κ and μ parameters in $\kappa-\mu$ fading and η and μ parameters in $\eta-\mu$ fading, the improvement in performance with increase in μ parameter dominates.

✓ **Average SER analysis of WP three-node DF relay system under Nakagami-m fading (EH at relay node):**

Next, we present SER analysis when data is transmitted over a WP three-node DF relay system. Average SER and throughput of the system are analyzed for M-PSK modulated data under Nakagami-m fading. Two cases are considered for the analysis; in the first case, direct (SD) link is considered for the analysis; while in the second case, it is assumed that direct link is in deep fade and hence its effect is ignored. Asymptotic average SER expressions are also derived at high SNRs to obtain DO of the system and allocate optimal resources, viz. energy, power, and time. Through numerical results, the following main observations are made: i) improvement in SR link quality results in better performance when compared to increase in that of RD link, ii) the performance improves if the relay node is placed close to either source or destination, optimal results are achieved when relay is placed close to source, and iv) average SER and throughput of the system with direct link is always better than the system without direct link.

✓ **Average SER analysis of WP three-node DF relay system under Nakagami-m and $\kappa-\mu$ shadowed fading (EH at source node):**

Lastly, we have analyzed the average SER of a WP two-hop DF relay system under Nakagami-m and $\kappa-\mu$ shadowed fading. Energy-constrained source node relies on the RF signal radiated by the relay node for EH. Data follows either M-PSK or orthogonal M-FSK modulation. Asymptotic average SERs are derived and used to analyze system's DO and optimal relay location. Through numerical results we observed that if the relay node is located near the source node then the performance improvement is more for the increase in fading parameters of the RD link when compared with that of the SR link. Otherwise, if the relay node is near to the destination node then the increase in fading parameters of the SR link dominates over that of the RD link. The optimal relay location lies between source node and destination node with inclination towards the node with poor link quality. Also, under $\kappa-\mu$ shadowed fading environment, the impact of μ is maximum on the performance improvement among the fading parameters κ, μ, and m, whereas increment in κ has the least impact.

6.2 Suggestions for Future Work

The possible future research directions in which our present work can be extended are listed below.

★ **Conventional relay systems:** The work in Chapter 3 can be further explored in the following directions.

- Average BER of conventional multihop DF relay system under $\kappa-\mu$ and $\eta-\mu$ fading for M-QAM scheme is analyzed in [119, 120]. In [121], outage probability is examined for conventional parallel DF relay system under $\kappa-\mu$ and $\eta-\mu$ fading. Outage probability under $\kappa-\mu$ shadowed fading is analyzed for conventional parallel AF and DF relay systems in [112]. In [81], average SER of parallel DF relay system under $\eta-\mu$ fading is analyzed for M-PSK and M-QAM modulation schemes. Average BER/SER of conventional parallel relay systems under $\kappa-\mu$ and/or $\kappa-\mu$ shadowed fading can be analyzed for M-ary modulation schemes.
- Outage probability and average BER of dual-hop DF relay system under $\eta-\mu$ fading in the presence of co-channel interference are examined in [118]. Binary modulation schemes are considered for the analysis. To the best of our knowledge, investigation of the average BER/SER for dual-hop, multihop, and/or parallel relay systems in the presence of co-channel interference is not reported in the literature for M-ary modulation schemes and generalized fading models. Because it can have mathematical challenges. The analysis can be simplified with the help of mathematical tools, such as Meijer-G function, Fox-H function, Mellin transform, etc.
- In [86], average BER of full-duplex dual-hop relay system under Rayleigh and Nakagami-m fading is analyzed for BPSK scheme. The analysis can be extended for higher order modulation schemes under $\kappa-\mu$, $\eta-\mu$, and/or $\kappa-\mu$ shadowed fading.

★ **WP relay systems:** The analysis for WP relay systems in Chapters 4 and 5 can be extended to following possible future directions.

- In [146], the average BER is investigated for binary modulation schemes under $\kappa-\mu$ and $\eta-\mu$ fading. The analysis can be extended for M-ary modulation schemes. Though, it may incur mathematical difficulties, which can be tackled with the help of mathematical tools, namely, Meijer-G function, Fox-H function, and Mellin transform.
- Instead of a single relay node, multiple relay nodes can be considered between source and destination. This would improve the diversity gain of the system. Full-duplex mimicking

[32] can be considered to improve the throughput. The analysis can be further extended for the system having nodes equipped with multiple antennas. Effects due to the presence of interference can also be investigated. In [141, 142], analysis of SWIPT networks in the presence of co-channel interferences in presented.

- In this thesis, we have made assumptions to simplify the analysis of the WP relay systems. The main assumptions are i) negligible power consumption in elementary circuitries, such as encoder, decoder, modulator, demodulator, etc., ii) linear EH model, and iii) harvest-use approach to process the incoming energy flow. In practical scenarios, power consumption in these circuitries cannot be neglected [148], and EH model is nonlinear [59, 175, 176]. Moreover, due to small RF-based energy arrival at harvester, the harvest-store-use approach for processing harvested energy can be more desirable [131]. This approach enables energy-constrained nodes to accumulate energy until a minimum amount of energy is stored. Then the accumulated energy can be used for data transmission. By considering these facts, the analysis can be extended to incorporate more practical scenarios.
- Performance analysis of WP heterogeneous cellular networks using stochastic geometry is also an interesting area of research [74, 139, 143]. In such networks, nodes are considered to be randomly deployed and their location is modeled using a Poisson point process. Performance of a system comprising one source, one destination, and multiple energy-constrained random relay nodes is analyzed in [143]. The transmission technique considered in Chapter 4 can be investigated for such systems on incorporating the appropriate modifications.

A

Derivation of $P_{e,\mathrm{EGC}}$, PDF $f_{\gamma_{\mathrm{EGC}}}(\gamma_{\mathrm{EGC}})$ and Its Asymptotic Approximation

Contents

A.1 Product of Two Nakagami-m Distributed Random Variables

The cumulative distribution function (CDF) of the random variable $t_2 = \nu_2|h_{SR}||h_{RD}|$, which is a scaled version of the product of two Nakagami-m distributed random variables, can be obtained by solving

$$\begin{aligned} F_{t_2}(t_2) &= \Pr[\nu_2|h_{SR}||h_{RD}| \leq t_2] \\ &= \int_0^\infty \Pr\left[|h_{SR}| \leq \frac{t_2}{\nu_2|h_{RD}|}\right] f_{|h_{RD}|}(|h_{RD}|)d|h_{RD}|. \end{aligned} \tag{A.1}$$

Equation (A.1) can be simplified using the PDF of $|h_{RD}|$ in (4.9) and the CDF of $|h_{SR}|$ given as

$$F_{|h_{SR}|}(|h_{SR}|) = \frac{1}{\Gamma(m_{SR})}\gamma\Big(m_{SR}, \frac{m_{SR}}{\lambda_{SR}}|h_{SR}|^2\Big),$$

where $\gamma(\cdot)$ is lower incomplete gamma function. Thus, (A.1) is

$$\begin{aligned} F_{t_2}(t_2) &= \int_0^\infty \frac{1}{\Gamma(m_{SR})}\gamma\left(m_{SR}, \frac{m_{SR}}{(\nu_2)^2\lambda_{SR}}\left(\frac{t_2}{|h_{RD}|}\right)^2\right) \\ &\quad \times \frac{2(m_{RD})^{m_{RD}}|h_{RD}|^{2m_{RD}-1}}{\Gamma(m_{RD})(\lambda_{RD})^{m_{RD}}}\exp\left(-\frac{m_{RD}|h_{RD}|^2}{\lambda_{RD}}\right)d|h_{RD}|. \end{aligned} \tag{A.2}$$

Using (B.2), the incomplete gamma function in (A.2) can be represented in terms of Meijer-G function, which on employing (4.13) can be written in integral form. Hence, on changing the order of integration (A.2) can be rewritten as

$$\begin{aligned} F_{t_2}(t_2) &= \frac{2(m_{RD})^{m_{RD}}}{\Gamma(m_{SR})\Gamma(m_{RD})(\lambda_{RD})^{m_{RD}}}\left(\frac{1}{2\pi\jmath}\right)\int_{\mathcal{C}}\frac{\Gamma(m_{SR}+p)\Gamma(-p)}{\Gamma(1-p)}\left(\frac{m_{SR}}{(\nu_2)^2\lambda_{SR}}(t_2)^2\right)^{-p} \\ &\quad \times \int_0^\infty |h_{RD}|^{2m_{RD}+2p-1}\exp\left(-\frac{m_{RD}|h_{RD}|^2}{\lambda_{RD}}\right)d|h_{RD}|\,dp. \end{aligned} \tag{A.3}$$

Now, on employing (B.7), the inner integral in (A.3) can be simplified in the terms of gamma function, thence (A.3) is written as

$$F_{t_2}(t_2) = \frac{1}{\Gamma(m_{SR})\Gamma(m_{RD})}\left(\frac{1}{2\pi\jmath}\right)\int_{\mathcal{C}}\frac{\Gamma(m_{SR}+p)\Gamma(m_{RD}+p)\Gamma(-p)}{\Gamma(1-p)}\left(\frac{m_{SR}m_{RD}}{\bar{\gamma}_2}(t_2)^2\right)^{-p}dp, \tag{A.4}$$

where $\bar{\gamma}_2 = \lambda_{SR}\lambda_{RD}(\nu_2)^2$. The PDF of t_2 is obtained by differentiating (A.4) with respect to t_2 and using the relation $x = \Gamma(1+x)/\Gamma(x)$ as

$$f_{t_2}(t_2) = \frac{2m_{SR}m_{RD}\,t_2}{\Gamma(m_{SR})\Gamma(m_{RD})\bar{\gamma}_2}\left(\frac{1}{2\pi\jmath}\right)\int_{\mathcal{C}}\Gamma(m_{SR}+p)\Gamma(m_{RD}+p)\left(\frac{m_{SR}m_{RD}}{\bar{\gamma}_2}(t_2)^2\right)^{-p-1}dp\,. \tag{A.5}$$

On replacing (p) by $(p-1)$ in (A.5), the expression can be rewritten in terms of Meijer-G function as in (4.16) with the help of (4.13).

A.2 PDF $f_{\gamma_{\mathbf{EGC}}}(\gamma_{\mathbf{EGC}})$

The CDF of a random variable z defined as $z = t_1 + t_2$ is given by

$$\begin{aligned} F_z(z) &= \Pr(t_1 + t_2 \leq z) \\ &= \int_0^z \Pr(t_1 \leq z - t_2) f_{t_2}(t_2) dt_2, \end{aligned} \tag{A.6}$$

where t_1 is Nakagami-m distributed with CDF $F_{t_1}(t_1) = \frac{1}{\Gamma(m_{SD})}\gamma\big(m_{SD}, \frac{m_{SD}}{\bar{\gamma}_1}(t_1)^2\big)$ and the PDF of t_2 is given by (A.5). (A.6) can be simplified by using the PDF in (A.5) and the integral form of $F_{t_1}(t_1)$ obtained from (B.2) and (4.13), followed by change in the order of integration. We get

$$\begin{aligned} F_z(z) &= \frac{2m_{SR}m_{RD}}{\Gamma(m_{SD})\Gamma(m_{SR})\Gamma(m_{RD})\bar{\gamma}_2}\left(\frac{1}{2\pi\jmath}\right)^2 \int_{\mathcal{C}_1}\int_{\mathcal{C}_2} \frac{\Gamma(m_{SR}-1+p)\Gamma(m_{RD}-1+p)}{\Gamma(1-q)} \\ &\times\Gamma(m_{SD}+q)\Gamma(-q)\left(\frac{m_{SD}}{\bar{\gamma}_1}\right)^{-q}\left(\frac{m_{SR}m_{RD}}{\bar{\gamma}_2}\right)^{-p}\left(\int_0^z t_2^{1-2p}(z-t_2)^{-2q}dt_2\right)dpdq. \end{aligned} \tag{A.7}$$

The innermost integral in (A.7) can be written in terms of the beta function $B(x,y) = \Gamma(x)\Gamma(y)/\Gamma(x+y)$ [166, eq. (3.191.1)]. Hence, (A.7) is simplified as

$$\begin{aligned} F_z(z) &= \frac{2m_{SR}m_{RD}z^2}{\Gamma(m_{SD})\Gamma(m_{SR})\Gamma(m_{RD})\bar{\gamma}_2}\left(\frac{1}{2\pi\jmath}\right)^2 \int_{\mathcal{C}_1}\int_{\mathcal{C}_2} \frac{\Gamma(m_{SR}-1+p)\Gamma(m_{RD}-1+p)\Gamma(2-2p)}{\Gamma(3-2p-2q)} \\ &\times\frac{\Gamma(m_{SD}+q)\Gamma(-q)\Gamma(1-2q)}{\Gamma(1-q)}\left(\frac{m_{SD}z^2}{\bar{\gamma}_1}\right)^{-q}\left(\frac{m_{SR}m_{RD}z^2}{\bar{\gamma}_2}\right)^{-p}dpdq\,. \end{aligned} \tag{A.8}$$

On differentiating (A.8) with respect to z and replacing q by $(q-1)$ in (A.8), the PDF $f_z(z)$ is

$$\begin{aligned} f_z(z) &= \frac{2m_{SD}m_{SR}m_{RD}z^3}{\Gamma(m_{SD})\Gamma(m_{SR})\Gamma(m_{RD})\bar{\gamma}_1\bar{\gamma}_2}\left(\frac{1}{2\pi\jmath}\right)^2 \int_{\mathcal{C}_1}\int_{\mathcal{C}_2} \frac{\Gamma(m_{SR}-1+p)\Gamma(m_{RD}-1+p)\Gamma(2-2p)}{\Gamma(4-2p-2q)} \\ &\times\frac{\Gamma(m_{SD}-1+q)\Gamma(1-q)\Gamma(3-2q)}{\Gamma(2-q)}\left(\frac{m_{SD}z^2}{\bar{\gamma}_1}\right)^{-q}\left(\frac{m_{SR}m_{RD}z^2}{\bar{\gamma}_2}\right)^{-p}dpdq\,. \end{aligned} \tag{A.9}$$

Using (A.9) and (4.14), the PDF of $\gamma_{\mathrm{EGC}} = z^2$ is obtained as in (4.17).

A.3 Simplification of $P_{e,\mathbf{EGC}}$

On substituting (4.25) in (4.26) and expanding the bivariate Fox-H function in contour integral form using (4.14), the average SER for EGC can be written as

$$\begin{aligned} P_{e,\mathrm{EGC}} &= \frac{a_M\, m_{SD} m_{SR} m_{RD}}{\pi\Gamma(m_{SD})\Gamma(m_{SR})\Gamma(m_{RD})\bar{\gamma}_1\bar{\gamma}_2 g^2}\left(\frac{1}{2\pi\jmath}\right)^2 \int_{\mathcal{C}_1}\int_{\mathcal{C}_2} \frac{\Gamma(2-p-q)\Gamma(m_{SR}-1+p)}{\Gamma(4-2p-2q)} \\ &\times \frac{\Gamma(m_{RD}-1+p)\Gamma(2-2p)\Gamma(m_{SD}-1+q)\Gamma(1-q)\Gamma(3-2q)}{\Gamma(2-q)} \\ &\times \left(\frac{m_{SD}}{g\bar{\gamma}_1}\right)^{-q}\left(\frac{m_{SR}m_{RD}}{g\bar{\gamma}_2}\right)^{-p}\left(\int_0^{\frac{\pi}{2}} (\sin^2(\theta))^{2-p-q} d\theta\right) dp dq. \end{aligned} \tag{A.10}$$

The innermost integral in (A.10) is solved using the substitution $\cos^2(\theta) = t$, applying (B.5), and using the relation $B(x,y) = \Gamma(x)\Gamma(y)/\Gamma(x+y)$ as

$$\int_0^{\frac{\pi}{2}} (\sin^2(\theta))^{2-p-q} d\theta = \frac{\sqrt{\pi}\Gamma(5/2-p-q)}{2\Gamma(3-p-q)}. \tag{A.11}$$

On substituting (A.11) in (A.10) and using (4.14), $P_{e,\mathrm{EGC}}$ is given as in (4.27).

A.4 Asymptotic Approximation of PDF $f_{\gamma_{\mathbf{EGC}}}(\gamma_{\mathbf{EGC}})$

Using (4.37) and the contour integral representation for the CDF of t_1 in (A.6), we get

$$\begin{aligned} F_z^{\infty}(z) &\approx \frac{-2}{\Gamma(m_{SD})(\Gamma(m_a))^2}\left(\frac{m_a^2}{\bar{\gamma}_2}\right)^{m_a}\left(\frac{1}{2\pi\jmath}\right)\int_{\mathcal{C}} \frac{\Gamma(m_{SD}+q)\Gamma(-q)}{\Gamma(1-q)} \\ &\times \left(\frac{m_{SD}}{\bar{\gamma}_1}\right)^{-q}\left(\int_0^z t_2^{2m_a-1}(z-t_2)^{-2q}\ln\left(\frac{4m_a^2t_2^2}{\bar{\gamma}_2}\right) dt_2\right) dq, \end{aligned} \tag{A.12}$$

where the inner integral is expanded as

$$\begin{aligned} \mathcal{I} &= \int_0^z (t_2)^{2m_a-1}(z-t_2)^{-2q}\ln\left(\frac{4m_a^2t_2^2}{\bar{\gamma}_2}\right) dt_2 \\ &= z^{2m_a-2q-1}\ln\left(\frac{4m_a^2z^2}{\bar{\gamma}_2}\right)\int_0^z \left(\frac{t_2}{z}\right)^{2m_a-1}\left(1-\frac{t_2}{z}\right)^{-2q} dt_2 \\ &\quad + 2z^{2m_a-2q-1}\int_0^z \left(\frac{t_2}{z}\right)^{2m_a-1}\left(1-\frac{t_2}{z}\right)^{-2q}\ln\left(\frac{t_2}{z}\right) dt_2. \end{aligned} \tag{A.13}$$

Using (B.5) and (B.8), followed by rearrangement of terms with the help of (B.11), we get

$$\mathcal{I} = z^{2m_a-2q}\frac{\Gamma(2m_a)\Gamma(1-2q)}{\Gamma(1+2m_a-2q)}\left(\ln\left(\frac{4(m_a)^2z^2}{\bar{\gamma}_2}\right)+\sum_{n=1}^{\infty}\frac{2(2m_a-1)}{n(2m_a+n-1)}-\sum_{n=1}^{\infty}\frac{2(2m_a-2q)}{n(2m_a-2q+n)}\right). \quad (A.14)$$

Using (A.14), (A.12) is rewritten as

$$F_z^{\infty}(z) \approx -\frac{2\Gamma(2m_a)z^{2m_a}}{\Gamma(m_{SD})(\Gamma(m_a))^2}\left(\frac{m_a^2}{\bar{\gamma}_2}\right)^{m_a}\left(\ln\left(\frac{4G^2(m_a)^2z^2}{\bar{\gamma}_2}\right)\times(\mathcal{J}_1)-\sum_{n=1}^{\infty}\frac{2}{n}\times(\mathcal{J}_2)\right), \quad (A.15)$$

where $\ln(G^2)=\sum_{n=1}^{\infty}(2(2m_a-1))/(n(2m_a+n-1))$,

$$\mathcal{J}_1 = \frac{1}{2\pi\jmath}\int_{\mathcal{C}_1}\frac{\Gamma(m_{SD}+q)\Gamma(-q)\Gamma(1-2q)}{\Gamma(1-q)\Gamma(2m_a+1-2q)}\left(\frac{m_{SD}z^2}{\bar{\gamma}_1}\right)^{-q}dq \quad (A.16)$$

and

$$\mathcal{J}_2 = \frac{1}{2\pi\jmath}\int_{\mathcal{C}_1}\frac{\Gamma(m_{SD}+q)\Gamma(-q)\Gamma(1-2q)\Gamma(2m_a+n-2q)}{\Gamma(1-q)\Gamma(2m_a-2q)\Gamma(1+2m_a+n-2q)}\left(\frac{m_{SD}z^2}{\bar{\gamma}_1}\right)^{q}dq. \quad (A.17)$$

The relation $x=\Gamma(x+1)/\Gamma(x)$ is used to obtain (A.17). Using (B.12), (A.16) and (A.17) can be represented in terms of univariate Fox-H function which on substitution in (A.15) give

$$\begin{aligned}F_z^{\infty}(z) \approx & -\frac{2\Gamma(2m_a)z^{2m_a}}{\Gamma(m_{SD})(\Gamma(m_a))^2}\left(\frac{(m_a)^2}{\bar{\gamma}_2}\right)^{m_a}\\ &\times\left(\ln\left(\frac{4G^2(m_a)^2z^2}{\bar{\gamma}_2}\right)H_{2,3}^{1,2}\left[\frac{m_{SD}z^2}{\bar{\gamma}_1}\middle|\begin{matrix}(1,1),(0,2)\\(m_{SD},1),(0,1),(-2m_a,2)\end{matrix}\right]\right.\\ &\left.-\sum_{n=1}^{\infty}\frac{2}{n}H_{3,4}^{1,3}\left[\frac{m_{SD}z^2}{\bar{\gamma}_1}\middle|\begin{matrix}(1,1),(0,2),(1-n-2m_a,2)\\(m_{SD},1),(0,1),(1-2m_a,2),(-2m_a-n,2)\end{matrix}\right]\right). \quad (A.18)\end{aligned}$$

In (A.18), Fox-H functions are dependent on $\bar{\gamma}_1$. Therefore, approximations of the Fox-H functions as $\bar{\gamma}_1\to\infty$ can be obtained to determine the high SNR expression for the CDF $F_z^{\infty}(z)$. Using [177, Th. 1.3], the Fox-H functions in (A.18) are expanded in power series form as

$$\begin{aligned}H_{2,3}^{1,2}\left[\frac{m_{SD}z^2}{\bar{\gamma}_1}\middle|\begin{matrix}(1,1),(0,2)\\(m_{SD},1),(0,1),(-2m_a,2)\end{matrix}\right] \sim & \sum_{l=0}^{\infty}\left(\frac{m_{SD}z^2}{\bar{\gamma}_1}\right)^{m_{SD}+l}\frac{(-1)^l}{l!}\\ &\times\frac{\Gamma(m_{SD}+l)\Gamma(1+2m_{SD}+2l)}{\Gamma(1+m_{SD}+l)\Gamma(1+2m_a+2m_{SD})+2l)} \quad (A.19)\end{aligned}$$

and

$$H_{3,4}^{1,3}\left[\frac{m_{SD}z^2}{\bar{\gamma}_1}\middle|\begin{matrix}(1,1),(0,2),(1-n-2m_a,2)\\(m_{SD},1),(0,1),(1-2m_a,2),(-2m_a-n,2)\end{matrix}\right]$$
$$\sim\sum_{l=0}^{\infty}\frac{(-1)^l}{l!}\frac{\Gamma(m_{SD}+l)\Gamma(1+2m_{SD}+2l)}{\Gamma(1+m_{SD}+l)\Gamma(2m_a+2m_{SD}+2l)}\frac{\Gamma(n+2m_a+2m_{SD}+2l)}{\Gamma(n+1+2m_a+m_{SD}+2l)}\left(\frac{m_{SD}z^2}{\bar{\gamma}_1}\right)^{m_{SD}+l}. \tag{A.20}$$

We consider only the first dominating term of the approximations as $\bar{\gamma}_1\to\infty$, thus the right hand side in (A.19) and (A.20) can be simplified as

$$\frac{\Gamma(m_{SD})\Gamma(1+2m_{SD})}{\Gamma(1+m_{SD})\Gamma(1+2m_{SD}+2m_a)}\left(\frac{m_{SD}z^2}{\bar{\gamma}_1}\right)^{m_{SD}} \tag{A.21}$$

and

$$\frac{\Gamma(m_{SD})\Gamma(1+2m_{SD})\Gamma(n+2m_{SD}+2m_a)}{\Gamma(1+m_{SD})\Gamma(2m_{SD}+2m_a)\Gamma(1+n+2m_{SD}+2m_a)}\left(\frac{m_{SD}z^2}{\bar{\gamma}_1}\right)^{m_{SD}}, \tag{A.22}$$

respectively. Substituting (A.21) and (A.22) in (A.18), the CDF is expressed as

$$\begin{aligned}F_z^{\infty}(z) \approx & -\frac{2\Gamma(2m_a)}{\Gamma(m_{SD})(\Gamma(m_a))^2}\left(\frac{m_{SD}z^2}{\bar{\gamma}_1}\right)^{m_{SD}}\left(\frac{m_a^2z^2}{\bar{\gamma}_2}\right)^{m_a}\\ &\times\left(\ln\left(\frac{4G^2m_a^2z^2}{\bar{\gamma}_2}\right)\frac{\Gamma(m_{SD})\Gamma(1+2m_{SD})}{\Gamma(1+m_{SD})\Gamma(1+2m_{SD}+2m_a)}\right.\\ &\left.-\sum_{n=1}^{\infty}\frac{2\Gamma(m_{SD})\Gamma(1+2m_{SD})\Gamma(n+2m_{SD}+2m_a)}{n\Gamma(1+m_{SD})\Gamma(2m_{SD}+2m_a)\Gamma(1+n+2m_{SD}+2m_a)}\right).\end{aligned} \tag{A.23}$$

Therefore, the approximate expression for the CDF $F_{\gamma_{\mathrm{EGC}}}^{\infty}(\gamma_{\mathrm{EGC}})$ is

$$\begin{aligned}F_{\gamma_{\mathrm{EGC}}}^{\infty}(\gamma_{\mathrm{EGC}}) \approx & -\frac{2\Gamma(2m_a)}{\Gamma(m_{SD})(\Gamma(m_a))^2}\left(\frac{m_{SD}}{\bar{\gamma}_1}\right)^{m_{SD}}\left(\frac{m_a^2}{\bar{\gamma}_2}\right)^{m_a}\\ &\times\gamma_{\mathrm{EGC}}^{(m_{SD}+m_a)}\left(\ln\left(\frac{4G^2m_a^2\gamma_{\mathrm{EGC}}}{\bar{\gamma}_2}\right)\frac{\Gamma(m_{SD})\Gamma(1+2m_{SD})}{\Gamma(1+m_{SD})\Gamma(1+2m_{SD}+2m_a)}\right.\\ &\left.-\sum_{n=1}^{\infty}\frac{2\Gamma(m_{SD})\Gamma(1+2m_{SD})\Gamma(n+2m_{SD}+2m_a)}{n\Gamma(1+m_{SD})\Gamma(2m_{SD}+2m_a)\Gamma(1+n+2m_{SD}+2m_a)}\right).\end{aligned} \tag{A.24}$$

Differentiating (A.24) with respect to γ_{EGC} results in the PDF (4.38).

B

Some Useful Mathematical Relations

Contents

B.1 Some Useful Mathematical Relations

Some of the useful mathematical relations used in this thesis are listed as follows.

★ Exponential function, lower incomplete gamma function, and modified Bessel's function of the second kind can be represented in terms of Meijer-G function using [162, eq. (8.4.3.1)], [162, eq. (8.4.16.1)] and [162, eq. (8.4.23.1)] as

$$\exp(-x) = G_{0,1}^{1,0}\left[x\middle|\begin{matrix}-\\0\end{matrix}\right], \tag{B.1}$$

$$\gamma(\nu,x) = G_{1,2}^{1,1}\left[x\middle|\begin{matrix}1\\\nu,\end{matrix}\right], \tag{B.2}$$

and

$$K_\nu(2\sqrt{x}) = \frac{1}{2}G_{0,2}^{2,0}\left[x\middle|\begin{matrix}-\\\nu/2,-\nu/2\end{matrix}\right], \tag{B.3}$$

respectively.

★ Univariate Meijer-G function to modified Bessel's function of the second kind using [178, eq. (07.34.03.0605.01)]

$$G_{0,2}^{2,0}\left[x\middle|\begin{matrix}-\\b,c\end{matrix}\right] = 2x^{(b+c)/2}K_{b-c}(2\sqrt{x}). \tag{B.4}$$

★ Beta function $B(\mu,\nu)=\Gamma(\mu)\Gamma(\nu)/\Gamma(\mu+\nu)$ in integral form is given by [166, eq. (3.191.1)]

$$B(\mu,\nu) = u^{1-\mu-\nu}\int_0^u x^{\mu-1}(u-x)^{\nu-1}dx. \tag{B.5}$$

★ The r-th order modified Bessel's function of the second kind, $K_r(y)$ can be approximated for $y\to 0$, $K_r(y)$ using [170, eqs. (9.6.6), (9.6.8) and (9.6.9)] as

$$K_r(y) \approx \begin{cases} -\ln(y), & r=0 \\ \frac{1}{2}\Gamma(|r|)\left(\frac{1}{2}y\right)^{-|r|}, & |r|>0 \end{cases}. \tag{B.6}$$

★ An integral involving product of algebraic and exponential functions [166, eq. (3.381.4)]

$$\int_0^\infty x^u \exp(-sx)dx = s^{-1-u}\Gamma(1+u) \tag{B.7}$$

★ An integral involving product of algebraic and logarithmic functions is given as [166, eq. (4.253.1)]

$$\int_0^1 x^{\mu-1}(1-x)^{\nu-1}\ln(x)\,dx \;=\; B(\mu,\nu)\Big(\psi(\mu)-\psi(\mu+\nu)\Big), \tag{B.8}$$

where $\psi(\cdot)$ is digamma function [170, eq. (6.3.1)].

★ An integral involving product of algebraic, logarithmic and exponential functions is given by [166, eq. (4.352.1)]

$$\int_0^\infty x^{\nu-1}\ln(x)\exp(-\mu x)\,dx \;=\; \mu^{-\nu}\Gamma(\nu)\Big(\psi(\nu)-\ln(\mu)\Big). \tag{B.9}$$

★ An integral involving functions of trigonometric function is given by [166, eq. (4.387.2)]

$$\int_0^{\pi/2}\ln(\sin(x))\sin^{\mu-1}(x)dx \;=\; \frac{\sqrt{\pi}\Gamma(\mu/2)}{4\Gamma((\mu+1)/2)}\left(\psi(\mu/2)-\psi((\mu+1)/2)\right). \tag{B.10}$$

★ Series form representation of digamma function is given as [170, eq. (6.3.16)]

$$\psi(1+x) \;=\; -\xi+\sum_{n=1}^{\infty}\frac{x}{n(n+x)}, \quad \text{for} \quad x\neq -1,-2,-3,\ldots \tag{B.11}$$

where $\xi = 0.577215$ is Euler-Mascheroni constant.

★ Univariate Fox-H function is represented in Mellin-Barnes integral form as [162, eq. (8.3.1.1)]

$$H_{p_1,q_1}^{m_1,n_1}\left[x\middle|\begin{matrix}(a_1,A_1),\ldots,(a_{p_1},A_{p_1})\\(b_1,B_1),\ldots,(b_{q_1},B_{q_1}))\end{matrix}\right] \;=\; \frac{1}{2\pi\jmath}\int_{\mathcal{C}}\theta(p)x^{-p}dp, \tag{B.12}$$

where

$$\theta(p) \;=\; \frac{\prod_{j=1}^{m_1}\Gamma(b_j+B_jp)\prod_{j=1}^{n_1}\Gamma(1-a_j-A_jp)}{\prod_{j=m_1+1}^{q_1}\Gamma(1-b_j-B_jp)\prod_{j=n_1+1}^{p_1}\Gamma(a_j+A_jp)}$$

.

★ The duplication formula of Gamma function is [164, Eq. (2.19)]

$$\Gamma(2r) \;=\; \frac{2^{2r}}{2\sqrt{\pi}}\Gamma(r)\Gamma(1/2+r). \tag{B.13}$$

★ An integration involving algebraic function and exponential function [179, eq. (2.3.16.1)]

$$\int_0^\infty x^{r-1}\exp(-px-q/x)dx \;=\; 2\left(\frac{q}{p}\right)^{r/2}K_r(2\sqrt{pq})), \tag{B.14}$$

where $K_r(\cdot)$ is the r-th order modified Bessel's function of the second kind.

★ An integration involving algebraic function, exponential function and the second kind Bessel's function [180, eq. (2.16.8.4)]

$$\int_0^\infty x^{a-1}\exp(-px^2)K_r(cx)dx = \frac{p^{(1-a)/2}}{2c}\Gamma\left(\frac{a+r}{2}\right)\Gamma\left(\frac{a-r}{2}\right)\exp\left(\frac{c^2}{8p}\right)W_{(1-a)/2,r/2}\left(\frac{c^2}{4p}\right), \tag{B.15}$$

where $W_{s,t}(\cdot)$ is Whittaker's function.

Bibliography

[1] B. P. Lathi, *Modern Digital and Analog Communication Systems*. 3rd ed. New York, NY, USA: Oxford University Press, 1998.

[2] B. Sklar, "Mitigating the degradation effects of fading channels," Accessed: August 25, 2018. [Online]. Available: http://citeseerx.ist.psu.edu/viewdoc/summary?doi=10.1.1.497.7527

[3] S. Haykin, *Communication Systems*. 4th ed. Singapore: John Wiley & Sons, 2004.

[4] T. S. Rappaport, *Wireless Communications: Principles and Practice*. 2nd ed. Upper Saddle River, New Jersey: Prentice Hall PTR, 2002.

[5] H. Inaltekin and S. B. Wicker, "The behavior of unbounded path-loss models and the effect of singularity on computed network interference," in *Proceedings of the IEEE Communications Society Conference on Sensor, Mesh and Ad Hoc Communications and Networks*, San Diego, June 18-21 2007, pp. 431–440.

[6] H. Inaltekin, M. Chiang, H. V. Poor, and S. B. Wicker, "On unbounded path-loss models: Effects of singularity on wireless network performance," *IEEE Journal on Selected Areas in Communications*, vol. 27, no. 7, pp. 1078–1092, September 2009.

[7] C. Zhang and Y. Chen, "Wireless power transfer strategies for cooperative relay system to maximize information throughput," *IEEE Access*, vol. 5, pp. 2573–2582, February 2017.

[8] S. Kurt and B. Tavli, "Path-loss modeling for wireless sensor networks: A review of models and comparative evaluations." *IEEE Antennas and Propagation Magazine*, vol. 59, no. 1, pp. 18–37, February 2017.

[9] M. Cheffena and M. Mohamed, "The application of lognormal mixture shadowing model for B2B channels," *IEEE Sensors Letters*, vol. 2, no. 3, pp. 1–4, September 2018.

[10] M. Nakagami, "The m-distribution—A general formula of intensity distribution of rapid fading," in *Proceedings of the Statistical Methods in Radio Wave Propagation*. Elsevier, Los Angeles, June 18-20, 1960, pp. 3–36. [Online]. Available: https://doi.org/10.1016%2Fb978-0-08-009306-2.50005-4

[11] M. D. Yacoub, "The $\kappa - \mu$ distribution and the $\eta - \mu$ distributuion," *IEEE Antennas and Propagation Magazine*, vol. 49, no. 1, pp. 68–81, February 2007.

[12] J. F. Paris, "Statistical characterization of $\kappa-\mu$ shadowed fading," *IEEE Transactions on Vehicular Technology*, vol. 63, no. 2, pp. 518–526, February 2014.

[13] S. L. Cotton, W. G. Scanlon, and J. Guy, "The $\kappa-\mu$ distribution applied to the analysis of fading in body to body communication channels for fire and rescue personnel," *IEEE Antennas and Wireless Propagation Letters*, vol. 7, pp. 66–69, April 2008.

[14] S. L. Cotton, "Human body shadowing in cellular device-to-device communications: Channel modeling using the shadowed $\kappa-\mu$ fading model," *IEEE Journal on Selected Areas in Communications*, vol. 33, no. 1, pp. 111–119, January 2015.

[15] Y. J. Chun, S. L. Cotton, H. S. Dhillon, F. J. Lopez-Martinez, J. F. Paris, and S. K. Yoo, "A comprehensive analysis of 5G heterogeneous cellular systems operating over $\kappa-\mu$ shadowed fading channels," *IEEE Transactions on Wireless Communications*, vol. 16, no. 11, pp. 6995–7010, November 2017.

[16] G. D. Durgin, T. S. Rappaport, and D. A. de Wolf, "New analytical models and probability density functions for fading in wireless communications," *IEEE Transactions on Communications*, vol. 50, no. 6, pp. 1005–1015, June 2002.

[17] M. D. Yacoub, "The $\alpha-\mu$ distribution: A physical fading model for the Stacy distribution," *IEEE Transactions on Vehicular Technology*, vol. 56, no. 1, pp. 27–34, January 2007.

[18] G. S. Rabelo and M. D. Yacoub, "The $\kappa-\mu$ extreme distribution," *IEEE Transactions on Communications*, vol. 59, no. 10, pp. 2776–2785, October 2011.

[19] A. Goldsmith, *Wireless Communications*. New York, NY, USA: Cambridge University Press, 2005.

[20] R. Padovani, "The application of spread spectrum to PCS has become a reality: Reverse link performance of 1S-95 based cellular systems," *IEEE Personal Communications*, vol. 1, no. 3, pp. 28–34, 3rd-quarter 1994.

[21] A. M. Sayeed and B. Aazhang, "Joint multipath-Doppler diversity in mobile wireless communications," *IEEE Transactions on Communications*, vol. 47, no. 1, pp. 123–132, January 1999.

[22] J. N. Laneman, D. N. C. Tse, and G. W. Wornell, "Cooperative diversity in wireless networks: Efficient protocols and outage behavior," *IEEE Transactions on Information Theory*, vol. 50, no. 12, pp. 3062–3080, December 2004.

[23] A. Stefanov and E. Erkip, "Cooperative space-time coding for wireless networks," *IEEE Transactions on Communications*, vol. 53, no. 11, pp. 1804–1809, November 2005.

[24] P. Clarke and R. C. de Lamare, "Joint transmit diversity optimization and relay selection for multi-relay cooperative MIMO systems using discrete stochastic algorithms," *IEEE Communications Letters*, vol. 15, no. 10, pp. 1035–1037, October 2011.

[25] K. Dhaka, R. K. Mallik, and R. Schober, "Performance analysis of decode-and-forward multi-hop communication: A difference equation approach," *IEEE Transactions on Communications*, vol. 60, no. 2, pp. 339–345, February 2012.

[26] J. Boyer, D. D. Falconer, and H. Yanikomeroglu, "Multihop diversity in wireless relaying channels," *IEEE Transactions on Communications*, vol. 52, no. 9, pp. 1605–1605, September 2004.

[27] Y. Xiao and L. J. Cimini, "Impact of overhead on spectral efficiency of cooperative relaying," *IEEE Transactions on Wireless Communications*, vol. 12, no. 5, pp. 2228–2239, May 2013.

[28] B. Klaiqi, X. Chu, and J. Zhang, "Energy-efficient and low signaling overhead cooperative relaying with proactive relay subset selection," *IEEE Transactions on Communications*, vol. 64, no. 3, pp. 1001–1015, March 2016.

[29] D. Hu, J. Wu, and P. Fan, "Minimizing end-to-end delays in linear multihop networks," *IEEE Transactions on Vehicular Technology*, vol. 65, no. 8, pp. 6487–6496, August 2016.

[30] B. Rankov and A. Wittneben, "Spectral efficient protocols for half-duplex fading relay channels," *IEEE Journal on Selected Areas in Communications*, vol. 25, no. 2, pp. 379–389, February 2007.

[31] R. Nikjah and N. C. Beaulieu, "Achievable rates and fairness in rateless coded decode-and-forward half-duplex and full-duplex opportunistic relaying," in *Proceedings of the IEEE International Conference on Communications*, Beijing, May 19-23, 2008, pp. 3701–3707.

[32] A. Ikhlef, J. Kim, and R. Schober, "Mimicking full-duplex relaying using half-duplex relays with buffers," *IEEE Transactions on Vehicular Technology*, vol. 61, no. 7, pp. 3025–3037, September 2012.

[33] Y. Chen, S. Kishore, and J. Li, "Wireless diversity through network coding," in *Proceedings of the IEEE Wireless Communications and Networking Conference*, vol. 3, Las Vegas, April 3-6, 2006, pp. 1681–1686.

[34] J. Lu, F. Wang, and T. J. Zhang, "Network-coded cooperative diversity in multi-hop cellular networks," in *Proceedings of the International Conference on Wireless Communications, Networking and Mobile Computing*, Beijing, September 24-26, 2009, pp. 1–4.

[35] L. Xiao, T. E. Fuja, J. Kliewer, and D. J. Costello, "A network coding approach to cooperative diversity," *IEEE Transactions on Information Theory*, vol. 53, no. 10, pp. 3714–3722, October 2007.

[36] G. L. Stüber, *Principles of Mobile Communication*. New York, NY, USA: Springer Science+Buisiness Media, 2011.

[37] M. O. Hasna and M. . Alouini, "End-to-end performance of transmission systems with relays over Rayleigh-fading channels," *IEEE Transactions on Wireless Communications*, vol. 2, no. 6, pp. 1126–1131, November 2003.

[38] M. Ku, W. Li, Y. Chen, and K. J. R. Liu, "Advances in energy harvesting communications: Past, present, and future challenges," *IEEE Communications Surveys & Tutorials*, vol. 18, no. 2, pp. 1384–1412, 2nd-quarter 2016.

[39] X. Lu, P. Wang, D. Niyato, D. I. Kim, and Z. Han, "Wireless charging technologies: Fundamentals, standards, and network applications," *IEEE Communications Surveys & Tutorials*, vol. 18, no. 2, pp. 1413–1452, 2nd-quarter 2016.

[40] C. Huang, R. Zhang, and S. Cui, "Throughput maximization for the gaussian relay channel with energy harvesting constraints," *IEEE Journal on Selected Areas in Communications*, vol. 31, no. 8, pp. 1469–1479, August 2013.

[41] A. A. Nasir, X. Zhou, S. Durrani, and R. A. Kennedy, "Relaying protocols for wireless energy harvesting and information processing," *IEEE Transactions on Wireless Communications*, vol. 12, no. 7, pp. 3622–3636, July 2013.

[42] "Qi (standard)," Accessed: August 25, 2018. [Online]. Available: https://en.wikipedia.org/wiki/Qi_(standard)

[43] "Rezence (wireless charging standard)," Accessed: August 25, 2018. [Online]. Available: https://en.wikipedia.org/wiki/Rezence_(wireless_charging_standard)

[44] "Airfuel: Charging is changing," Accessed: August 25, 2018. [Online]. Available: https://www.airfuel.org/about/

[45] "WiTricity," Accessed: August 25, 2018. [Online]. Available: https://en.wikipedia.org/wiki/WiTricity

[46] "Cota: Real wireless power," Accessed: August 25, 2018. [Online]. Available: http://www.ossia.com/cota/

[47] "Powercast," Accessed: August 25, 2018. [Online]. Available: http://www.powercastco.com/company/about/

[48] "WattUp: Wire-free charging technology," Accessed: August 25, 2018. [Online]. Available: http://energous.com/

[49] L. R. Varshney, "Transporting information and energy simultaneously," in *Proceedings of the IEEE International Symposium on Information Theory*, Toronto, July 6-11, 2008, pp. 1612–1616.

[50] R. Zhang, R. G. Maunder, and L. Hanzo, "Wireless information and power transfer: From scientific hypothesis to engineering practice," *IEEE Communications Magazine*, vol. 53, no. 8, pp. 99–105, August 2015.

[51] Q. Liu, J. Wu, P. Xia, S. Zhao, W. Chen, Y. Yang, and L. Hanzo, "Charging unplugged: Will distributed laser charging for mobile wireless power transfer work?" *IEEE Vehicular Technology Magazine*, vol. 11, no. 4, pp. 36–45, December 2016.

[52] K. David and H. Berndt, "6G vision and requirements: Is there any need for beyond 5g?" *IEEE Vehicular Technology Magazine*, vol. 13, no. 3, pp. 72–80, September 2018.

[53] X. Zhou, R. Zhang, and C. K. Ho, "Wireless information and power transfer: Architecture design and rate-energy tradeoff," in *Proceedings of the IEEE Global Communications Conference*, Anaheim, December 3-7, 2012, pp. 3982–3987.

[54] R. Zhang and C. K. Ho, "MIMO broadcasting for simultaneous wireless information and power transfer," *IEEE Transactions on Wireless Communications*, vol. 12, no. 5, pp. 1989–2001, May 2013.

[55] F. Zhao, L. Wei, and H. Chen, "Optimal time allocation for wireless information and power transfer in wireless powered communication systems," *IEEE Transactions on Vehicular Technology*, vol. 65, no. 3, pp. 1830–1835, March 2016.

[56] K. Chi, Y. H. Zhu, Y. Li, L. Huang, and M. Xia, "Minimization of transmission completion time in wireless powered communication networks," *IEEE Internet of Things Journal*, vol. 4, no. 5, pp. 1671–1683, October 2017.

[57] M. M. N. Aboelwafa, K. G. Seddik, and M. ElNainay, "Cooperation in multi-user wireless powered communication networks," in *Proceedings of the IEEE International Conference on Wireless and Mobile Computing, Networking and Communications*, Rome, October 9-11, 2017, pp. 1–6.

[58] M.-L. Ku, W. Li, Y. Chen, and K. J. R. Liu, "Advances in energy harvesting communications: Past, present, and future challenges," *IEEE Communications Surveys & Tutorials*, vol. 18, no. 2, pp. 1384–1412, 2nd-quarter 2016.

[59] E. Boshkovska, D. W. K. Ng, N. Zlatanov, and R. Schober, "Practical non-linear energy harvesting model and resource allocation for SWIPT systems," *IEEE Communications Letters*, vol. 19, no. 12, pp. 2082–2085, December 2015.

[60] Y. Zeng, B. Clerckx, and R. Zhang, "Communications and signals design for wireless power transmission," *IEEE Transactions on Communications*, vol. 65, no. 5, pp. 2264–2290, May 2017.

[61] E. Bayguzina and B. Clerckx, "Modulation design for wireless information and power transfer with nonlinear energy harvester modeling," in *Proceedings of the IEEE International Workshop on Signal Processing Advances in Wireless Communications*, Kalamata, June 25-28, 2018, pp. 1–5.

[62] Y. Dong, M. J. Hossain, and J. Cheng, "Performance of wireless powered amplify and forward relaying over Nakagami-*m* fading channels with nonlinear energy harvester," *IEEE Communications Letters*, vol. 20, no. 4, pp. 672–675, April 2016.

[63] C. R. Valenta and G. D. Durgin, "Harvesting wireless power: Survey of energy-harvester conversion efficiency in far-field, wireless power transfer systems," *IEEE Microwave Magazine*, vol. 15, no. 4, pp. 108–120, June 2014.

[64] B. Clerckx, A. Costanzo, A. Georgiadis, and N. B. Carvalho, "Toward 1G mobile power networks: RF, signal, and system designs to make smart objects autonomous," *IEEE Microwave Magazine*, vol. 19, no. 6, pp. 69–82, September 2018.

[65] S. Y. Lee, T. Y. Chen, C. Tsou, and Y. S. Chu, "Wireless energy-harvesting circuit and system with error-correction ASK demodulator for body sensor network with ultra-high-frequency RFID healthcare system," *IET Wireless Sensor Systems*, vol. 8, no. 1, pp. 36–44, January 2018.

[66] Y. Alsaba, S. K. A. Rahim, and C. Y. Leow, "Beamforming in wireless energy harvesting communications systems: A survey," *IEEE Communications Surveys & Tutorials*, vol. 20, no. 2, pp. 1329–1360, 2nd-quarter 2018.

[67] H. Zhang and W. X. Zheng, "Robust transmission power management for remote state estimation with wireless energy harvesting," *IEEE Internet of Things Journal*, vol. 5, no. 4, pp. 2682–2690, February 2018.

[68] S. Sudevalayam and P. Kulkarni, "Energy harvesting sensor nodes: Survey and implications," *IEEE Communications Surveys & Tutorials*, vol. 13, no. 3, pp. 443–461, 3rd-quarter 2011.

[69] P. Liu, S. Gazor, I. Kim, and D. Kim, "Energy harvesting noncoherent cooperative communications," *IEEE Transactions on Wireless Communications*, vol. 14, no. 12, pp. 6722–6737, December 2015.

[70] Y. Gu and S. Aïssa, "RF-based energy harvesting in decode-and-forward relaying systems: Ergodic and outage capacities," *IEEE Transactions on Wireless Communications*, vol. 14, no. 11, pp. 6425–6434, November 2015.

[71] M. Babaei, U. Aygölü, and E. Basar, "BER analysis of dual-hop relaying with energy harvesting in Nakagami-*m* fading channel," *IEEE Transactions on Wireless Communications*, vol. 17, no. 7, pp. 4352–4361, July 2018.

[72] W. Su, A. K. Sadek, and K. J. R. Liu, "SER performance analysis and optimum power allocation for decode-and-forward cooperation protocol in wireless networks," in *Proceedings of the IEEE Wireless Communications and Networking Conference*, vol. 2, New Orleans, March 13-17, 2005, pp. 984–989.

[73] Y. Lee and M.-H. Tsai, "Performance of decode-and-forward cooperative communications over Nakagami-m fading channels," *IEEE Transactions on Vehicular Technology*, vol. 58, no. 3, pp. 1218–1228, March 2009.

[74] H. H. Yang, J. Lee, and T. Q. S. Quek, "Heterogeneous cellular network with energy harvesting-based D2D communication," *IEEE Transactions on Wireless Communications*, vol. 15, no. 2, pp. 1406–1419, February 2016.

[75] D. D. Tran, D. B. Ha, H. V. Tran, and G. Kaddoum, "Wireless information transfer in relay networks with energy harvesting over non-identical channels," in *Proceedings of the International Conference on Communications, Management and Telecommunications*, DaNang, December 28-30, 2015, pp. 172–177.

[76] Y. Gao, Y. Chen, and A. Hu, "Throughput and BER of wireless powered DF relaying in Nakagami$-m$ fading," *Science China Information Sciences*, vol. 60, no. 10, pp. 102 306:1– 13, June 2017.

[77] Z. Yang, W. Xu, Y. Pan, C. Pan, and M. Chen, "Energy efficient resource allocation in machine-to-machine communications with multiple access and energy harvesting for IoT," *IEEE Internet of Things Journal*, vol. 5, no. 1, pp. 229–245, February 2018.

[78] M. Wen, X. Cheng, A. Huang, and B. Jiao, "Asymptotic performance analysis of multihop relaying with co-channel interference in Nakagami-m fading channels," *IEEE Communications Letters*, vol. 16, no. 9, pp. 1450–1453, September 2012.

[79] Y. Liang and T. Li, "End-to-end throughput in multihop wireless networks with random relay deployment," *IEEE Transactions on Signal and Information Processing over Networks*, vol. 4, no. 3, pp. 613–625, September 2018.

[80] P. L. Yeoh, M. Elkashlan, Z. Chen, and I. B. Collings, "Ser of multiple amplify-and-forward relays with selection diversity," *IEEE Transactions on Communications*, vol. 59, no. 8, pp. 2078–2083, August 2011.

[81] M. K. Fikadu, P. C. Sofotasios, S. Muhaidat, Q. Cui, G. K. Karagiannidis, and M. Valkama, "Error rate and power allocation analysis of regenerative networks over generalized fading channels," *IEEE Transactions on Communications*, vol. 64, no. 4, pp. 1751–1768, April 2016.

[82] H. Ilhan, "Performance analysis of two-way AF relaying systems over cascaded Nakagami-m fading channels," *IEEE Signal Processing Letters*, vol. 19, no. 6, pp. 332–335, June 2012.

[83] X. Sun, K. Xu, and Y. Xu, "Performance analysis of multi-pair two-way amplify-and-forward relaying with imperfect CSI over Ricean fading channels," *IET Communications*, vol. 12, no. 3, pp. 261–270, March 2018.

[84] E. Li, X. Wang, Z. Wu, S. Hao, and Y. Dong, "Outage analysis of decode-and-forward two-way relay selection with different coding and decoding schemes," *IEEE Systems Journal*, pp. 1–12, May 2018 (early access). [Online]. Available: https://ieeexplore.ieee.org/document/8353825

[85] H. Alves, D. B. da Costa, R. D. Souza, and M. Latva-aho, "Performance of block-Markov full duplex relaying with self interference in Nakagami-m fading," *IEEE Wireless Communications Letters*, vol. 2, no. 3, pp. 311–314, June 2013.

[86] R. Li, L. Wang, W. Chen, M. Song, and Z. Han, "Bit error rate analysis in hybrid full duplex/half duplex relay cooperative networks," in *Proceedings of the International Conference on Wireless Communications Signal Processing*, Yangzhou, October 13-15, 2016, pp. 1–5.

[87] B. C. Nguyen, X. N. Tran, and D. T. Tran, "Performance analysis of in-band full-duplex amplify-and-forward relay system with direct link," in *Proceedings of the International Conference on Recent Advances in Signal Processing, Telecommunications Computing*, Ho Chi Minh City, January 29-31, 2018, pp. 192–197.

[88] W. Tang, S. Kang, and B. Ren, "Performance analysis of cooperative pattern division multiple access (Co-PDMA) in uplink network," *IEEE Access*, vol. 5, pp. 3860–3868, April 2017.

[89] J. Men, J. Ge, and C. Zhang, "Performance analysis for downlink relaying aided non-orthogonal multiple access networks with imperfect CSI over Nakagami-m fading," *IEEE Access*, vol. 5, pp. 998–1004, March 2017.

[90] S. Poursajadi, M. H. Madani, and H. K. Bizaki, "Power allocation and outage probability analysis of af relaying systems with multiple antennas at terminal nodes," *IEEE Transactions on Vehicular Technology*, vol. 66, no. 1, pp. 377–384, January 2017.

[91] B. Kumbhani and R. S. Kshetrimayum, "Error performance of two-hop decode and forward relaying systems with source and relay transmit antenna selection," *Electronics Letters*, vol. 51, no. 6, pp. 530–532, March 2015.

[92] C. Kundu, S. Ghose, and R. Bose, "Secrecy outage of dual-hop regenerative multi-relay system with relay selection," *IEEE Transactions on Wireless Communications*, vol. 14, no. 8, pp. 4614–4625, August 2015.

[93] R. Sinha and P. Jindal, "Performance analysis of cooperative schemes under total transmit power constraint in single hop wireless relaying system," in *Proceedings of the International Conference on Communication Control and Intelligent Systems*, Mathura, November 18-20 2016, pp. 28–31.

[94] R. Zhao, Y. Yuan, L. Fan, and Y. He, "Secrecy performance analysis of cognitive decode-and-forward relay networks in Nakagami-m fading channels," *IEEE Transactions on Communications*, vol. 65, no. 2, pp. 549–563, February 2017.

[95] T. K. Baranwal, D. S. Michalopoulos, and R. Schober, "Outage analysis of multihop full duplex relaying," *IEEE Communications Letters*, vol. 17, no. 1, pp. 63–66, January 2013.

[96] D. Gunduz, M. A. Khojastepour, A. Goldsmith, and H. V. Poor, "Multi-hop MIMO relay networks: diversity-multiplexing trade-off analysis," *IEEE Transactions on Wireless Communications*, vol. 9, no. 5, pp. 1738–1747, May 2010.

[97] J. Men and J. Ge, "Non-orthogonal multiple access for multiple-antenna relaying networks," *IEEE Communications Letters*, vol. 19, no. 10, pp. 1686–1689, Oct. 2015.

[98] Z. Wang, S. Dang, and D. T. Kennedy, "Multi-hop index modulation-aided OFDM with decode-and-forward relaying," *IEEE Access*, vol. 6, pp. 26 457–26 468, May 2018.

[99] X. Yue, Y. Liu, S. Kang, A. Nallanathan, and Y. Chen, "Modeling and analysis of two-way relay non-orthogonal multiple access systems," *IEEE Transactions on Communications*, vol. 66, no. 9, pp. 3784–3796, September 2018.

[100] S. Wang, W. Yang, and W. Xu, "Outage analysis of OFDM full duplex relaying systems," in *Proceedings of the International Conference on Wireless Communications Signal Processing*, Nanjing, October 15-17, 2015, pp. 1–4.

[101] C. Zhong and Z. Zhang, "Non-orthogonal multiple access with cooperative full-duplex relaying," *IEEE Communications Letters*, vol. 20, no. 12, pp. 2478–2481, December 2016.

[102] M. O. Hasna and M.-S. Alouini, "A performance study of dual-hop transmissions with fixed gain relays," *IEEE Transactions on Wireless Communications*, vol. 3, no. 6, pp. 1963–1968, November 2004.

[103] M. O. Hasna and M. S. Alouini, "Harmonic mean and end-to-end performance of transmission systems with relays," *IEEE Transactions on Communications*, vol. 52, no. 1, pp. 130–135, January 2004.

[104] D. Chen and J. N. Laneman, "Modulation and demodulation for cooperative diversity in wireless systems," *IEEE Transactions on Wireless Communications*, vol. 5, no. 7, pp. 1785–1794, July 2006.

[105] T. Wang, A. Cano, G. B. Giannakis, and J. N. Laneman, "High-performance cooperative demodulation with decode-and-forward relays," *IEEE Transactions on Communications*, vol. 55, no. 7, pp. 1427–1438, July 2007.

[106] P. A. Anghel and M. Kaveh, "Exact symbol error probability of a cooperative network in a Rayleigh fading environment," *IEEE Transactions on Wireless Communications*, vol. 3, no. 5, pp. 1416–1421, September 2004.

[107] H. Shin and J. B. Song, "MRC analysis of cooperative diversity with fixed-gain relays in Nakagami-m fading channels," *IEEE Transactions on Wireless Communications*, vol. 7, no. 6, pp. 2069–2074, June 2008.

[108] K. P. Peppas, G. C. Alexandropoulos, and P. T. Mathiopoulos, "Performance analysis of dual-hop AF relaying systems over mixed $\eta-\mu$ and $\kappa-\mu$ fading channels," *IEEE Transactions on Vehicular Technology*, vol. 62, no. 7, pp. 3149–3163, September 2013.

[109] Y. Zhang, J. Xue, T. Ratnarajah, and C. Zhong, "Error exponents analysis of dual-hop $\eta-\mu$ and $\kappa-\mu$ fading channel with amplify-and-forward relaying," *IET Communications*, vol. 9, no. 11, pp. 1367–1379, July 2015.

[110] A. Hussain, K. Lee, S. Kim, S. Chang, and D. I. Kim, "Performance analysis of dual-hop variable-gain relaying with beamforming over $\kappa-\mu$ fading channels," *IET Communications*, vol. 11, no. 10, pp. 1587–1593, August 2017.

[111] J. Yang, L. Chen, X. Lei, K. P. Peppas, and T. Q. Duong, "Dual-hop cognitive amplify-and-forward relaying networks over $\eta-\mu$ fading channels," *IEEE Transactions on Vehicular Technology*, vol. 65, no. 8, pp. 6290–6300, August 2016.

[112] A. Kodide, T. M. C. Chu, and H. Zepernick, "Outage probability of multiple relay networks over $\kappa-\mu$ shadowed fading," in *Proceedings of the International Conference on Signal Processing and Communication Systems*, Gold Coast, December 19-21, 2016, pp. 1–7.

[113] A. K. Sadek, W. Su, and K. J. R. Liu, "Performance analysis for multi-node decode-and-forward relaying in cooperative wireless networks," in *Proceedings of the IEEE International Conference on Acoustics, Speech, and Signal Processing*, vol. 3, Philadelphia, March 23-23, 2005, pp. III: 521–524.

[114] H. A. Suraweera, P. J. Smith, and J. Armstrong, "Outage probability of cooperative relay networks in Nakagami-m fading channels," *IEEE Communications Letters*, vol. 10, no. 12, pp. 834–836, December 2006.

[115] S. S. Ikki and M. H. Ahmed, "Performance of decode-and-forward cooperative diversity networks over Nakagami-m fading channels," in *Proccedings of the IEEE Global Telecommunications Conference*, Washington, November 26-30, 2007, pp. 4328–4333.

[116] W.-G. Li, H.-M. Chen, and M. Chen, "Outage probability of dual-hop decode-and-forward relaying systems over generalized fading channels," *European Transactions on Telecommunications*, vol. 21, no. 1, pp. 86–89, January 2010.

[117] N. Biswas, B. Ghosh, and A. Chandra, "Energy efficient relay node placement in a eta-mu fading channel," in *Proceedings of the IEEE Conference on Information & Communication Technologies*, Thuckalay, April 11-12, 2013, pp. 824–828.

[118] K. P. Peppas, "Dual-hop relaying communications with cochannel interference over $\eta-\mu$ fading channels," *IEEE Transactions on Vehicular Technology*, vol. 62, no. 8, pp. 4110–4116, October 2013.

[119] D. Dixit and P. R. Sahu, "Performance of multihop communication systems with regenerative relays in $\eta-\mu$ fading channels," in *Proceedings of the IEEE Vehicular Technology Conference (Spring)*, Seoul, May 18-21 2014, pp. 1–5.

[120] ——, "Exact closed-form ABER for multi-hop regenerative relay systems over $\kappa\mu$ fading," *IEEE Wireless Communications Letters*, vol. 6, no. 2, pp. 246–249, April 2017.

[121] ——, "Outage probability of cooperative relay networks in $\eta-\mu$, $\kappa-\mu$ and mixed fading channels," in *Proceedings of the IEEE Vehicular Technology Conference (Fall)*, Toronto, September 24-27, 2017, 2017, pp. 1–5.

[122] S. Kumar and S. Chouhan, "Outage probability analysis of cognitive decode-and-forward relay networks over $\kappa-\mu$ shadowed channels," in *Proceedings of the Asia-Pacific Conference on Communications*, Kyoto, October 14-16, 2015, pp. 433–437.

[123] ——, "Performance analysis of cognitive decode-and-forward dual-hop relay networks over $\kappa-\mu$ shadowed channels," *AEU - International Journal of Electronics and Communications*, vol. 70, no. 9, pp. 1241–1248, September 2016.

[124] M. Poreddy, T. M. C. Chu, and H. Zepernick, "On outage probability of cooperative cognitive radio networks over $\kappa-\mu$ shadowed fading," in *Proceedings of the IEEE Wireless Communications and Networking Conference*, San Francisco, March 19-22, 2017, pp. 1–6.

[125] A. A. Nasir, X. Zhou, S. Durrani, and R. A. Kennedy, "Throughput and ergodic capacity of wireless energy harvesting based DF relaying network," in *Proceedings of the IEEE International Conference on Communications*, Sydney, June 10-14, 2014, pp. 4066–4071.

[126] D. Mishra, S. De, and C. F. Chiasserini, "Joint optimization schemes for cooperative wireless information and power transfer over Rician channels," *IEEE Transactions on Communications*, vol. 64, no. 2, pp. 554–571, February 2016.

[127] E. Chen, M. Xia, D. B. da Costa, and S. Aïssa, "Multi-hop cooperative relaying with energy harvesting from cochannel interferences," *IEEE Communications Letters*, vol. 21, no. 5, pp. 1199–1202, May 2017.

[128] H. Chen, X. Zhou, Y. Li, P. Wang, and B. Vucetic, "Wireless-powered cooperative communications via a hybrid relay," in *Proceedings of the IEEE Information Theory Workshop*, Hobart, November 2-5, 2014, pp. 666–670.

[129] X. Huang and N. Ansari, "Optimal cooperative power allocation for energy-harvesting-enabled relay networks," *IEEE Transactions on Vehicular Technology*, vol. 65, no. 4, pp. 2424–2434, April 2016.

[130] D. S. Michalopoulos, H. A. Suraweera, and R. Schober, "The impact of relay selection on the trade-off between information transmission and wireless energy transfer," in *Proceedings of the IEEE Global Communications Conference*, Austin, December 8-12, 2014, pp. 4191–4196.

[131] A. A. Nasir, X. Zhou, S. Durrani, and R. A. Kennedy, "Wireless-powered relays in cooperative communications: Time-switching relaying protocols and throughput analysis," *IEEE Transactions on Communications*, vol. 63, no. 5, pp. 1607–1622, May 2015.

[132] G. Li and H. Jiang, "Performance analysis of wireless powered incremental relaying networks with an adaptive harvest-store-use strategy," *IEEE Access*, vol. 6, pp. 48 531–48 542, September 2018.

[133] Z. Zhou, M. Peng, Z. Zhao, W. Wang, and R. S. Blum, "Wireless-powered cooperative communications: Power-splitting relaying with energy accumulation," *IEEE Journal on Selected Areas in Communications*, vol. 34, no. 4, pp. 969–982, April 2016.

[134] J. Men, J. Ge, and C. Zhang, "A joint relay-and-antenna selection scheme in energy-harvesting MIMO relay networks," *IEEE Signal Processing Letters*, vol. 23, no. 4, pp. 532–536, April 2016.

[135] M. Ashraf, A. Shahid, J. W. Jang, and K. Lee, "Energy harvesting non-orthogonal multiple access system with multi-antenna relay and base station," *IEEE Access*, vol. 5, pp. 17 660–17 670, September 2017.

[136] Y. Zeng and R. Zhang, "Full-duplex wireless-powered relay with self-energy recycling," *IEEE Wireless Communications Letters*, vol. 4, no. 2, pp. 201–204, April 2015.

[137] M. Mao, N. Cao, Y. Chen, and Y. Zhou, "Multi-hop relaying using energy harvesting," *IEEE Wireless Communications Letters*, vol. 4, no. 5, pp. 565–568, October 2015.

[138] Z. Chen, B. Xia, and H. Liu, "Wireless information and power transfer in two-way amplify-and-forward relaying channels," in *Proceedings of the IEEE Global Conference on Signal and Information Processing*, Atlanta, December 3-5, 2014, pp. 168–172.

[139] Z. Yan, S. Chen, X. Zhang, and H. Liu, "Outage performance analysis of wireless energy harvesting relay-assisted random underlay cognitive networks," *IEEE Internet of Things Journal*, vol. 5, no. 4, pp. 2691–2699, August 2018.

[140] D. Wang, H. Yu, J. Zhang, G. Pan, H. Lei, T. Li, and Y. Chen, "On outage of dual-hop relay SWIPT system with antenna selection and GSC over Nakagami-m fading channels," in *Proceedings of the IEEE International Conference on Communication Systems*, Shenzhen, December 14-16, 2016, pp. 1–6.

[141] Y. Chen, "Energy-harvesting AF relaying in the presence of interference and Nakagami-m fading," *IEEE Transactions on Wireless Communication*, vol. 15, no. 2, pp. 1008–1017, February 2016.

[142] H. Yu, D. Wang, G. Pan, R. Shi, J. Zhang, and Y. Chen, "On outage of WPC system with relay selection over nakagami-m fading channels," *IEEE Transactions on Vehicular Technology*, vol. 66, no. 9, pp. 8590–8594, September 2017.

[143] J. Ye, H. Lei, Y. Liu, G. Pan, D. B. da Costa, Q. Ni, and Z. Ding, "Cooperative communications with wireless energy harvesting over Nakagami-m fading channels," *IEEE Transactions on Communications*, vol. 65, no. 12, pp. 5149–5164, December 2017.

[144] A. Hussain, Z. Ahmed, N. H. Phulpoto, S. Soomro, and I. Ali, "Energy harvesting in opportunistic relaying network with multiple antennas," *International Journal of Computer Science and Network Security*, vol. 18, no. 5, pp. 125–129, May 2018.

[145] A. Hussain, N. H. Phulpoto, U. Rajput, F. Abbas, and Z. A. Baloch, "Non-linear energy harvesting dual-hop DF relaying system over $\eta-\mu$ fading channels," *International Journal of Advanced Computer Science and Applications*, vol. 9, no. 6, pp. 423–426, June 2018.

[146] O. S. Badarneh, F. S. Almehmadi, I. S. Ansari, and X. Yang, "Wireless energy harvesting in cooperative decode-and-forward relaying networks over mixed generalized $\eta-\mu$ and $\kappa-\mu$ fading channels," *Transactions on Emerging Telecommunications Technologies*, vol. 29, no. 2, pp. 1–18, November 2017.

[147] A. Hussain, I. Ali, Z. Ahmed, and S.-H. Kim, "Energy harvesting relaying network in a delay-tolerant transmission mode over $\kappa-\mu$ shadowed fading channels," *International Journal of Computer Science and Network Security*, vol. 18, no. 3, pp. 119–125, March 2018.

[148] M. Haghifam, B. Makki, M. Nasiri-Kenari, and T. Svensson, "On joint energy and information transfer in relay networks with an imperfect power amplifier," in *Proceedings of the IEEE Annual International Symposium on Personal, Indoor, and Mobile Radio Communications*, Valencia, September 4-8, 2016, pp. 1–6.

[149] H. Ju and R. Zhang, "User cooperation in wireless powered communication networks," in *Proceedings of the IEEE Global Communications Conference*, Austin, December 8-12, 2014, pp. 1430–1435.

[150] X. Di, K. Xiong, P. Fan, H. Yang, and K. B. Letaief, "Optimal resource allocation in wireless powered communication networks with user cooperation," *IEEE Transactions on Wireless Communications*, vol. 16, no. 12, pp. 7936–7949, December 2017.

[151] H. Chen, L. Xiao, D. Yang, T. Zhang, and L. Cuthbert, "User cooperation in wireless powered communication networks with a pricing mechanism," *IEEE Access*, vol. 5, pp. 16 895–16 903, August 2017.

[152] N. Zlatanov, D. W. K. Ng, and R. Schober, "Capacity of the two-hop relay channel with wireless energy transfer from relay to source and energy transmission cost," *IEEE Transactions on Wireless Communications*, vol. 16, no. 1, pp. 647–662, January 2017.

[153] S. Luo, G. Yang, and K. C. Teh, "Throughput of wireless-powered relaying systems with buffer-aided hybrid relay," *IEEE Transactions on Wireless Communications*, vol. 15, no. 7, pp. 4790–4801, July 2016.

[154] M. D. Selvaraj, R. K. Mallik, and R. Goel, "Optimum receiver performance with binary phase-shift keying for decode-and-forward relaying," *IEEE Transactions on Vehicular Technology*, vol. 60, no. 4, pp. 1948–1954, May 2011.

[155] N. Y. Ermolova, "Useful integrals for performance evaluation of communication systems in generalised $\eta - \mu$ and $\kappa - \mu$ fading channels," *IET Communications*, pp. 303–308, February 2009.

[156] M. K. Simon and M.-S. Alouni, *Digital Communications over Fading Channels*. New Jersey: Wiley, 2005.

[157] M. E. H. Ismail and J. Pitman, "Algebraic evaluations of some Euler integrals, duplication formulae for Appell's hypergeometric function F_1, and Brownian variations," Department of Statistics, University of California, Tech. Rep., August 1999, Rep. no. 554.

[158] S. Boyd and L. Vandenberghe, *Convex Optimization*. Cambridge: Cambridge University Press, 2004.

[159] P. Kumar and P. R. Sahu, "Analysis of M-PSK with MRC receiver over $\kappa - \mu$ fading channels with outdated CSI," *IEEE Wireless Communications Letters*, vol. 3, no. 6, pp. 557–560, December 2014.

[160] W. Lin, G. Wu, L. Zhang, and S. Li, "SER performance analysis and optimal relay location of cooperative communications with distributed Alamouti code," in *Proceedings of the Conference on Information Sciences and Systems*, Baltimore, March 18-20, 2009, pp. 646–651.

[161] Z. Mo, W. Su, S. Batalama, and J. D. Matyjas, "Cooperative communication protocol designs based on optimum power and time allocation," *IEEE Transactions on Wireless Communications*, vol. 13, no. 8, pp. 4283–4296, August 2014.

[162] A. P. Prudnikov, Y. A. Brychkov, O. I. Marichev, and G. G. Gould, *Integrals and Series: More Special Functions*. Vol. 3. Amsterdam: Gordon and Breach Science, 1990.

[163] K. C. Gupta and P. K. Mital, "Integrals involving a generalized function of two variables," *Indian Journal of Pure and Applied Mathematics*, vol. 5, no. 5, pp. 430–437, January 1972.

[164] G. Fikioris, *Mellin-Transform Method for Integral Evaluation: Introduction and Applications to Electromagnetics*. San Rafael: Morgan & Claypool, 2007.

[165] K. P. Peppas, "A new formula for the average bit error probability of dual-hop amplify-and-forward relaying systems over generalized shadowed fading channels," *IEEE Wireless Communications Letters*, vol. 1, no. 2, pp. 85–88, April 2012.

[166] I. S. Gradshteyn and I. M. Ryzhik, *Table of Integrals, Series and Products*. 6th ed. New York: Academic Press, 2000.

[167] E. Zedini, H. Soury, and M. S. Alouini, "On the performance analysis of dual-hop mixed FSO/RF systems," *IEEE Transactions on Wireless Communications*, vol. 15, no. 5, pp. 3679–3689, May 2016.

[168] E. A. Ansari and N. Rajatheva, "Exact SER analysis of OSTBC MIMO-OFDM systems over uncorrelated Nakagami-m fading channels," in *Proceedings of the IEEE International Multitopic Conference*, Islamabad, December 14-15, 2009, pp. 1–6.

[169] S. P. Goyal and R. K. Agrawal, "Bivariate distributions and the multivariate H-function," *Indian Journal of Pure and Applied Mathematics*, vol. 12, no. 3, pp. 380–387, March 1981.

[170] M. Abramowitz and I. A. Stegun, *Handbook of Mathematical Functions with Formulas, Graphs, and Mathematical Tables*. Washington: Government Printing Office, 1970.

[171] "Least-Squares Fitting," Accessed: August 25, 2018. [Online]. Available: https://in.mathworks.com/help/curvefit/least-squares-fitting.html.

[172] W. H. Press, S. A. Teukolsky, W. T. Vetterling, and B. P. Flannery, *Numerical Recipes in Fortran 77: The Art of Scientific Computing*. 2nd ed. Cambridge University Press, 1992.

[173] S. Parthasarathy and R. K. Ganti, "Coverage analysis in downlink Poisson cellular network with $\kappa-\mu$ shadowed fading," *IEEE Wireless Communications Letters*, vol. 6, no. 1, pp. 10–13, February 2017.

[174] M. D. Selvaraj and R. K. Mallik, "Error analysis of the decode and forward protocol with selection combining," *IEEE Transactions on Wireless Communications*, vol. 8, no. 6, pp. 3086–3094, June 2009.

[175] Y. Dong, M. J. Hossain, and J. Cheng, "Performance of wireless powered amplify and forward relaying over Nakagami-m fading channels with nonlinear energy harvester," *IEEE Communications Letters*, vol. 20, no. 4, pp. 672–675, April 2016.

[176] W. Liu, X. Zhou, S. Durrani, and P. Popovski, "SWIPT with practical modulation and RF energy harvesting sensitivity," in *Proceedings of the IEEE International Conference on Communications*, Kuala Lumpur, May 22-27 2016, pp. 1–7.

[177] A. A. Kilbas and M. Saigo, *H-Tansforms: Theory and Applications*. Boca Raton: CRC press LLC, 2004.

[178] "MeijerG," Accessed: August 25, 2018. [Online]. Available: http://functions.wolfram.com/PDF/MeijerG.pdf.

[179] A. P. Prudnikov, Y. A. Brychkov, O. I. Marichev, N. M. Queen, *Integrals and Series: Elementary Functions*. New York: Gordon and Breach Science, 1998, vol. 1.

[180] A. P. Prudnikov, Y. A. Brychkov, O. I. Marichev, and G. G. Gould, *Integrals and Series: Special Functions*. New York: Gordon and Breach Science, 1992, vol. 2.

Bio-Data

1.	Name:	Pawan Kumar
2.	Date of Birth:	25-July-1990
3.	Educational Qualification:	June-2011, B.Tech. in Electronics Engineering (69.88 %) Dr. Ambedkar Institute of Technology for Handicapped Kanpur, Uttar Pradesh, India June-2013, M.Tech. in Communication Engineering (7.44/10 CGPA), Indian Institute of Technology Guwahati Guwahati, Assam, India May-2019, Ph.D Indian Institute of Technology Guwahati Guwahati, Assam, India
4.	Permanent Address:	Pawan Kumar s/o Mr. Ramakant Prasad Opp. Bansdih Inter College Post: Bansdih District: Ballia Uttar Pradesh, India Pincode-277202
5.	Contact Address:	Pawan Kumar, Communication Lab 2 Dept. of EEE Indian Institute of Technology Guwahati Guwahati, Assam, India Pincode-781039
6.	Contact Number:	(+91)-8638265824

Abstract-TH-2151_136102001